



The Development of Vinylheteroarene Linkers for Proteinogenic
Cysteine Modification
and
Studies Towards Applying (+)-Discodermolide as a Novel Payload in
Antibody-Drug Conjugates

Hikaru Seki

Trinity College
University of Cambridge
December 2021

Supervised by Professor David R. Spring

This thesis is submitted for the degree of Doctor of Philosophy

Declaration

This thesis is the result of my own work carried out between October 2018 and December 2021. It includes nothing which is the outcome of work done in collaboration except where specifically indicated in the text. It is not substantially the same as any work that has already been submitted before for any degree or other qualification. It does not exceed the prescribed word limit for the Physics and Chemistry Degree Committee.

Hikaru Seki

December 2021

Abstract

The Development of Vinylheteroarene Linkers for Proteinogenic Cysteine Modification and Studies Towards Applying (+)-Discodermolide as a Novel Payload in Antibody-Drug Conjugates

Hikaru Seki

Antibody-drug conjugates (ADCs) are an emerging class of anticancer agents which combine the cell-targeting properties of a monoclonal antibody and the cytotoxicity of a small molecule drug. The antibody, cytotoxin and the covalent linker which connects the two units must be optimised for the ADC to have favourable pharmacokinetic, toxicology, and overall pharmacological profiles.

The first project describes the design, synthesis, and evaluation of vinylheteroarene linkers for the post-translational modification of proteinogenic cysteine residues (**Figure a**). It was hypothesised that the variable heteroarene ring electronics would greatly affect the conjugate addition reaction rate and resulting bioconjugate stability. Thus, a panel of vinylheteroarenes with differing heterocyclic groups were synthesised and evaluated for their suitability. Using small molecule model systems, vinylheteroarene linkers were assessed for cysteine reactivity and chemoselectivity, and conjugate stability to identify the optimum linker. The lead linker was utilised to modify a number of protein substrates with various functionality, including the synthesis of a homogeneous, stable and biologically active ADC. The reagent was also efficient in labelling proteome-wide cysteines in cell lysates. The efficiency and selectivity of these reagents as well as the stability of the products makes them suitable for the generation of biotherapeutics or studies in chemical biology.

The second project describes studies towards using (+)-discodermolide as a cytotoxic payload in ADCs (**Figure b**). Discodermolide is a polyketide natural product which displays potent activity as an antimetabolic agent and is known to be effective against a range of malignancy types. It was desired to attach discodermolide to an antibody using a cleavable linker which would enable traceless release of the cytotoxin. The alcohol groups in discodermolide presented an opportunity to achieve this in a chemically tractable way. Thus, a valine-alanine-*para*-aminobenzylcarbonyl-hemiaminal linker was designed for the selective cleavage and payload release by lysosomal cathepsin enzymes. Importantly, this linker strategy allows the synthesis of linker-payloads in one synthetic step, making this a promising approach for the

rapid assembly of ADCs using unexplored alcohol cytotoxins. Using this linker, a discodermolide ADC was successfully synthesised which can be used for biological evaluation.

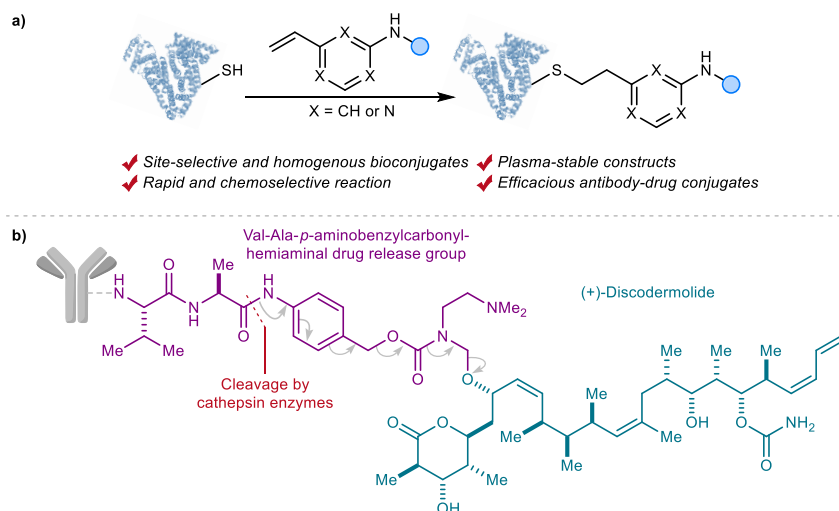


Figure. a) Project One: The development of vinylheteroarene linkers for proteinogenic cysteine modification and **b)** Project Two: Studies towards applying (+)-discodermolide as a novel payload in antibody-drug conjugates.

Acknowledgements

Firstly, I would like to thank Professor David Spring for giving me the opportunity to work in the group, encouragement, and advice. Your trust and support have made my PhD a wonderful experience. I would also like to acknowledge Trinity College Cambridge for funding my studies through the Geoffrey Moorhouse Gibson Studentship.

Special thanks to Steve, who I was fortunate enough to be mentored by throughout my PhD. You somehow managed to develop me to where I am now, and I am grateful for your encouragement, support, and friendship.

Jessy – thank you for being around to talk about things. I enjoyed working on projects with you. You're a great role model.

I'm grateful to be part of an amazing cohort with Andrew, Beth, Ellie, and Tom. I had so much fun with you – going to Trinity for lunch and formals, punting, going on walks during lockdown, and visiting Greggs.

'Bay 1 and the no. 1 Bae' – Nicola, Jiyan, and Abbie. I really had a great time sharing a bay with you. I'm now convinced that Jiyan and Nicola's taste in music was not that horrible after all, and I will miss all the shenanigans that happened in the bay. Only a genius can come up with 'bin laden', 'condens/condoms', and 'TEA' in fumehoods. Also, who brings a gun to work?

I would also like to thank all the past and present Spring Group members for making the three years in the group so enjoyable. I will miss having lunch together, tea at 3 pm, and Alma trips! Thank you to Steve, Javi, Nicola, Josie, Tom, and Mahri for proofreading this thesis.

College pals – Aaron, Josh, Miriam, Kasia, Nat, and Steph. I will miss going to formal, brunching, and having fish and chips for lunch. Thanks for being around.

Finally, I'd like to thank *oka-san* for her continued support and Ilma for the great food.

Abbreviations

Ac	Acetyl
ADC	Antibody-drug conjugate
Ala	Alanine
Alloc	Allyloxycarbonyl
app	Apparent
BBN	9-Borabicyclo[3.3.1]nonane
Bn	Benzyl
Boc	<i>tert</i> -Butyloxycarbonyl
br	Broad
Bu	Primary butyl
^t Bu	Tertiary butyl
Bz	Benzoyl
Cit	Citruline
CuAAC	Copper-catalysed alkyne-azide cycloaddition
Cys	Cysteine
d	Doublet
Da	Dalton(s)
DAR	Drug-to-antibody ratio
DBCO	Dibenzocyclooctyne
DBU	1,8-Diazabicyclo[5.4.0]undec-7-ene
DDQ	2,3-Dichloro-5,6-dicyano- <i>para</i> -benzoquinone
DIBAL	Diisobutylaluminum hydride
DMF	<i>N,N</i> -Dimethylformamide
DMSO	Dimethyl sulfoxide
DNA	Deoxyribonucleic acid
dppf	1,1'-Bis(diphenylphosphino)ferrocene
DTT	Dithiothreitol
DVP	Divinylpyrimidine
EDC	<i>N</i> -Ethyl- <i>N'</i> -(3-dimethylaminopropyl)carbodiimide
EDTA	Ethylenediaminetetraacetic acid
EEDQ	<i>N</i> -Ethoxycarbonyl-2-ethoxy-1,2-dihydroquinoline
eq.	Equivalent(s)
ESI	Electron spray ionisation
Et	Ethyl
Fab	Fragment antigen binding
Fc	Fragment crystallisable
FDA	Food and Drug Administration
Fmoc	Fluorenylmethyloxycarbonyl
g	Gram(s)
Gly	Glycine
h	Hour(s)
HATU	<i>N</i> -[(Dimethylamino)-1 <i>H</i> -1,2,3-triazolo-[4,5- <i>b</i>]pyridin-1-ylmethylene]- <i>N</i> -methylmethanaminium hexafluorophosphate <i>N</i> -oxide
HC	Heavy chain
HER2	Human epidermal growth factor receptor 2
^c Hex	Cyclohexyl
HPLC	High performance liquid chromatography
HRMS	High resolution mass spectrometry
HSA	Human serum albumin
Hz	Hertz
IC50	Half-maximal inhibitory concentration
IEDDA	Inverse electron-demand Diels-Alder
Ig	Immunoglobulin
Ipc	Isopinocampheyl
IR	Infrared
<i>J</i>	Coupling constant(s)

k_2	Second order rate constant(s)
KHDMS	Potassium bis(trimethylsilyl)amide
L	Litre(s)
LC	Light chain or liquid chromatography
LCMS	Liquid chromatography mass spectroscopy
LRMS	Low resolution mass spectrometry
Lys	Lysine
M	molar, mol/L
m	Multiplet or meter(s)
Me	Methyl
min	Minute(s)
MMAE	Monomethyl auristatin E
MMAF	Monomethyl auristatin F
mol	mole(s)
MWCO	Molecular weight cutoff
NaPi	Sodium phosphate
NBD	Nitrobenzoxadiazole
NMR	Nuclear magnetic resonance
PAB	<i>para</i> -Aminobenzyl
PBS	Phosphate buffered saline
PDB	Pyrrolobenzodiazepine
PEG	Polyethylene glycol
pent	Pentet
Ph	Phenyl
Phe	Phenylalanine
PMB	<i>para</i> -Methoxybenzyl
PMP	<i>para</i> -Methoxyphenyl
PNGase F	Peptide: <i>N</i> -glycosidase F
ppm	Parts per million
ⁱ Pr	Isopropyl
Py	Pyridine
q	Quartet
R _f	Retention factor
RNA	Ribonucleic acid
rt	Room temperature
s	Second(s) or singlet
SDS-PAGE	Sodium dodecyl sulphate–polyacrylamide gel electrophoresis
SPAAC	Strain-promoted alkyne-azide cycloaddition
Su	Succinimide
t	Triplet or time
TBS	Tris buffered saline or <i>tert</i> -butyldimethylsilyl
TCEP	Tris(2-carboxyethyl)phosphine
TEMPO	2,2,6,6-Tetramethylpiperidine 1-oxyl
Tf	Trifluoromethylsulfonyl
THF	Tetrahydrofuran
THPTA	Tris(benzyltriazolylmethyl)amine
TLC	Thin layer chromatography
TMS	Trimethylsilane
Tris	Tris(hydroxymethyl)aminomethane
Ts	Toluenesulfonyl
UV	Ultraviolet
V	Volt(s)
Val	Valine
Vis	Visible
%	Percent
°C	Degrees Celsius
ε	Molar extinction coefficient
δ	Chemical shift
ν _{max}	Absorption maxima

Table of contents

Declaration.....	i
Abstract.....	ii
Acknowledgements.....	iv
Abbreviations.....	v
Chapter 1. Introduction.....	1
1.1. Cancer chemotherapy.....	1
1.2. Antibody-drug conjugates.....	2
1.3. Monoclonal antibodies.....	5
1.4. Payloads.....	6
1.5. Linker technologies.....	9
Chapter 2. Rapid and robust cysteine bioconjugation with vinylheteroarenes.....	21
2.1. Introduction.....	21
2.2. Project aims and overview.....	22
2.3. Design of linker.....	23
2.4. Synthesis of model vinylheteroarene linkers.....	23
2.5. Reactivity studies of vinylheteroarene linkers.....	24
2.6. Stability of vinylheteroarene-thiol conjugates.....	30
2.7. Modification of human serum albumin.....	32
2.8. Modification of antibodies and biological evaluation of antibody-drug conjugates.....	38
2.9. Labelling of cysteine-containing proteins in cell lysate.....	44
2.10. Plasma stability.....	45
2.11. Conclusion.....	48
2.12. Future work.....	49

Chapter 3. Studies towards applying (+)-discodermolide as a cytotoxic payload in antibody-drug conjugates	50
3.1. Introduction	50
3.2. Project background.....	53
3.3. Project aims	54
3.4. Project design	55
3.5. Synthesis and isolation of aminomethylene chloride	59
3.6. Optimisation of conjugation with aminomethylene chloride	62
3.7. Synthesis of azide-discodermolide.....	63
3.8. Synthesis of trastuzumab-discodermolide ADC	65
3.9. Conclusion.....	68
3.10. Future work.....	68
Chapter 4. Experimental	70
4.1. General experimental	70
4.2. Kinetic studies of conjugate addition	73
4.3. Thioether stability studies	73
4.4. Chemical synthesis – Chapter 2	73
4.5. Chemical synthesis – Chapter 3	86
4.6. Protein chemistry – Chapter 2.....	92
4.7. Protein chemistry – Chapter 3.....	114
Chapter 5. References.....	117
Chapter 6. Appendix.....	122
6.1. Spectra from kinetic studies	122
6.2. Spectra from thioether stability studies.....	129
6.3. Spectra of small molecules.....	131
6.4. Chromatography traces	158
6.5. Publication list.....	159

Chapter 1. Introduction

1.1. Cancer chemotherapy

Cancer is a disease which is characterised by the rapid and uncontrolled division of cells.¹ It is a leading cause of death worldwide, accounting for nearly 10 million deaths in 2020 and its annual economic impact is estimated to be 1.2 trillion US dollars.²

The formation of cancer cells is initiated by mutations in genetic material. This can occur randomly during cell replication or can be triggered by external factors, such as smoking, alcohol use, poor diet, obesity, or lack of physical activity.³ These factors can activate oncogenes or inhibit of tumour-suppressing genes, leading to cancer development. Since there are over 200 cancer types with a high inter-individual variability in origin, each disease must be diagnosed and treated differently.⁴

Cancer is typically treated by a combination of chemotherapy, radiotherapy, and surgery.¹ For solid tumours, the most effective therapy is surgical removal of the tumour, whereas chemotherapy is preferred for metastatic and haematological cancers.⁵ Although chemotherapy has shown effectiveness for curing these tumour types, its low tumour specificity is often associated with numerous and severe side effects. Indeed, early chemotherapy drugs were toxic against both healthy and tumorous cells; these drugs' selectivity for tumour cells exclusively relied on rapid growth and proliferation of these cells, which are characterised by a greater intake of drugs and nutrients relative to healthy cells.^{1,6}

Aiming at decreasing severe side effects, therapeutics with greater selectivity for tumour cells have been developed. For example, modern chemotherapy agents are designed to bind to receptors that are overexpressed in cancer cells, such as kinases.^{6,7} Furthermore, monoclonal antibodies,⁸ small interfering RNA,⁹ and antisense oligonucleotides¹⁰ have been used to treat patients with high tumour cell selectivity.

1.2. Antibody-drug conjugates

Antibody-drug conjugates (ADCs) are a class of targeted drug delivery agent comprised of an antibody and a cytotoxin connected *via* a covalent linker (**Figure 1**). The antibody acts as a vehicle to deliver highly potent cytotoxins to antigen-overexpressing cells with exquisite selectivity. Compared to non-selective chemotherapy agents, ADCs have reduced side effects while being effective to irradiate tumour cells with lowered doses, resulting in an overall increase in the therapeutic window.¹¹ Although ADCs are primarily used in cancer treatment, there are recent examples where they are used as antibiotics.^{12,13}

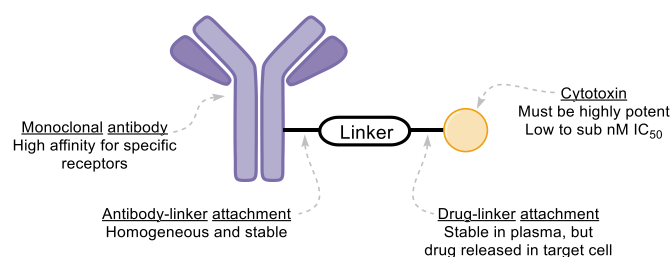


Figure 1. General structure of ADCs and their overall requirements

Once an ADC is administered to the patient, it circulates the body until it reaches the target cell, where the antibody binds to its antigen. This triggers endocytosis, where the ADC–antigen complex is internalised and trafficked to the endosome and then to the lysosome. At this point, the antibody is degraded to its constituent amino acids and the payload is released from the antibody. This payload can either cause cell death, or if sufficiently membrane permeable, diffuse out of the cell and kill neighbouring tumour cells (**Figure 2**).¹⁴

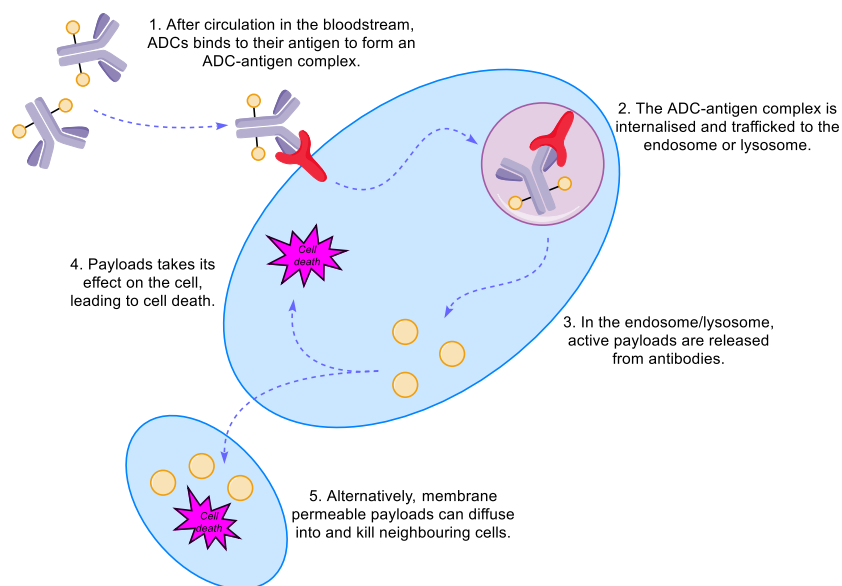


Figure 2. Mechanism of action of ADCs.

The first report of using antibodies for drug delivery was made in the 1950s, but the field of ADCs only matured in recent decades with clinical trials began in 1980s; this led to the approval of the first ADC in 2000.^{15–18} Currently, there are 11 FDA-approved ADCs, which are all used for cancer treatment, with seven of these approved since 2019 (**Figure 3**).^{19,20,29,21–28}

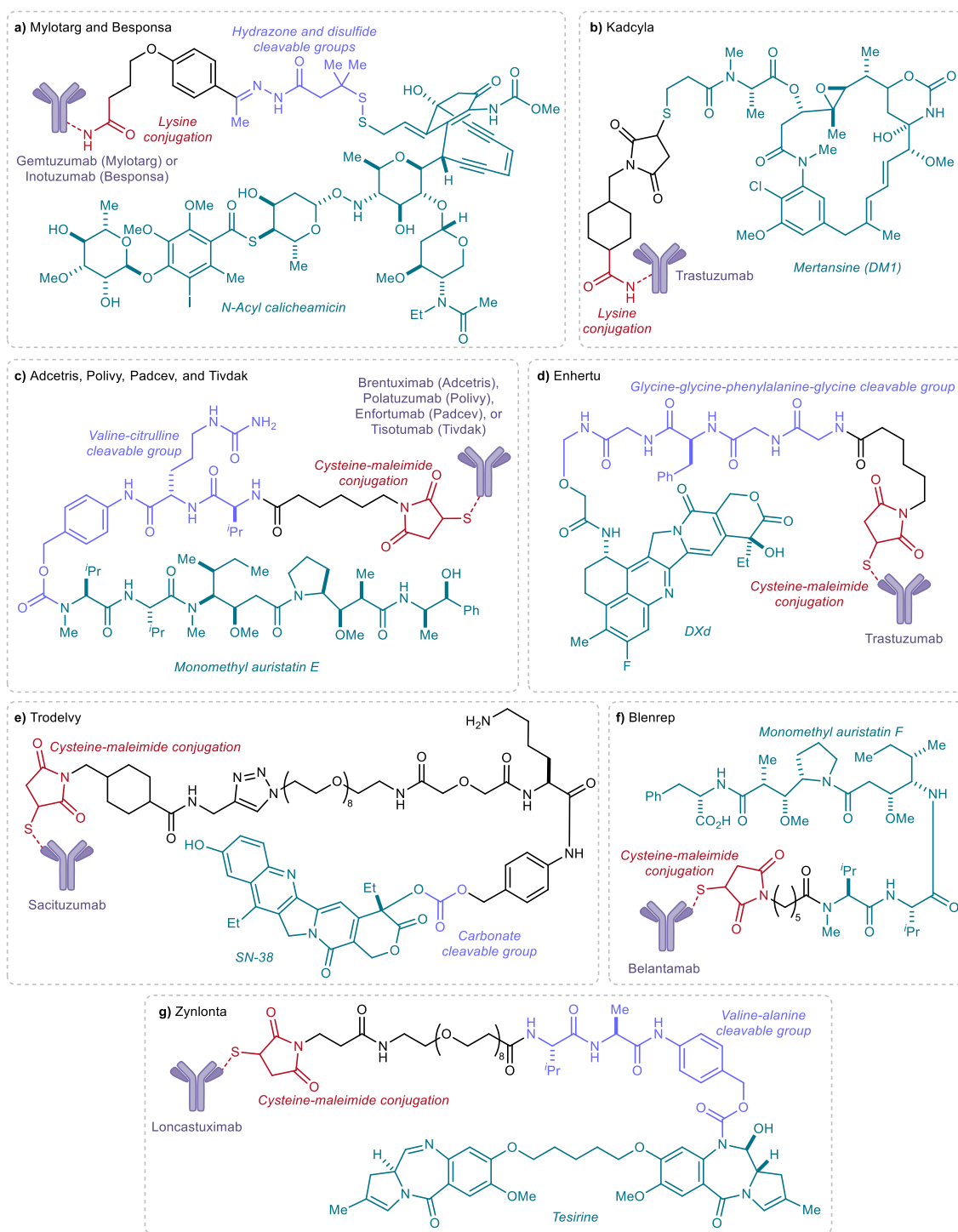


Figure 3. Structures of FDA-approved ADCs. **a)** Gemtuzumab ozogamicin (Mylotarg[®]; approved 2000, withdrawn 2010, re-approved 2017)^{16,17} and Inotuzumab ozogamicin (Besponsa[®], approved 2017).¹⁹ **b)** Trastuzumab emtansine (Kadcyla[®], approved 2013).²⁰ **c)** Brentuximab vedotin (Adcetris[®], approved 2011),²¹ Polatuzumab vedotin (Polivy[®], approved 2019),²² Enfortumab vedotin (Padcev[®], approved 2019),^{23,24} and Tisotumab vedotin (Tivdak[®], approved 2021).²⁵ **d)** Trastuzumab deruxtecan (Enhertu[®], approved 2019).²⁶ **e)** Sacituzumab govitecan (Trodelvy[®], approved 2020).²⁷ **f)** Belantamab mafodotin (Belrep[®], approved 2020).²⁸ **g)** Loncastuximab tesirine (Zynlonta[®], approved 2021).²⁹

1.3. Monoclonal antibodies

Antibodies or immunoglobins (Ig) are large glycoproteins which bind to target antigens with high affinity and selectivity (**Figure 4**). They comprise two heavy and two light polypeptide chains which are covalently connected by disulfide bonds. The polypeptide chains can be further subcategorised into the fragment antigen binding (Fab) region and the fragment crystallisable (Fc) region.³⁰ Both of the Fab and Fc regions are important for biotherapeutic development: the Fab region contains the complementarity-determining regions which are responsible for antigen binding, whereas the Fc region provides long half-lives through FcRn recycling.^{30,31} In addition to the four polypeptide chains comprising the antibody, there is a glycan group on the conserved asparagine 297 residue.³⁰

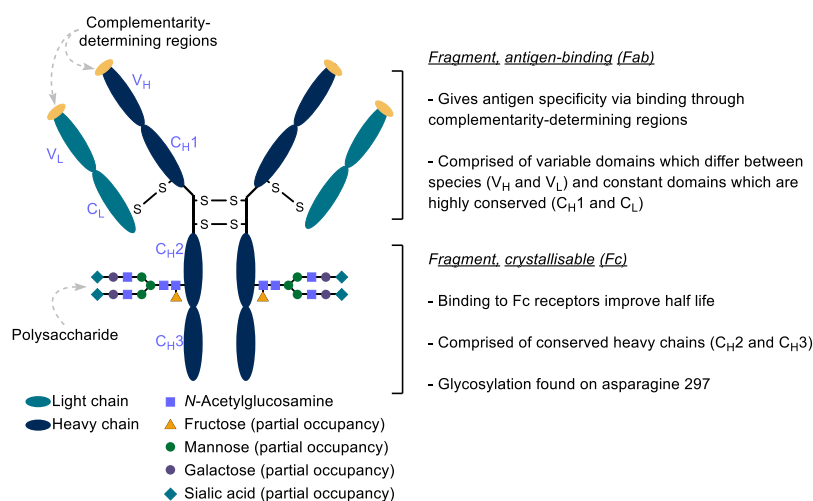


Figure 4. Structure of an antibody.³⁰

For successful ADC development, the antibody must meet a number of requirements. They must a) have an exquisite selectivity for a highly expressed antigen on the target-cell surface, allowing a targeted drug delivery; b) be internalised by the target cell and metabolised effectively to achieve maximum cytotoxicity; c) have extended half-life of >2 weeks; and d) have low immunogenicity.^{32,33}

1.4. Payloads

Early ADCs were designed with the aim of targeted delivery of traditional chemotherapy drugs such as methotrexate and doxorubicin (**Figure 5**).^{18,34} However, ADCs using these drugs gave insufficient potency due to limited cytotoxin delivery as i) ADCs that can be internalised to the target cell are limited by the density of antigens on the cell surface and ii) ADC-antigen complex's internalisation and lysosomal processing can have poor efficiency, which reduces the release of active cytotoxin within the cell. To overcome the poor cytotoxin delivery to target cells, highly potent cytotoxins with subnanomolar IC50 values are desirable to achieve complete cell-killing.^{11,14,18,35} Cytotoxic warheads which have been used in FDA-approved ADCs can be categorised into five classes, according to their chemical structure: auristatins, matansinoids, calicheamicins, camptothecins analogues, and pyrrolobenzodiazepine dimers.

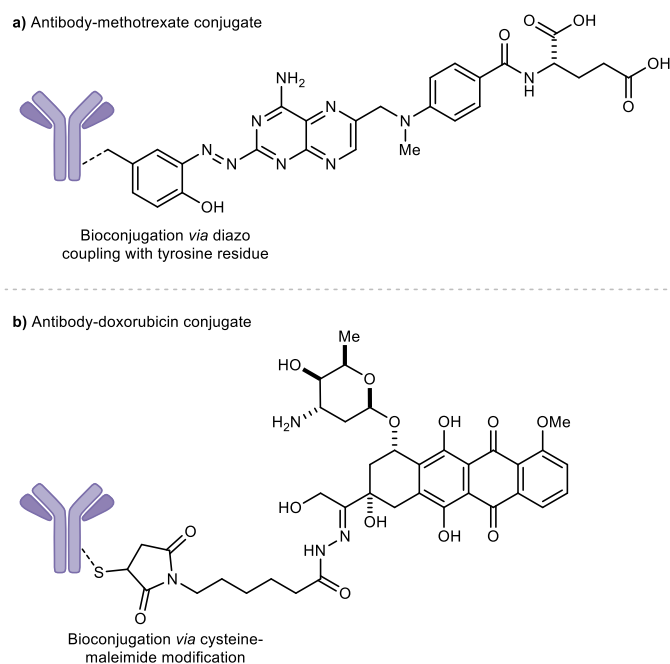


Figure 5. Structures of ADCs where **a)** methotrexate and **b)** doxorubicin were used as payloads.^{18,34}

Auristatins are synthetic analogues of the marine natural product dolastatin 10 and are widely used in ADC development. Both auristatins and dolastatins inhibit tubulin polymerisation, thus preventing mitosis. In contrast to dolastatin 10 which possesses a tertiary amine, monomethyl auristatin E (MMAE)³⁶ and monomethyl auristatin F (MMAF)³⁷ have a secondary amine which can be used to attach a linker. MMAE is used as the payload for Adcetris[®], Polivy[®], Padcev[®], and Tivdak[®], whereas MMAF is found in Blenrep[®] (**Figure 6a**).

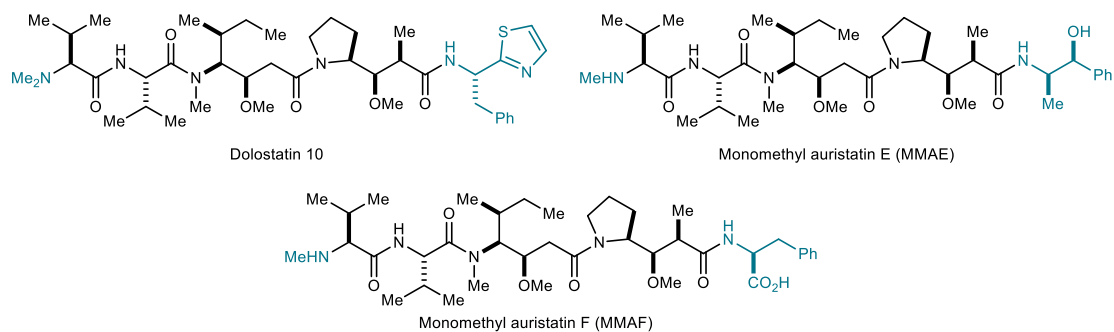
Maytansinoids are the synthetic analogue of maytansine, a natural product originally isolated from the Ethiopian shrub *Maytenus serrata*.³⁸ Similar to auristatins, maytansine and matansinoids act as tubulin disrupters with sub-nanomolar potency.³⁹ Maytansinoids used as ADC payloads have an additional thiol group, which allows attachment either *via* a thiosuccinimide or disulfide. A family of maytansinoids have been developed which have varying steric hindrance around this thiol, allowing tuneable stability of the drug attachment site.⁴⁰ The maytansinoid DM1 is used as a payload in Kadcyra[®] (**Figure 6b**).

Calicheamicins are DNA damaging agents which bind to the minor groove of DNA and cause DNA scission. Their cytotoxic properties are revealed by a reduction of the trisulfide group which triggers the formation of the active diradical species *via* a Bergman cyclisation.^{41,42} This payload is used in Mylotarg[®] and Besponsa[®] (**Figure 6c**).

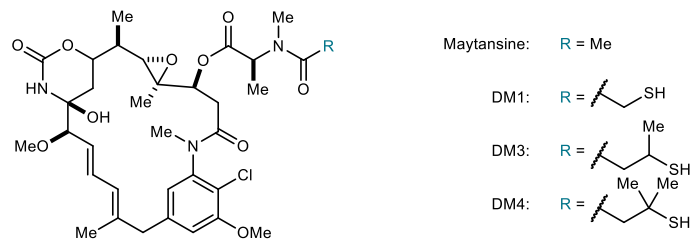
Camptothecins act as cytotoxins by stabilising the topoisomerase 1-DNA complex, thus preventing DNA re-ligation and causing cell death. Currently, two camptothecins analogues with nanomolar potencies are used as ADC payloads – DXd in Enhertu[®] and SN-38 in Trodelvy[®] (**Figure 6d**).^{43,44}

Pyrrrolobenzodiazepine (PDB) dimers are highly toxic DNA alkylating agents with low picomolar cytotoxicity. They act as DNA crosslinking agents, with the imine group reacting with the amine group on guanine bases. PDB dimers are one of the most potent cytotoxins and show great potential, however the linker must be optimised to balance the high hydrophobicity of the payload.^{45,46} Currently the PDB dimer tesirine is used in Zynlonta[®] (**Figure 6e**).

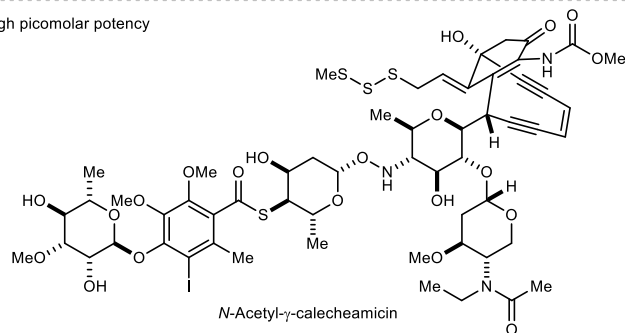
a) Auristatins - low to high picomolar potency



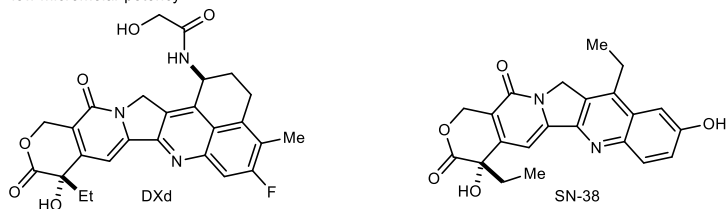
b) Maytansinoids - mid to high picomolar potency



c) Calecheamincins - mid to high picomolar potency



d) Camptothecin analogues - low micromolar potency



e) Pyrrolobenzodiazepine (PDB) dimers - low femtomolar to low nanomolar potency

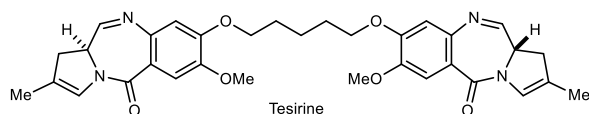


Figure 6. Structures and potency ranges of payloads used in FDA-approved ADCs.⁴⁷

1.5. Linker technologies

The purpose of the linker is to provide a covalent attachment between the antibody and a drug molecule. The properties of the linker are crucial for the clinical success of the ADC, as the linker influences its pharmacokinetics, pharmacodynamics, and therapeutic window. Crucially, the linker must have high plasma stability to prevent premature cleavage during circulation; linkers with poor stability in circulation result in systemic toxicity and reduce payload delivery to tumour cells.^{48,49} Linkers can be categorised into two components – the linker-antibody attachment point and the linker-drug attachment point.

1.5.1. Linker-antibody attachment

This section discusses the requirements for ADC bioconjugation and the methods for its synthesis.

1.5.1.1. General considerations

The chemistry used for the linker-antibody attachment has a significant influence on the pharmacology of an ADC. For example, a key parameter of an ADC that influences these properties is the stoichiometry of the linker-payloads to the antibody, referred to the drug-to-antibody ratio (DAR). Given the limited number of ADCs reaching the target cell, it is desirable to maximise DAR to have high potency. However, since cytotoxins used in ADC development are lipophilic, having an excessively large drug loading could lead to ADC aggregation and rapid clearance, thus reducing safety and efficacy. For these reasons, the DAR must be optimised for each antibody and linker-payload combination.⁵⁰⁻⁵² Typically, antibodies are modified with two to four linker-payloads, but for Enhertu[®] and Trodelvy[®], the use of hydrophilic linker-payloads permits drug-to-antibody ratios of 7.6 (average) and 8, respectively.^{26,27}

Another consideration in ADC development is the conjugation site. To ensure the attached linker-payloads do not interfere with the ADC antigen binding and internalisation, the modification should be distal from the antigen-binding surface region. Furthermore, the local environment around the attachment site can influence ADC plasma stability, which may lead to premature linker cleavage.^{49,53}

To achieve the best efficacy and safety, synthetic methods are required to predictably modify antibodies to afford ADCs with uniform DAR and modification site. Although stochastic modification of lysine and cysteine residues has been widely employed, the use of site-selective modification techniques have been developed to give improved control. These modification methods include disulfide rebridging, cysteine engineering, enzymatic modification, and incorporation of non-proteinogenic amino acids.⁵⁴

1.5.1.2. Stochastic modification

Early ADC development relied on the stochastic modification of naturally occurring lysine and cysteine residues. Lysine modification offers a general method of antibody modification due to its high natural abundance and solvent accessibility.⁵⁵ Indeed, the FDA-approved ADCs Mylotarg[®], Kadcyła[®], and Besponsa[®] attach the linker-payload through an amide bond with the antibody's lysine residues using *N*-hydroxysuccinimide reagents (**Figure 7a**). Nevertheless, since antibodies have approximately 85 accessible lysine residues, this bioconjugation method leads to mixtures where each antibody varies in DAR and site of modification. For example, Mylotarg[®] – which has an average DAR of 3 – is comprised of a mixture where ~50% of the antibodies are unmodified while the remaining antibodies have an average of approximately 6 drugs per antibody.⁵⁶

Cysteine residues are also an attractive target for antibody modification. The thiol's inherent reactivity as a soft nucleophile allows the chemoselective modification of these residues. Furthermore, there are limited solvent-exposed cysteines on an antibody surface, thus reducing the eventual variability in DAR and the number of regioisomers that can be formed. In native antibodies, there are 8 exposed cysteine residues forming four interchain disulfide bridges. To reveal the nucleophilicity of cysteine residues, the disulfide bonds are first reduced to their thiol form, which is subsequently modified. Since modification of all thiol residues yield drug loadings which are typically higher than desired, the disulfides are partially reduced and then reacted to afford an average drug loading between 2 and 4.⁵⁷ Although this partial modification method also leads to mixtures, the level of heterogeneity is dramatically lower than that for ADCs synthesised by lysine modification.

For cysteine modification, the conjugate addition to *N*-substituted maleimide reagents is the most widely used due to their remarkable conjugation efficiency (**Figure 7b**). Indeed, all FDA-

approved ADCs that use a cysteine modification approach employ maleimide reagents to attach linker-payloads. However, despite the utility of the maleimide linker, the resulting thiosuccinimide linkage has demonstrated poor stability, caused by E₁cB-type elimination. Instability of the protein-payload linkage can greatly affect the pharmacological properties of biotherapeutics such as ADCs, given that premature release of cytotoxic payload can decrease its targeted delivery and cause off-target toxicity.^{48,58} To address this, modified maleimide reagents have been developed to increase the stability of the bioconjugate.^{59,60} One approach involves the use of self-hydrolysing maleimides which catalyse hydrolytic opening of the thiosuccinimide ring, thus reducing its susceptibility towards deconjugation (**Figure 7c**).^{61,62}

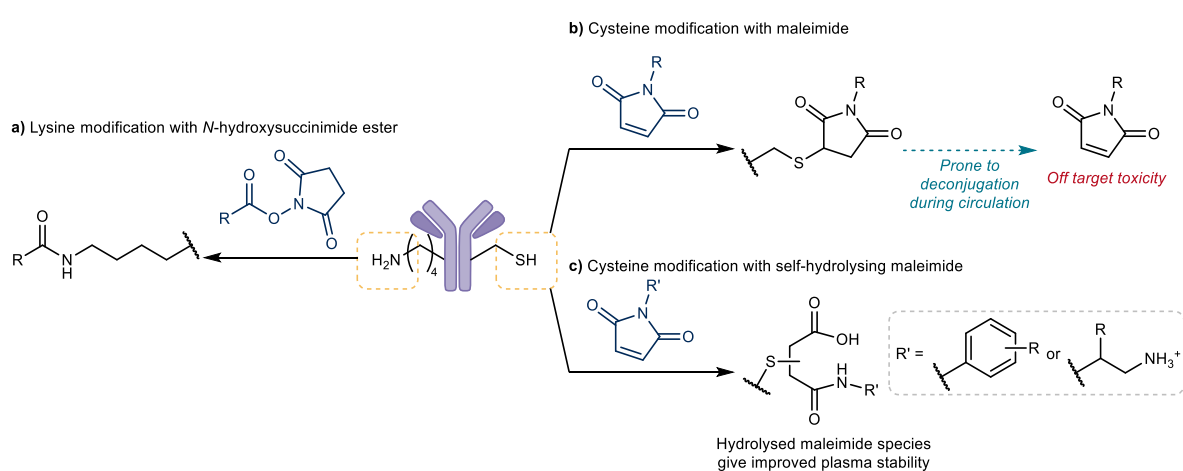


Figure 7. Methods of stochastic protein modification can be accomplished by **a)** *N*-hydroxysuccinimide esters; **b)** maleimides; and **c)** self-hydrolysing maleimides.

1.5.1.3. Disulfide rebridging

Antibody modification methods using bis-reactive reagents have been developed for disulfide rebridging. To achieve this, the interchain disulfides are reduced and the resulting thiols are treated with the bis-reactive reagents to furnish disulfide rebridged products. Then, drug molecules are installed onto the antibody while maintaining a covalent bond between the polypeptide chains of the antibody. Since the IgG1 antibodies commonly used for ADC development have four solvent exposed disulfide bonds, this methodology gives rise to ADCs with a drug loading of four. This is an effective method for synthesising homogeneous ADCs from native antibodies.⁶³

Bis-reactive reagents which accomplish disulfide rebridging include dibromomaleimides (**Figure 8a**),⁶⁴ pyridazinediones (**Figure 8b**),⁶⁵ bis-sulfones (**Figure 8c**),⁶⁶ and diethynyl

phosphinates (**Figure 8d**).⁶⁷ Recently, divinylpyrimidine (DVP) reagents were developed by the Spring Group (**Figure 8e**).^{54,68} ADCs synthesised using divinylpyrimidine linkers displayed selective cytotoxicity against antigen-positive cells, demonstrating that the native function of the antibody was preserved. This methodology was extended with divinyltriazine reagents, which have greater reactivity and allow modification of antibodies using near stoichiometric quantities of linker (**Figure 8e**).⁶⁹

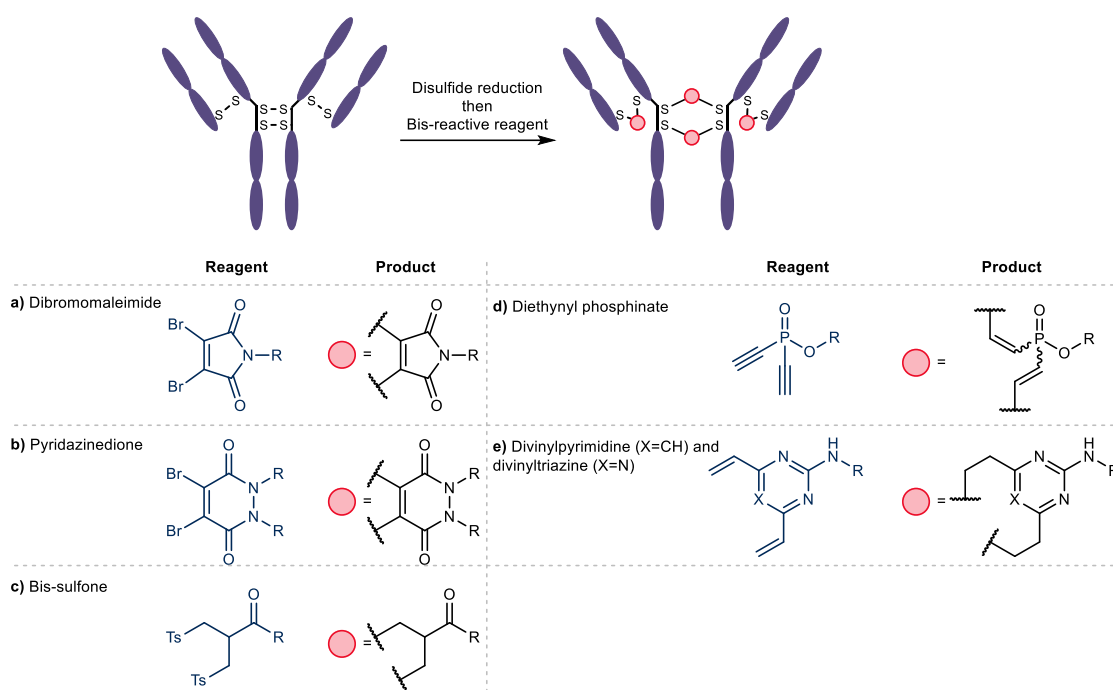


Figure 8. Examples of disulfide rebridging reagents used for antibody modification. R = drug or functional moiety.

1.5.1.4. Engineered cysteine residues

Genetic modification to incorporate additional engineered cysteine residues on an antibody surface has emerged as a popular method to achieve the desired site-selective and homogeneous modification. This approach offers a number of advantages: 1) modification of these unpaired cysteines with payloads will give homogeneous ADCs with a defined attachment site and drug stoichiometry; and 2) all native immunoglobulin disulfide bonds will be retained, potentially improving the stability and inherent function of the antibody. The site of cysteine incorporation can influence the stability of the conjugation linkage, potentially altering the pharmacological properties of the ADC. Thus, the site of cysteine incorporation must be carefully selected and optimised to synthesise ADCs with high linker stability, target antigen binding, internalisation, and potency.

The most common method of modifying an engineered cysteine residue is by using an appropriate electrophilic reagent. Although maleimides are the most common cysteine-selective reagents, a variety of novel linkers have been used to functionalise engineered cysteines in this fashion. For example, maleimides (**Figure 9a**), iodoacetamides (**Figure 9b**),⁷⁰ bromomaleimides (**Figure 9c**),⁷¹ carbonylacrylic reagents (**Figure 9d**),^{72,73} and *N*-alkyl vinylpyridine salts (**Figure 9e**)⁷⁴ have been used to modify the engineered cysteine residue to synthesise ADCs.

Drug attachment can be also achieved through formation of a mixed disulfide bond at the engineered cysteine.^{75,76} The ADCs synthesised using this method are stable in plasma, as the antibody shields the disulfide bond from glutathione and other thiols present in plasma that may potentially reduce the linkage. The disulfide bioconjugation can be achieved by either treating the antibody with a drug molecule bearing an activated thiol group, or by first activating the antibody's cysteine residues with 2,2'-dithiobis(5-nitropyridine), followed by reaction with a thiol-bearing drug molecule (**Figure 9f**).

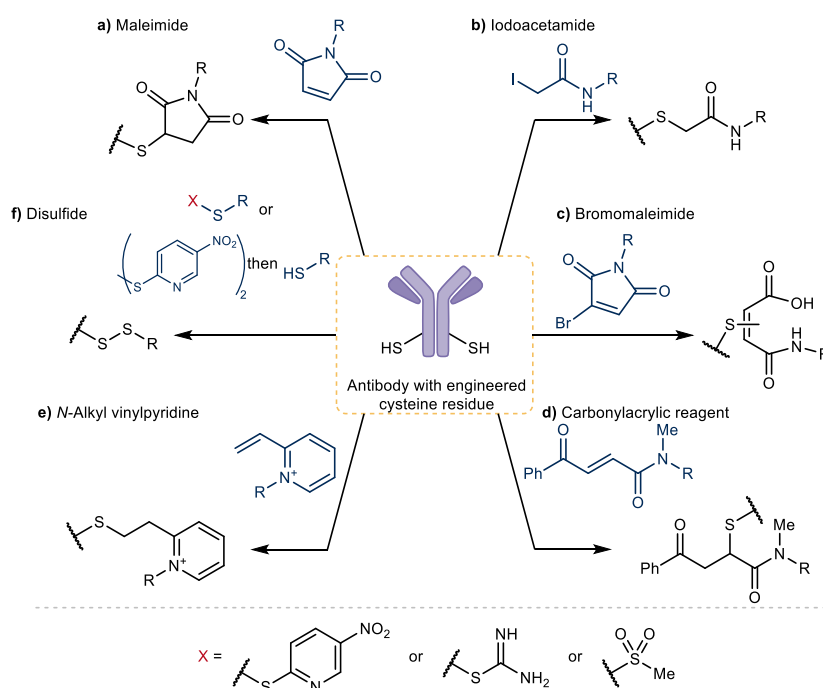


Figure 9. Strategies to functionalise cysteine-engineered antibodies. R = drug or functional moiety.

1.5.1.5. Enzymatic modification and non-canonical amino acids

Enzymes have been used to achieve site-selective antibody modification due to their high specificity and mild reaction conditions. Microbial transglutaminases catalyse the formation of an amide bond between a sequence-specific glutamine residue and an amine reagent.⁷⁷ In terms of native antibody modification, heavy chain glutamine 295 is commonly targeted for modification. First, the antibody is treated with peptide:*N*-glycosidase F which removes the glycan chains attached on asparagine 297 and makes glutamine 295 more accessible. Then, the deglycosylated antibody can be reacted with a payload-bearing amine reagent and microbial transglutaminase, which functionalises glutamine 295 (**Figure 10**).^{49,77}

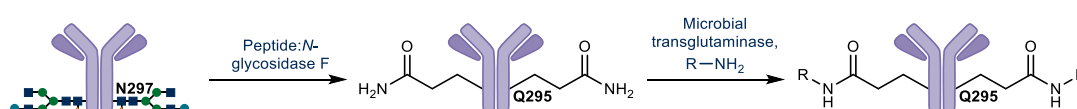


Figure 10. Microbial transglutaminase-mediated modification of an antibody. R = drug or functional moiety.

Another method to achieve site-specific modification involves protein engineering to incorporate non-native amino acids which bear bioorthogonal functional groups. Ketones (**Figure 11a**),⁷⁸ cyclopropenes (**Figure 11b**),⁷⁹ and azides (**Figure 11c**)⁸⁰ have been successfully engineered into antibodies, and can be modified using oxime ligation, inverse electron-demand Diels-Alder (IEDDA), and strain-promoted alkyne-azide cycloaddition (SPAAC), respectively. Similarly, the atypical selenocysteine amino acid can also be incorporated, and its highly nucleophilic selenol group was modified with iodoacetamide reagents (**Figure 11d**).⁸¹ The use of unnatural amino acids allows the synthesis of highly homogeneous bioconjugates through robust bioorthogonal ligation reactions.

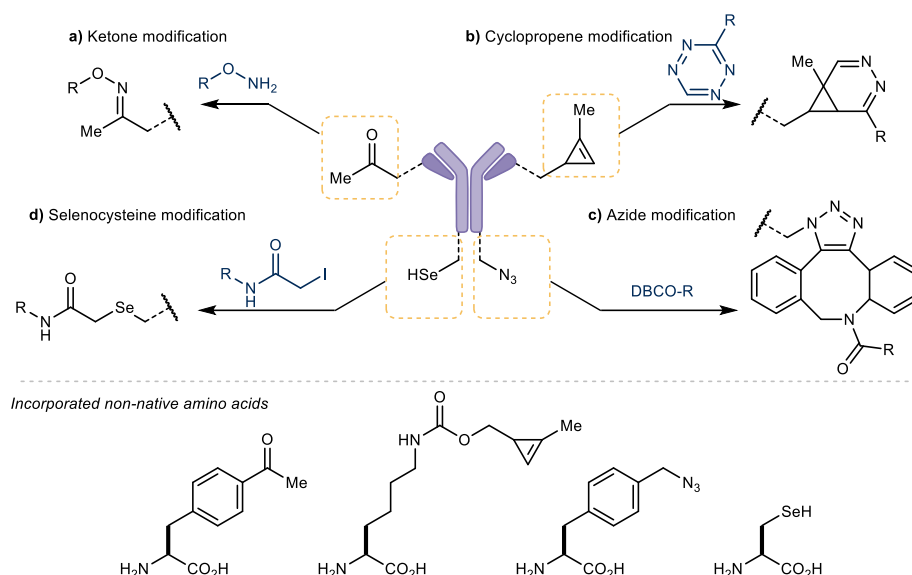


Figure 11. Bioorthogonal functional handles which allow downstream modification can be installed onto antibodies *via* the incorporation of non-native amino acids. DBCO = dibenzocyclooctyne. R = drug or functional moiety.

1.5.1.6. Cysteine functionalisation in protein substrates

Apart from the methodologies for cysteine modification for antibodies, a variety of reagents have been developed to modify cysteine residues in proteins.⁸² To achieve chemoselective modification of the soft cysteine nucleophiles over the harder lysines and *N*-termini, many of these reagents act as soft electrophiles. For example, conjugate addition to the cyclopropenyl ketone can modify cysteine residues extremely fast, which can be attributed to the release of the highly strained cyclopropene moiety upon conjugation (**Figure 12a**).⁸³ The unfavourable re-formation of the cyclopropene moiety makes the bioconjugate stable towards elimination. Similarly, cyanoethyl benzenes (**Figure 12b**),⁸⁴ azabicyclic vinyl sulfones (**Figure 12c**),⁸⁵ and a family of α,β -unsaturated carbonyls (**Figure 12d**)⁸⁶ have been developed for cysteine modification.

In some instances, traceless linkers can be useful for *in vitro* and *in vivo* applications. These linkers are stable under physiologically relevant conditions but allow the detachment of the linker-payload to regenerate the unmodified protein under defined conditions.⁸⁷ For example, 5-methylene pyrrolones (**Figure 12e**)⁸⁸ and 4-acetoxy cyclopentenones (**Figure 12f**)⁸⁹ are examples of traceless linkers; the unmodified protein can be reformed from the bioconjugate by the treatment with glutathione or β -mercaptoethanol, respectively. It is worth highlighting

that the bioconjugate formed using the 4-acetoxy cyclopentenone linker has increased stability towards β -elimination, because of the antiaromatic property of the resulting cyclopentadione.

Although many methodologies exploit the inherent nucleophilicity of cysteine residues, there are examples which achieve bioconjugation without the use of electrophilic linkers. A notable example is the umpolung reactivity of cysteine residues which can be revealed with a bis-alkylating agent (**Figure 12g**). The resulting dehydroalanine residue can be treated with thiol reagents to return the modified protein.⁹⁰ Recently, a metal-mediated cross coupling methodology has been reported which involves the use of an aryl palladium (II) salt (**Figure 12h**).^{91,92}

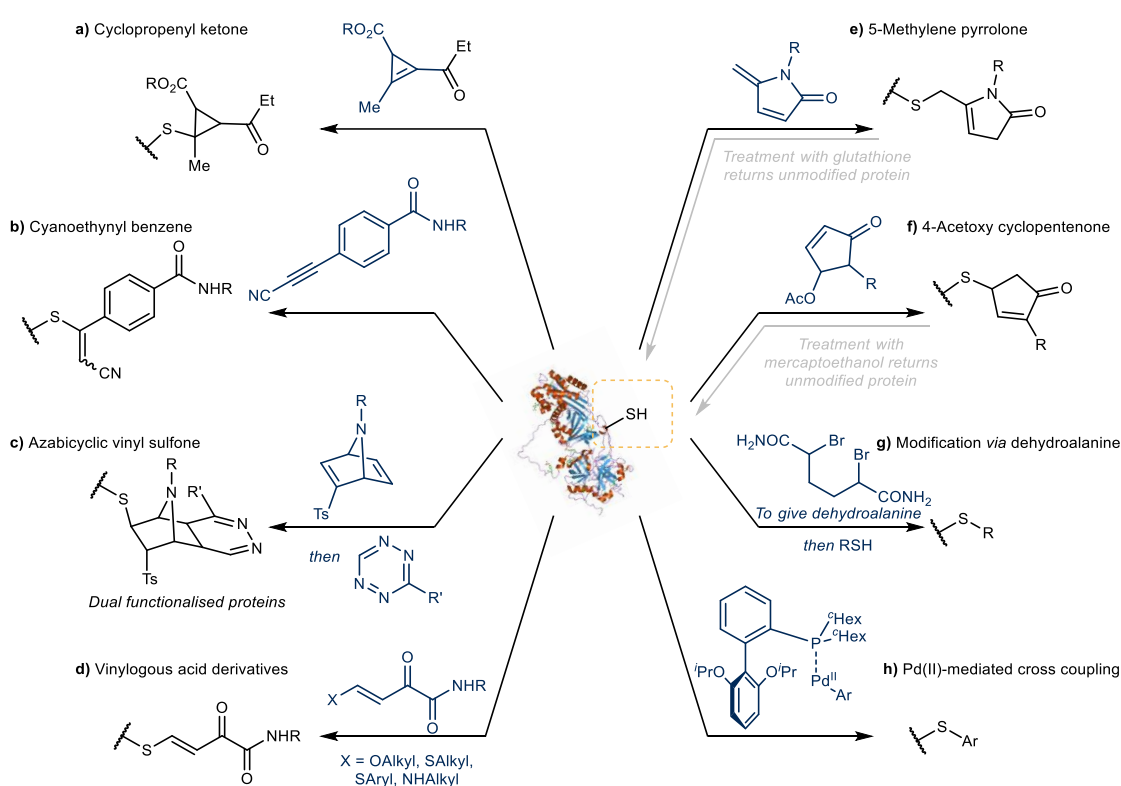


Figure 12. Reagents developed for the modification of cysteine residues in proteins. R and R' = drug or functional moiety.

1.5.2. Linker-drug attachment

The second role of the linker is drug attachment. The linker must provide a secure connection between the drug and the antibody while allowing the release of an active cytotoxic group inside the target cell. Broadly, the linker-drug attachment can be classed as non-cleavable or cleavable.⁹³

1.5.2.1. Non-cleavable linkers

Non-cleavable linkers lack a chemical trigger to release payloads. Upon ADC internalisation and lysosomal protein degradation, the payload molecule with an amino acid appendage used for bioconjugation will still be present. One benefit of non-cleavable linkers is their improved serum stability, since the presence of a drug release group increases the possibility of premature drug release.⁹⁴ However, this approach is only effective for payloads which retain their cytotoxic activity even with the amino acid group attached to their structure. Furthermore, due to the zwitterionic nature of the amino acid, the released cytotoxins are unable to diffuse into and kill neighbouring non-antigen expressing cancer cells. For this reason, non-cleavable linkers are only effective for tumour types with high antigen expression.^{11,93,94}

Despite these limitations, non-cleavable linkers are found in the FDA-approved ADCs Kadcyła[®] and Blenrep[®]. Kadcyła[®] contains a succinimidyl-4-(*N*-maleimidomethyl) cyclohexane-1-carboxylate group which attaches the thiol group of the mertansine payload to a lysine residue of an antibody (**Figure 13a**),⁹⁵ whereas Belnrep[®] uses an maleimidocaproyl linker-MMAF linker-payload for cysteine bioconjugation (**Figure 13b**).⁹⁶ Therefore, the released payloads for Kadcyła[®] and Belenrep[®] will have a lysine and cysteine amino acid appendage, respectively.

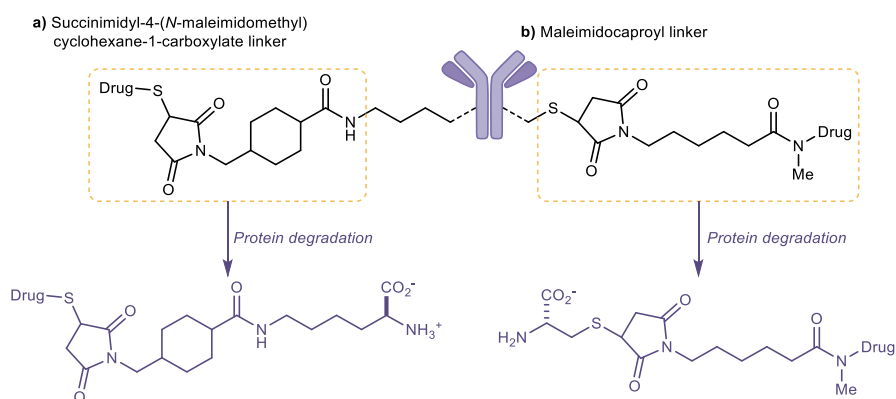


Figure 13. Non-cleavable linkers found in Kadcyła[®] and Blenrep[®].

1.5.2.2. Cleavable linkers

Cleavable linkers have a built-in mechanism which releases the unmodified cytotoxin under specific conditions. The use of cleavable linkers is generally preferred to non-cleavable linkers, as the release of the unmodified drug without an amino acid appendage gives a more predictable cytotoxicity. Most commonly, the acidic condition of endosomes or lysosomes; the reducing environment of cytosol; or hydrolytic enzymes found in the lysosomes are exploited to trigger the drug release.⁹³

Acid cleavable linkers

Acid cleavable linkers exploit the acidity of endosomes (pH 5.5 to 6.2) and lysosomes (pH 4.5 to 5.0) to allow drug release, while maintaining high stability in plasma (pH 7.3). For example, the linker in Mylotarg[®] and Besponsa[®] contains an *N*-acyl hydrazone moiety that is hydrolysed to a ketone and a drug-bearing hydrazine group that is cleaved further (**Figure 14a**).^{19,97} Stability studies *in vivo* revealed the hydrazone group in Besponsa[®] to be hydrolysed in circulation at a rate of 1.5% to 2% per day, suggesting linker instability even at neutral pH.⁹³

The carbonate moiety has also been used in acid-triggered drug release (**Figure 14b**). In Trodelvy[®], a carbonate group connects the linker to the tertiary alcohol found in SN-38. The serum half-life of the carbonate linkage was found to be only 21.6 h, yet again demonstrating the difficulty of balancing stability in circulation with acid-triggered drug release.^{98,99}

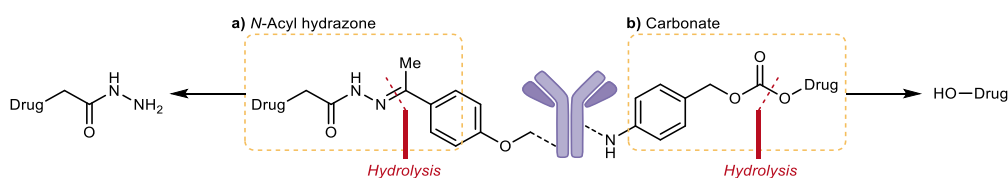


Figure 14. Acid cleavable linkers used in ADC development.

Reducible disulfides

Disulfide bonds have also been used in drug release, capitalising on their stability under physiological pH and facile cleavage with thiol compounds. In human plasma, the most dominant thiol species is the cysteine residue in human serum albumin which is found at concentrations of ~400 μ M. However, since this thiol group is partially solvent-exposed, it has limited reactivity as a disulfide reducing agent. In contrast to the low levels of reactive thiol in plasma, the cytosol contains a high level of glutathione (1 to 10 mM), which can be used to

trigger drug release. It is worth noting that tumour cells can produce higher levels of glutathione compared to healthy cells, facilitating drug release of disulfide-linked drugs.⁷⁵ Examples of disulfide groups are found in Mylotarg[®] and Besponsa[®]. After the acid-catalysed hydrazone hydrolysis described in the previous section, the disulfide bond is cleaved by glutathione to release a calicheamicin molecule (**Figure 15**).^{19,97}

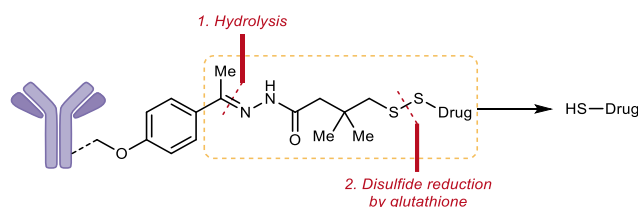


Figure 15. Release of *N*-acyl calicheamicin payloads in Mylotarg[®] and Besponsa[®]. First the hydrazone group is hydrolysed, then the disulfide is reduced by glutathione to release the payload.

Enzyme cleavable linkers

Upon internalisation, ADCs are typically trafficked to the lysosome where high concentrations of hydrolytic enzymes are found. Since these enzymes can be overexpressed in tumour cells, enzyme cleavable linkers exploit them for drug release.^{93,100}

Drug release mediated by cathepsin enzymes is the most widely used enzyme cleavable linker. Indeed, they are found in six of the ten FDA-approved ADCs. The most common groups used for cathepsin-mediated drug release are the valine-citruline (**Figure 16a**) and valine-alanine dipeptides (**Figure 16b**).^{101,102} The enzyme recognises the dipeptide sequence and cleaves the *C*-terminus amide. To ensure general cleavage irrespective of the payload's steric bulk, a *para*-aminobenzyl carbamate immolation group is used as a spacer between the dipeptide and the payload.¹⁰³ Although valine-citruline gives faster enzymolysis, the less hydrophobic valine-alanine group is effective when used in conjunction with the highly hydrophobic PDB dimer payload to prevent ADC aggregation.^{102,104} More recently, the glycine-glycine-phenylalanine-glycine tetrapeptide was used to release the alcohol payload DXd in Enhertu[®] (**Figure 16c**). Owing to the high hydrophilicity of the linker-payload in Enhertu[®], the trastuzumab antibody was successfully modified with eight linker-payloads.⁴⁴

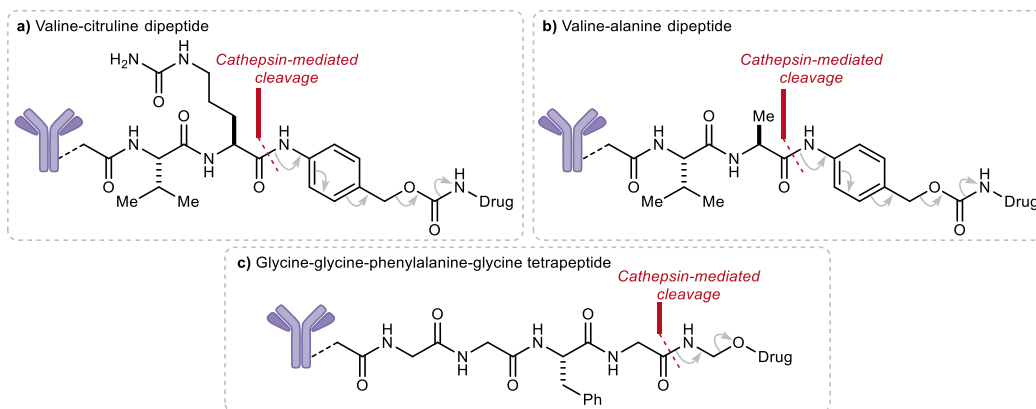


Figure 16. Cathepsin cleavable linkers to release amine and alcohol cytotoxins.

Despite the success of cathepsin cleavable linkers, their hydrophobicity limits their utility. To address this, hydrophilic enzyme cleavable linkers have been developed. Payloads have been released successfully from ADCs *via* enzymatic cleavage by β -galactosidases (**Figure 17a**),¹⁰⁵ β -glucuronidases (**Figure 17b**),^{51,106} phosphatases (**Figure 17c**),^{107,108} and arylsulfatases (**Figure 17d**).^{109,110}

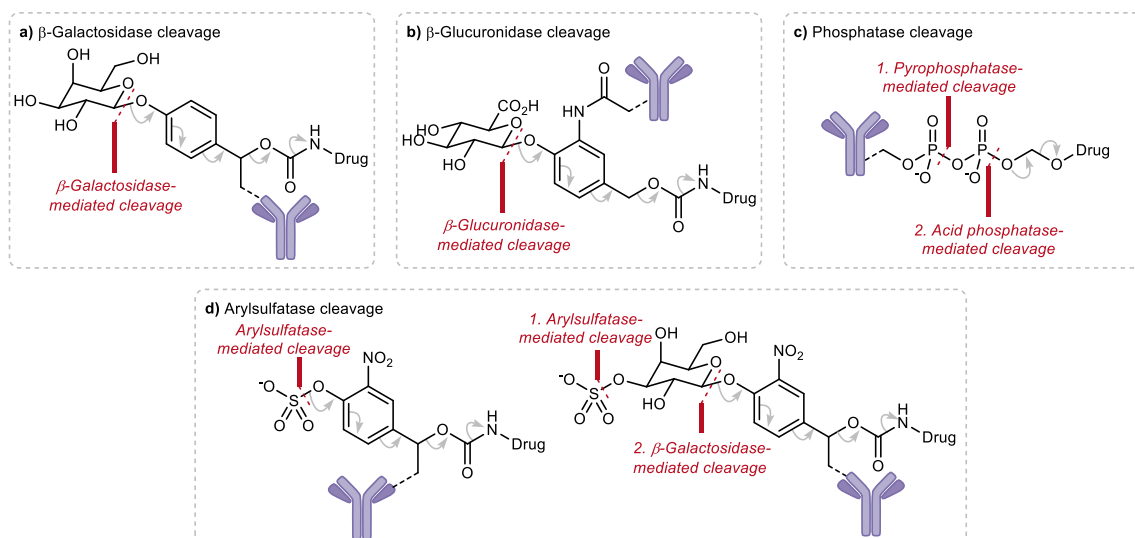


Figure 17. ADC payload release by β -galactosidases, β -glucuronidases, phosphatases, and arylsulfatases. These linkers are endowed with improved hydrophilicity, which reduces antibody aggregation.

Chapter 2. Rapid and robust cysteine bioconjugation with vinylheteroarenes

2.1. Introduction

The chemical modification of proteins has a crucial role in enabling the interrogation of biology and providing improved medicines.^{111,112} However, the controlled modification of these highly complex macromolecules remains challenging. To preserve the native structure and function of metastable proteins, mild reaction conditions are required. Furthermore, site-selective modification is often desirable, meaning that the transformation must be chemo- and regioselective for a target residue.⁵⁴ Cysteine modification is particularly attractive due to its high nucleophilicity under biocompatible conditions, solvent accessibility, and low natural abundance.⁸²

Work within the Spring Group led to the development of divinylheteroarene linkers for cysteine cross-linking^{69,93,110,113–116} (**Figure 18**). These linkers reacted selectively with cysteine residues within proteins and peptides, and the resulting bioconjugates showed excellent stability.¹¹³ Although initial studies focused on divinylpyrimidine linkers,¹¹³ this methodology was expanded with divinyltriazine linkers^{69,114} which showed faster bioconjugation kinetics. Using these divinylheteroarene linkers, the Fab region of trastuzumab and several therapeutic peptides were modified. Furthermore, homogenous ADCs were produced by reduction of the four interchain disulfide bonds in the anti-HER2 antibody trastuzumab, followed by cysteine rebridging with these linkers.

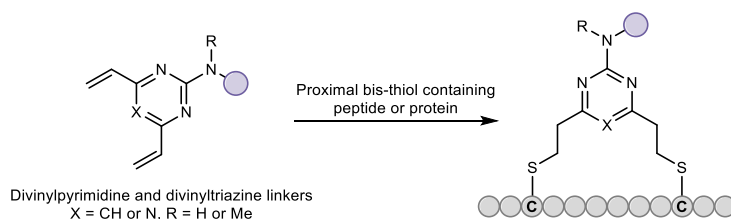


Figure 18. Divinylpyrimidine and divinyltriazine reagents effectively cross-link a bis-thiol containing peptides and proteins.^{69,93,110,113–116}

2.2. Project aims and overview

The aim of this project was to develop monovinylheteroarene linkers for the efficient and selective modification of cysteine residues. While stable and functional modification of proteins or peptides was achieved with the divinylpyrimidine and divinyltriazine reagents, they require two proximal cysteine residues are present in the protein of interest. Thus, monovinylheteroarene reagents for single-cysteine modification would expand the scope and generality of this scaffold, allowing the modification of cysteine residues regardless of spatial arrangement (**Figure 19**).

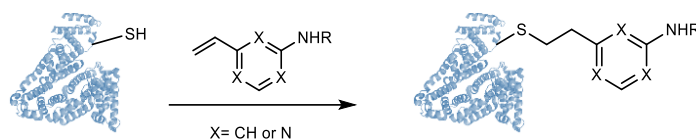


Figure 19. Monovinylheteroarene linkers for the general modification of cysteine residues.

The monovinylheteroarene linkers developed in this work will be required to satisfy a number of requirements:

- The linker should show chemoselective and rapid reactivity towards cysteine residues.
- The linker should allow the bioconjugation of a wide range of protein substrates.
- The linker should tolerate the attachment of a range of biologically-relevant payloads.
- The modification of the protein with the linker should not affect the protein's structure or function.
- The bioconjugates should be stable in human plasma for >1 week.

Initial investigations focused on determining the reactivity and stability profiles for a series of vinylheteroarene linkers. Studies on small molecule and protein substrates allowed the identification of an optimum vinylheteroarene scaffold for selective cysteine modification. Using this lead linker, a number of protein substrates were modified with various functionalities, culminating in the synthesis of a homogeneous, stable, and biologically active antibody-drug conjugate (ADC).¹¹⁷

2.3. Design of linker

To commence investigations, it was hypothesised alteration of heteroarene ring electronics would greatly affect the reactivity of the vinyl group, with increasing electron deficiency proposed to increase the rate of thiol addition. However, increased electrophilicity may also cause increased reactivity towards other proteinogenic nucleophiles (e.g., lysine or *N*-terminus), or lead to increased rates of deconjugation *via* an elimination reaction. Thus, to determine the optimal scaffold for cysteine modification, a panel of monovinylheteroarenes with varying heterocycle electron deficiencies was studied (**Figure 20**).

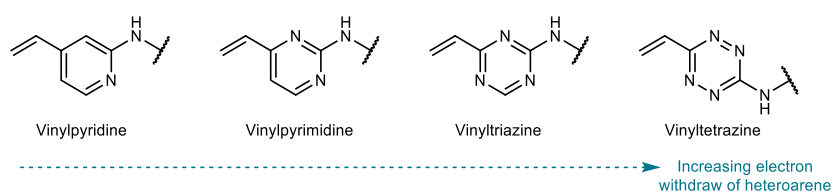
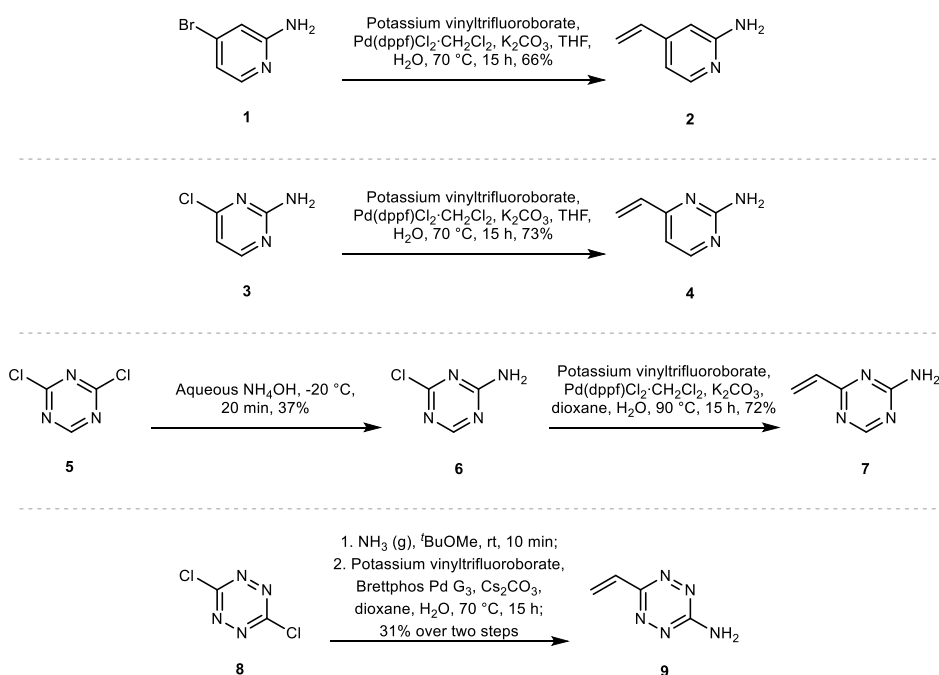


Figure 20. Monovinylheteroarenes investigated in this study.

2.4. Synthesis of model vinylheteroarene linkers

To evaluate the reactivity and stability of the various monovinylheteroarenes (hereafter referred to as vinylheteroarenes), model linker systems were synthesised (**Scheme 1**). Vinylpyridine **2** and vinylpyrimidine **4** were synthesised in good yields from commercially available halides **1** and **3**, respectively, *via* a Suzuki-Miyaura coupling reaction with potassium vinyltrifluoroborate. Vinyltriazine **7** was synthesised from dichlorotriazine **5** *via* monoamination with aqueous ammonium hydroxide which afforded amine **6** in 37% yield, followed by Suzuki-Miyaura coupling which gave **7** in good yield. Similarly, vinyltetrazine **9** was synthesised from dichlorotetrazine **8** (starting material prepared by A. J. Counsell) by treatment with ammonia gas¹¹⁸ followed by cross coupling¹¹⁹ to give **9** in moderate yield.



Scheme 1. Synthesis of model vinylheteroarene linkers **2**, **4**, **7**, and **9**.

2.5. Reactivity studies of vinylheteroarene linkers

Successful cysteine modification reagents will have rapid reactivity towards thiols, whilst having low reactivity towards other nucleophilic residues, e.g. lysine residues and *N*-termini. Thus, it was imperative to quantify the reactivity of the linkers towards these biological nucleophiles by determining the second order rate constants (k_2).

To successfully monitor these rapid reactions, a method of *in situ* monitoring of reaction mixtures using ¹H NMR spectroscopy was required. In an NMR tube, linkers **2**, **4**, **7**, and **9** (10 mM) were incubated with one equivalent of cysteine, lysine, and alanine (modelling the *N*-terminus), and the reaction progress was monitored *via* ¹H NMR spectroscopy. The linker vinyl peaks were integrated to determine the concentration of remaining starting material allowing the calculation of the second order rate constants from the following equations. The use of equimolar linker and nucleophile were used which simplified the calculation of the rate constants (**Equation 1**).

Equation 1. Determination of second order rate constant for equimolecular reactions. In these equations, k_2 refers to the second order rate constant, t is the time since start of reaction, $[\text{Linker}]_t$ and $[\text{Linker}]_{t=0}$ is the linker concentration at time t and start of reaction respectively, and $[\text{Amino acid}]$ is the amino acid concentration.

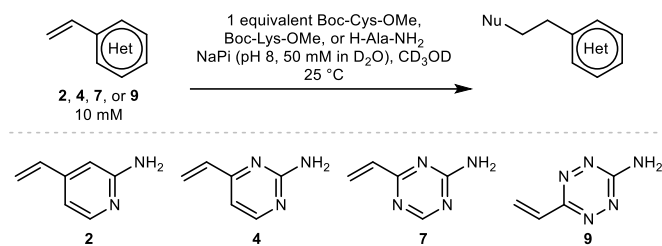
$$\begin{aligned} & \frac{d[\text{Linker}]}{dt} = -k_2[\text{Linker}][\text{Amino acid}] \\ \text{When } [\text{Linker}] &= [\text{Amino acid}], \quad \frac{d[\text{Linker}]}{dt} = -k_2[\text{Linker}]^2 \\ \text{Integration over time gives } & \frac{1}{[\text{Linker}]_t} = k_2t + \frac{1}{[\text{Linker}]_{t=0}} \end{aligned}$$

Thus, the second order rate constant k_2 can be determined by plotting $y = \frac{1}{[\text{Linker}]_t}$ versus $x = t$; the gradient is equal to k_2 .

2.5.1. Vinylheteroarene reactivity towards thiols

First, the second order rate constants with a model cysteine residue were established. Studies were conducted by treating the four vinylheteroarene linkers with Boc-Cys-OMe, a model substrate for protein cysteines. To model bioconjugation conditions, a mixture of sodium phosphate (NaPi, pH 8, 50 mM in D₂O) and CD₃OD was used. Kinetic analysis revealed that vinylpyrimidine **4** and vinyltriazine **7** were most reactive, displaying second order rate constants of 0.375 M⁻¹ s⁻¹ and 3.10 M⁻¹ s⁻¹, respectively (**Table 1** and **Figure 21**). For comparison, traceless Staudinger ligations and strain-promoted alkyne-azide cycloadditions (SPAAC) have rate constants of 10⁻³ M⁻¹ s⁻¹ and 10⁻² M⁻¹ s⁻¹, respectively, and are widely used for protein modification.¹²⁰ With this in mind, the reaction on vinylpyrimidine and vinyltriazine scaffolds was deemed sufficiently fast for cysteine modification.

Table 1. The second order rate constants for the reaction of vinylpyridine **2**, vinylpyrimidine **4**, vinyltriazine **7**, and vinyltetrazine **9** with Boc-Cys-OMe, Boc-Lys-OMe or H-Ala-NH₂. Average of two replicates; error bars represent standard deviation of the mean. †No reaction observed. ‡Significant side reaction observed.



Linker	Second order rate constants (k_2), $\times 10^{-3} \text{ M}^{-1} \cdot \text{s}^{-1}$		
	Boc-Cys-OMe	Boc-Lys-OMe	H-Ala-NH ₂
Vinylpyridine 2	4.91 ± 0.01	0 †	0 †
Vinylpyrimidine 4	375 ± 30	0 †	0 †
Vinyltriazine 7	3100 ± 30	0.323 ± 0.006	0.944 ± 0.090
Vinyltetrazine 9	n/a ‡	-	-

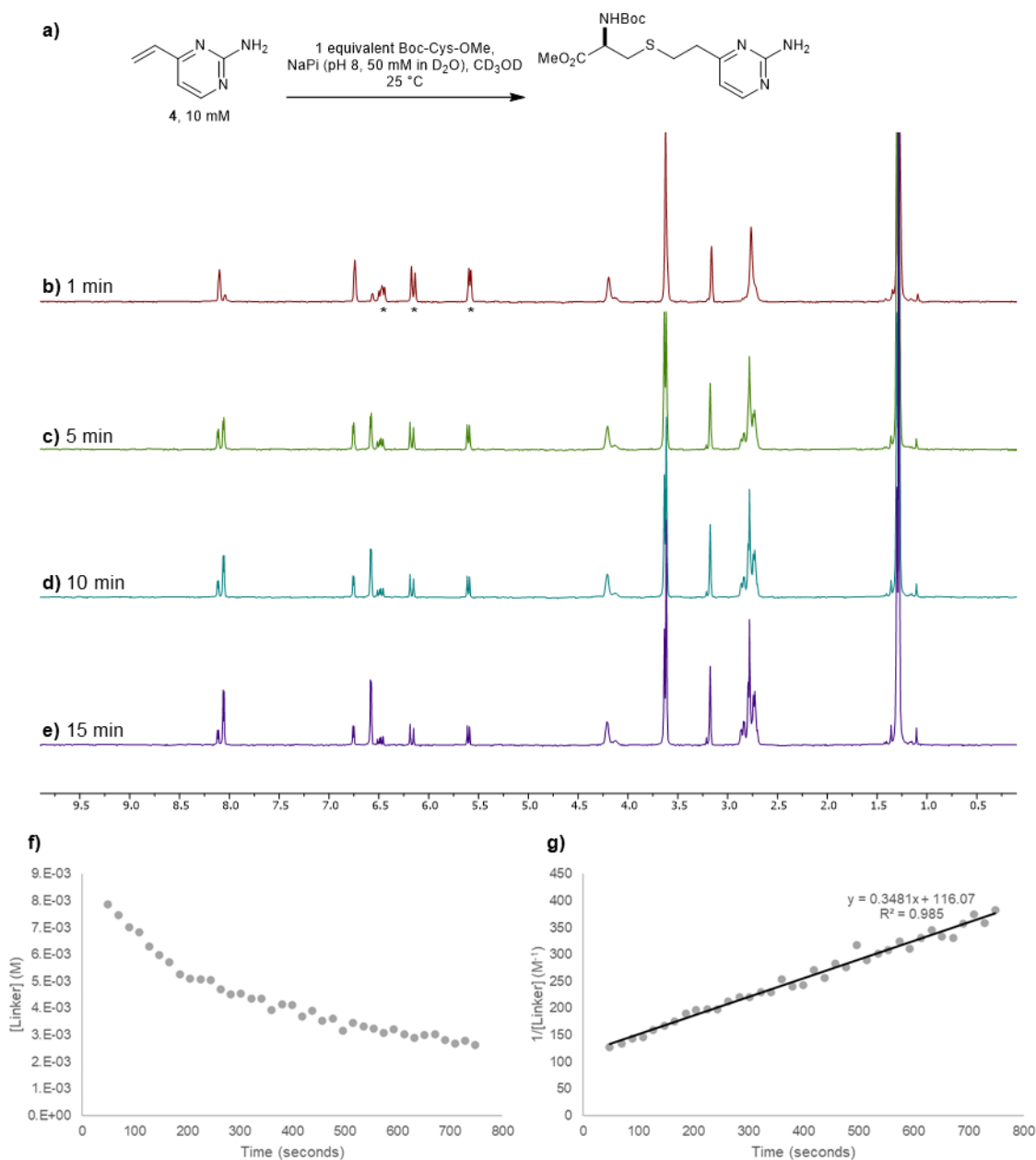


Figure 21. Representative workflow for the determination of second order rate constants. **a)** Vinylpyrimidine **4** is treated with Boc-Cys-OMe. **b) to e)** Reaction monitoring using ^1H NMR spectroscopy. The vinyl protons of **4** are marked with an asterisk. **f)** Graph of $y = \text{linker concentration}$ versus $x = \text{time}$. **g)** Graph of $y = 1/(\text{linker concentration})$ versus $x = \text{time}$. The gradient is equal to the second order rate constant.

Given the excellent reaction rates observed for vinylpyrimidine **4** and vinyltriazine **7**, the cysteine reactivity of the vinylpyridine and vinyltetrazine scaffold was explored. Vinylpyridine **2** reactivity with Boc-Cys-OMe was significantly slower with a rate constant of $4.91 \cdot 10^{-3} \text{ M}^{-1} \text{ s}^{-1}$ which was considered too low for the effective bioconjugation for wide range of protein substrates. Surprisingly, no reaction with the vinyl group was observed upon

treatment of vinyltetrazine **9** with Boc-Cys-OMe. Instead, a second set of vinyl peaks were observed in the ^1H NMR spectra (**Figure 22a to 22d**), suggestive of direct nucleophilic attack on the tetrazine ring (**Figure 22e**) – a previously documented type of reactivity.^{121,122} As such, vinylpyrimidines and vinyltetrazines were discounted from further studies.

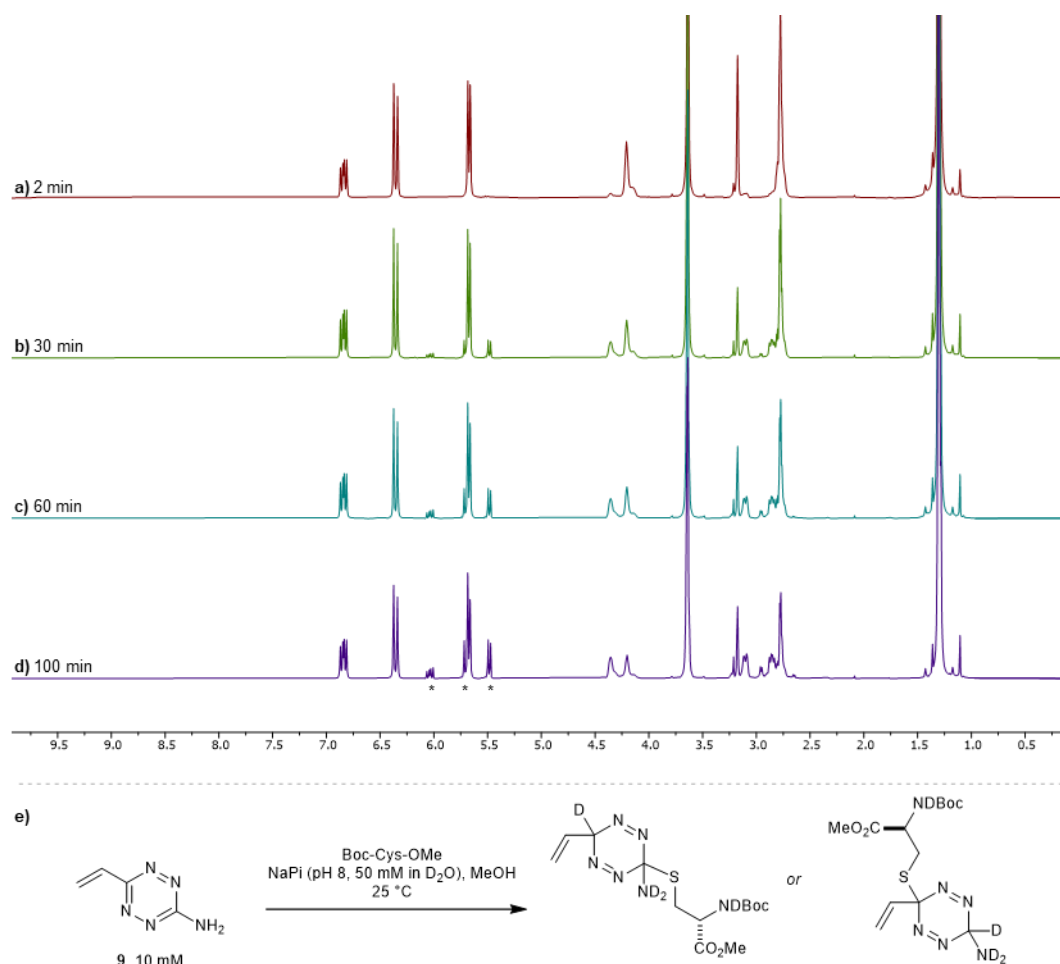


Figure 22. a) to d) ^1H NMR spectra of the reaction of vinyltetrazine **9** with Boc-Cys-OMe in a mixture of CD_3OD and NaPi (pH 8, 50 mM in D_2O). Rather than the depletion of vinyl peaks (which indicate conjugate addition), a new set of vinyl peaks arise over time at 6.04 ppm (dd, $J = 18.0, 11.3$ Hz), 5.70 (overlapping) and 5.48 (dd, $J = 11.3, 1.6$ Hz). These peaks are marked with an asterisk. e) Proposed reaction products.

2.5.2. Vinylheteroarene reactivity towards amines

Attention turned towards ascertaining the reactivity for other nucleophilic groups. Thus, to aid comparison, vinylheteroarenes **2**, **4** and **7** were incubated with either Boc-Lys-OMe or H-Ala- NH_2 (representative of the protein *N*-terminus) under the same conditions used in the reactions with Boc-Cys-OMe [i.e. 10 mM vinylheteroarene, 10 mM amino acid, NaPi (pH 8, 50 mM in D_2O), CD_3OD]. Pleasingly, no reactivity was observed between vinylpyridine **2** and

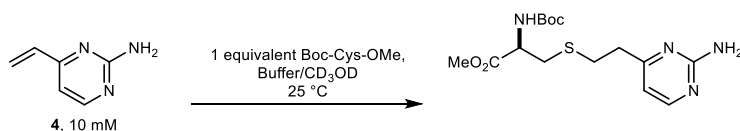
vinylpyrimidine **4** with Boc-Lys-OMe or H-Ala-NH₂. Gratifyingly, the minimal reactivity that was observed between vinyltriazine **7** with the *N*-nucleophiles translates to >3200-fold selectivity for cysteine. This represents a significant improvement compared to maleimides – the state-of-the-art linker for cysteine modification – which are known to react with both cysteine and lysine residues^{123–125} (**Table 1**).

2.5.3. Effect of buffer on vinylheteroarene-cysteine reactivity

To explore the effect of varying buffer systems on the conjugation reaction rates, further investigations were conducted using vinylpyrimidine **4** as a model substrate (**Table 2**). To explore the effect of buffer pH on reactivity, vinylpyrimidine **4** reacted with Boc-Cys-OMe over a range of biologically relevant pHs. Second order rate constants of 0.375 M⁻¹ s⁻¹, 0.510 M⁻¹ s⁻¹, 0.636 M⁻¹ s⁻¹, and 0.851 M⁻¹ s⁻¹ were observed when reactions were conducted at pH 8, 7, 6, and 5, respectively (Entries 1, 2, 3, and 4). These results suggest bioconjugation reactions are tolerant of a wide range of buffer pH and reaction conditions can be tailored to suit the specific protein or biomolecule of interest.

To study the effect of buffer concentration on reaction kinetics, the reaction was conducted using different reaction media. A reduction of the second order rate constants was observed when more dilute NaPi (pH 8; 50 mM, 25 mM, or 10 mM) was used as the reaction medium (Entries 1, 5, and 6). These data suggest that vinylheteroarenes react with cysteines *via* general base catalysis.

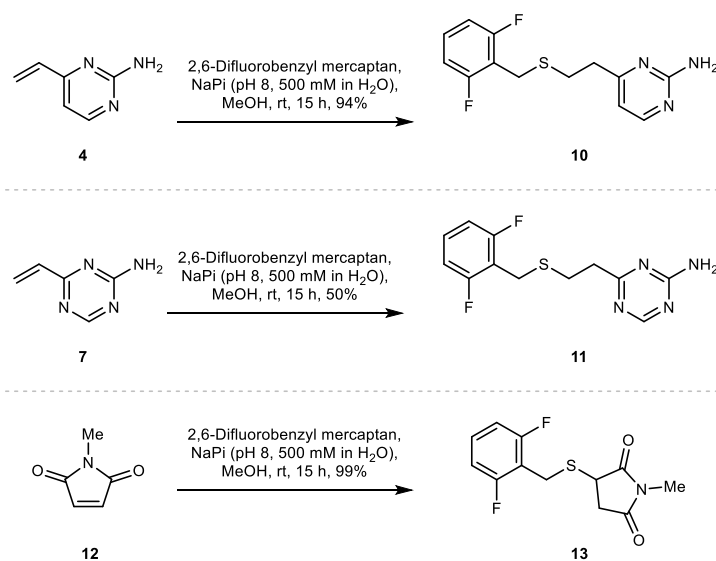
Table 2. The effect of buffer concentration and pH on the conjugate addition of Boc-Cys-OMe with vinylpyrimidine **4**.



Entry	Aqueous buffer	Second order rate constant (k_2), $\times 10^{-3} \text{ M}^{-1} \cdot \text{s}^{-1}$
1	NaPi (pH 8, 50 mM in D ₂ O)	375 ± 30
2	NaPi (pH 7, 50 mM in D ₂ O)	510 ± 1
3	NaPi (pH 6, 50 mM in D ₂ O)	636 ± 10
4	CD ₃ CO ₂ Na (pH 5, 50 mM in D ₂ O)	851 ± 7
5	NaPi (pH 8, 25 mM in D ₂ O)	330 ± 6
6	NaPi (pH 8, 10 mM in D ₂ O)	213 ± 2

2.6. Stability of vinylheteroarene-thiol conjugates

Given the favourable reaction rates and cysteine selectivity observed for both vinylpyrimidine and vinyltriazine scaffolds, attention turned towards determining the stability of the corresponding linker-thiol conjugates. It was proposed that vinylheteroarene conjugation to a fluorinated thiol would enable the use of ^{19}F NMR spectroscopy to monitor the rate of conjugate decomposition, given the quantitative nature and high sensitivity of this technique. Thus, conjugates **10**, **11**, and **13** were synthesised by reacting 2,6-difluorobenzyl mercaptan with **4**, **7**, and *N*-methylmaleimide **12**, respectively (**Scheme 2**).



Scheme 2. Synthesis of fluorinated thioethers **10**, **11**, and **13**.

To measure the stability of the linker-thiol conjugates under physiologically relevant conditions, thioethers **10**, **11**, and **13** were incubated in a mixture of NaPi (pH 7.4, 50 mM in H_2O) and MeCN with an excess of 1-thioglycerol at 37 °C (**Figure 23a**). 1-Thioglycerol was added to mimic biological thiols such as glutathione or human serum albumin and would trap any reactive species formed from conjugate decomposition. Integration of ^{19}F NMR peaks of the starting material and comparison with an internal standard (sodium trifluoroacetate) allowed the quantification of remaining starting material. These studies revealed that pyrimidinyl thioether **10** and triazinyl thioether **11** were exceptionally stable over the ten-day monitoring period with <5% decomposition observed (**Figure 23b**, **23c**, and **23e**). In contrast, the maleimide-derived conjugate **13** was unstable under these conditions, with approximately 60% starting material remaining after ten days incubation (**Figure 23d** and **23e**). These results

suggest that both vinyl-pyrimidine and -triazine scaffolds have the desired stability profile required for widespread biotherapeutic development.

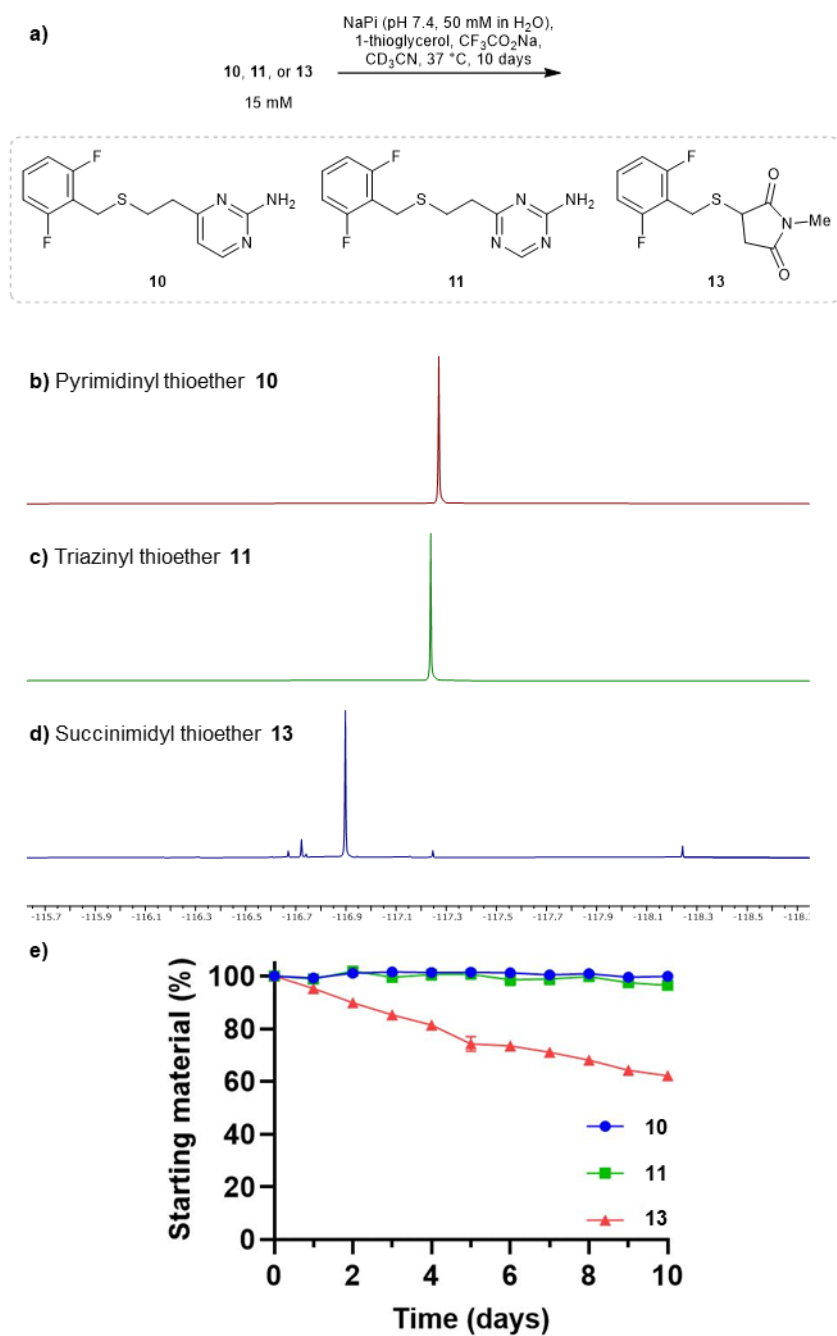


Figure 23. Stability studies for thioethers **10**, **11**, and **13**. **a)** Scheme of stability study. The reaction was monitored daily using ¹⁹F NMR spectroscopy over 10 days. **b)** ¹⁹F NMR spectra of **10** on day 10. **c)** ¹⁹F NMR spectra of **11** on day 10. **d)** ¹⁹F NMR spectra of **13** on day 10. **e)** Remaining starting material over the 10-day study.

2.7. Modification of human serum albumin

Having evaluated the reactivity and stability of the vinylheteroarene scaffolds in small molecule assays, investigating focused on determining if these favourable results could be translated onto cysteine-containing proteins. Human serum albumin (HSA) is the most abundant protein found in plasma, which has also been utilised as a biomacromolecular delivery system in protein-drug conjugates.¹²⁶ Among the 35 cysteines encoded in the HSA peptide sequence, 34 are present as disulfide bonds; one cysteine (Cys-34) is found unpaired.¹²⁶ Thus, HSA was deemed to be an ideal substrate to commence protein modification investigations.

2.7.1. Preparation of unprotected human serum albumin

The purity of commercially available HSA was analysed by protein LCMS, which revealed HSA's cysteine residue to be partially protected as a disulfide – thus existing as a mixture of the free Cys-34 form **14** (66445 Da) and the cysteinylated form **15** (66566 Da; **Figure 24b**). Thus, reduction of the cysteinylated form was required before bioconjugation.

Treatment of the commercially available mixture of **14** and **15** with 2 equivalents dithiothreitol (DTT) gave fully uncapped HSA **14**, as determined by protein LCMS (**Figure 24a** and **24c**). It was imperative to ascertain that the reduction procedure did not reduce any interchain disulfide bonds. Since the over-reduced species will be difficult to observe on LCMS due to the small mass difference between the disulfide and reduced bis-thiol species, an aliquot of the DTT-treated HSA **14** was reacted with a large excess of vinylpyrimidine **4**. If any interchain disulfides had been reduced, these resulting thiols would also be modified. Pleasingly, LCMS revealed that one modification had taken place giving **16**, demonstrating the mild DTT reduction protocol to only reveal the unpaired Cys-34 (**Figure 24d**).

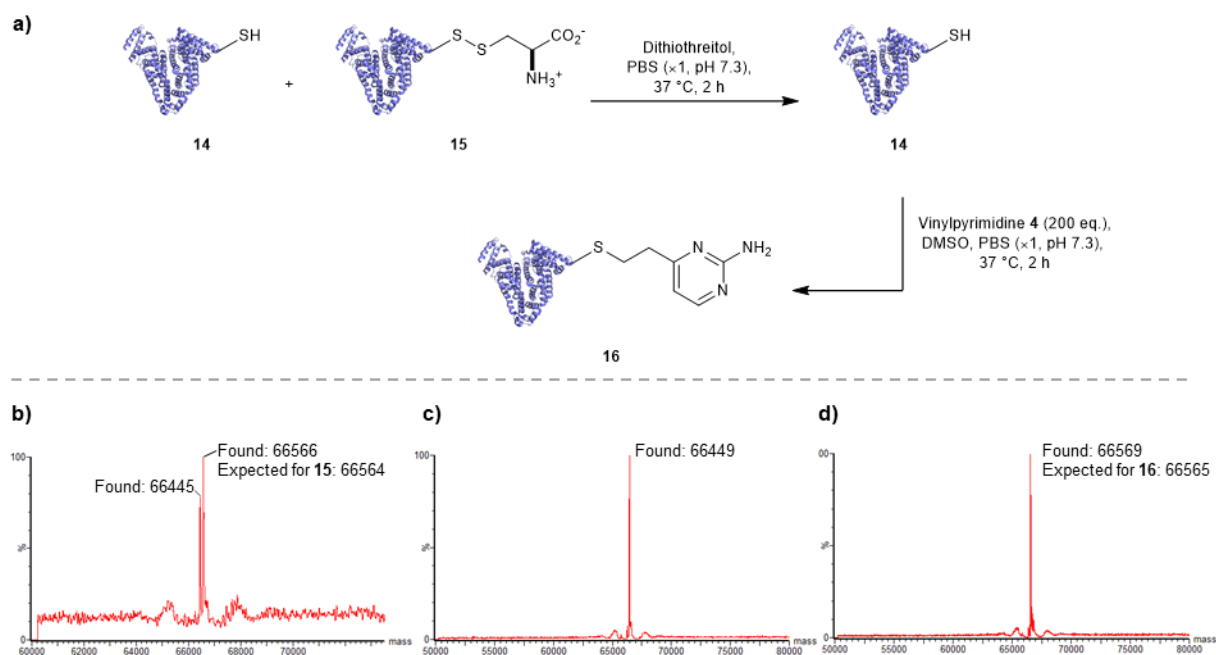


Figure 24. a) The commercially available mixture of uncapped human serum albumin **14** and cysteinylated human serum albumin **15** were reduced to give **14**. b) Deconvoluted mass spectrum of the commercially available mixture of **14** and **15**. c) Deconvoluted mass spectrum of the uncapped species **14**. d) Deconvoluted mass spectrum of **16**, which was synthesised by treating **14** with a large excess of **4**. Only the singly modified species was detected, which demonstrates that only the unpaired thiols were revealed during DTT treatment.

2.7.2. Optimisation of serum albumin modification with vinylpyrimidine reagents

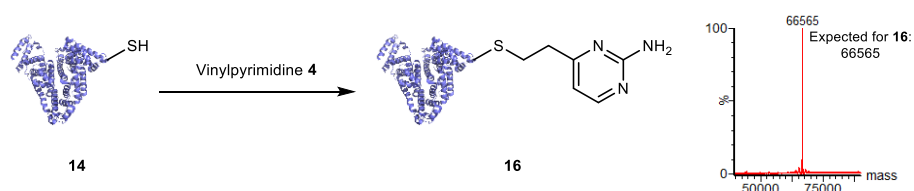
With uncapped HSA **14** in hand, efforts focused on modifying its cysteine residue. To determine the reactivity of model vinylpyrimidine **4** with HSA, extensive screening was carried out. For every reaction condition studied, aliquots of the reaction mixture were taken, and any unreacted linker was quenched with an excess of 1-thioglycerol before analysis by LCMS.

To determine the optimal buffer system for bioconjugation, reactions were conducted in phosphate buffered saline (PBS, $\times 1$) and trisaminomethane (Tris·HCl, pH 8, 50 mM in H₂O). For every entry, Tris·HCl (pH 8, 50 mM in H₂O) gave higher conversion than PBS, which suggests the former reaction medium to be more suitable (**Table 3**).

The effect of protein concentration on bioconjugation rate was also determined. Between the two HSA concentrations tested (10 μ M and 35 μ M), reactions with higher protein concentrations gave greater conversions at each timepoint; a larger excess of linker **4** was required for >95% conversion for the more dilute reactions. From these optimisation studies,

it was determined that the most suitable bioconjugation condition is 20 equivalents of **4** at 37 °C for 2 h in Tris·HCl (pH 8, 50 mM) (Entry 3, **Table 3**).

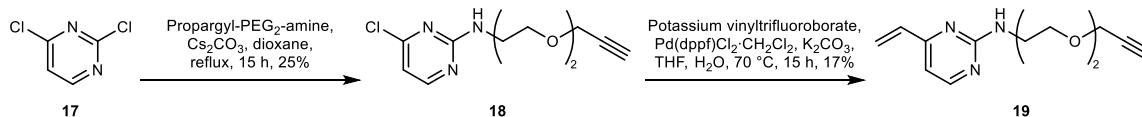
Table 3. Screening of conjugation reactions between HSA **14** and vinylpyrimidine **4**. Reactions were performed at 37 °C in buffer solutions containing 5% DMSO. Aliquots of the reaction mixture were taken and quenched using 1-thioglycerol at the required timepoints prior to LCMS analysis. A hyphen refers to a measurement which was not taken. Percentage conversions are reported to the nearest 5%. Representative deconvoluted mass spectrum for the product **16** is shown.



Entry	[HSA]	Linker eq.	Percentage conversion							
			PBS (×1)				Tris·HCl (pH 8, 50 mM)			
			1 h	2 h	3 h	4 h	1 h	2 h	3 h	4 h
1		5	30	40	50	60	40	60	70	75
2	35 μM	10	45	65	70	75	50	70	75	>95
3		20	65	75	75	80	75	>95	-	-
4	10 μM	20	35	45	55	65	50	70	75	>95
5		50	55	70	70	75	75	>95	-	-

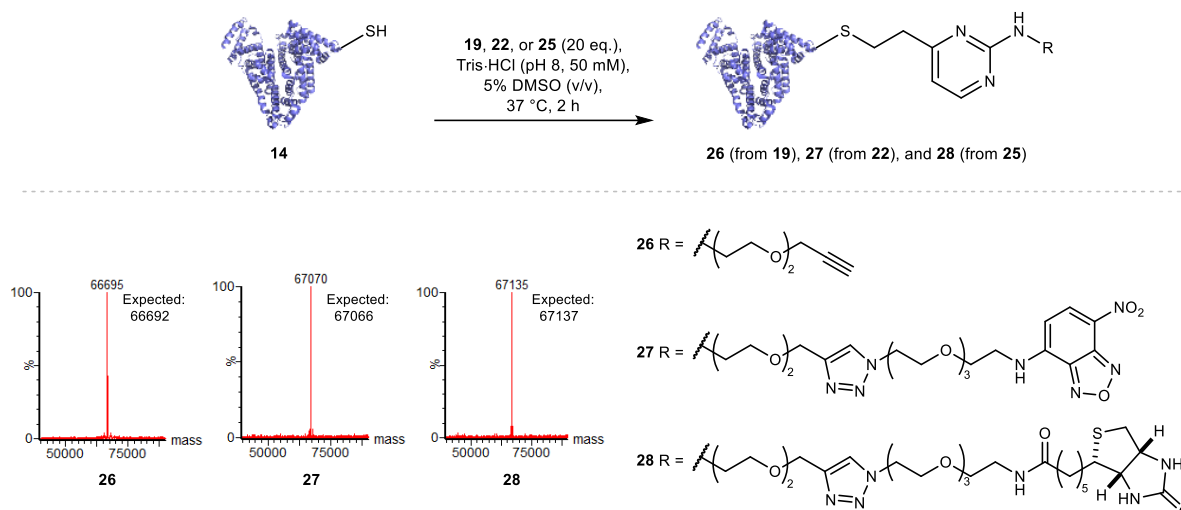
2.7.3. Modification of human serum albumin with functional payloads using vinylpyrimidine reagents

To explore the generality of the vinylpyrimidine reagent, HSA was modified with a range of biologically useful moieties. To achieve this, several vinylpyrimidine reagents were first synthesised. First, dichloropyrimidine **17** was reacted with propargyl-PEG₂-amine to give **18** in 25% yield. The chlorine group within **18** was then reacted under Suzuki-Miyaura conditions to give vinylpyrimidine-alkyne **19** in 17% yield (**Scheme 3**).



Scheme 3. Synthesis of vinylpyrimidine-alkyne **19**.

Fluorophore-bearing linkers have shown great utility for use in microscopy studies.¹¹⁵ To synthesise vinylpyrimidine reagents with a nitrobenzoxadiazole (NBD) fluorophore, NBD

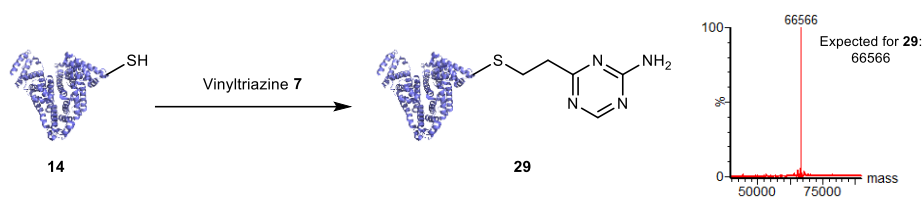


Scheme 6. Synthesis of albumin-alkyne **26**, albumin-NBD **27**, and albumin-biotin **28**.

2.7.4. Optimisation of serum albumin modification with vinyltriazine reagents

The suitability of vinyltriazines for protein modification was also investigated, as initial studies suggested these reagents would yield faster bioconjugation reaction kinetics than vinylpyrimidine linkers. Using a similar method to vinylpyrimidine screening, vinyltriazine **7** was reacted with HSA **14** under different buffer systems and protein concentrations (**Table 4**). The conditions that provided the best balance of short reaction times and low linker excess were treatment of HSA **14** (35 μM) with vinyltriazine **7** (20 molar equivalents) for 1 h at 37 $^{\circ}\text{C}$, in PBS (Entry 5, **Table 4**). This is a great improvement compared to vinylpyrimidine linkers, as >95% conversion to the corresponding bioconjugate was achieved in a shorter reaction time in a milder buffer system.

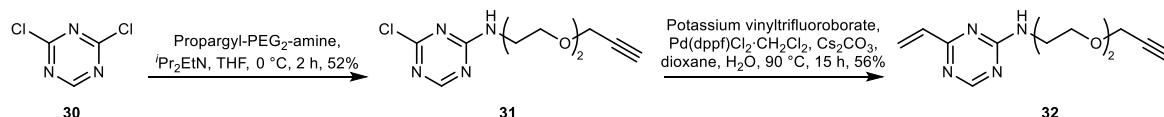
Table 4. Screening of conjugation reactions between HSA **14** and vinyltriazine **7**. Reactions were performed at 37 °C in buffer solutions containing 5% DMSO. Aliquots of the reaction mixture were taken and quenched using 1-thioglycerol at the required timepoints prior to LCMS analysis. A hyphen refers to a measurement which was not taken. Percentage conversion reported to the nearest 5%. Representative deconvoluted mass spectrum for the product **29** is shown.



Entry	[HSA]	Linker eq.	Percentage conversion			
			PBS (×1)		Tris·HCl (pH 8)	
			30 min	1 h	30 min	1 h
1	35 μM	1	<5	25	<5	<5
2		2	<5	40	<5	25
3		5	<5	45	35	45
4		10	35	70	55	70
5		20	50	>95	75	>95
6	10 μM	1	<5	<5	<5	<5
7		2	<5	<5	<5	<5
8		5	<5	<5	<5	25
9		10	<5	25	30	40
10		20	25	35	40	55

2.7.5. Modification of human serum albumin with functional payloads using vinyltriazine reagents

It was hypothesised that a vinyltriazine linker with an alkyne group would aid the synthesis of functional protein conjugates. To this end, dichlorotriazine **30** was reacted with propargyl-PEG₂-amine to give **31** in 52% yield. Subsequent Suzuki coupling gave the required vinyltriazine-alkyne linker **32** in 56% yield (**Scheme 7**).



Scheme 7. Synthesis of vinyltriazine-alkyne **32**.

With **32** in hand, modification of HSA **14** was pursued. Although a range of reaction conditions were attempted, a mixture of unmodified, singly modified and doubly modified protein was

observed upon LCMS analysis (**Figure 25**). This suggests that vinyltriazine **32** is reacting with another nucleophilic site, e.g., the *N*-terminus or lysine residues of HSA **14**. Despite the success of HSA **14** modification with model linker **7**, the lack of selectivity for linker **32** suggests that the vinyltriazine scaffold is unsuitable for general and robust cysteine modification. Thus, the vinylpyrimidine scaffolds were concluded to have the best selectivity and stability for general widespread use in protein modification.

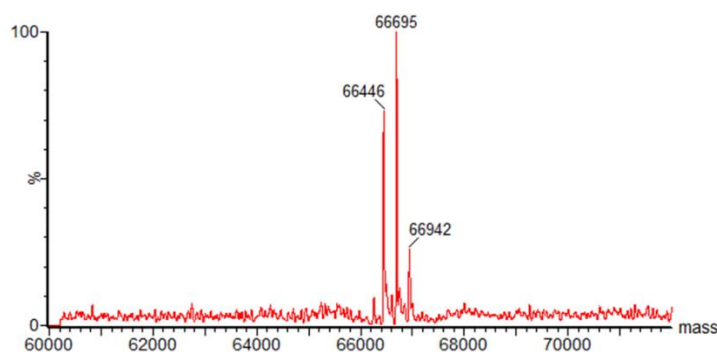


Figure 25. Representative deconvoluted mass spectrum for the reaction between human serum albumin **14** and vinyltriazine-alkyne **32**. The undesired double modification product (66942 Da) is observed together with the unmodified protein (66446 Da) and single modification product (66695 Da). These data suggest vinyltriazine-alkyne **32** has poor cysteine selectivity. Here, human serum albumin **14** was treated with 20 equivalents of **32** in PBS ($\times 1$) and DMSO, at 37 °C for 2 h.

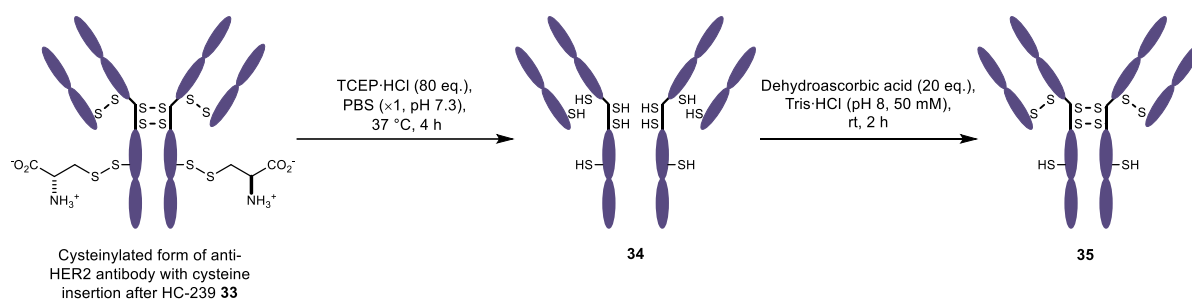
2.8. Modification of antibodies and biological evaluation of antibody-drug conjugates

Encouraged by the positive properties of vinylpyrimidine reagents, efforts focused towards generating a homogeneous and functional ADC using these linkers. One approach for generating ADCs uses antibodies engineered with additional surface-exposed cysteines, which allows conjugation of cytotoxic payloads to produce highly homogeneous ADCs with a defined modification site and drug-to-antibody ratio.^{54,127} Antibodies targeting the extracellular domain of the HER2 receptor tyrosine kinase have demonstrated immense clinical benefit for many years, particularly for the treatment of HER2-positive breast cancer.¹²⁸ Several ADCs targeting HER2 have also undergone development with Kadcylla^{®20} and Enhertu^{®26} obtaining FDA approval. Thus, to evaluate the utility of vinylpyrimidine linkers, it was decided to synthesise ADCs using cysteine-engineered anti-HER2 antibodies.

2.8.1. Uncapping of engineered cysteine residues

It was envisaged that using an anti-HER2 antibody **33** which has cysteine insertion after position 239 in each heavy chain could be used to synthesise ADCs.¹²⁹ To functionalise the engineered cysteine residues of antibody **33**, they must be first uncapped as they are found protected as a disulfide with cysteine. Thus, **33** was subjected towards a reduction-partial reoxidation protocol.

Following literature procedure,¹²⁹ **33** was first treated TCEP·HCl to reduce all six surface-exposed disulfides, before purification to remove the cleaved molecular cysteine (**Scheme 8**). The reduced antibody species **34** was then treated with dehydroascorbic acid to facilitate the re-oxidation of the four pairs of proximal thiols to give partially-reduced antibody **35**.

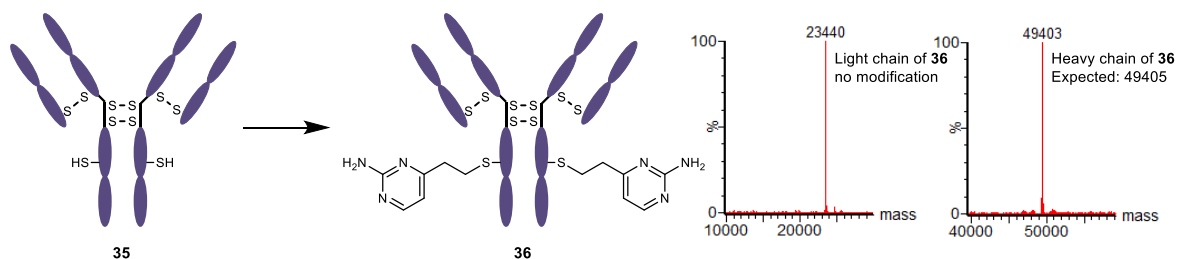


Scheme 8. Preparation of uncapped cysteine-inserted antibody **35**.

2.8.2. Modification of antibody with model linker

With the reactive antibody species **35** in hand, the reactivity of its exposed cysteine with model linker **4** was assessed. To determine the optimal modification conditions, antibody **35** at 30 μM was treated with varying equivalents of linker **4** in Tris·HCl (pH 8, 50 mM), and incubated at 37 °C for 1, 2, and 4 h (**Table 5**). This study revealed that treatment with 20 equivalents of linker **4** for 4 h yielded >95% conversion (Entry 4, **Table 5**). Pleasingly, modification was only observed on the heavy chains, where the engineered cysteines are located. Crucially, no modification was observed on the light chains, highlighting the excellent chemoselectivity of vinylpyrimidines for cysteine residues.

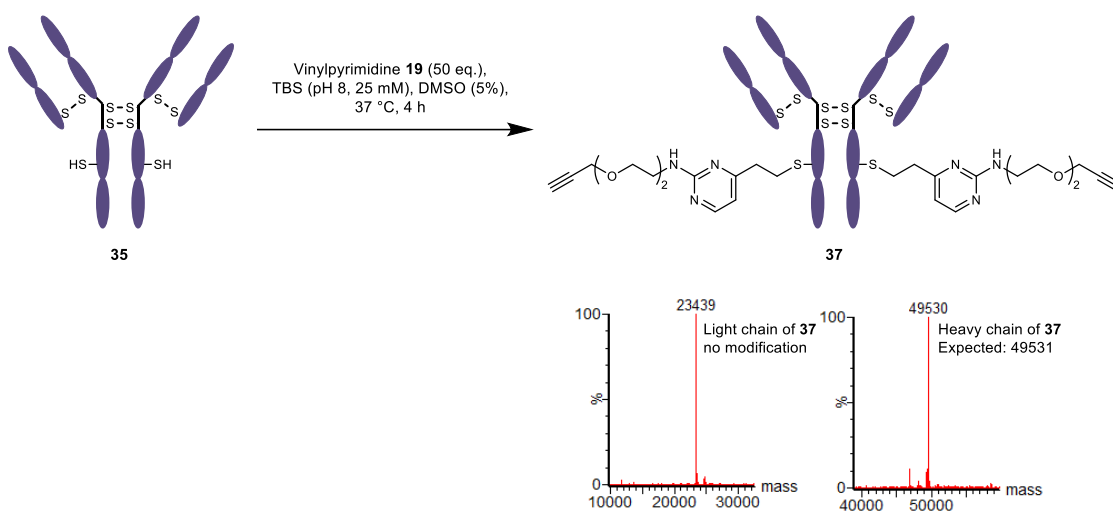
Table 5. Screening of conjugation reactions between antibody **35** and vinylpyrimidine **4**. Reactions were performed at 37 °C in buffer solutions containing 5% DMSO. Aliquots of the reaction mixture were taken, purified, deglycosylated and reduced prior to LCMS analysis. A hyphen refers to a measurement which was not taken. Percentage conversion reported to the nearest 5%. Representative deconvoluted mass spectra for the product **36** are shown.



Entry	Linker eq.	Percentage conversion		
		1 h	2 h	4 h
1	50	75	80	>95
2	40	-	85	>95
3	30	-	-	>95
4	20	-	-	>95
5	10	-	-	85

2.8.3. Modification of antibody with vinylpyrimidine-alkyne

Given the favourable reactivity profiles of model linker **4**, it was hypothesised that modification of antibody **35** with vinylpyrimidine-alkyne **19** would allow further functionalisation of the protein *via* CuAAC reactions (**Scheme 9**). Thus, **35** was treated with 20 equivalents of **19** for 4 h, which were the optimal conditions for model linker **4**. However, these conditions gave ~80% conversion. Pleasingly, increasing the linker equivalents to 50 equivalents gave >95% conversion to the desired bioconjugate, as determined by LCMS analysis.



Scheme 9. Synthesis of antibody-alkyne **37**. Antibody species **35** was deglycosylated and reduced before analysis. LCMS analysis revealed >95% conversion to the desired conjugate. Modifications have taken place on the heavy chain only; no modification was found for the light chain. Representative deconvoluted mass spectra for the product **37** are shown.

2.8.4. Synthesis of antibody-biotin and -AlexaFluor conjugates

With the antibody-alkyne conjugate **37** in hand, its ability to be modified with functional payloads was investigated. First, azido-biotin **25** was reacted in the presence of $\text{CuSO}_4 \cdot 5\text{H}_2\text{O}$, THPTA, and sodium ascorbate, with LCMS analysis revealing >95% conversion to the desired conjugate **38** (**Figure 26a** and **26b**). Similarly, **37** was reacted with Alexa Fluor 488 azide **40**, yielding a fluorophore-to-antibody ratio of 1.9 *via* UV-Vis analysis, indicating a near-complete conversion to the desired **39** (**Figure 26c**). To ascertain that the modifications were taking place on the antibody's heavy chains, antibody-fluorophore conjugate **39** was analysed using SDS-PAGE under reducing conditions. Fluorescence was observed only on the heavy chains of conjugate **39** (**Figure 26d**). The successful synthesis of **38** and **39** demonstrate that the alkyne-bearing vinylpyrimidine linker is compatible with on-protein CuAAC reactions.

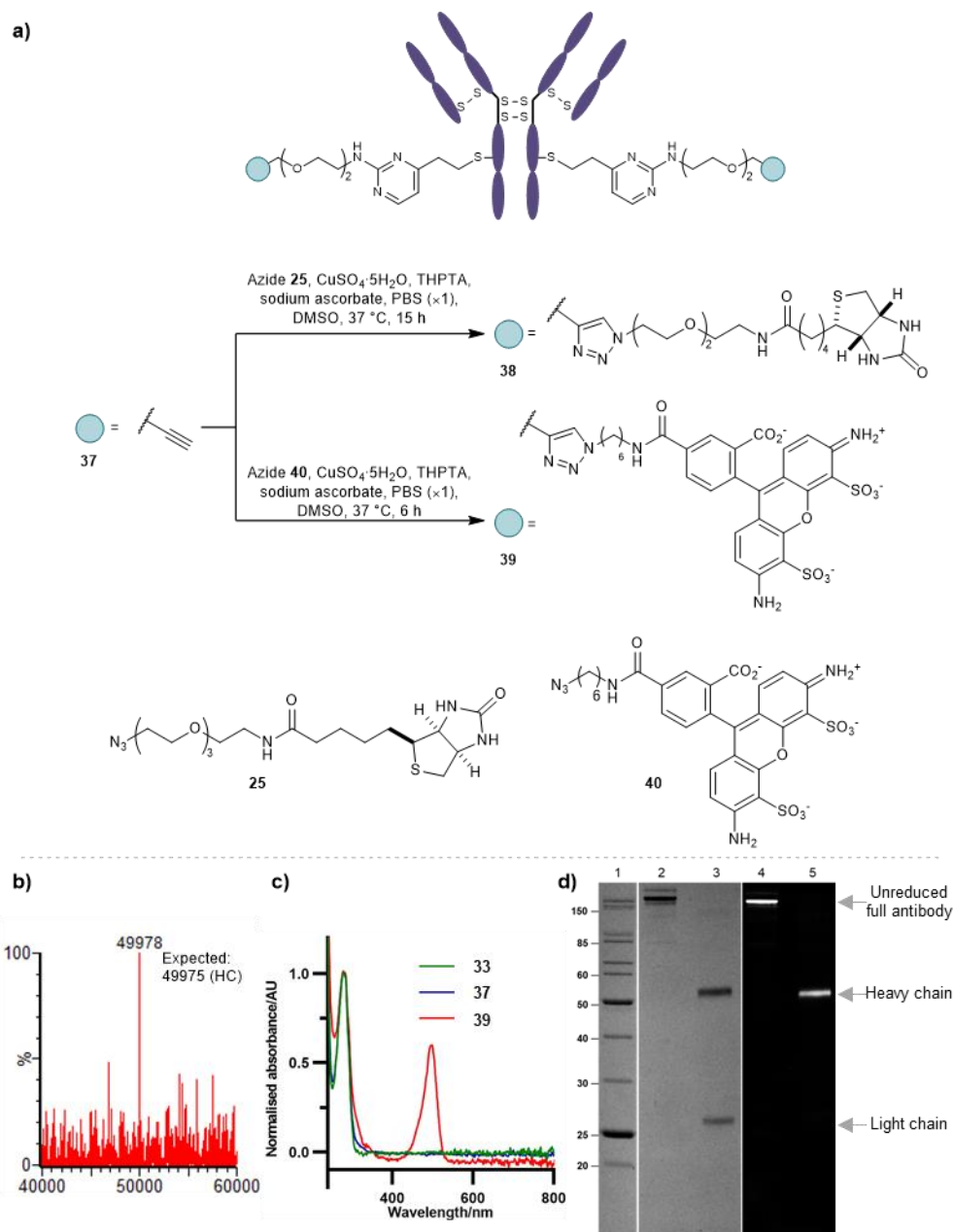


Figure 26. Synthesis of antibody-biotin conjugate **38** and antibody-AlexaFluor conjugate **39**. **a)** Antibody-alkyne **37** was reacted with azides **25** and **40** to give **38** and **39**, respectively. **b)** Deconvoluted mass spectra of **38** heavy chain. **c)** UV-Vis analysis of **33**, **37** and **39**. Antibody-AlexaFluor conjugate **39** gave a fluorophore-to-antibody ratio of 1.9, whereas **33** and **37** lacked absorbance around 495 nm. **d)** SDS-PAGE analysis of antibody-AlexaFluor **39** reveals fluorescence is present only on the heavy chain. Lane 1 – molecular weight ladder (annotations in kDa); Lane 2 – Coomassie stained, non-reduced **39**; Lane 3 – Coomassie stained, reduced **39**; Lane 4 – in gel fluorescence, non-reduced **39**; Lane 5 – in gel fluorescence, reduced **39**.

2.8.5. Synthesis of antibody-drug conjugate

With these promising results in hand, it was proposed that this linker system would be suitable for the generation of an ADC. Thus, an appropriate azide-modified cytotoxic warhead was

2.8.6. *In vitro* cytotoxicity of antibody-drug conjugate

With the anti-HER2 ADC **41** in hand, it was imperative to evaluate its efficacy by *in vitro* cytotoxicity studies in HER2-positive SKBR3 cells and HER2-negative MCF7 cells (cytotoxicity studies conducted by Dr. Stephen Walsh). Pleasingly, potent dose-dependent cytotoxicity was observed in SKBR3 cells. In contrast, the ADC had little effect on the viability of the HER2-negative MCF7 cells at the concentrations tested. This demonstrates that the bioconjugation to a vinylpyrimidine linker does not negatively affect the antibody's biological processes in terms of receptor specificity, binding, or internalisation. These *in vitro* studies highlight the potential of the vinylpyrimidine platform to generate clinically relevant biotherapeutics (**Figure 28**).

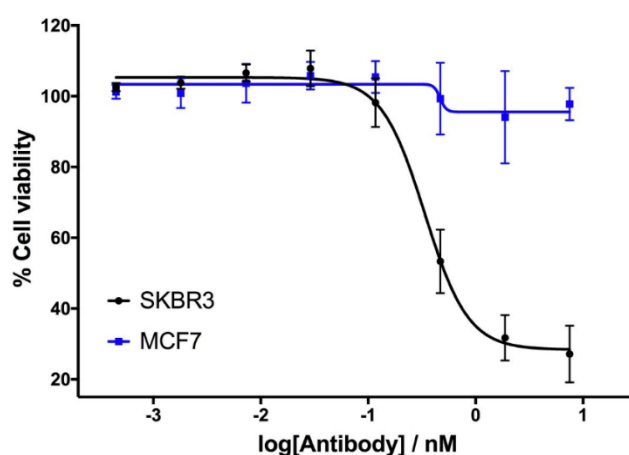


Figure 28. Cytotoxicity data for ADC **41**. The HER2 positive cell line (SKBR3) have dose dependent cell killing by **41**, whereas for the HER2-negative cell line (MCF7) is unaffected. Viability data shows the mean of three independent experiments and error bars represent standard error of the mean.

2.9. Labelling of cysteine-containing proteins in cell lysate

With the chemoselective modification of cysteine residues validated in isolated protein and antibody systems, it was hypothesised that the linker could be used to probe the presence of proteome-wide cysteine residues. Accordingly, MCF7 cell lysates (at 1 mg/mL) were treated with varying concentrations of vinylpyrimidine probe **19** (0 to 400 μ M) at rt for 2 h. The alkyne-tagged lysates were then labelled with AlexaFluor 488 azide **40** in the presence of $\text{CuSO}_4 \cdot 5\text{H}_2\text{O}$, THPTA, and sodium ascorbate (**Figure 29c**). The AlexaFluor 488-labelled proteins were separated *via* SDS-PAGE followed by visualisation by in-gel fluorescence scanning, which revealed concentration-dependent labelling of lysates (**Figure 29a** and **29b**). Crucially, when MCF7 cell lysates were pre-treated with iodoacetamide before incubating with probe **19**, no

labelling was observed. These data provide further evidence that vinylpyrimidine **19** reacts with cysteine residues with exceptional chemoselectivity. These studies demonstrate that vinylpyrimidine linkers can successfully label lysates and offers a complementary approach to lysate-labelling methodologies found in the literature.^{86,130}

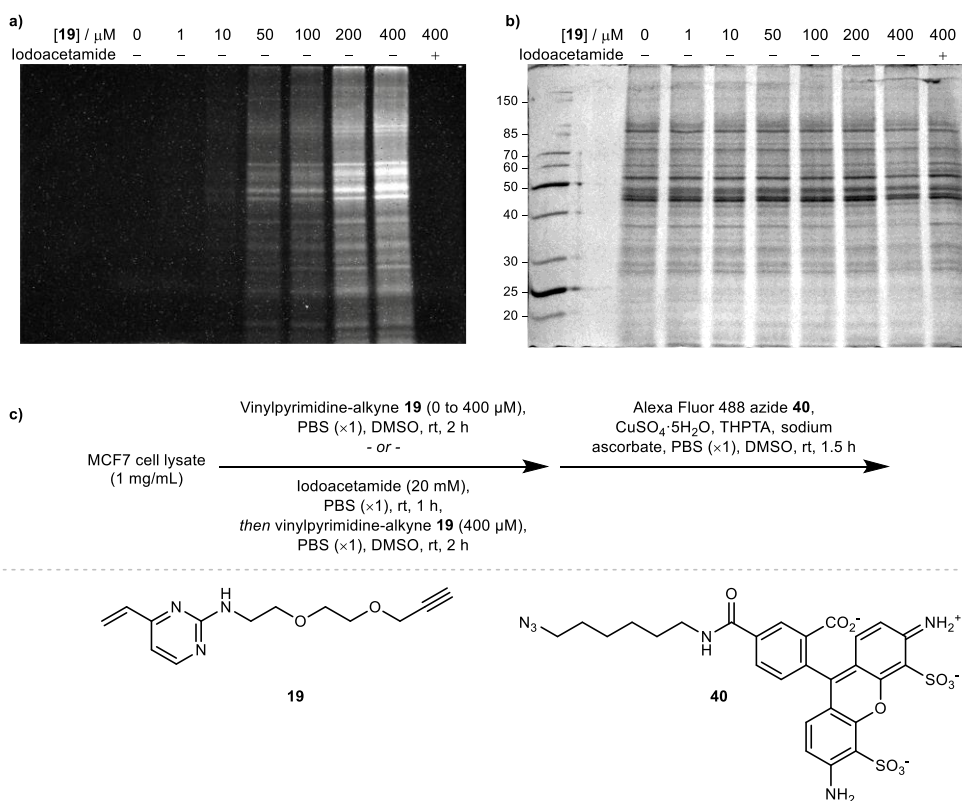
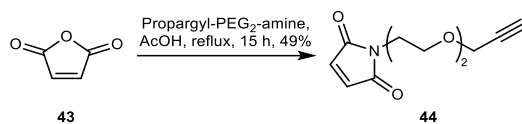


Figure 29. SDS-PAGE analysis of MCF7 cell lysate labelling studies. **a)** In-gel fluorescence of cell lysates. **b)** Coomassie staining of cell lysates. All lanes were prepared under reducing conditions. Molecular weight ladder in kDa. **c)** Cell lysates were first labelled with varying concentrations of probe **19**, and further modified with Alexa Fluor 488 azide **40** via a CuAAC reaction. For cysteine blockage studies, cell lysates were first pre-incubated with iodoacetamide.

2.10. Plasma stability

Finally, to determine the stability of bioconjugates in human plasma, the plasma stability of the vinylpyrimidine bioconjugates was determined and compared to those synthesised using maleimide bioconjugation. It was anticipated that the study of antibody-fluorophore conjugates would enable qualitative analysis of the stability profiles of the linkers using SDS-PAGE.^{69,86,113}

To aid the stability comparison with vinylpyrimidine linker **19**, the corresponding maleimide linker was synthesised. Thus, maleic anhydride **43** was treated with the corresponding amine in refluxing AcOH to afford maleimide **44** in 49% yield (**Scheme 10**).



Scheme 10. Synthesis of maleimide linker **44**.

With the required linkers **19** and **44** in hand, efforts were made to synthesise the antibody-fluorophore conjugates. First, the interchain disulfides of the native anti-HER2 antibody trastuzumab **45** were reduced with TCEP·HCl to reveal eight reactive thiols. Then, the reduced antibody was reacted with vinylpyrimidine **19** or maleimide **44** to generate the corresponding alkynyl antibodies. Finally, the resulting alkynes were subjected to CuAAC with AlexaFluor 488 azide in the presence of CuSO₄·5H₂O, THPTA and sodium ascorbate (**Figure 30a** and **30b**). Analysis *via* UV-Vis spectroscopy revealed that the antibody-fluorophore conjugates **47** and **49** had a fluorophore-antibody ratio of 6.0 and 5.8, respectively. With similar fluorophore-antibody ratios between the two bioconjugates, these species were deemed suitable for use in the comparative stability study (**Figure 30c**).

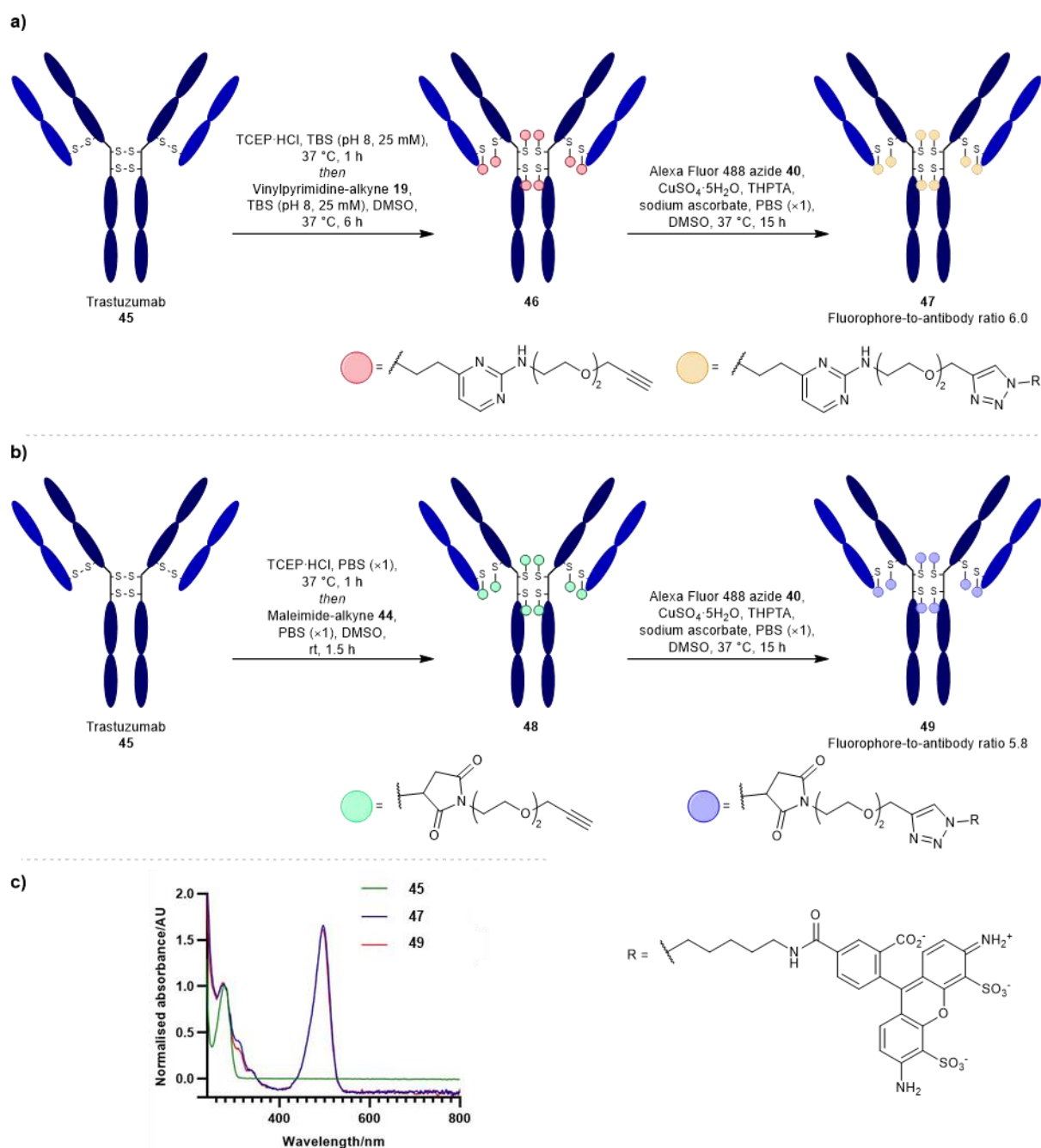


Figure 30. a) Synthesis of antibody-fluorophore conjugate **47**. b) Synthesis of antibody-fluorophore conjugate **49**. c) UV-Vis spectra for **45**, **47**, and **49**.

To determine plasma stability, the antibody-fluorophore conjugates **47** and **49** were incubated in human plasma at 37 °C for eight days (**Figure 31a** and **31b**). Analysis by SDS-PAGE revealed that maleimide conjugate **49** over time formed a new fluorescence band at ~67 kDa. This corresponds to the product formed from linker deconjugation followed by interception with serum albumin, in accordance with previous reports⁸⁴ (**Figure 31c**). In contrast, no transfer of fluorescence to any of the plasma proteins was observed for the vinylpyrimidine

analogue **47** over the eight-day monitoring period. These plasma stability data confirm the exquisite stability of vinylpyrimidine conjugates.

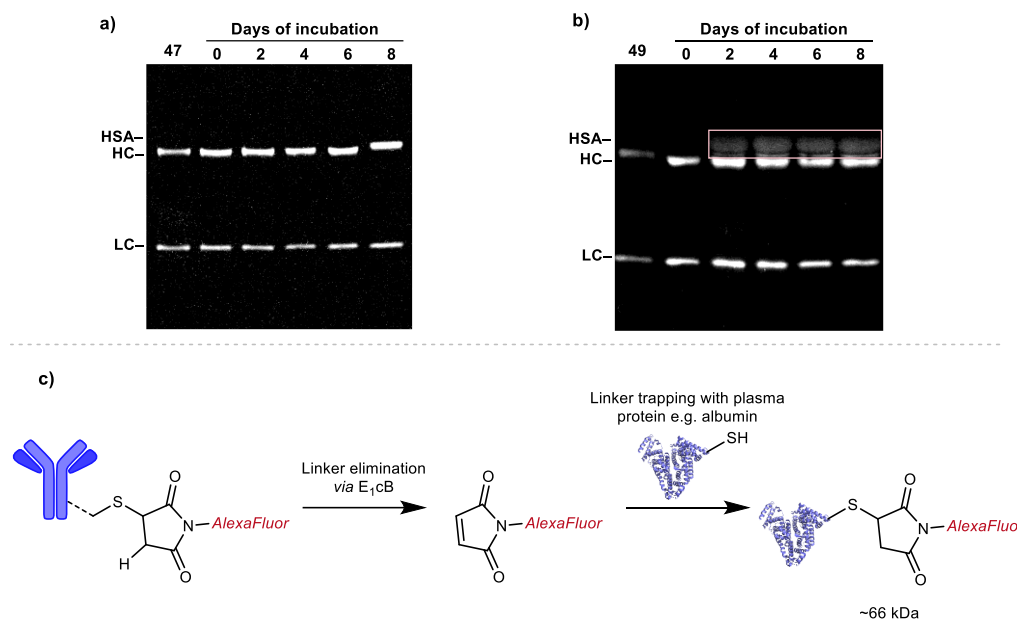


Figure 31. Plasma stability analysis for **a)** vinylpyrimidine conjugate **47** and **b)** maleimide conjugate **49**. All lanes were prepared under reducing conditions. In-gel fluorescence analysis displays no transfer of fluorescence for **47**, whereas fluorescence transfer to serum proteins was observed for **49**. **c)** It is thought that the instability of **49** had occurred *via* deconjugation to give maleimide, which was then trapped by serum proteins e.g., human serum albumin.

2.11. Conclusion

In this work, a series of vinylheteroarene scaffolds were explored for cysteine modification. Through several small molecule reactivity, chemoselectivity, and stability assays, vinylpyrimidine reagents emerged as the most promising candidates for selective modification of proteinogenic cysteine residues. Vinylpyrimidine reagents demonstrated rapid reactivity and chemoselectivity towards cysteines, and the resulting conjugates were exceptionally stable under physiologically relevant conditions. These reagents were then elaborated to modify cysteine residues in protein substrates, culminating in the synthesis of a homogeneous ADC. Biological assays revealed the modified proteins retain their biological function, as demonstrated by cell-specific cytotoxicity. Utilising the linker's cysteine selective reactivity, the linkers were used as a probe for proteinogenic cysteine residues in cell lysates. Finally, the bioconjugates exhibited superior stability in human plasma compared to the widely used maleimide reagents. The advantageous properties and synthetic accessibility of the

vinylheteroarene scaffold lends itself toward widespread usage, both in the development of biological probes and next generation biotherapeutics.

2.12. Future work

The vinylheteroarene linker technology can be further developed by combining the cysteine-reactive properties of vinyl heterocycles with the reactivity of 1,2,4-triazines (**Figure 32**). The inverse electron demand cycloaddition between unsymmetrical 1,2,4-triazines with *trans*-cyclooctene^{121,131–133} and cyclooctynes^{134–136} has been used to modify a range of biomolecules. Thus, it is envisaged that use of an appropriate vinyl-1,2,4-triazine linker **50** may enable the rapid synthesis of functionalised protein conjugate **52** via a cysteine bioconjugation reaction to give **51** followed by an inverse electron demand cycloaddition to attach a functional moiety. This modification method will be an improvement from the current approach – the use of a triazene bioorthogonal handle will allow a range of *in vitro* and *in vivo* studies to be conducted which would not have been possible with linker systems requiring CuAAC reactions due to the toxicity of the Cu(I) species.

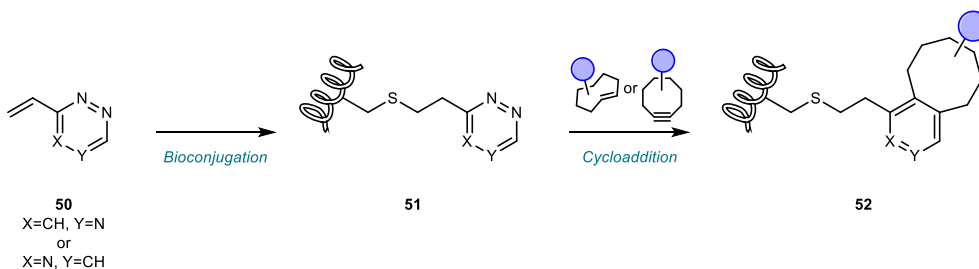


Figure 32. Use of vinyl-1,2,4-triazines which allow cysteine bioconjugation and subsequent functionalisation via inverse electron demand Diels Alder reactions.

Chapter 3. Studies towards applying (+)-discodermolide as a cytotoxic payload in antibody-drug conjugates

3.1. Introduction

(+)-Discodermolide (+)-**53** (hereafter referred to as ‘discodermolide **53**’) is a polyketide natural product isolated by the Harbor Branch Oceanographic Institution in 1990 from extracts of the Caribbean deep water marine sponge *Discodermia dissoluta* (**Figure 33**).¹³⁷ Its favourable antimetabolic activity made it a promising anticancer agent. Discodermolide **53** has been shown to be potent against a variety of malignancy types, including breast, colon, lung, ovarian, and prostate cell lines with IC₅₀ values between 3 and 80 nM.^{138–140} In a comparative study with Taxol, another antimetabolic agent, discodermolide **53** displayed 100-fold greater potency and 160-fold higher aqueous solubility.¹⁴¹ In 1998, **53** was licensed to Novartis by Harbor Branch Oceanographic Institution for its development as an anticancer drug, and this candidate progressed to Phase I clinical trials.¹⁴²

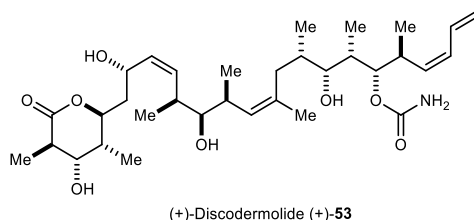


Figure 33. Structure of (+)-discodermolide (+)-**53**.

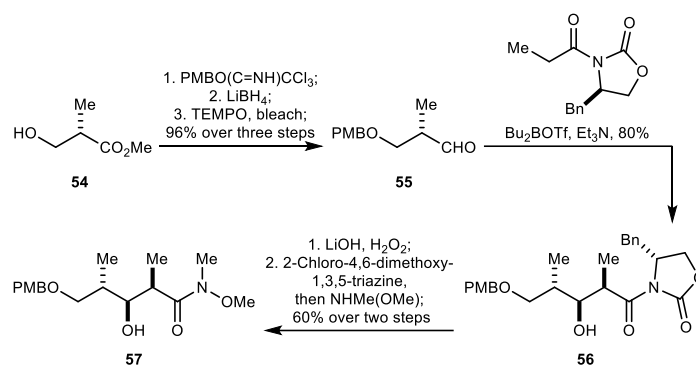
3.1.1. Total synthesis of discodermolide

Discodermolide **53** has gained great attention from both academia and pharmaceutical industry, and has consequently been a popular target in total synthesis research.¹⁴² Since the first total synthesis by Schreiber and co-workers in 1993,¹⁴³ the groups of Smith,¹⁴⁴ Myles,¹⁴⁵ Marshall,¹⁴⁶ and Paterson¹⁴⁰ have also explored synthetic strategies toward discodermolide.

To support Novartis’ clinical trial efforts, a process chemistry route to synthesise **53** was developed by Mickel and co-workers. Using a highly convergent approach, three fragments –

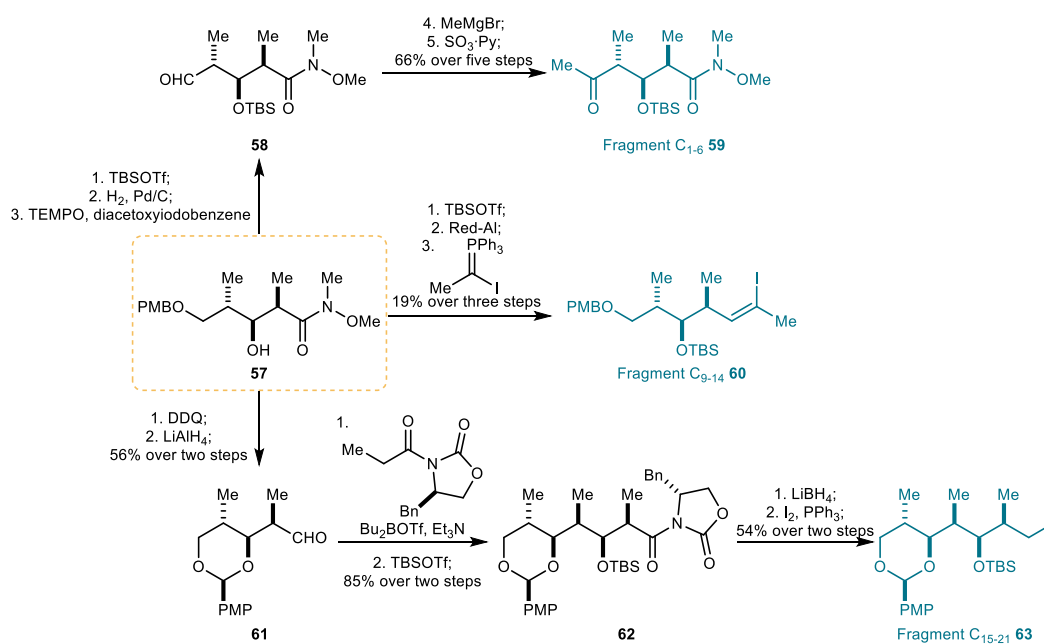
59, **60**, and **63** – were synthesised from common intermediate **57** using a route based on Smith's total synthesis, and fragment union using chemistry developed by Paterson's route allowed the successful synthesis of 64 grams of **53**.^{147–151}

Mickel's synthesis commenced from the enantiopure hydroxy ester **54**, where *O*-PMB protection, ester reduction to the corresponding alcohol, and TEMPO-mediated oxidation gave aldehyde **55**. Evans aldol reaction between **55** and enantiopure *N*-propionic oxazolidinone gave **56** as a single diastereoisomer. Finally, hydrolysis of the chiral auxiliary followed by amide coupling furnished Weinreb amide **57** (**Scheme 11**).



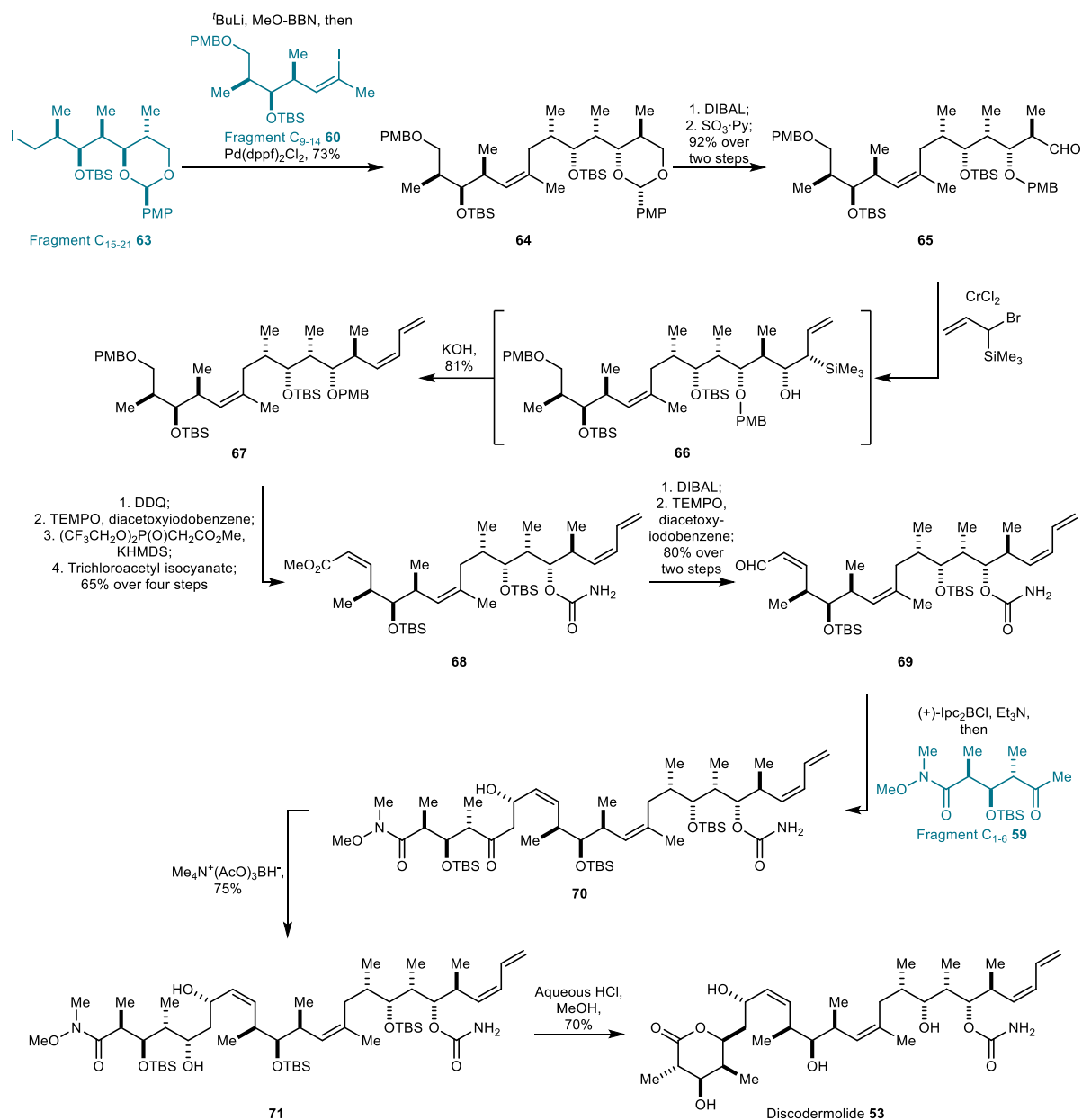
Scheme 11. Synthesis of intermediate **57**.¹⁴⁷

The key intermediate **57** was further diversified to give three key fragments: 'Fragment C₁₋₆' **59**, 'Fragment C₉₋₁₄' **60**, and 'Fragment C₁₅₋₂₁' **63**. Fragment C₁₋₆ **59** was synthesised by *O*-silylation, debenzoylation by hydrogenolysis, and oxidation, which gave aldehyde **58**. Treatment of **58** with MeMgBr followed by Parikh-Doering oxidation gave the required ketone **59** (**Scheme 12**, top). Synthesis of Fragment C₉₋₁₄ **60** commenced with *O*-silylation of **57**, which was followed by amide reduction to the corresponding aldehyde. To complete the fragment, Wittig olefination gave *cis*-olefin **60** with high selectivity (**Scheme 12**, middle). The third fragment **63** was synthesised by treating **57** with DDQ which gave the corresponding *para*-methoxybenzylidene acetal. The amide group was reduced with LiAlH₄ which gave aldehyde **61**. Evans aldol reaction with *N*-propionic oxazolidinone followed by *O*-silylation gave **62**. Compound **62** was further treated with LiBH₄ which reduced the amide group to the corresponding alcohol. Subjection of the alcohol to Appel conditions gave iodide **63** (**Scheme 12**, bottom).



Scheme 12. Synthesis of fragments **59**, **60**, and **63** from **57**.^{148,149}

Finally, linkage of the three fragments was required to complete the synthesis of **53**. Coupling of fragment **63** and **60** under Suzuki conditions gave **64**. The acetal group within **64** was reduced which gave a primary alcohol, which was oxidised to aldehyde **65**. Chromium(II)-mediated Nozaki-Hiyama allylation gave β -hydroxysilane **66**, and base mediated *syn*-elimination of this group furnished *cis*-olefin **67**. Removal of the two PMB ethers within **67** followed by selective oxidation of the primary alcohol to the aldehyde, Still-Gennari *cis*-selective olefination, and carbamate formation at the secondary alcohol gave **68**. Transformation of the methyl ester **68** to aldehyde **69**, and aldol coupling with fragment **59** gave **70**. Evans-Saksena reduction of the ketone group within **70** gave the corresponding 1,3-*anti* diol **71**. Finally, global deprotection and lactone formation in aqueous HCl furnished (+)-**53** in 39 total synthetic steps (**Scheme 13**).



Scheme 13. Synthesis of **53** from **63**, **60**, and **59**.^{150,151} Ipc = isopinocampheyl.

3.2. Project background

Discodermolide has low nanomolar cytotoxicity against a range of cancer cell types and high aqueous solubility, characteristics which are both favourable for ADC payloads. This prompted investigations towards synthesis and biological characterisation of antibody-discodermolide conjugates. As part of previous research conducted in the group by Dr. Elaine Fowler and Dr. Stephen Walsh, the modification of the C7 hydroxyl group of **53** as a benzoyl ester enabled its attachment to trastuzumab (an anti-HER2 antibody) (**Figure 34**). It was hypothesised that this

benzoyl ester would act as a stable ‘non-cleavable’ drug linkage, where upon lysosomal protein degradation the active drug contains the amino acid appendage used in bioconjugation (**Section 1.5.2.1**). However, *in vitro* cell cytotoxicity studies revealed little cell discrimination between HER2-positive and HER2-negative cell lines. These results suggest the benzoyl ester linkage was not stable in cell media and aqueous hydrolysis was releasing the drug before cell internalisation.

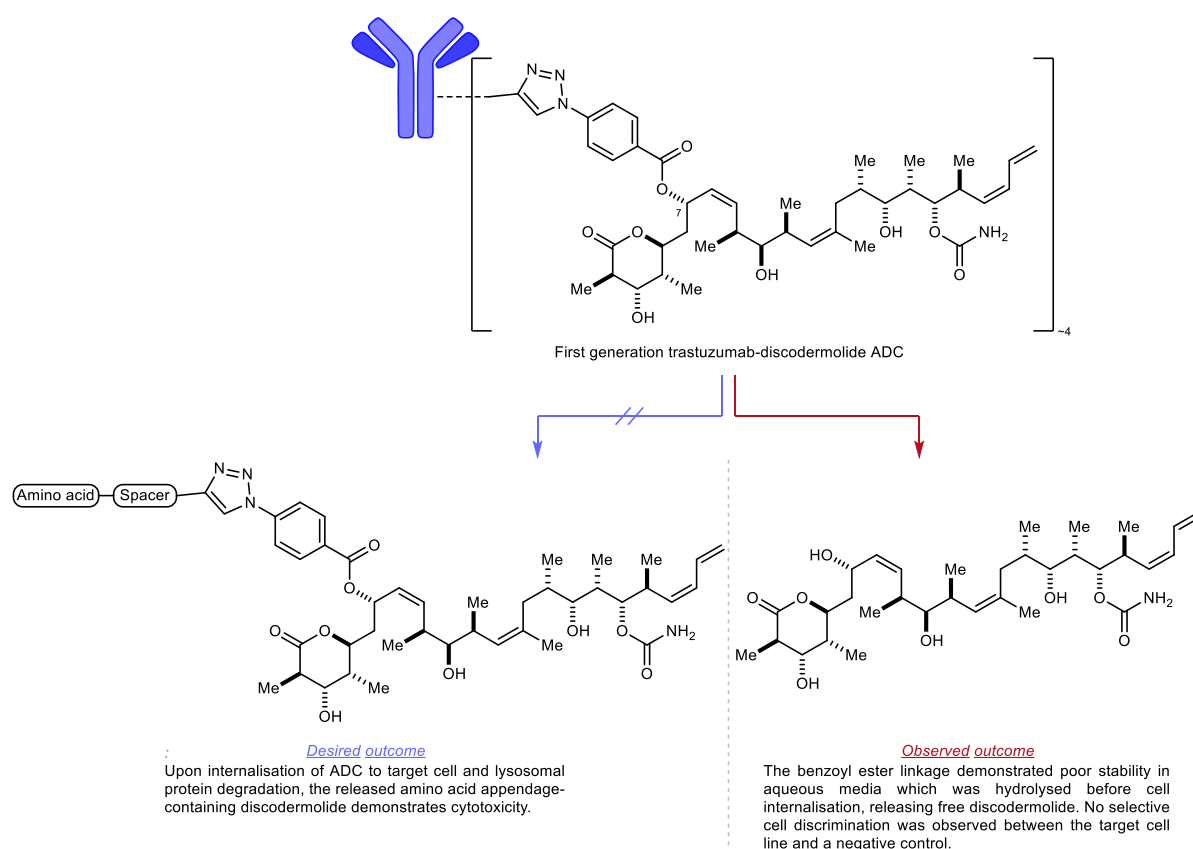


Figure 34. Trastuzumab-discodermolide ADC synthesised by Dr. Elaine Fowler and Dr. Stephen Walsh, based on a non-cleavable benzoyl ester linkage, and the outcome from *in vitro* cytotoxicity studies.

3.3. Project aims

To overcome the pitfalls observed in the initial non-cleavable design, a ‘cleavable linker’ strategy was proposed (**Section 1.5.2.2**). It was envisaged that using a cleavable linker to modify discodermolide **53** would generate an ADC with sufficient cytotoxicity against target cells and a wider therapeutic window over non-target cells.⁹³ A prerequisite of a cleavable linker is using a suitable leaving group to release the drug. Since the alcohol groups within

discodermolide **53** will serve as the best leaving group, attention focused on the modification of this functionality.

The aims of this project are:

1. The design and synthesis of discodermolide **53** linker-payload, which connects discodermolide **53** to a protein attachment handle through a drug release group.
2. Bioconjugation of this linker-payload to a therapeutic antibody to synthesise an ADC.
3. Determination of *in vitro* cytotoxicity of ADCs with discodermolide payloads.

3.4. Project design

A number of strategies are documented in literature to release aliphatic alcohol payloads. However, these strategies were deemed unsuitable to synthesise discodermolide ADCs: carbonates suffer from poor plasma stability (**Figure 35a**),²⁷ Gly-Gly-Phe-Gly-hemiaminal ethers are not amenable to releasing a wide range of alcohol payloads (**Figure 35b**),²⁶ and diphosphate modified cytotoxins require laborious synthesis (**Figure 35c**)^{152,153}

Attention focused on the key work conducted by Seattle Genetics (**Figure 35d**).¹⁰⁶ This method uses a key hemiaminal ether spacer which connects the alcohol group of auristatin E with the linker. Upon β -glucuronide-catalysed cleavage of the glycosidic bond, a cascade of elimination reactions occurs which first releases an amine group. This intermediate then hydrolyses spontaneously to give the unmodified drug. Less than 1% of released auristatin E was detected after incubation in mouse plasma for seven days, and the ADC demonstrated selective cell killing for the target CD30+ cell line in both *in vitro* cell studies and in mouse xerografts.¹⁰⁶

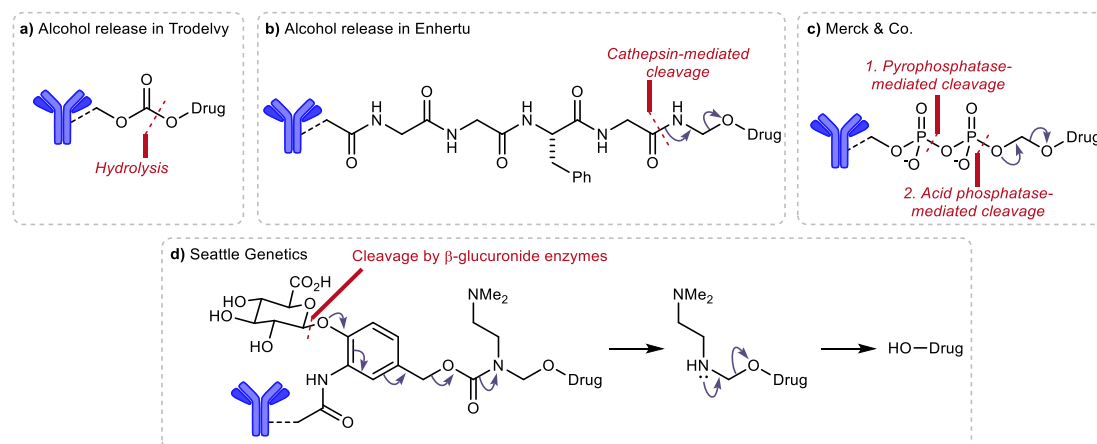
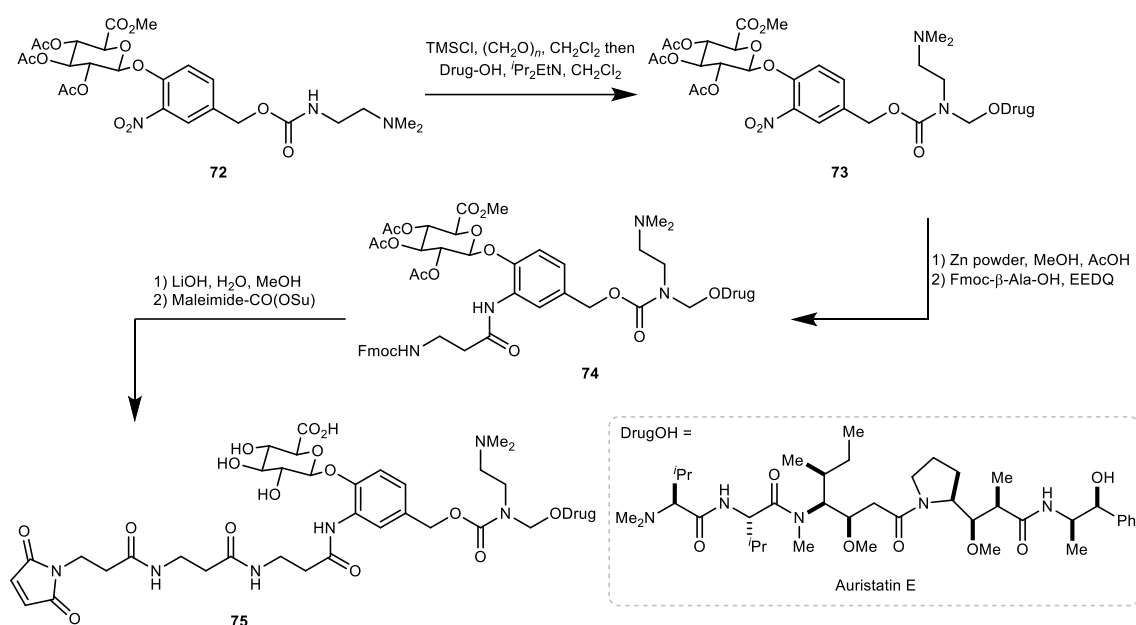


Figure 35. Summary of alcohol release strategies found in literature.

Despite the effective drug release, this method possessed a significant synthetic challenge (**Figure 14**). Namely, after the drug is functionalised with the protected drug release group **72** to give **73** the resulting conjugate was subjected to a further four synthetic steps to synthesise maleimide-auristatin E **75**, which could finally be used to modify the antibody of interest.¹⁰⁶ Given many of these steps used relatively harsh conditions, this route may not be amenable to payloads which have delicate functional groups.



Scheme 14. Synthetic route to the maleimide-auristatin E conjugate **75**, which possesses an alcohol drug release group developed by Seattle Genetics.

To improve on the approach developed by Seattle Genetics, a dipeptide drug release trigger could be combined with hemiaminal ether spacer. The valine-alanine-*para*-aminobenzoyloxycarbonyl dipeptide has been used widely to release amine drugs,⁹³ and indeed this moiety is found in the FDA-approved ADC Zynlonta[®].²⁹ In Zynlonta[®], upon recognition of the dipeptide unit by cathepsin enzymes in lysosomes, the enzyme selectively cleaves the alanine C-terminus amide bond giving an aniline. Upon 1,6-elimination, the unmodified tesirine drug is released (**Figure 36a**). By attaching a hemiaminal ether spacer to this linkage strategy, an alcohol-containing drug such as discodermolide could be released using a valine-alanine-*para*-aminobenzoyloxycarbonyl group. Previous studies have shown that the inclusion of an *N*-ethyl dimethylamine group on the carbamate nitrogen improves the aqueous stability of the hemiaminal ether group, thus this moiety is included in the design (**Figure 36b**).¹⁰⁶

Using a Val-Ala dipeptide trigger was an advantage over Seattle Genetics' approach as this significantly shortens the synthetic sequence and avoids harsh reaction conditions. Azido-discodermolide **76** could be used for antibody attachment using a copper-catalysed azide-alkyne cycloaddition reaction to synthesise the required ADC (**Figure 36c**). It was envisaged that **76** could be constructed from aminomethylene chloride **77** and discodermolide **53** in one synthetic step, which greatly shortens the synthetic sequence compared to Seattle Genetics' linker.

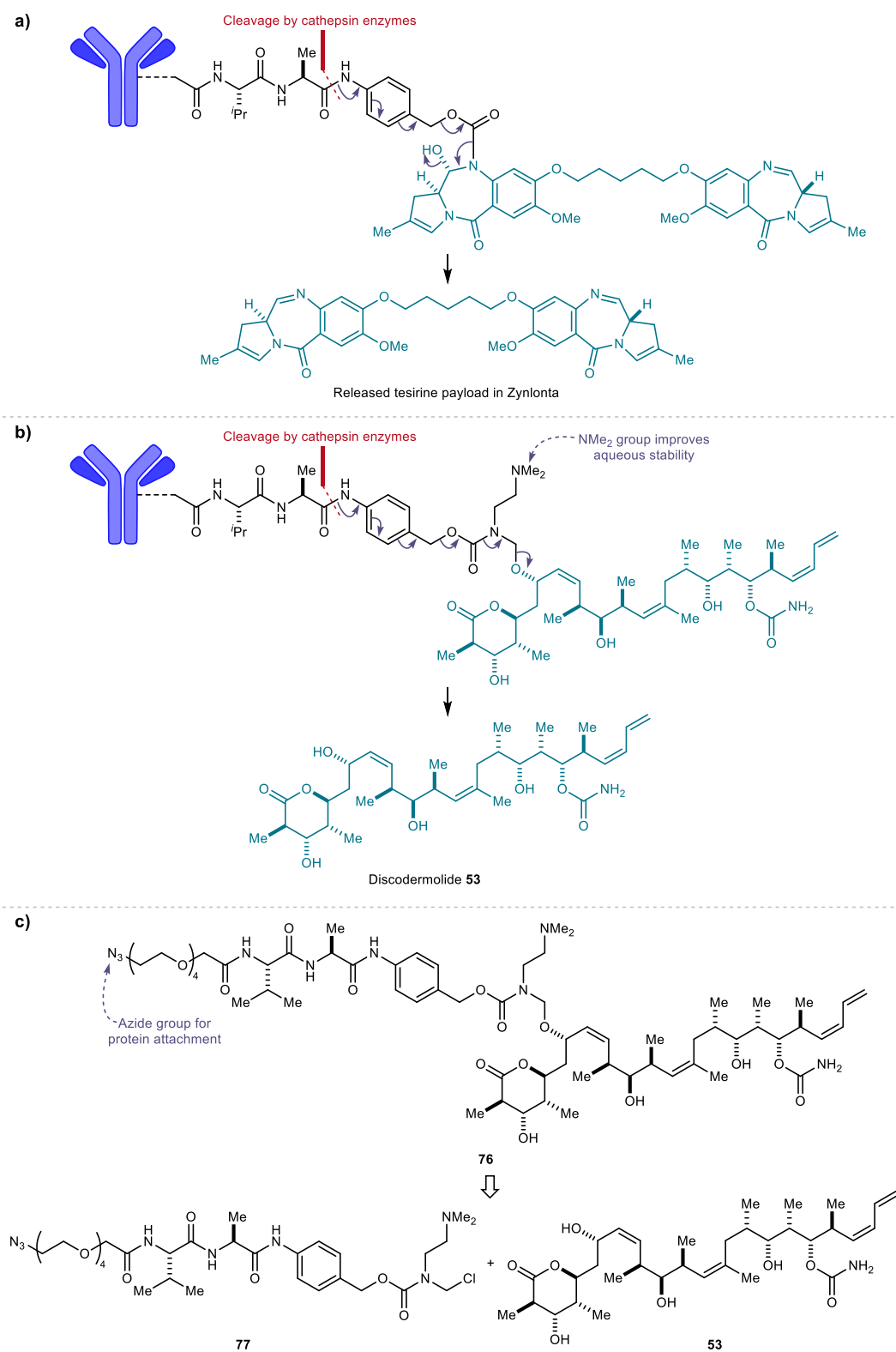


Figure 36. Drug release using valine-alanine-*para*-aminobenzylcarbonyl groups. **a)** Amine release in Zynlonta[®]. Upon aniline release by cleavage by cathepsins, a cascade of elimination reactions occurs which releases the payload in Zynlonta[®]. **b)** It is envisaged that by using a hemiaminal ether spacer, discodermolide **53** can be released by using a similar strategy. **c)** It was hypothesised that discodermolide-azide **76** can be synthesised from aminomethylene chloride **77** and discodermolide **53** in one synthetic step.

3.5. Synthesis and isolation of aminomethylene chloride

Initial efforts focused on the development of a robust route to synthesise aminomethylene chloride **77** (Figure 37).

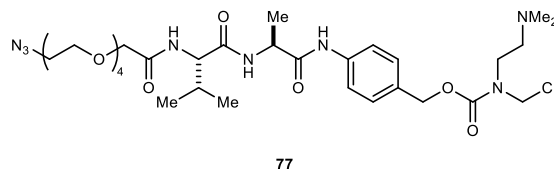
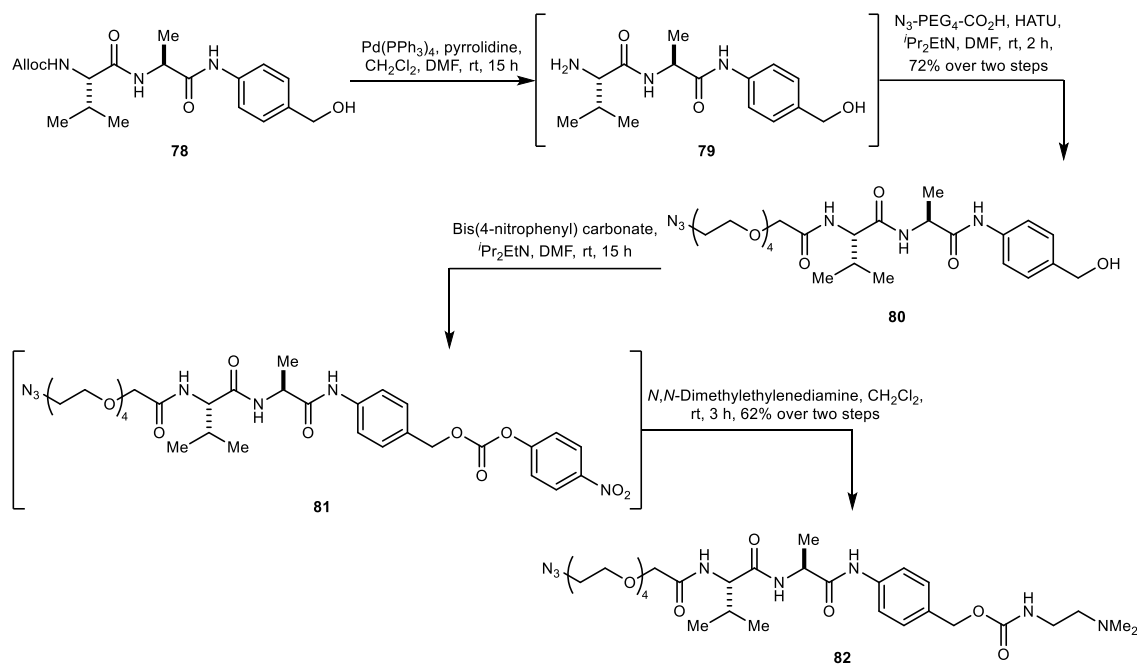


Figure 37. Structure of aminomethylene chloride **77**.

3.5.1. First generation route

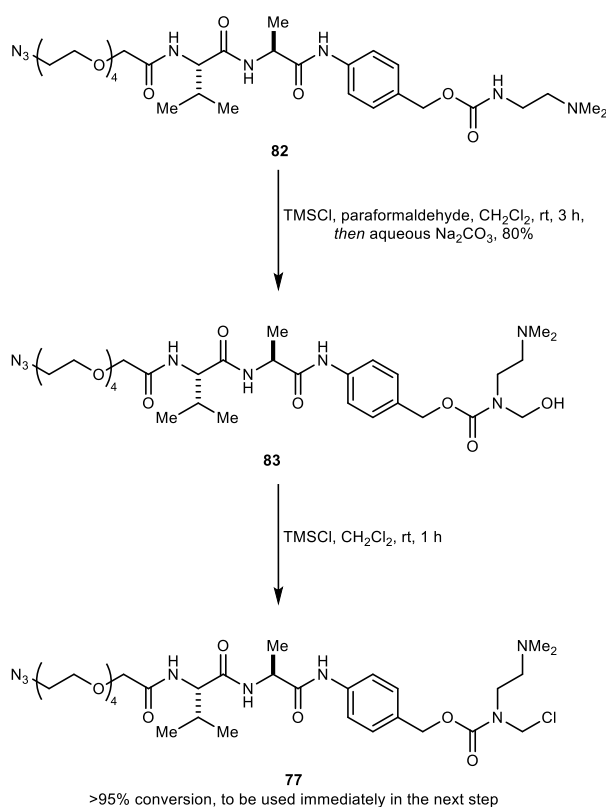
Synthesis of aminomethylene chloride **77** began from Alloc-Val-Ala-*para*-aminobenzylalcohol **78** (Scheme 15). First, **78** was treated with Pd(PPh₃)₄ and pyrrolidine to give amine **79**. Crude **79** was then treated with N₃-PEG₄-CO₂H and HATU, which gave the corresponding amide **80** in 72% yield over two steps. To functionalise the alcohol group within **80**, the compound was treated with bis(4-nitrophenyl) carbonate to give the corresponding mixed carbonate **81**. Crude **81** was treated with *N,N*-dimethylethylenediamine to give the desired carbamate **82** in good yield.



Scheme 15. Synthesis of carbamate **82**.

3.5.2. Second generation route

Given the limitation of the first approach was in the purification of **77**, an alternative two-step route was devised. By doing so, the purification protocol for the reactive intermediate **77** is simplified as filtration steps are no longer required, therefore reducing handling steps and increasing the reproducibility of its synthesis. Thus, carbamate **82** was treated with TMSCl and paraformaldehyde to form aminomethylene chloride **77**, before treating the reaction mixture with aqueous Na_2CO_3 (**Scheme 17**). This gave hemiaminal **83** in 80% isolated yield. Then, hemiaminal **83** was re-subjected to TMSCl and concentrated *in vacuo*. LCMS analysis of the methanol-quenched sample indicated the complete conversion to aminomethylene chloride **77** from hemiaminal **83**; no hydrolysis product or starting material was observed. Activated compound **77** could then be used immediately by treatment with a variety of alcohol drugs to obtain azide-functionalised payloads.



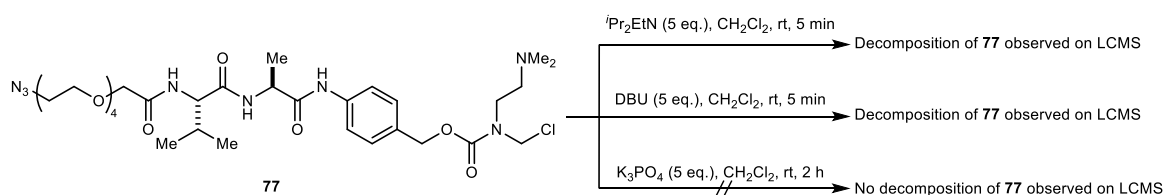
Scheme 17. Synthesis of aminomethylene chloride **77** from carbamate **82** via hemiaminal **83**.

3.6. Optimisation of conjugation with aminomethylene chloride

With a route established that gave aminomethylene chloride **77**, efforts were made to optimise the reaction between **77** and model alcohols.

3.6.1. Base compatibility

To facilitate the conjugation reaction between electrophile **77** and alcohols, it was proposed a mild, non-nucleophilic base would be required. Accordingly, *i*Pr₂EtN, 1,8-diazabicyclo[5.4.0]undec-7-ene (DBU), and K₃PO₄ were screened for compatibility. Five equivalents of base were added to a solution of **77** in CH₂Cl₂ and the reactions were incubated at room temperature. To monitor the reactions, aliquots were taken, quenched with MeOH, and analysed *via* LCMS. Surprisingly, both *i*Pr₂EtN and DBU gave rapid decomposition of **77** within 5 minutes. However, **77** and K₃PO₄ showed excellent compatibility: when **77** was incubated with K₃PO₄, no decomposition of **77** was observed after 2 h. (**Scheme 18**).

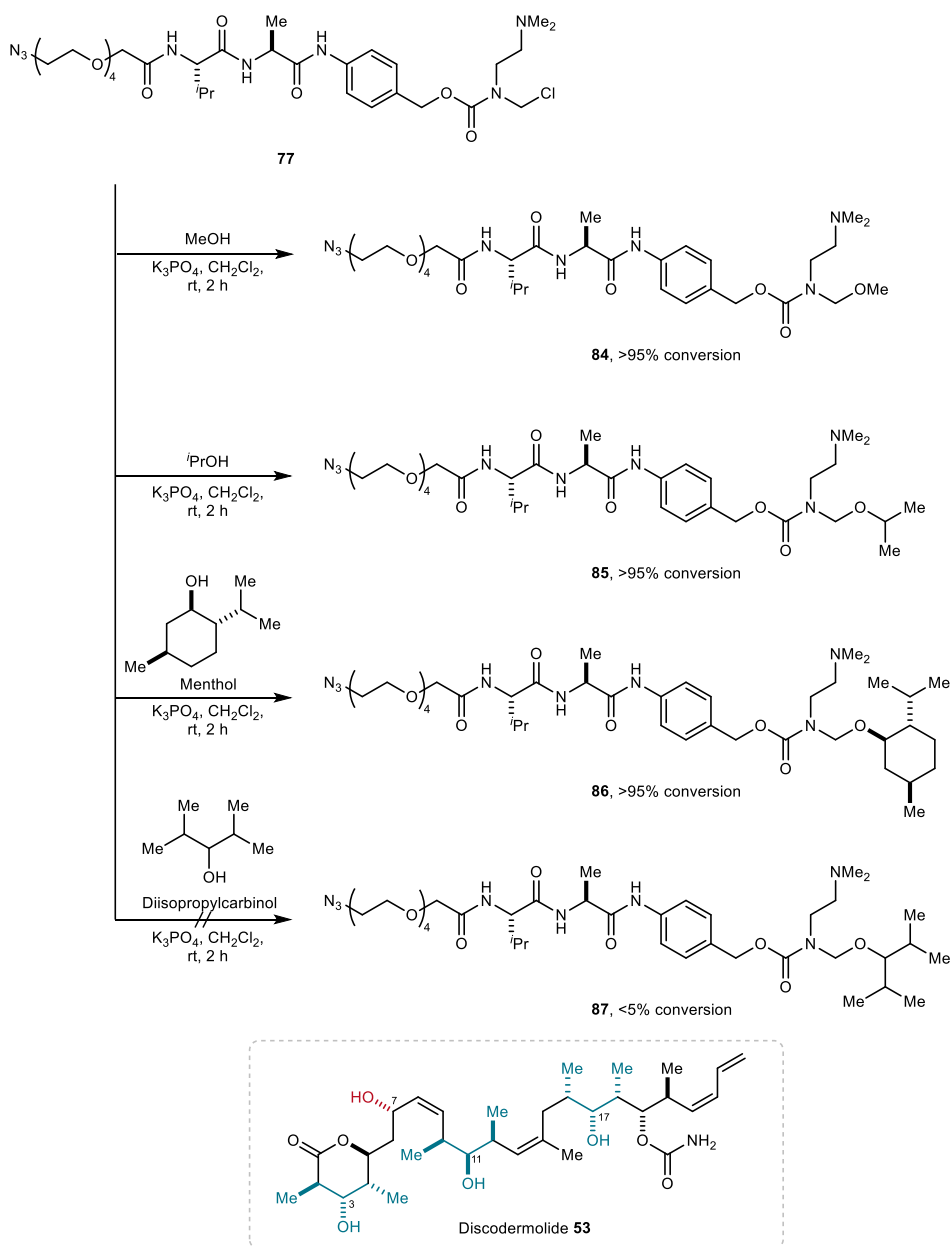


Scheme 18. Base compatibility studies for **77**. While *i*Pr₂EtN and DBU were too nucleophilic and caused rapid decomposition, K₃PO₄ was compatible with **77**.

3.6.2. Alcohol compatibility

With the most suitable base determined, it was imperative to determine the scope of alcohols which can react with **77**. Since the steric environment around the alcohol functionality would influence reactivity, a panel of alcohols with varying steric properties was examined for conjugation. Accordingly, aminomethylene chloride **77** in the presence of K₃PO₄ was reacted with 1.2 equivalents of MeOH, *i*PrOH, menthol, or diisopropylcarbinol (**Scheme 19**). After 2 h, analysis by LCMS revealed >95% conversion to the corresponding hemiaminal ethers **84**, **85**, and **86** from alcohols MeOH, *i*PrOH, and menthol, respectively. However, under the same conditions, <5% conversion to **87** was observed for diisopropylcarbinol. The lack of reactivity for diisopropylcarbinol is a significant result – this demonstrates that aminomethylene chloride **77** is a sufficiently mild reagent to discriminate between alcohols with different levels of steric hinderance. Since discodermolide **53** possesses alcohols on C3, C11, and C17 (marked in

turquoise, **Scheme 19**) which are flanked by two secondary carbons similar to the alcohol group of diisopropylcarbinol, it is thought that the less hindered alcohol on C7 (marked in red) will react selectively with aminomethylene chloride **77**.

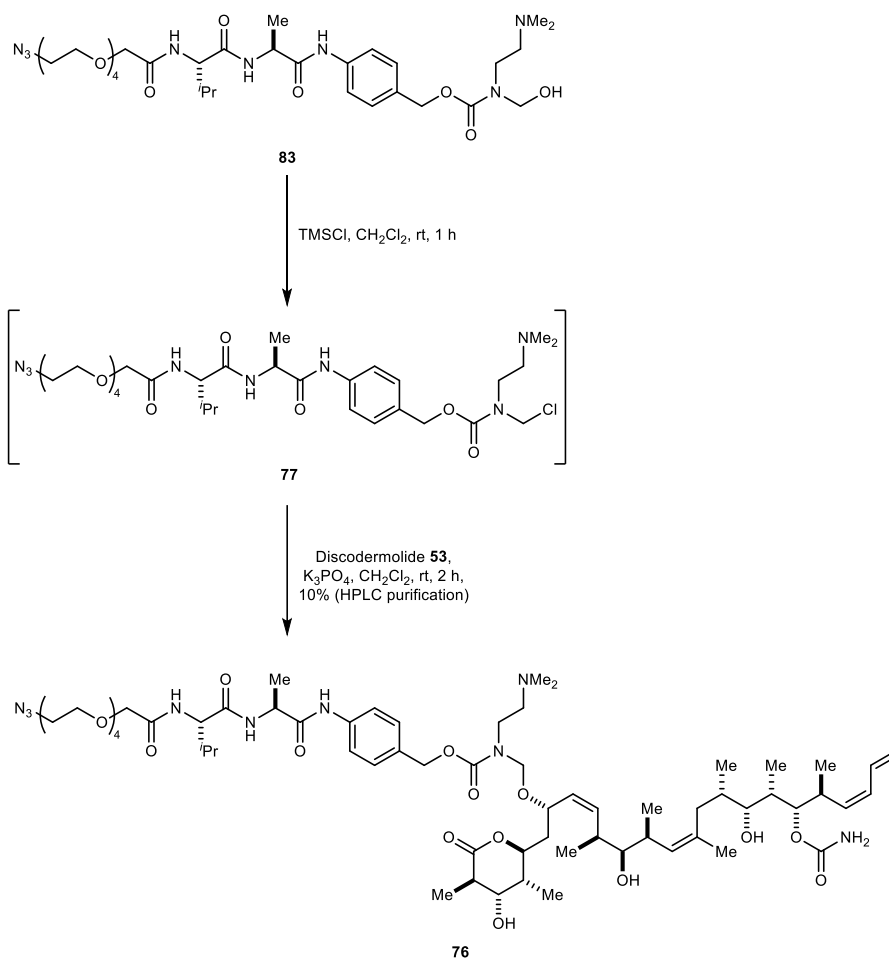


Scheme 19. Reactivity studies of aminomethylene chloride **77** with a variety of alcohols. While less sterically hindered alcohols reacted with **77**, the highly hindered diisopropylcarbinol showed <5% conversion.

3.7. Synthesis of azide-discodermolide

With conjugation reactions optimised, studies commenced to attach discodermolide (provided by Dr. Elaine Fowler and Paterson Group) on the linker. Thus, 1.2 equivalents of hemiaminal

83 were activated with TMSCl to give aminomethyl chloride **77**, which was used immediately in the next step (**Scheme 20**). Reagent **77** was treated with 1.0 equivalent of discodermolide **53** and K_3PO_4 in CH_2Cl_2 . LCMS analysis of the reaction mixture revealed the formation of a single regioisomer, which was isolated *via* preparatory HPLC in 10% yield. NMR spectroscopy studies to fully elucidate the regiochemistry of the azide-discodermolide conjugate were not conducted due to the complexity of this compound and the small amount that was isolated. However, based on studies with model systems, it is hypothesised that the least hindered alcohol on C7 had reacted, giving **76**. Importantly, due to the cleavable linker releasing unmodified **53** within the target cell, it is unlikely that the linker attachment site has a significant influence on the cytotoxicity of the resulting ADC. A sufficient amount of **76** was isolated to pursue subsequent antibody modification studies.

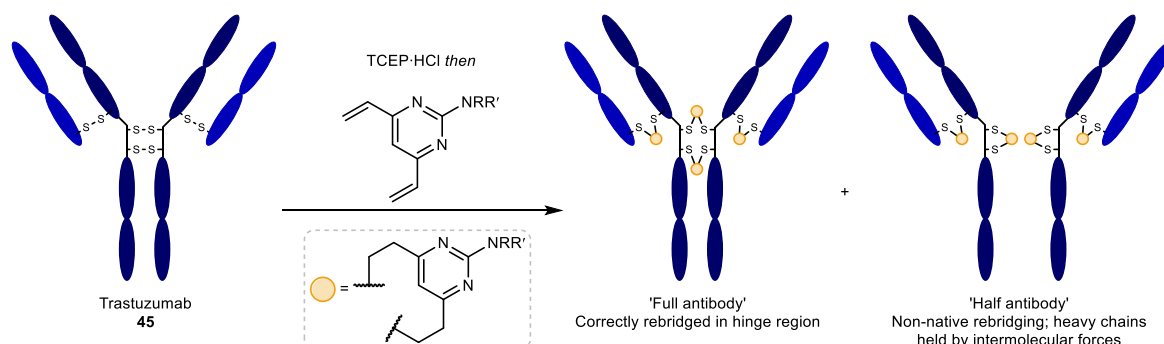


Scheme 20. Synthesis of azide-discodermolide **76** using a two-step telescope approach from **83**.

3.8. Synthesis of trastuzumab-discodermolide ADC

Having successfully synthesised azide-discodermolide **76**, studies focused on attaching this compound on a therapeutic antibody. The anti-HER2 antibody trastuzumab **45** was chosen as an antibody substrate for its widespread use in ADC research.^{69,109,113,115}

Previously in the Spring Group, divinylpyrimidine (DVP) rebridging reagents were developed for the synthesis of homogeneous and stable antibody conjugates (**Scheme 21**).¹¹³ In this approach, the four solvent-exposed interchain disulfide bonds in trastuzumab **45** are reduced with TCEP·HCl, and the resulting species with eight thiols is treated with a DVP reagent. This gives two disulfide-rebridged products – the correct rebridged ‘full antibody’ species, and the ‘half antibody’ species which arises from intrachain misbridging in the hinge region. Although the half antibody does not have the two heavy chains linked by a covalent bond, non-covalent interactions fully retain the antibody’s structure, antigen-binding, or internalisation functionalities.^{54,113} Thus, the formation of a mixture of full and half antibody species was deemed not to be problematic for this study.

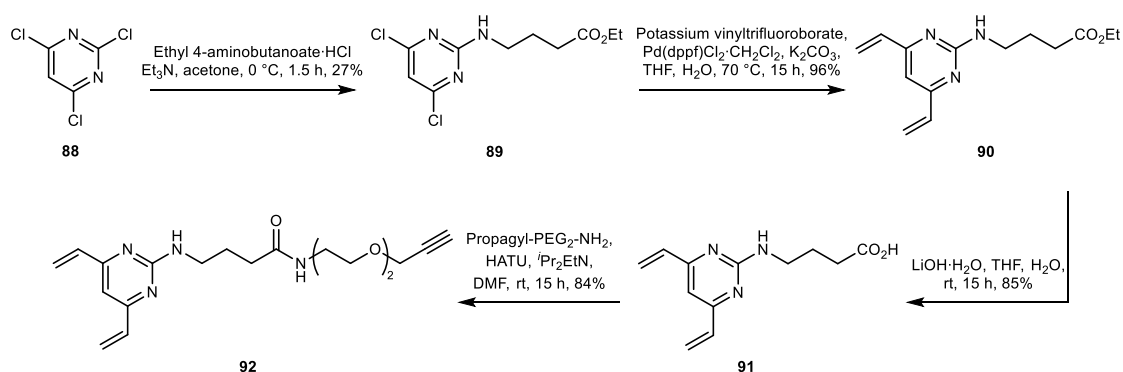


Scheme 21. The formation of full and half antibody species by the divinylpyrimidine disulfide rebridging reagent. Drugs and other biologically relevant moieties were attached at R and R’.

To synthesise the trastuzumab-discodermolide ADC, a two-step procedure was proposed. First, reaction of trastuzumab **45** with a DVP reagent containing an alkyne functional handle would be conducted. Next, the installed alkyne could be further functionalised with discodermolide-azide **76** using CuAAC chemistry.

To facilitate antibody conjugation, DVP-alkyne **92** was required (**Scheme 22**).¹¹⁵ Thus, trichloropyrimidine **88** was treated with ethyl 4-aminobutanoate hydrochloride, which gave the 2-substituted product **89** in moderate yield. Suzuki coupling with potassium vinyltrifluoroborate gave **90** in excellent yield, then the ester group within **91** was hydrolysed

to the corresponding carboxylic acid in excellent yield. Finally, a HATU-mediated amide coupling between **91** and propargyl-PEG₂-amine gave the desired amide **92** in good yield (**Scheme 22**).



Scheme 22. Synthesis of DVP-alkyne **92**.

With the required DVP-alkyne linker **92** in hand, attention focused on the synthesis of antibody-discodermolide conjugate. Using literature conditions, trastuzumab **45** was first reacted with TCEP·HCl, followed by DVP-alkyne **92** to furnish antibody-alkyne **93** (**Figure 38a** and **38b**).^{113,115} Analysis of **93** *via* SDS-PAGE revealed that the conjugate is predominantly in the half antibody form with smaller amounts of full antibody and unreacted heavy and light chains; this is in line with SDS-PAGE results reported in literature (**Figure 38c**).^{113,115}

With antibody-alkyne **93** in hand, synthesis of the required ADC **94** was pursued. Treatment of antibody-alkyne **93** with azide-discodermolide **76** in the presence of CuSO₄·5H₂O, THPTA, and sodium ascorbate produced the required antibody-discodermolide conjugate **94** as determined by LCMS analysis (**Figure 38d**; the synthesis of **94** from **93** was conducted by Dr. Stephen Walsh). Thus, the synthesis of ADC **94** was achieved to support investigation of its biological properties using *in vitro* cell assays.

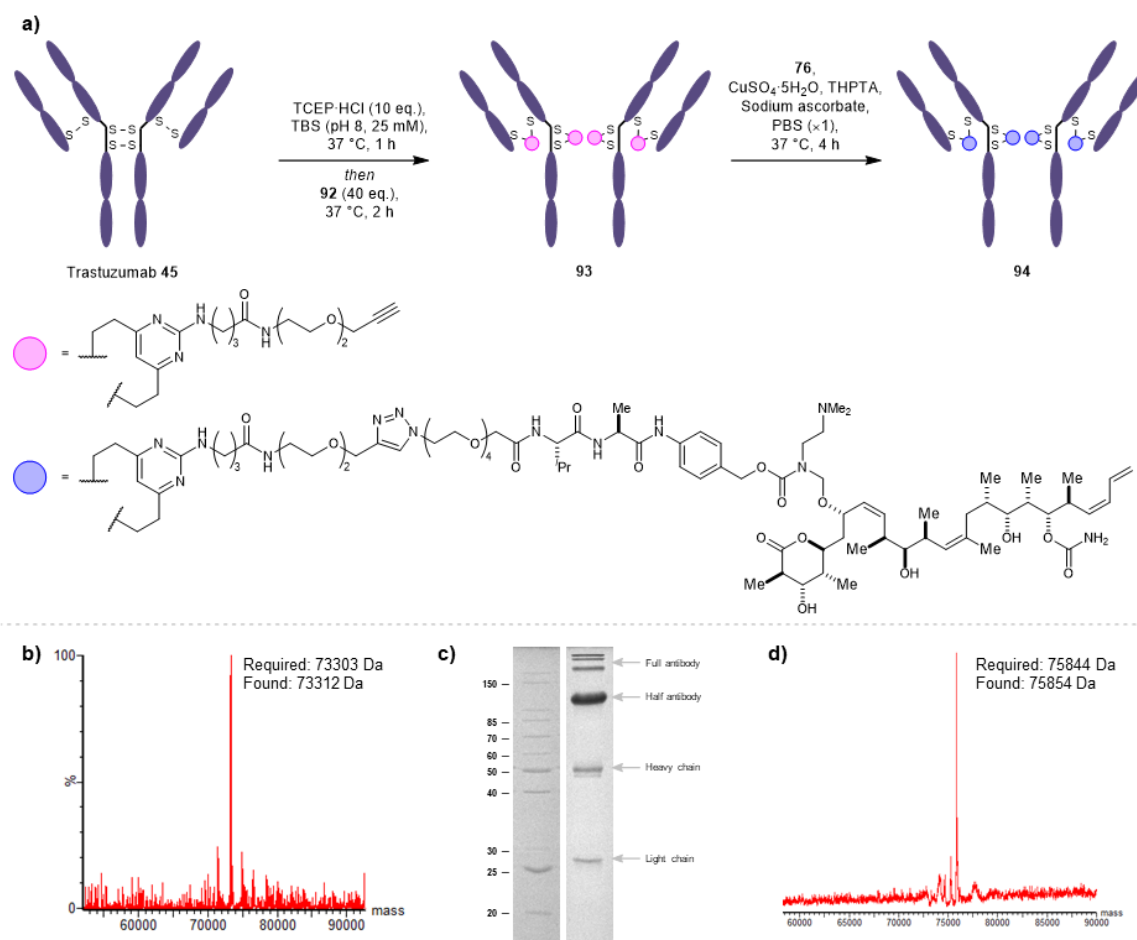


Figure 38. **a)** Synthesis of antibody-discodermolide conjugate **94** from trastuzumab **45** using divinylpyrimidine-alkyne linker **92**. **b)** LCMS analysis of **93** detected the formation of half antibody species. **c)** SDS-PAGE analysis of **93** under reducing conditions revealed the formation of predominantly the half antibody species, with trace amounts of full antibody, unreacted heavy chain, and unreacted light chain. **d)** LCMS analysis of **94** revealed >95% conversion from **93**.

3.9. Conclusion

This chapter describes the synthesis of a novel trastuzumab-discodermolide ADC **94**, the first ADC to employ discodermolide as a cytotoxic payload. A Val-Ala-hemiaminal ether linker was designed to release the cytotoxin in the target cell. The key azide-discodermolide linker-payload **76** was synthesised from aminomethylene chloride reagent **77** in one synthetic step, greatly improving the ease of synthesis compared to other alcohol-releasing linker technologies. The azide-discodermolide **76** was then used to modify trastuzumab, yielding an anti-HER2 ADC **94**.

3.10. Future work

3.10.1. Biological evaluation of discodermolide ADCs

With the successful synthesis of trastuzumab-discodermolide ADC **94**, it is imperative to determine its cytotoxic activity. This will be evaluated in HER2-positive SKBR3 cells and HER2-negative MCF7 cells to demonstrate the selective cell killing of the target cell line.

3.10.2. Confirmation of cleavage mechanism

The Val-Ala dipeptide and the hemiaminal ether motifs have been used separately for ADC drug release, and are well documented.^{93,106} However, it would be useful to determine stability and drug release kinetics for the combined approach that has been developed in this study. This can be achieved by synthesising model systems with a hydroxymethylcoumarin or a fluorinated benzylalcohol group which will assist reaction monitoring by fluorimetry or ¹⁹F NMR spectroscopy, respectively (**Figure 39**). These model systems can be incubated in human plasma for stability studies or reacted with isolated cathepsin enzymes to determine drug release kinetics.

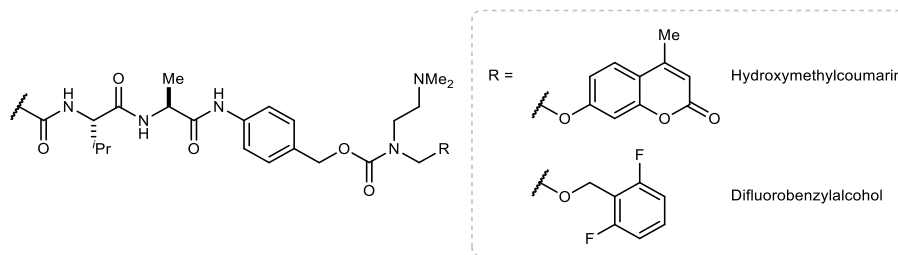


Figure 39. Potential model substrates to interrogate the kinetics and stability of the Val-Ala-*para*-aminobenzylcarbonyl-hemiaminal ether moiety.

3.10.3. Application to other alcohol payloads

Given the success of synthesising trastuzumab-discodermolide ADC **94**, it was envisaged that this approach could be applied to other alcohol cytotoxins. Taxol **95** is a tubulin depolymerisation inhibitor approved by the FDA in 1992 as an anticancer drug, and is listed on World Health Organisation's List of Essential Medicines.¹⁵⁴ Similarly, SN-38 **96** is a topoisomerase I inhibitor, and it is the active component within the prodrug irinotecan **97** – a therapeutic for colon cancer.¹⁵⁵ Both Taxol and SN-38 have low nanomolar potency against their respective targets and have been used as payloads in ADC research. Indeed, SN-38 is the cytotoxic warhead found in the FDA-approved ADC Trodelvy®.²⁷ Given the success of Taxol and SN-38 in generating biologically-active ADCs, it was thought these alcohol drugs would be well suited to explore the scope of the alcohol-release linker (**Figure 40**).

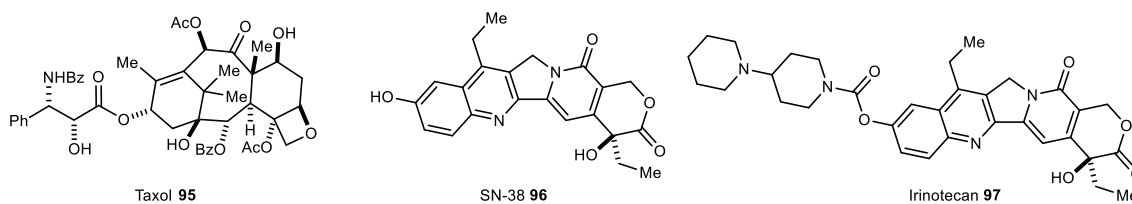


Figure 40. Structure of Taxol **95**, SN-38 **96**, and irinotecan **97**.

Chapter 4. Experimental

4.1. General experimental

All solvents and reagents were used as received unless otherwise stated. Ethyl acetate, methanol, dichloromethane, acetonitrile, and toluene were distilled from calcium hydride. Diethyl ether was distilled from a mixture of lithium aluminium hydride and calcium hydride. Petroleum ether refers to the fraction between 40–60 °C upon distillation. Tetrahydrofuran was dried using Na wire and distilled from a mixture of lithium aluminium hydride and calcium hydride with triphenylmethane as indicator.

Non-aqueous reactions were conducted under a stream of dry nitrogen using oven dried glassware. Temperatures of 0 °C were maintained using an ice-water bath. Room temperature (rt) refers to ambient temperature.

Yields refer to spectroscopically and chromatographically pure compounds unless otherwise stated. Reactions were monitored by thin layer chromatography (TLC) or liquid chromatography mass spectroscopy (LCMS). TLC was performed using glass plates pre-coated with Merck silica gel 60 F254 and visualized by quenching of UV fluorescence ($\lambda_{\text{max}} = 254 \text{ nm}$) or by staining with potassium permanganate, ceric ammonium molybdate, or *para*-anisaldehyde. Retention factors (R_f) are quoted to 0.01.

LCMS was carried out using a Waters ACQUITY HClass UPLC with an ESCi Multi-Mode Ionisation Waters SQ Detector 2 spectrometer using MassLynx 4.1 software; EI refers to the electrospray ionisation technique; LC system: solvent A: 2 mM NH_4OAc in $\text{H}_2\text{O}/\text{MeCN}$ (95:5); solvent B: MeCN; solvent C: 2% formic acid; column: ACQUITY UPLC[®] CSH C18 (2.1 mm \times 50 mm, 1.7 μm , 130 Å) at 40 °C; gradient: 5 – 95 % B with constant 5 % C over 1 min at flow rate of 0.6 mL/min; detector: PDA e λ Detector 220 – 800 nm, interval 1.2 nm.

Flash column chromatography was carried out using slurry-packed Merck 9385 Kieselgel 60 SiO_2 (230-400 mesh) under positive pressure.

Reverse-phase flash column chromatography was carried out using a Combiflash Rf200 automated chromatography system with Redisep[®] reverse-phase C18-silica flash columns (20-40 μm).

Analytical high performance liquid chromatography (HPLC) was performed on Agilent 1260 Infinity machine, using a Supelcosil™ ABZ+PLUS column (150 mm × 4.6 mm, 3 μm) with a linear gradient system (solvent A: 0.05% (v/v) TFA in H₂O; solvent B: 0.05% (v/v) TFA in MeCN) over 20 min at a flow rate of 1 mL/min, and UV detection ($\lambda_{\text{max}} = 220 - 254 \text{ nm}$).

Infrared (IR) spectra were recorded neat on a Perkin-Elmer Spectrum One spectrometer with internal referencing. Selected absorption maxima (ν_{max}) are reported in wavenumbers (cm^{-1}).

Proton and carbon nuclear magnetic resonance (NMR) were recorded using an internal deuterium lock on Bruker DPX-400 (400 MHz, 101 MHz), Bruker Avance 400 QNP (400 MHz, 101 MHz) and Bruker Avance 500 Cryo Ultrashield (500 MHz, 126 MHz). In ¹H NMR, chemical shifts (δ_{H}) are reported in parts per million (ppm), to the nearest 0.01 ppm and are referenced to the residual non-deuterated solvent peak (*CHCl*₃: 7.26, *CHD*₂OD: 3.31, HOD: 4.79). Coupling constants (*J*) are reported in Hertz (Hz) to the nearest 0.1 Hz. Data are reported as follows: chemical shift, integration, multiplicity (s = singlet; d = doublet; t = triplet; q = quartet; pent = pentet; m = multiplet; app = apparent; br = broad; or as a combination of these, e.g. dd, dt etc.), and coupling constant(s). ¹H coupling constants are not corrected. In ¹³C NMR, chemical shifts (δ_{C}) are quoted in ppm, to the nearest 0.1 ppm, and are referenced to the residual non-deuterated solvent peak (*CDCl*₃: 77.16, *CD*₃OD: 49.00).

High resolution mass spectrometry (HRMS) measurements were recorded with a Micromass Q-TOF mass spectrometer or a Waters LCT Premier Time of Flight mass spectrometer. Mass values are reported within the error limits of ±5 ppm mass units. ESI refers to the electrospray ionisation technique.

Protein LCMS was performed on a Xevo G2-S TOF mass spectrometer coupled to an Acquity UPLC system using an Acquity UPLC BEH300 C4 column (1.7 μm, 2.1 × 50 mm). H₂O with 0.1% formic acid (solvent A) and 95% MeCN and 5% water with 0.1% formic acid (solvent B), were used as the mobile phase at a flow rate of 0.2 mL/min. The gradient was programmed as follows: 95% A for 0.93 min, then a gradient to 100% B over 4.28 min, then 100% B for 1.04 minutes, then a gradient to 95% A over 1.04 min. The electrospray source was operated with a capillary voltage of 2.0 kV and a cone voltage of 40 or 150 V. Nitrogen was used as the desolvation gas at a total flow of 850 L/h. Total mass spectra were reconstructed from the ion series using the MaxEnt algorithm preinstalled on MassLynx software (v4.1 from Waters) according to the manufacturer's instructions.

Non-reducing Tris-Glycine SDS-PAGE with 12% acrylamide with 4% stacking gel was performed as standard. Broad range molecular weight marker (10-200 kDa, New England BioLabs) was run in all gels. Samples were prepared by mixing with loading dye and heated to 90 °C for 5 minutes. Loading dye containing β -mercaptoethanol was used to prepare samples under reducing conditions. Gels were run at constant voltage (160 V) for 70 min to 90 min in $\times 1$ Laemmli running buffer. All gels were stained with Coomassie brilliant blue dye and imaged on a Syngene gel imaging system.

Monoclonal antibodies were deglycosylated and reduced prior to LCMS analysis. This was typically performed by adding 0.1 μ L of peptide:*N*-glycosidase F (PNGase F; New England BioLabs Catalogue number P0704S) to a solution of antibody (10 μ L at 1 μ M) and was left to stand at rt for 15 h. To this solution, TCEP·HCl (1 μ L, 5 mM in H₂O) was added and was left to stand at rt for 10 minutes before analysis.

UV-visible (UV-vis) spectra were obtained using a NanoDrop™ One spectrophotometer (ThermoFisher). Raw data was plotted using GraphPad Prism. The following equation¹¹⁷ was used to calculate fluorophore-to-antibody ratio for AlexaFluor488-containing antibodies, where $\epsilon_{280} = 215380 \text{ M}^{-1} \text{ cm}^{-1}$ is the molar extinction coefficient trastuzumab at 280 nm; $\epsilon_{495} = 71000 \text{ M}^{-1} \text{ cm}^{-1}$ is the molar extinction coefficient for AlexaFluor488 at 495 nm; Abs₄₉₅ and Abs₂₈₀ are absorbance at 495 nm and 280 nm, respectively. A correction factor of 0.11 was used to account for AlexaFluor488 absorbance at 280 nm.

$$\text{Fluorophore to antibody ratio} = \frac{\text{Abs}_{495}/\epsilon_{495}}{[\text{Abs}_{280} - 0.11\text{Abs}_{495}]/\epsilon_{280}}$$

4.2. Kinetic studies of conjugate addition

To a solution of linker **2**, **4**, **7**, or **9** [0.7 mL, 20 mM in 3:7 CD₃OD/buffer] in an NMR tube, a solution of Boc-Cys-OMe, Boc-Lys-OMe·HCl, or H-Ala-NH₂·HCl [0.7 mL, 20 mM in 3:7 CD₃OD/buffer] was added and mixed by vigorous shaking.

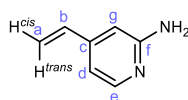
After the first ¹H NMR spectrum (with water suppression) was acquired, subsequent measurements were taken every ~10 minutes for all nucleophile-vinylheteroarene combinations, apart from the reactions between Boc-Cys-OMe and **4**, **7**, or **9**, where measurements were taken every ~15 seconds. The vinyl peaks at 5.52 ppm, 5.75 ppm, and 5.96 ppm were integrated to determine the concentration of substrates **2**, **4**, and **7**, respectively.

4.3. Thioether stability studies

A solution of linker-difluorobenzyl mercaptan conjugate **10**, **11**, or **13** (15 mM), 1-thioglycerol (150 mM), and sodium trifluoroacetate (4.5 mM) in 1:1 (v/v) CD₃CN/NaPi (pH 7.4, 50 mM in H₂O) was prepared. This solution was transferred to an NMR tube, and the atmosphere was purged with argon gas before the tube was sealed. The samples were placed in a water bath at 37 °C for 10 days. ¹⁹F NMR spectra was acquired every day, and the integral of **10**, **11**, or **13** were compared with that of the sodium trifluoroacetate internal standard in order to determine the amount of starting material. The CD₃CN co-solvent was required to ensure solubilisation of substrates in an aqueous solution.

4.4. Chemical synthesis – Chapter 2

4-Vinylpyridin-2-amine (2)

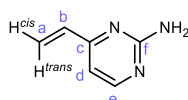


A stirred mixture of 4-bromopyridin-2-amine (250 mg, 1.45 mmol), potassium vinyltrifluoroborate (223 mg, 1.66 mmol), Pd(dppf)Cl₂·CH₂Cl₂ (59 mg, 0.072 mmol) and K₂CO₃ (240 mg, 1.74 mmol) in THF/H₂O (10:1, 5.5 mL) was heated at 70 °C for 14 h. The reaction mixture was filtered through Celite (eluent EtOAc) and the resultant filtrate was

concentrated *in vacuo*. The resulting residue was purified by flash column chromatography (MeOH/CH₂Cl₂, 1:19 with 0.5% Et₃N) to give vinylpyridine **2** (115 mg, 0.957 mmol, 66%) as a dark brown solid.

R_f (SiO₂; MeOH/CH₂Cl₂ 1:10 with 1% Et₃N) 0.60; **v_{max}** (neat/cm⁻¹) 3434, 3291, 3160, 1620, 1598, 1541; **¹H NMR** (MeOD, 400 MHz) δ 7.82 (1H, d, *J* = 5.6 Hz, H_e), 6.70 (1H, dd, *J* = 5.6, 1.6 Hz, H_d), 6.65 – 6.54 (2H, m, H_b, H_g), 5.93 (1H, dd, *J* = 17.6, 0.8 Hz, H_{a^{trans}}), 5.42 (1H, d, *J* = 10.8 Hz, H_{a^{cis}}); **¹³C NMR** (MeOD, 101 MHz) δ 161.3 (C_f), 148.5 (C_c), 147.9 (C_e), 136.5 (C_b), 118.5 (C_a), 111.1 (C_d), 107.7 (C_g); **HRMS** (ESI) [M+H]⁺ required for C₇H₉N₂⁺ 121.0760, found 121.0763,

4-Vinylpyrimidin-2-amine (**4**)

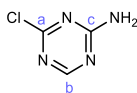


A stirred mixture of 4-chloropyrimidin-2-amine (257 mg, 1.98 mmol), potassium vinyltrifluoroborate (798 mg, 5.96 mmol), Pd(dppf)Cl₂·CH₂Cl₂ (162 mg, 0.198 mmol) and K₂CO₃ (1.65 g, 11.9 mmol) in THF/H₂O (10:1, 6.6 mL) was heated to 70 °C for 16 h. The reaction mixture was filtered through Celite (eluent EtOAc) and the filtrate was concentrated *in vacuo*. The resulting residue was purified by flash column chromatography (EtOAc/petroleum ether, 2:1) to give vinylpyrimidine **4** (175 mg, 1.44 mmol, 73%) as a light brown solid.

R_f (SiO₂; EtOAc/petroleum ether, 2:1) 0.28; **v_{max}** (neat/cm⁻¹) 3335, 3173, 1655, 1565; **¹H NMR** (MeOD, 400 MHz) δ 8.20 (1H, d, *J* = 5.2 Hz, H_e), 6.72 (1H, d, *J* = 5.2 Hz, H_d), 6.60 (1H, dd, *J* = 17.5, 10.7 Hz, H_b), 6.35 (1H, dd, *J* = 17.4, 1.3 Hz, H_{a^{trans}}), 5.62 (1H, dd, *J* = 10.7, 1.3 Hz, H_{a^{cis}}); **¹³C NMR** (MeOD, 101 MHz) δ 165.4 (C_c), 164.7 (C_f), 159.6 (C_e), 136.7 (C_b), 123.0 (C_a), 108.7 (C_d); **HRMS** (ESI) [M+H]⁺ required for C₆H₈N₃⁺ 122.0713, found 122.0715.

Data in accordance with literature.¹¹³

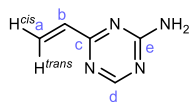
4-Chloro-1,3,5-triazin-2-amine (6)



2,4-Dichloro-1,3,5-triazine (500 mg, 3.33 mmol) was added to a stirred solution of 35% aqueous NH_3 (22.2 mL, 402 mmol) at $-20\text{ }^\circ\text{C}$, and the resulting solution was stirred for 20 min. The reaction mixture was then extracted with EtOAc/*i*PrOH (10:1, $\times 5$). The combined organic extracts were washed with brine ($\times 1$), dried, and concentrated *in vacuo*. The residue was purified by flash column chromatography (EtOAc/petroleum ether, 2:3) to give aminotriazine **6** (162 mg, 1.24 mmol, 37%) as a white solid.

R_f (SiO₂; EtOAc/petroleum ether, 1:1) 0.46; **v_{max}** (neat/cm⁻¹) 3239, 2480, 2396, 2322, 1632, 1500; **¹H NMR** (MeOD, 400 MHz) δ 8.31 (1H, s, H_b); **¹³C NMR** (MeOD, 101 MHz) δ 171.2 (C_a), 168.7 (C_c), 168.2 (C_b); **HRMS** (ESI) [M+H]⁺ required for C₃H₄³⁵ClN₄⁺ 131.0119, found 131.0121.

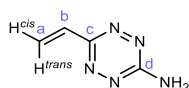
4-Vinyl-1,3,5-triazin-2-amine (7)



A mixture of 4-chloro-1,3,5-triazin-2-amine **6** (148 mg, 1.20 mmol), potassium vinyltrifluoroborate (243 mg, 1.82 mmol), Pd(dppf)Cl₂·CH₂Cl₂ (50 mmol, 0.061 mmol) and K₂CO₃ (200 mg, 1.45 mmol) in 1,4-dioxane/H₂O (10:1, 4.5 mL) was stirred at 90 °C for 15 h. The resulting reaction mixture was filtered through Celite (eluent EtOAc) and the filtrate was concentrated *in vacuo*. The resulting residue was purified by flash column chromatography (EtOAc/petroleum ether, 2:1) to give vinyltriazine **7** (107 mg, 0.876 mmol, 72%) as a white solid.

R_f (SiO₂; EtOAc/petroleum ether, 4:1) 0.47; **v_{max}** (neat/cm⁻¹) 3291, 3142, 1689, 1537, 1504, 1433; **¹H NMR** (MeOD, 400 MHz) δ 8.43 (1H, s, H_d), 6.67 (1H, dd, $J = 17.3, 1.9$ Hz, H_a^{trans}), 6.53 (1H, dd, $J = 17.3, 10.4$ Hz, H_b), 5.81 (1H, dd, $J = 10.4, 1.9$ Hz, H_a^{cis}); **¹³C NMR** (MeOD, 101 MHz) δ 171.8 (C_c), 168.1 (C_e), 167.2 (C_d), 136.3 (C_b), 127.6 (C_a); **HRMS** (ESI) [M+H]⁺ required for C₅H₇N₄⁺ 123.0665, found 123.0668,

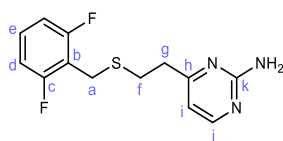
6-Vinyl-1,2,4,5-tetrazin-3-amine (9)



To a stirred solution of 3,6-dichloro-1,2,4,5-tetrazine **8** (100 mg, 0.662 mmol) in ^tBuOMe (3 mL) at rt, ammonia gas was continuously bubbled from a cannister for 10 min. The reaction mixture was then filtered through Celite, and the resulting solution was concentrated *in vacuo*. The residue was dissolved in 1,4-dioxane/H₂O (5:1, 4 mL), and potassium vinyltrifluoroborate (124 mg, 0.927 mmol), Brettphos Pd G3 (30 mg, 0.033 mmol) and Cs₂CO₃ (647 mg, 2.00 mmol) was added. The resulting mixture was stirred at 70 °C over 15 h, filtered through Celite, and the filtrate was concentrated *in vacuo*. The resulting residue was purified by flash column chromatography (petroleum ether/EtOAc, 3:1) to give vinyltetrazine **9** (26 mg, 0.21 mmol, 31% over two steps) as a bright red solid.

R_f (SiO₂; EtOAc/petroleum ether, 1:1) 0.52; **v_{max}** (neat/cm⁻¹) 3291, 3152, 1618, 1553, 1505; **¹H NMR** (MeOD, 400 MHz) δ 6.94 (1H, dd, *J* = 17.6, 11.1 Hz, H_b), 6.51 (1H, dd, *J* = 17.6, 1.3 Hz, H_a^{trans}), 5.68 (1H, dd, *J* = 11.0, 1.3 Hz, H_a^{cis}); **¹³C NMR** (MeOD, 101 MHz) δ 164.3 (C_d), 161.1 (C_c), 131.8 (C_b), 121.2 (C_a); **LRMS** (ESI) [M+H]⁺ required for C₄H₆N₅⁺ 124, found 124,

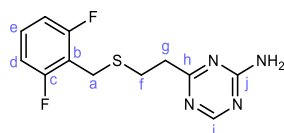
4-(2-((2,6-Difluorobenzyl)thio)ethyl)pyrimidin-2-amine (10)



A solution of vinylpyrimidine **4** (112 mg, 0.938 mmol) and (2,6-difluorophenyl)methanethiol (300 mg, 1.88 mmol) in MeOH (5 mL) and NaPi (pH 8, 500 mM in H₂O, 0.5 mL) was stirred at rt for 15 h. The reaction mixture was concentrated *in vacuo*, and the resulting residue was diluted with H₂O. The aqueous phase was extracted with CH₂Cl₂ (×3), and the combined organic extracts were dried, and concentrated *in vacuo*. The resulting residue was purified *via* flash column chromatography (EtOAc/petroleum ether, 2:1) to give thioether **10** (248 mg, 0.883 mmol, 94%) as a white solid.

R_f (SiO₂; EtOAc/petroleum ether, 2:1) 0.36; **v_{max}** (neat/cm⁻¹) 3333, 3158, 1662, 1646, 1563; **¹H NMR** (CDCl₃, 400 MHz) δ 8.18 (1H, d, *J* = 5.0 Hz, H_j), 7.21 (1H, tt, *J* = 8.4, 6.4 Hz, H_e), 6.95 – 6.83 (2H, m, H_d), 6.48 (1H, d, *J* = 5.1 Hz, H_i), 5.07 (2H, s, NH₂), 3.79 (2H, t, *J* = 1.2 Hz, H_a), 2.92 – 2.80 (4H, m, H_f, H_g); **¹³C NMR** (CDCl₃, 101 MHz) δ 169.7 (C_h), 163.1 (C_k), 161.3 (dd, *J* = 248.6, 7.9 Hz, C_c), 158.3 (C_j), 128.8 (t, *J* = 10.3 Hz, C_e), 115.4 (t, *J* = 19.3 Hz, C_b), 111.5 (dd, *J* = 19.0, 6.6 Hz, C_d), 111.0 (C_i), 37.6 (C_g), 30.5 (C_f), 22.9 (t, *J* = 2.9 Hz, C_a); **¹⁹F NMR** (CDCl₃, 376 MHz) δ -114.96 (t, *J* = 6.8 Hz, F_c); **HRMS** (ESI) [M+H]⁺ required for C₁₃H₁₄F₂N₃S⁺ 282.0876, found 282.0886.

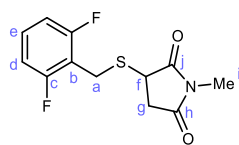
4-(2-((2,6-Difluorobenzyl)thio)ethyl)-1,3,5-triazin-2-amine (11)



A solution of vinyltriazine **7** (114 mg, 0.938 mmol) and (2,6-difluorophenyl)methanethiol (300 mg, 1.88 mmol) in MeOH (5 mL) and NaPi (pH 8, 500 mM in H₂O, 0.5 mL) was stirred at rt for 15 h. The reaction mixture was concentrated *in vacuo*, and the resulting residue was diluted with H₂O. The aqueous phase was extracted with CH₂Cl₂ (×3), and the combined organic extracts were dried, and concentrated *in vacuo*. The resulting residue was purified *via* flash column chromatography (EtOAc/petroleum ether, 2:1) to give thioether **11** (132 mg, 0.468 mmol, 50%) as a white solid.

R_f (SiO₂; EtOAc/petroleum ether, 2:1) 0.29; **v_{max}** (neat/cm⁻¹) 3302, 3171, 3171, 1673, 1626, 1578; **¹H NMR** (CDCl₃, 400 MHz) δ 8.52 (1H, s, H_i), 7.20 (1H, tt, *J* = 8.4, 6.5 Hz, H_e), 6.94 – 6.83 (2H, m, H_d), 5.42 (2H, s, NH₂), 3.81 (2H, t, *J* = 1.2 Hz, H_a), 3.04 – 2.92 (4H, m, H_f, H_g); **¹³C NMR** (CDCl₃, 101 MHz) δ 177.8 (C_h), 166.6 (C_i), 166.3 (C_j), 161.3 (dd, *J* = 248.7, 7.9 Hz, C_c), 128.7 (t, *J* = 10.3 Hz, C_e), 115.4 (t, *J* = 19.3 Hz, C_b), 111.5 (dd, *J* = 19.0, 6.6 Hz, C_d), 38.4 (C_g), 29.0 (C_f), 22.8 (t, *J* = 2.9 Hz, C_a); **¹⁹F NMR** (CDCl₃, 376 MHz) δ -114.93 (t, *J* = 6.7 Hz, F_c); **HRMS** (ESI) [M+H]⁺ required for C₁₂H₁₃F₂N₄S⁺ 283.0829, found 283.0818.

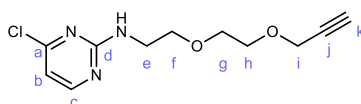
3-((2,6-Difluorobenzyl)thio)-1-methylpyrrolidine-2,5-dione (**13**)



A solution of *N*-methyl maleimide **12** (100 mg, 0.901 mmol) and (2,6-difluorophenyl)methanethiol (216 mg, 1.35 mmol) in MeOH (5 mL) and NaPi (pH 8, 500 mM in H₂O, 0.5 mL) was stirred at rt for 15 h. The reaction mixture was concentrated *in vacuo*, and the resulting residue was purified *via* flash column chromatography (EtOAc/petroleum ether, 1:5) to give thioether **13** (241 mg, 0.888 mmol, 99%) as a light yellow oil.

R_f (SiO₂; EtOAc/petroleum ether, 1:5) 0.14; ν_{\max} (neat/cm⁻¹) 1694; **¹H NMR** (CDCl₃, 400 MHz) δ 7.31 – 7.19 (1H, m, H_e), 6.97 – 6.86 (2H, m, H_d), 4.25 (1H, dt, J = 13.6, 1.1 Hz, H_a^A), 3.99 (1H, dt, J = 13.6, 1.3 Hz, H_a^B), 3.80 (1H, dd, J = 9.1, 4.1 Hz, H_f), 3.11 (1H, dd, J = 18.7, 9.2 Hz, H_g^A), 3.02 (3H, s, H_i), 2.50 (1H, dd, J = 18.7, 4.1 Hz, H_g^B); **¹³C NMR** (CDCl₃, 101 MHz) δ 176.5 (C_{h/j}), 174.7 (C_{h/j}), 161.3 (dd, J = 249.3, 7.7 Hz, C_c), 129.5 (t, J = 10.3 Hz, C_e), 114.2 (t, J = 19.3 Hz, C_b), 111.7 (dd, J = 19.0, 6.4 Hz, C_d), 39.7 (C_f), 36.2 (C_g), 25.3 (C_i), 23.1 (t, J = 3.1 Hz, C_a); **¹⁹F NMR** (CDCl₃, 376 MHz) δ -114.46 (t, J = 6.8 Hz, F_c); **HRMS** (ESI) [M+H]⁺ required for C₁₂H₁₂F₂NO₂S⁺ 272.0557, found 272.0546.

4-Chloro-*N*-(2-(2-(prop-2-yn-1-yloxy)ethoxy)ethyl)pyrimidin-2-amine (**18**)

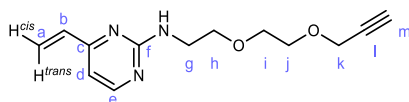


A mixture of 2,4-dichloropyrimidine **17** (458 mg, 3.07 mmol), 2-(2-(prop-2-yn-1-yloxy)ethoxy)ethan-1-amine (400 mg, 2.79 mmol), and Cs₂CO₃ (2.73 g, 8.37 mmol) in dioxane (8 mL) was heated under reflux for 15 h. The resulting suspension was filtered through cotton wool, and the filtrate was concentrated *in vacuo*. The resulting residue was purified *via* flash column chromatography (EtOAc/petroleum ether, 2:3) to give aminopyrimidine **18** (181 mg, 0.708 mmol, 25%) as a colourless oil.

R_f (SiO₂; EtOAc/petroleum ether, 1:1) 0.45; ν_{\max} (neat/cm⁻¹) 3286, 1573, 1522; **¹H NMR** (CDCl₃, 400 MHz) δ 8.14 (1H, d, J = 5.2 Hz, H_a), 6.55 (1H, d, J = 5.1 Hz, H_b), 5.80 (1H, s, NH), 4.21 (2H, d, J = 2.4 Hz, H_i), 3.72 – 3.59 (8H, m, H_e, H_f, H_g, H_h), 2.46 (1H, t, J = 2.4 Hz,

H_k); ¹³C NMR (CDCl₃, 101 MHz) δ 162.4 (C_d), 161.4 (C_a), 159.2 (C_c), 110.1 (C_b), 79.7 (C_j), 74.8 (C_k), 70.3 (C_{f/g/h}), 69.8 (C_{f/g/h}), 69.2 (C_{f/g/h}), 58.6 (C_i), 41.3 (C_e); HRMS (ESI) [M+H]⁺ required for C₁₁H₁₅³⁵ClN₃O₂⁺ 256.1505, found 255.9449.

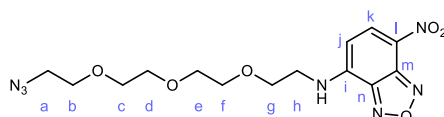
***N*-(2-(2-(Prop-2-yn-1-yloxy)ethoxy)ethyl)-4-vinylpyrimidin-2-amine (19)**



A mixture of **18** (592 mg, 2.31 mmol), potassium vinyltrifluoroborate (930 mg, 6.94 mmol), K₂CO₃ (1.92 g, 13.9 mmol) and Pd(dppf)Cl₂·CH₂Cl₂ (189 mg, 0.232 mmol) in THF/H₂O (10:1, 8 mL) was stirred at 70 °C for 15 h. The resulting suspension was cooled to rt, and EDTA (300 mg, 0.721 mmol) was added. The solution was stirred at rt for 1 h, filtered through Celite, and the filtrate was concentrated *in vacuo*. The resulting residue was purified *via* flash column chromatography (EtOAc/petroleum ether, 1:2) to give vinylpyrimidine **19** (97 mg, 0.39 mmol, 17%) as a colourless oil.

R_f (SiO₂; EtOAc/petroleum ether, 1:1) 0.40; **v_{max}** (neat/cm⁻¹) 3290, 1571; ¹H NMR (CDCl₃, 500 MHz) δ 8.24 (1H, d, *J* = 5.0 Hz, H_e), 6.62 – 6.51 (2H, m, H_b, H_d), 6.34 (1H, dd, *J* = 17.4, 1.5 Hz, H_{a^{trans}}), 5.57 (1H, dd, *J* = 10.6, 1.5 Hz, H_{a^{cis}}), 5.50 (1H, s, NH), 4.22 (2H, d, *J* = 2.4 Hz, H_k), 3.74 – 3.62 (8H, m, H_g, H_h, H_i, H_j), 2.45 (1H, t, *J* = 2.4 Hz, H_m); ¹³C NMR (CDCl₃, 126 MHz) δ 163.2 (C_c), 162.5 (C_f), 158.6 (C_e), 136.0 (C_b), 121.8 (C_a), 108.0 (C_d), 79.7 (C_i), 74.8 (C_m), 70.3 (C_{h/i/j}), 70.2 (C_{h/i/j}), 69.2 (C_{h/i/j}), 58.6 (C_k), 41.2 (C_g); HRMS (ESI) [M+H]⁺ required for C₁₃H₁₈N₃O₂⁺ 248.2051, found 248.1396.

***N*-(2-(2-(2-(2-Azidoethoxy)ethoxy)ethoxy)ethyl)-7-nitrobenzo[*c*][1,2,5]oxadiazol-4-amine (21)**

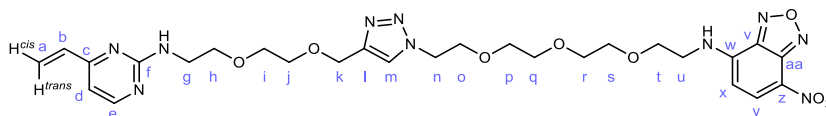


A solution of 4-chloro-7-nitrobenzo[*c*][1,2,5]oxadiazole **20** (200 mg, 1.00 mmol), 2-(2-(2-(2-azidoethoxy)ethoxy)ethoxy)ethan-1-amine (238 μL, 1.20 mmol), and Et₃N (139 μL, 1.00 mmol) in DMF (6 mL) was stirred at rt for 4 h. The resulting solution was diluted with 3 M

LiCl and extracted with EtOAc (×3). The combined organic extracts were washed sequentially with 1 M aqueous HCl (×3), 3 M aqueous LiCl (×3), saturated aqueous Na₂CO₃ (×3), and brine (×2). The organic extracts were dried and concentrated *in vacuo* to provide NBD-azide **21** (280 mL, 0.734 mmol, 73%) as an intensely coloured brown oil.

ν_{\max} (neat/cm⁻¹) 2097, 1579; ¹H NMR (MeOD, 400 MHz) δ 8.38 (1H, d, *J* = 8.9 Hz, H_k), 6.32 (1H, d, *J* = 8.9 Hz, H_j), 3.79 (2H, t, *J* = 5.1 Hz, H_a), 3.70 – 3.53 (12H, m, H_b, H_c, H_d, H_e, H_f, H_g), 3.37 – 3.27 (1H, app m, overlapping with solvent peak, H_h); ¹³C NMR (MeOD, 101 MHz) δ 146.7 (C_{i/l/m/n}), 145.7 (C_{i/l/m/n}), 145.4 (C_{i/l/m/n}), 138.3 (C_k), 123.1 (C_{i/l/m/n}), 100.1 (C_j), 71.6 (C_{b/c/d/e/f/g}), 71.6 (C_{b/c/d/e/f/g}), 71.5 (C_{b/c/d/e/f/g}), 71.5 (C_{b/c/d/e/f/g}), 71.1 (C_{b/c/d/e/f/g}), 69.8 (C_{b/c/d/e/f/g}), 51.7 (C_a), 44.8 (C_h); HRMS (ESI) [M+H]⁺ required for C₁₄H₂₀N₇O₆⁺ 382.1470, found 382.1429.

7-Nitro-N-(2-(2-(2-(2-(4-((2-(2-((4-vinylpyrimidin-2-yl)amino)ethoxy)ethoxy)methyl)-1H-1,2,3-triazol-1-yl)ethoxy)ethoxy)ethoxy)ethyl)benzo[*c*][1,2,5]oxadiazol-4-amine (22)

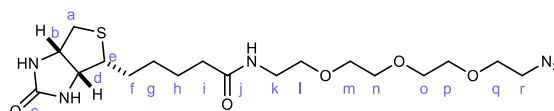


A solution of **19** (24 mg, 0.097 mmol), **21** (56 mg, 0.147 mmol), CuSO₄·5H₂O (30 mg, 0.12 mmol), sodium ascorbate (100 mg, 0.500 mmol) and THPTA (130 mg, 0.300 mmol) in ^tBuOH/H₂O/CH₂Cl₂ (1:1:1, 6 mL) was stirred at rt for 15 h. To this solution, EDTA (100 mg, 0.240 mmol) was added, and the solution was stirred at rt for 1 h. The resulting solution was concentrated under a stream of N₂, and the resulting residue was purified by reverse phase flash column chromatography (10 – 90% solvent B in solvent A. Solvent A: 0.1 M aqueous ammonium hydroxide. Solvent B: MeCN) and lyophilised to give vinylpyrimidine-NBD **22** (25 mg, 0.040 mmol, 41%) as a brown oil.

¹H NMR (MeOD, 700 MHz) δ 8.48 (1H, d, *J* = 8.7 Hz, H_y), 8.16 (1H, d, *J* = 5.1 Hz, H_e), 8.01 (1H, s, H_m), 6.61 (1H, d, *J* = 5.1 Hz, H_d), 6.55 (1H, dd, *J* = 17.4, 10.7 Hz, H_b), 6.38 (1H, d, *J* = 8.8 Hz, H_x), 6.33 (1H, d, *J* = 17.4 Hz, H_a^{cis}), 5.57 (1H, dd, *J* = 10.6, 1.4 Hz, H_a^{trans}), 4.60 (2H, s, H_k), 4.53 (2H, t, *J* = 5.1 Hz, H_n), 3.84 (2H, t, *J* = 5.0 Hz, H_o), 3.78 (2H, t, *J* = 5.2 Hz, H_t), 3.71 – 3.62 (10H, m, H_{h/i/j/p/q/r/s}, H_u), 3.58 – 3.52 (8H, m, H_g, H_{h/i/j/p/q/r/s}); ¹³C NMR (MeOD, 176 MHz) δ 164.8 (C_c), 163.6 (C_f), 159.4 (C_e), 146.7 (C_{v/w/z/aa}), 145.9 (C_{v/w/z/aa}), 145.7 (C_l), 145.5 (C_{v/w/z/aa}), 138.5 (C_y), 136.9 (C_b), 125.9 (C_m), 123.2 (C_{v/w/z/aa}), 122.6 (C_a), 108.5 (C_d),

100.2 (C_x), 71.6 (C_{h/i/j/p/q/r/s}), 71.4 (C_{h/i/j/p/q/r/s}), 71.4 (C_{h/i/j/p/q/r/s}), 71.3 (C_{h/i/j/p/q/r/s}), 70.8 (C_{h/i/j/p/q/r/s}), 70.8 (C_{h/i/j/p/q/r/s}), 70.3 (C_o), 69.8 (C_l), 65.0 (C_k), 51.4 (C_n), 44.8 (C_u), 42.0 (C_g); **HRMS** (ESI) [M+H]⁺ required for C₂₇H₃₇N₁₀O₈⁺ 629.2769, found 629.2819.

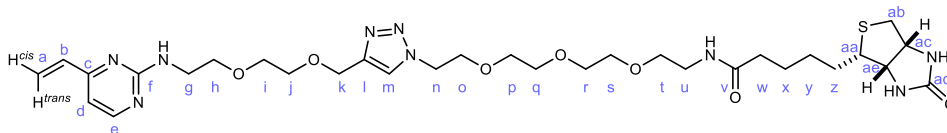
***N*-(2-(2-(2-(2-Azidoethoxy)ethoxy)ethoxy)ethyl)-5-((3*aR*,4*R*,6*aS*)-2-oxohexahydro-1*H*-thieno[3,4-*d*]imidazol-4-yl)pentanamide (24)**



A solution of biotin **23** (460 mmol, 1.89 mmol), EDC·HCl (725 mg, 3.78 mmol), DMAP (460 mg, 3.76 mmol) and ⁱPr₂EtN (983 μL, 5.65 mmol) in DMF (15 mL) was stirred at rt for 20 min. To this solution, 2-(2-(2-(2-azidoethoxy)ethoxy)ethoxy)ethan-1-amine (557 μL, 2.81 mmol) was added before stirring at rt for 15 h. The solution was concentrated *in vacuo* and the resulting residue was purified *via* flash column chromatography (neat CH₂Cl₂ with 1% AcOH → 1:10 MeOH/CH₂Cl₂ with 1% AcOH) to give biotin-azide **24** (686 mg, 1.54 mmol, 84%) as a white solid.

R_f (SiO₂; CH₂Cl₂/MeOH, 10:1) 0.30; **v_{max}** (neat/cm⁻¹) 2103, 1682, 1639; **¹H NMR** (MeOD, 400 MHz) δ 4.50 (1H, ddd, *J* = 7.9, 5.0, 1.0 Hz, H_b), 4.31 (1H, dd, *J* = 7.9, 4.4 Hz, H_d), 3.71 – 3.60 (10H, m, H_{l/m/n/o/p/q}), 3.55 (2H, t, *J* = 5.5 Hz, H_{l/m/n/o/p/q}), 3.40 – 3.34 (4H, m, H_k, H_r), 3.21 (1H, ddd, *J* = 8.8, 5.9, 4.5 Hz, H_e), 2.93 (1H, dd, *J* = 12.8, 5.0 Hz, H_a^A), 2.71 (1H, d, *J* = 12.7 Hz, H_a^B), 2.22 (2H, t, *J* = 7.4 Hz, H_i), 1.80 – 1.53 (4H, m, H_{f/g/h}), 1.44 (2H, pent, *J* = 7.5 Hz, H_{f/g/h}); **¹³C NMR** (MeOD, 101 MHz) δ 174.7 (C_j), 164.7 (C_c), 70.2 (C_{l/m/n/o/p/q}), 70.2 (C_{l/m/n/o/p/q}), 70.1 (C_{l/m/n/o/p/q}), 69.9 (C_{l/m/n/o/p/q}), 69.7 (C_{l/m/n/o/p/q}), 69.2 (C_{l/m/n/o/p/q}), 62.0 (C_d), 60.2 (C_b), 55.6 (C_e), 50.4 (C_r), 39.7 (C_a), 39.0 (C_k), 35.3 (C_i), 28.4 (C_{f/g/h}), 28.1 (C_{f/g/h}), 25.5 (C_{f/g/h}); **HRMS** (ESI) [M+Na]⁺ required for C₁₈H₃₂N₆O₅SNa⁺ 467.2047, found 467.1966.

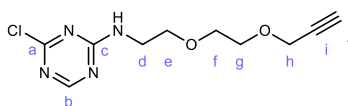
5-((3a*S*,4*S*,6a*R*)-2-Oxohexahydro-1*H*-thieno[3,4-*d*]imidazol-4-yl)-*N*-(2-(2-(2-(2-(4-((2-(2-((4-vinylpyrimidin-2-yl)amino)ethoxy)ethoxy)methyl)-1*H*-1,2,3-triazol-1-yl)ethoxy)ethoxy)ethoxy)ethyl)pentanamide (25)



A solution of **19** (30 mg, 0.12 mmol), **24** (107 mg, 0.243 mmol), CuSO₄·5H₂O (37 mg, 0.15 mmol), THPTA (158 mg, 0.364 mmol) and sodium ascorbate (121 mg, 0.607 mmol) in ^tBuOH/CH₂Cl₂/H₂O (1:1:1, 6 mL) was stirred at rt for 15 h. To this solution, EDTA (100 mg, 0.240 mmol) was added, and the solution was stirred at rt for 1 h. The resulting solution was concentrated under a stream of N₂, and the resulting residue was purified by reverse phase flash column chromatography (10 – 90% solvent B in solvent A. Solvent A: 0.1 M aqueous ammonium hydroxide. Solvent B: MeCN) and lyophilised to give vinylpyrimidine-biotin **25** (19 mg, 0.028 mmol, 23%) as a white solid.

¹H NMR (MeOD, 400 MHz) δ 8.20 (1H, d, *J* = 5.1 Hz, H_e), 8.04 (1H, s, H_m), 6.66 (1H, d, *J* = 5.2 Hz, H_d), 6.60 (1H, dd, *J* = 17.4, 10.6 Hz, H_b), 6.37 (1H, dd, *J* = 17.5, 1.5 Hz, H_a^{trans}), 5.60 (1H, dd, *J* = 10.7, 1.5 Hz, H_a^{cis}), 4.64 (2H, s, H_k), 4.58 (2H, dd, *J* = 5.6, 4.6 Hz, H_n), 4.48 (1H, ddd, *J* = 7.9, 5.0, 1.0 Hz, H_{ac}), 4.29 (1H, dd, *J* = 7.9, 4.4 Hz, H_{ae}), 3.89 (2H, dd, *J* = 5.6, 4.6 Hz, H_o), 3.70 – 3.57 (16H, m, H_{g/h/i/j/p/q/r/s}), 3.52 (2H, t, *J* = 5.5 Hz, H_t), 3.34 (2H, t, *J* = 5.5 Hz, H_u), 3.19 (1H, ddd, *J* = 8.9, 5.9, 4.4 Hz, H_{aa}), 2.91 (1H, dd, *J* = 12.7, 5.0 Hz, H_a^A), 2.69 (1H, d, *J* = 12.7 Hz, H_a^B), 2.19 (2H, t, *J* = 7.5 Hz, H_w), 1.79 – 1.52 (4H, m, H_{x/y/z}), 1.49 – 1.34 (2H, m, H_{x/y/z}); **¹³C NMR** (MeOD, 101 MHz) δ 176.1 (C_v), 166.1 (C_{ad}), 164.9 (C_c), 163.7 (C_f), 159.5 (C_e), 145.8 (C_l), 137.0 (C_b), 125.9 (C_m), 122.6 (C_a), 108.5 (C_d), 71.5 (C_{h/i/j/p/q/r/s}), 71.5 (C_{h/i/j/p/q/r/s}), 71.4 (C_{h/i/j/p/q/r/s}), 71.3 (C_{h/i/j/p/q/r/s}), 71.2 (C_{h/i/j/p/q/r/s}), 70.8 (C_{h/i/j/p/q/r/s}), 70.8 (C_{h/i/j/p/q/r/s}), 70.6 (C_t), 70.4 (C_o), 65.1 (C_k), 63.4 (C_{ae}), 61.6 (C_{ac}), 57.0 (C_{aa}), 51.4 (C_n), 42.0 (C_g), 41.0 (C_{ab}), 40.3 (C_u), 36.7 (C_v), 29.8 (C_{x/y/z}), 29.5 (C_{x/y/z}), 26.8 (C_{x/y/z}); **HRMS** (ESI) [M+H]⁺ required for C₃₁H₅₀N₉O₇S⁺ 692.3549, found 692.3698.

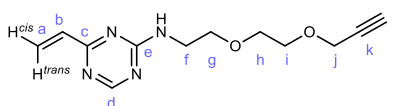
4-Chloro-*N*-(2-(2-(prop-2-yn-1-yloxy)ethoxy)ethyl)-1,3,5-triazin-2-amine (**31**)



2-(2-(Prop-2-yn-1-yloxy)ethoxy)ethan-1-amine (99 μ L, 0.698 mmol) was added to a solution of 2,4-dichloro-1,3,5-triazine **30** (104 mg, 0.698 mmol) and t Pr₂EtN (365 μ L, 0.838 mmol) in THF (5 mL) at 0 °C. The resulting solution was stirred at 0 °C for 2 h. The solution was concentrated *in vacuo*, and the resulting residue was purified *via* flash column chromatography (EtOAc/petroleum ether, 1:2) to give aminotriazine **31** (90 mg, 0.362 mmol, 52%) as a colourless oil.

R_f (SiO₂; EtOAc/petroleum ether, 1:1) 0.22; **v_{max}** (neat/cm⁻¹) 3279, 2118, 1587, 1561; **¹H NMR** (CDCl₃, 400 MHz, mixture of rotamers) δ 8.37 (1H, app d, $J = 29.6$ Hz, H_b), 6.40 (1H, app d, $J = 73.1$ Hz, NH), 4.22 (2H, app dd, $J = 2.4, 1.3$ Hz, H_a), 3.76 – 3.62 (8H, m, H_{d/e/f/g}), 2.46 (1H, app td, $J = 2.4, 1.0$ Hz, H_j); **¹³C NMR** (CDCl₃, 101 MHz, mixture of rotamers) δ 170.9 (C_a), 170.1 (C_a), 167.4 (C_b), 166.7 (C_b), 165.7 (C_c), 165.6 (C_c), 79.5 (C_d), 79.5 (C_d), 74.9 (C_{e/f/g}), 70.5 (C_{e/f/g}), 70.4 (C_{e/f/g}), 69.3 (C_{e/f/g}), 69.3 (C_{e/f/g}), 69.2 (C_{e/f/g}), 69.2 (C_{e/f/g}), 58.6 (C_h), 58.6 (C_h), 41.2 (C_j), 41.0 (C_j); **HRMS** (ESI) [M+H]⁺ required for C₁₀H₁₄³⁵ClN₄O₂⁺ 257.0800, found 257.0795.

N-(2-(2-(Prop-2-yn-1-yloxy)ethoxy)ethyl)-4-vinyl-1,3,5-triazin-2-amine (**32**)

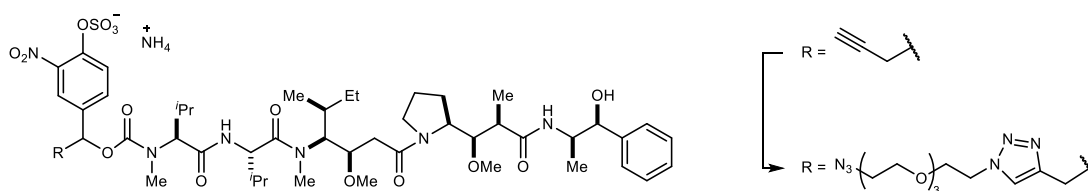


A mixture of **31** (369 mg, 1.44 mmol), potassium vinyltrifluoroborate (630 mg, 4.71 mmol), Cs₂CO₃ (3.07 g, 9.42 mmol) and Pd(dppf)Cl₂·CH₂Cl₂ (128 mg, 0.157 mmol) in dioxane/H₂O (10:1, 8 mL) was heated to 90 °C for 15 h. The resulting mixture was cooled to rt, and EDTA (300 mg, 0.721 mmol) was added. The suspension was stirred at rt for 1 h, filtered through Celite, and the filtrate was concentrated *in vacuo*. The resulting residue was purified *via* flash column chromatography (EtOAc/petroleum ether, 1:1) to give vinyltriazine **32** (200 mg, 0.805 mmol, 56%) as a colourless oil.

R_f (SiO₂; EtOAc) 0.58; **v_{max}** (neat/cm⁻¹) 1591; **¹H NMR** (CDCl₃, 400 MHz, mixture of rotamers) δ 8.53 (1H, app d, $J = 31.0$ Hz, H_d), 6.73 – 6.47 (2H, m, H_{a^{trans}}, H_b), 6.11 (1H, app d,

$J = 44.5$ Hz, NH), 5.79 (1H, dd, $J = 10.3, 2.2$ Hz, H_a^{cis}), 4.22 (2H, d, $J = 2.4$ Hz, H_j), 3.69 (8H, ddd, $J = 8.6, 6.2, 3.4$ Hz, H_f, H_g, H_h, H_i), 2.46 (1H, t, $J = 2.4$ Hz, H_l); ^{13}C NMR (CDCl_3 , 101 MHz, mixture of rotamers) δ 170.8 (C_c), 170.5 (C_c), 166.4 (C_d), 166.1 (C_d), 165.4 (C_e), 165.3 (C_e), 136.0 (C_b), 135.6 (C_b), 126.9 (C_a), 79.6 (C_k), 74.9 (C_l), 70.4 ($C_{g/h/i}$), 69.7 ($C_{g/h/i}$), 69.2 ($C_{g/h/i}$), 58.6 (C_j), 40.8 (C_f), 40.6 (C_f); **HRMS** (ESI) $[\text{M}+\text{H}]^+$ required for $\text{C}_{12}\text{H}_{17}\text{N}_4\text{O}_2^+$ 249.2003, found 249.1345.

Azide-PEG₃-arylsulfate-MMAE (42)

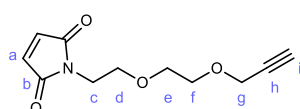


Compound synthesised by J. D. Bargh.

A degassed solution of $\text{CuSO}_4 \cdot 5\text{H}_2\text{O}$ (0.24 mg, 0.95 μmol), THPTA (0.83 mg, 1.9 μmol) and sodium ascorbate (0.76 mg, 3.8 μmol) in $\text{H}_2\text{O}/\text{BuOH}$ (0.2 mL, 1:1) was added to a degassed solution of alkynyl-arylsulfate-MMAE (2.00 mg, 1.91 μmol ; synthesised according to literature procedures¹⁰⁹) and $\text{N}_3\text{-PEG}_3\text{-N}_3$ (1.99 μL , 9.54 μmol) in $\text{H}_2\text{O}/\text{BuOH}$ (0.1 mL, 1:1). The reaction mixture was stirred at rt for 15 min before being purified by reverse-phase flash column chromatography (25-100% solvent B in solvent A. Solvent A: 0.1 M NH_4OH (aq). Solvent B: MeCN) and lyophilised to yield azide **42** (1.56 mg, 1.21 μmol , 63%) as a white solid.

LRMS (ESI) m/z found $[\text{M}-\text{H}^+]$ 1274.0 $\text{C}_{58}\text{H}_{89}\text{N}_{12}\text{O}_{18}^{32}\text{S}^-$ required 1273.6; **HPLC** retention time 12.180 min.

1-(2-(2-(Prop-2-yn-1-yloxy)ethoxy)ethyl)-1H-pyrrole-2,5-dione (44)



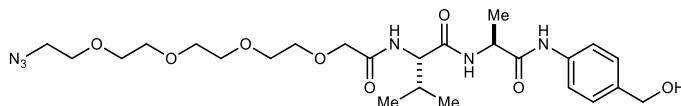
A solution of 2-(2-(prop-2-yn-1-yloxy)ethoxy)ethan-1-amine (122 mg, 0.852 mmol) and maleic anhydride **43** (84 mg, 0.85 mmol) was heated under reflux for 15 h. The resulting

solution was concentrated *in vacuo* and purified *via* flash column chromatography (EtOAc/petroleum ether, 1:2) to give maleimide **44** (94 mg, 0.42 mmol, 49%) as a light yellow oil.

R_f (SiO₂; EtOAc/petroleum ether, 1:1) 0.47; **v_{max}** (neat/cm⁻¹) 1699; **¹H NMR** (CDCl₃, 400 MHz) δ 6.72 (2H, s, H_a), 4.17 (2H, app d, *J* = 2.4 Hz, H_g), 3.74 (2H, app td, *J* = 5.6, 0.9 Hz, H_c), 3.67 – 3.62 (6H, m, H_d, H_e, H_f), 2.44 (1H, app t, *J* = 2.4 Hz, H_i); **¹³C NMR** (CDCl₃, 101 MHz) δ 170.7 (C_b), 134.2 (C_a), 79.7 (C_h), 74.6 (C_i), 69.9 (C_{e/f}), 69.1 (C_{e/f}), 67.9 (C_d), 58.4 (C_g), 37.1 (C_g); **HRMS** (ESI) [M+H]⁺ required for C₁₁H₁₄NO₄⁺ 224.0918, found 224.1000.

4.5. Chemical synthesis – Chapter 3

14-Azido-*N*-((*S*)-1-(((*S*)-1-(4-(hydroxymethyl)phenyl)amino)-1-oxopropan-2-yl)amino)-3-methyl-1-oxobutan-2-yl)-3,6,9,12-tetraoxatetradecanamide (**80**)



Step 1:

A solution of Alloc-Val-Ala-PAB-OH **78** (189 mg, 0.500 mmol), Pd(PPh₃)₄ (29 mg, 0.03 mmol), and pyrrolidine (84 μL, 1.0 mmol) in CH₂Cl₂/DMF (7:1, 20 mL) was stirred at rt over 15 h. The resulting solution was concentrated *in vacuo*.

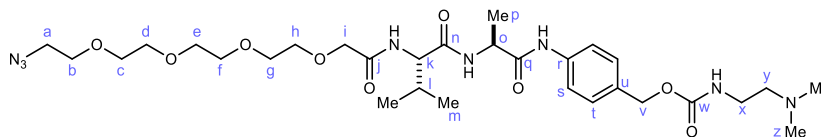
Step 2:

HATU (200 mg, 0.525 mmol) was added to a solution of 14-azido-3,6,9,12-tetraoxa-1-tetradecanoic acid (0.5 M in ^tBuOMe, 1.1 mL, 0.52 mmol) and ^tPr₂EtN (348 μL, 2.00 mmol) in DMF (8 mL), and the resulting solution was stirred at rt for 5 min. The solution was transferred to the flask containing the residue from the previous step, and the resulting solution was stirred at rt for 2 h. The solution was concentrated *in vacuo* and purified *via* reverse phase flash column chromatography (5% to 100 MeCN in 0.5% aqueous formic acid). Lyophilisation gave **80** (198 mg, 0.358 mmol, 72% over two steps) as a white powder.

R_f (SiO₂; MeOH/CH₂Cl₂, 100:5) 0.29; **¹H NMR** (MeOD, 400 MHz) δ 7.59 – 7.51 (2H, m), 7.33 – 7.27 (2H, m), 4.56 (2H, s), 4.48 (1H, q, *J* = 7.1 Hz), 4.31 (1H, d, *J* = 7.0 Hz), 4.06 (2H, s), 3.74 – 3.59 (14H, m), 3.34 (2H, t, *J* = 4.9 Hz), 2.21 – 2.06 (1H, m, *J* = 6.8 Hz), 1.44 (3H, d, *J* = 7.1 Hz), 0.99 (6H, dd, *J* = 15.1, 6.8 Hz); **¹³C NMR** (MeOD, 101 MHz) δ 173.0, 172.9, 172.7, 138.8, 138.6, 128.6, 121.1, 72.2, 71.6, 71.6, 71.5, 71.4, 71.1, 71.1, 64.8, 59.4, 51.7, 51.1, 32.4, 19.8, 18.7, 18.0; **LRMS** (ESI) [M+H]⁺ required for C₂₅H₄₁N₆O₈⁺ 553, found 553.

Data in accordance with literature.¹¹⁶

4-((2*S*,5*S*)-20-Azido-5-isopropyl-2-methyl-4,7-dioxo-9,12,15,18-tetraoxa-3,6-diazaicosanamido)benzyl (2-(dimethylamino)ethyl)carbamate (82**)**



Step 1:

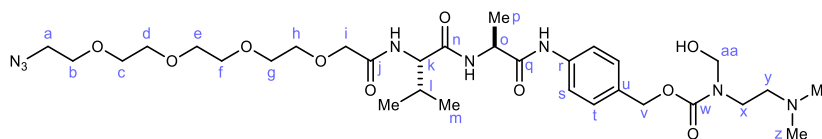
A solution of **80** (149 mg, 0.270 mmol), bis(4-nitrophenyl) carbonate (205 mg, 0.675 mmol), i Pr₂EtN (376 μ L, 2.16 mmol) in DMF (5 mL) was stirred at rt for 15 h. The resulting solution was diluted with EtOAc and washed successively with 3 M aqueous LiCl ($\times 3$), aqueous saturated Na₂CO₃ ($\times 10$) and brine ($\times 1$). The organic extract was dried and concentrated *in vacuo*.

Step 2:

The residue from Step 1 was dissolved in CH₂Cl₂ (5 mL), and *N,N*-dimethylethylenediamine (295 μ L, 2.70 mmol) was added to the solution. The resulting solution was stirred at rt for 3 h, before concentrating *in vacuo*. The residue was diluted with saturated aqueous Na₂CO₃ and extracted with EtOAc ($\times 3$). The combined organic extracts were washed with brine ($\times 1$), dried (Na₂SO₄), and concentrated *in vacuo*. Purification of the resulting residue *via* flash column chromatography (MeOH/CH₂Cl₂, 5:100 \rightarrow 15:100) gave **82** (111 mg, 0.166 mmol, 62% over two steps) as a light yellow oil.

R_f (SiO₂; MeOH/CH₂Cl₂, 15:85) 0.31; ν_{\max} (neat/cm⁻¹) 3272, 2103, 1690, 1637, 1532; **¹H NMR** (CDCl₃, 400 MHz) δ 8.67 (1H, s, NH), 7.57 – 7.50 (2H, m, H_s), 7.34 (1H, d, $J = 8.1$ Hz, NH), 7.29 (2H, d, $J = 8.4$ Hz, H_t), 6.95 (1H, d, $J = 7.1$ Hz, NH), 5.35 (1H, s, NH), 5.03 (2H, s, H_v), 4.63 (1H, pent, $J = 7.1$ Hz, H_o), 4.28 (1H, dd, $J = 8.1, 6.8$ Hz, H_k), 4.13 – 4.00 (2H, m, H_i), 3.78 – 3.58 (14H, m, H_b, H_c, H_d, H_e, H_f, H_g, H_h), 3.37 (2H, t, $J = 5.0$ Hz, H_a), 3.28 (2H, q, $J = 5.8$ Hz, H_x), 2.43 (2H, t, $J = 6.0$ Hz, H_y), 2.23 (7H, s, H_k, H_z), 1.45 (3H, d, $J = 7.1$ Hz, H_p), 0.97 (6H, dd, $J = 6.8, 3.6$ Hz, H_m); **¹³C NMR** (CDCl₃, 101 MHz) δ 171.6 (C_n), 171.0 (C_j), 170.1 (C_q), 156.6 (C_w), 137.9 (C_r), 132.6 (C_u), 129.1 (C_i), 119.9 (C_s), 71.3 (C_{b/c/d/e/f/g/h/i}), 70.8 (C_{b/c/d/e/f/g/h/i}), 70.8 (C_{b/c/d/e/f/g/h/i}), 70.77 (C_{b/c/d/e/f/g/h/i}), 70.72 (C_{b/c/d/e/f/g/h/i}), 70.5 (C_{b/c/d/e/f/g/h/i}), 70.4 (C_{b/c/d/e/f/g/h/i}), 70.2 (C_{b/c/d/e/f/g/h/i}), 66.4 (C_v), 58.9 (C_k), 58.2 (C_y), 50.8 (C_a), 49.8 (C_o), 45.2 (C_z), 38.4 (C_x), 30.6 (C_i), 19.5 (C_m), 18.4 (C_m), 17.2 (C_p); **HRMS** (ESI) [M+H]⁺ required for C₃₀H₅₁N₈O₉⁺ 667.3779, found 667.3786.

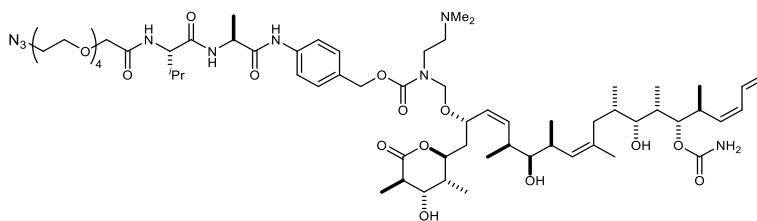
4-((2*S*,5*S*)-20-Azido-5-isopropyl-2-methyl-4,7-dioxo-9,12,15,18-tetraoxa-3,6-diazaicosanamido)benzyl (2-(dimethylamino)ethyl)(hydroxymethyl)carbamate (83**)**



A solution of **82** (111 mg, 0.166 mmol), paraformaldehyde (100 mg, 3.33 mmol as monomer), and TMSCl (200 μ L, 1.59 mmol) in CH₂Cl₂ (5 mL) was stirred at rt for 3 h. To this reaction mixture saturated aqueous Na₂CO₃ (1 mL) was added, and the resulting solution was concentrated *in vacuo*. The residue was diluted with saturated aqueous Na₂CO₃ and extracted with EtOAc (\times 3). The combined organic extracts were dried and concentrated *in vacuo*, before purification *via* flash column chromatography (MeOH/CH₂Cl₂, 2.5:100 \rightarrow 10:100) to give **83** (93 mg, 0.13 mmol, 80%) as a yellow oil.

R_f (SiO₂; MeOH/CH₂Cl₂, 10:90) 0.23; **v_{max}** (neat/cm⁻¹) 3292, 2923, 2107, 1651, 1516; **¹H NMR** (CDCl₃, 400 MHz, rotameric) δ 8.78 (1H, d, J = 16.8 Hz, NH), 7.54 (2H, t, J = 7.8 Hz, H_s), 7.36 (1H, d, J = 8.2 Hz, NH), 7.34 – 7.25 (2H, m, H_t), 7.14 (1H, d, J = 7.3 Hz, NH), 5.11 (2H, d, J = 6.3 Hz, H_v), 4.74 (2H, d, J = 8.9 Hz, H_{aa}), 4.63 (1H, pent, J = 7.1 Hz, H_o), 4.32 (1H, dd, J = 9.4, 7.0 Hz, H_k), 4.13 – 4.00 (2H, m, H_i), 3.72 – 3.64 (14H, m, H_b, H_c, H_d, H_e, H_f, H_g, H_h), 3.49 (2H, ddd, J = 12.0, 7.5, 3.8 Hz, H_x), 3.37 (2H, t, J = 5.0 Hz, H_a), 2.48 – 2.35 (2H, m, H_y), 2.30 (6H, d, J = 13.6 Hz, H_z), 2.25 – 2.13 (1H, m, H_l), 1.44 (3H, d, J = 7.3 Hz, H_p), 0.97 (6H, dd, J = 6.8, 4.2 Hz, H_m); **¹³C NMR** (CDCl₃, 101 MHz, rotameric) δ 171.5 (C_n), 170.94 (C_j), 170.85 (C_j), 170.3 (C_q), 170.2 (C_q), 155.7 (C_w), 155.6 (C_w), 138.1 (C_r), 137.9 (C_r), 132.5 (C_u), 132.3 (C_u), 129.0 (C_t), 128.9 (C_t), 120.0 (C_s), 119.9 (C_s), 73.3 (C_{aa}), 72.7 (C_{aa}), 71.4 (C_{b/c/d/e/f/g/h/i}), 71.3 (C_{b/c/d/e/f/g/h/i}), 70.8 (C_{b/c/d/e/f/g/h/i}), 70.7 (C_{b/c/d/e/f/g/h/i}), 70.7 (C_{b/c/d/e/f/g/h/i}), 70.7 (C_{b/c/d/e/f/g/h/i}), 70.5 (C_{b/c/d/e/f/g/h/i}), 70.4 (C_{b/c/d/e/f/g/h/i}), 70.1 (C_{b/c/d/e/f/g/h/i}), 67.1 (C_v), 59.2 (C_y), 58.7 (C_k), 58.4 (C_y), 50.8 (C_a), 49.8 (C_o), 47.1 (C_x), 46.6 (C_x), 45.0 (C_z), 44.9 (C_z), 30.7 (C_l), 19.4 (C_m), 18.4 (C_m), 17.3 (C_p); **HRMS** (ESI) [M+H]⁺ required for C₃₁H₅₃N₈O₁₀⁺ 697.3879, found 697.3885.

Azide-discodermolide (**76**)



Step 1:

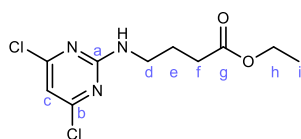
A solution of hemiaminal **83** (5.2 mg, 7.5 μmol) and TMSCl (40 μL , 370 μmol) in CH_2Cl_2 (400 μL) was stirred at rt for 1 h. The resulting reaction mixture was concentrated *in vacuo* to give aminomethylene chloride **77**.

Step 2:

To the residue from previous step K_3PO_4 (1.4 mg, 6.6 μmol), (+)-discodermolide **53** (2.4 mg, 4.0 μmol) and CH_2Cl_2 (200 μL) were added, and the resulting mixture was stirred at rt for 3 h. The resulting reaction mixture was quenched with H_2O (20 μL), concentrated *in vacuo*, and purified *via* preparatory HPLC (5% to 95% Solvent B in Solvent A. Solvent A: 0.1% (v/v) TFA in water. Solvent B: 0.05% (v/v) TFA in MeCN) to give azide-discodermolide **76** (0.6 mg, 0.5 μmol , 12%) as a light yellow oil.

LC 1.31 min; HRMS (ESI) $[\text{M}+\text{H}]^+$ required for $\text{C}_{64}\text{H}_{106}\text{N}_9\text{O}_{17}^+$ 1272.7701, found 1272.7720.

Ethyl 4-((4,6-dichloropyrimidin-2-yl)amino)butanoate (**89**)



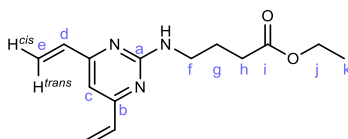
A solution of 2,4,6-trichloropyrimidine **88** (2.00 g, 10.9 mmol), ethyl 4-aminobutanoate hydrochloride (1.83 g, 10.9 mmol), and Et_3N (3.80 mL, 27.3 mmol) in acetone was stirred at 0 $^\circ\text{C}$ for 1.5 h. The resulting solution was concentrated *in vacuo* and purified *via* flash column chromatography (EtOAc/petroleum ether, 1:5) to give **89** (819 mg, 2.95 mmol, 27%) as a colourless oil.

R_f (SiO_2 ; EtOAc/petroleum ether, 1:4) 0.38; $^1\text{H NMR}$ (CDCl_3 , 700 MHz) δ 6.55 (1H, dd, $J = 3.3, 1.8$ Hz, H_c), 6.18 (1H, s, NH), 4.11 (2H, app qd, $J = 7.2, 2.2$ Hz, H_h), 3.47 (2H, q, $J = 6.6$

Hz, H_d), 2.36 (2H, td, $J = 7.3, 2.0$ Hz, H_f), 1.93 – 1.88 (2H, m, H_e), 1.22 (3H, td, $J = 7.2, 2.4$ Hz, H_i); ¹³C NMR (CDCl₃, 176 MHz) δ 173.2 (C_g), 161.9 (C_a), 108.9 (C_c), 60.6 (C_h), 40.9 (C_d), 31.6 (C_f), 24.6 (C_e), 14.3 (C_i) [¹³C NMR peak for C_b was not observed]; LRMS (ESI) [M+H]⁺ required for C₁₀H₁₄³⁵Cl₂N₃O₂⁺ 278, found 278.

These data correspond with those in literature.¹⁰⁹

Ethyl 4-((4,6-divinylpyrimidin-2-yl)amino)butanoate (**90**)

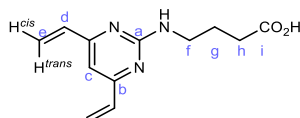


A solution of **89** (819 mg, 2.95 mmol), potassium trifluorovinylborate (2.37 g, 17.7 mmol), K₂CO₃ (4.89 g, 35.4 mmol), Pd(dppf)Cl₂·CH₂Cl₂ (490 mg, 0.600 mmol), and H₂O (2 mL) in THF (20 mL) was heated under reflux for 15 h. The solution was cooled, filtered through Celite, and concentrated *in vacuo*. The resulting residue was purified *via* flash column chromatography (EtOAc/petroleum ether, 1:4) to give **90** (737 mg, 2.83 mmol, 96%) as a colourless oil.

R_f (SiO₂; EtOAc/petroleum ether, 1:3) 0.35; **v_{max}** (neat/cm⁻¹) 3295, 1728, 1539; **¹H NMR** (CDCl₃, 400 MHz) δ 6.56 (2H, dd, $J = 17.4, 10.6$ Hz, H_e^{trans}), 6.51 (1H, s, H_c), 6.34 (2H, d, $J = 17.3$ Hz, H_d), 5.54 (2H, dd, $J = 10.6, 1.7$ Hz, H_e^{cis}), 5.21 (1H, t, $J = 6.2$ Hz, NH), 4.11 (2H, q, $J = 7.1$ Hz, H_j), 3.52 (2H, q, $J = 6.6$ Hz, H_f), 2.39 (2H, t, $J = 7.4$ Hz, H_h), 1.94 (2H, app pent, $J = 7.1$ Hz, H_g), 1.22 (3H, t, $J = 7.1$ Hz, H_k); **¹³C NMR** (CDCl₃, 101 MHz) δ 173.6 (C_i), 163.8 (C_b), 162.7 (C_a), 136.0 (C_d), 121.4 (C_e), 105.8 (C_c), 60.5 (C_j), 40.8 (C_f), 31.9 (C_h), 25.2 (C_g), 14.3 (C_k); **HRMS** (ESI) [M+H]⁺ required for C₁₄H₂₀N₃O₂⁺ 262.1550, found 262.1556.

These data correspond with those reported in literature.¹⁰⁹

4-((4,6-Divinylpyrimidin-2-yl)amino)butanoic acid (**91**)

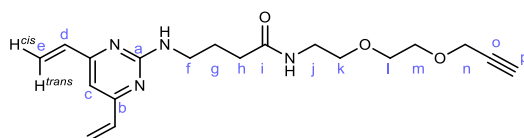


A solution of **90** (737 mg, 2.82 mmol) and LiOH monohydrate (280 mg, 6.68 mmol) in THF (18 mL) and H₂O (18 mL) was stirred at rt for 15 h. The resulting solution was concentrated *in*

vacuo to remove organic volatiles, and the resulting aqueous solution was acidified to pH 4 with 1 M aqueous HCl and extracted with EtOAc ($\times 3$). The combined organic extracts were dried (Na_2SO_4) and concentrated *in vacuo* to give **91** (559 mg, 2.40 mmol, 85%) as a white solid.

R_f (SiO_2 ; EtOAc/petroleum ether,); **v_{max}** (neat/ cm^{-1}) 3273, 2512, 1704, 1567; **¹H NMR** (CDCl_3 , 400 MHz) δ 6.95 (1H, t, $J = 5.9$ Hz, NH), 6.61 – 6.47 (3H, m, H_c and H_d), 6.28 (2H, app br d, $J = 13.5$ Hz, $\text{H}_e^{\text{trans}}$), 5.58 (2H, dd, $J = 10.7, 1.3$ Hz, H_e^{cis}), 3.57 (2H, q, $J = 6.0$ Hz, H_f), 2.46 (2H, t, $J = 7.0$ Hz, H_i), 2.01 (2H, app pent, $J = 6.8$ Hz, H_g); **¹³C NMR** (CDCl_3 , 101 MHz) δ 178.1 (C_i), 163.9 (C_b), 162.1 (C_a), 135.3 (C_d), 122.5 (C_e), 103.8 (C_c), 40.9 (C_f), 32.3 (C_i), 24.9 (C_h); **HRMS** (ESI) $[\text{M}-\text{H}]^-$ required for $\text{C}_{12}\text{H}_{14}\text{N}_3\text{O}_2^-$ 232.1086, found 232.1091.

4-((4,6-Divinylpyrimidin-2-yl)amino)-N-(2-(2-(prop-2-yn-1-yloxy)ethoxy)ethyl)butanamide (92)



A solution of **91** (30 mg, 0.130 mmol), HATU (98 mg, 0.260 mmol), and Pr_2EtN (112 μL , 0.643 mmol) in DMF (2 mL) was stirred at rt for 10 min. To this solution, 2-(2-(prop-2-yn-1-yloxy)ethoxy)ethan-1-amine (37 mg, 0.260 mmol) was added and the resulting solution was stirred at rt for 15 h. The reaction mixture solution was directly purified *via* reverse phase column chromatography (5 to 95% MeCN in 50 mM aqueous NH_4OH) to give **92** (39 mg, 0.110 mmol, 84%) as a light yellow oil.

R_f (SiO_2 ; EtOAc) 0.25; **v_{max}** (neat/ cm^{-1}) 1637, 1539; **¹H NMR** (MeOD, 400 MHz) δ 6.69 (1H, d, $J = 1.1$ Hz, H_c), 6.61 (2H, dd, $J = 17.4, 10.7$ Hz, H_d), 6.37 (2H, d, $J = 17.4$ Hz, $\text{H}_e^{\text{trans}}$), 5.57 (2H, dd, $J = 10.6, 1.5$ Hz, H_e^{cis}), 4.17 (2H, t, $J = 1.7$ Hz, H_n), 3.65 (2H, dd, $J = 5.9, 3.3$ Hz, H_m), 3.60 (2H, dd, $J = 5.9, 3.5$ Hz, H_i), 3.52 (2H, t, $J = 5.4$ Hz, H_k), 3.47 (2H, t, $J = 6.8$ Hz, H_f), 3.35 (2H, t, $J = 5.5$ Hz, H_j), 2.85 (1H, t, $J = 1.9$ Hz, H_p), 2.29 (2H, t, $J = 7.5$ Hz, H_h), 1.92 (2H, pent, $J = 7.1$ Hz, H_g); **¹³C NMR** (MeOD, 101 MHz) δ 175.9 (C_i), 165.3 (C_b), 164.0 (C_a), 137.1 (C_d), 122.1 (C_e), 105.8 (C_c), 80.5 (C_o), 76.0 (C_p), 71.0 (C_l), 70.6 (C_k), 70.1 (C_m), 59.1 (C_n), 41.6 (C_f), 40.3 (C_j), 34.5 (C_h), 26.9 (C_g); **HRMS** (ESI) $[\text{M}+\text{H}]^+$ required for $\text{C}_{19}\text{H}_{27}\text{N}_4\text{O}_3^+$ 359.2083, found 359.2068.

4.6. Protein chemistry – Chapter 2

4.6.1. Modification of human serum albumin

Reduction of human serum albumin

The purity of commercially available recombinant human serum albumin (HSA; purchased from Sigma Aldrich; product code A9731) was determined by protein LCMS. This revealed a mixture of the free Cys-34 form **14** (66445 Da) and the cysteinylated form **15** (i.e. disulfide bonded with cysteine; 66566 Da).

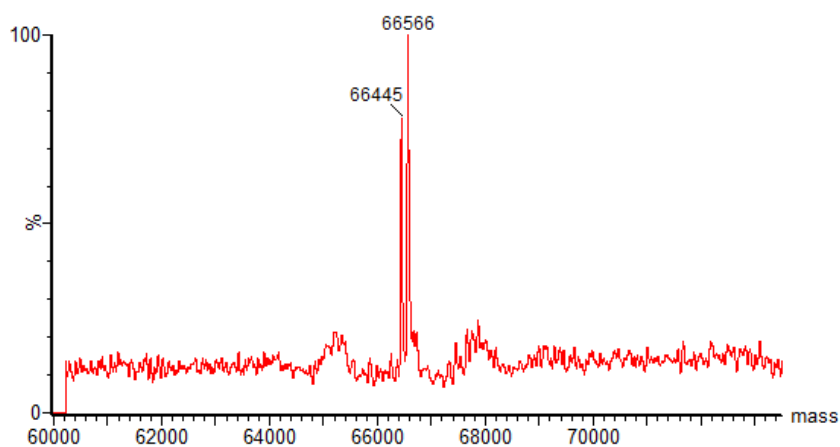
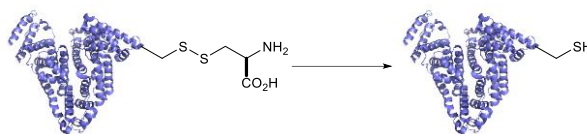


Figure 41. Deconvoluted mass spectrum of commercially available HSA. The mass difference between the two signals corresponds to cysteinylation of the Cys-34 residue. Expected mass difference from cysteinylation: 119 Da; observed mass difference: 121 Da.

A sample of the free Cys-34 HSA **14** was required for bioconjugation. This was achieved *via* reduction with dithiothreitol (DTT).



Dithiothreitol (DTT, 1.81 μL , 5 mM in PBS ($\times 1$)) was added to a solution of HSA (17.9 μL , 253 μM , mixture of **14** and **15**) in PBS (100 μL , $\times 1$). The resulting solution was vortexed and incubated at 37 $^{\circ}\text{C}$ for 2 h. Removal of excess reagents and buffer exchange to the required solvent was achieved by repeated ultracentrifugation into PBS ($\times 1$) or Tris·HCl (pH 8, 50 mM) using an Amicon-Ultra centrifugal filter (10k MWCO, Merck Millipore) to give uncapped HSA **14**.

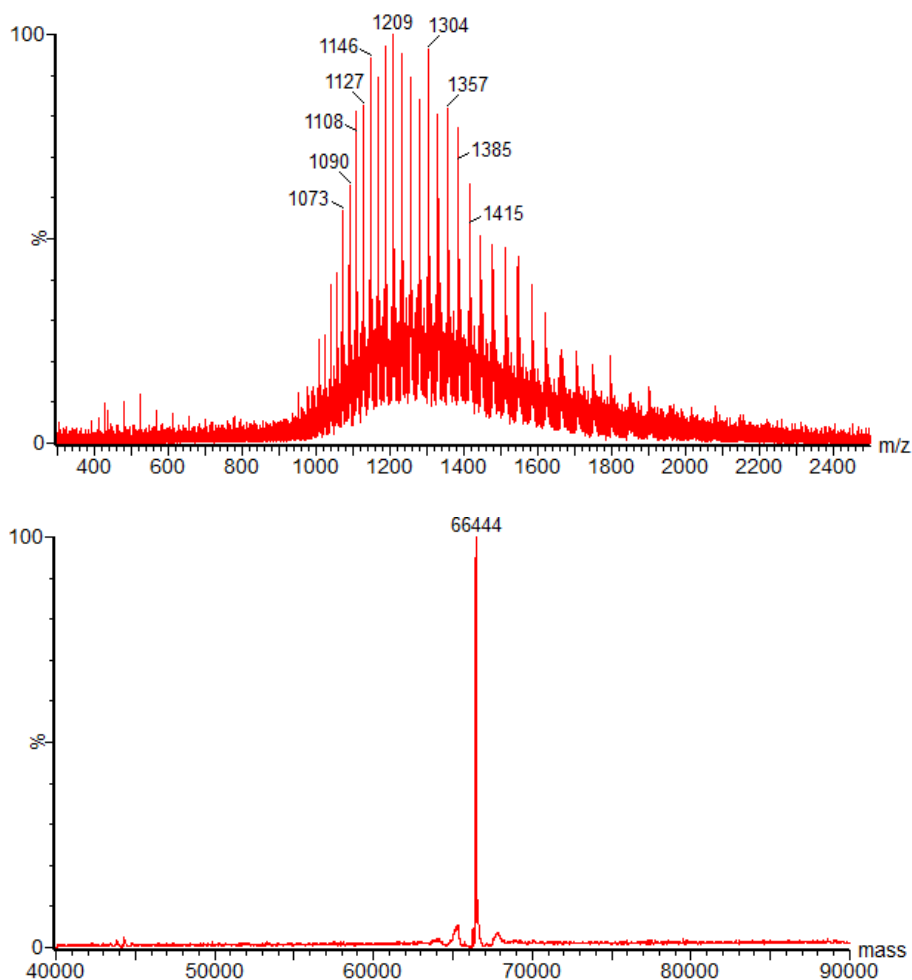
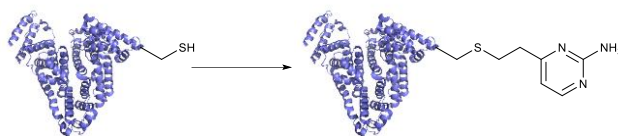


Figure 42. Non-deconvoluted (top) and deconvoluted (bottom) mass spectrum of the free Cys-34 HSA **14**.

Synthesis of **16**



Linker **4** (0.77 μL , 20 mM in DMSO), Tris·HCl (18.8 μL , pH 8, 50 mM) and DMSO (0.33 μL) were added to a solution of HSA (Cys-34 free form, 2.0 μL , 384 μM in Tris·HCl (pH 8, 50mM)). After incubation at 37 °C for 2 h, the solution was purified *via* Zeba Spin desalting column (7k MWCO, ThermoFisher, pre-equilibrated with Tris·HCl (pH 8, 50 mM)) to give **16**.

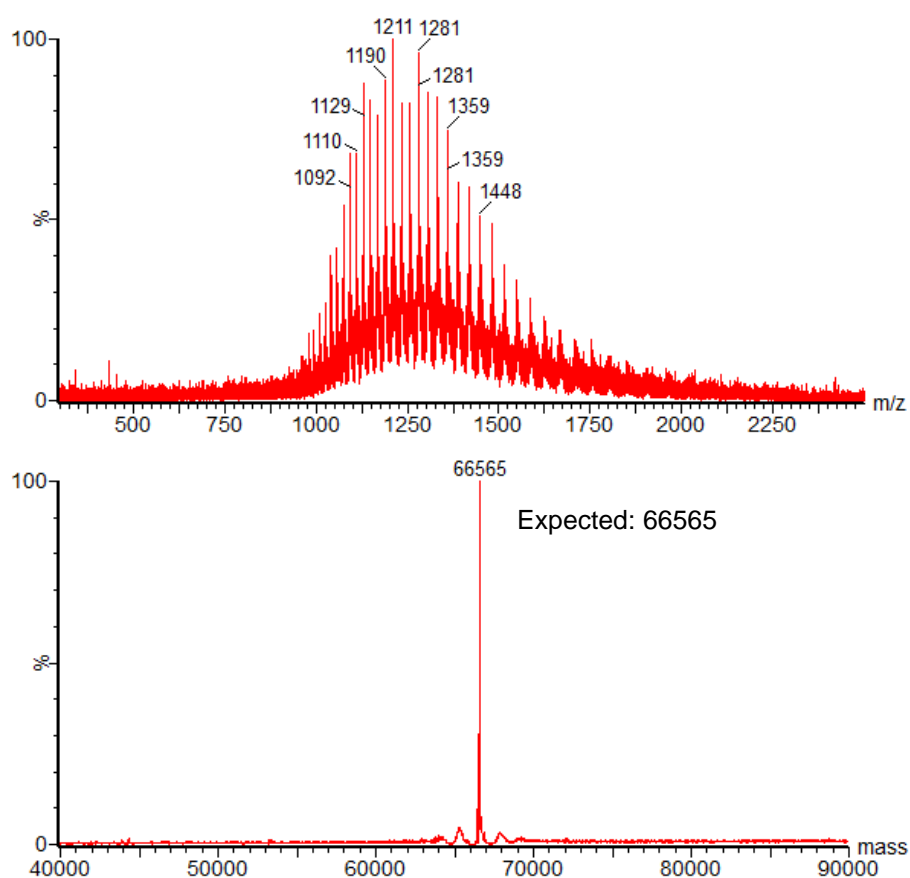
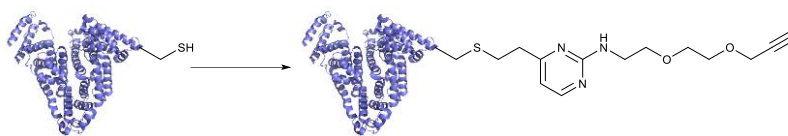


Figure 43. Non-deconvoluted (top) and deconvoluted (bottom) mass spectrum of **16**. Expected 66565 Da; observed 66565 Da.

Synthesis of **26**



Linker **19** (16.8 μL , 20 mM in DMSO), Tris·HCl (413 μL , pH 8, 50 mM) and DMSO (7.15 μL) were added to a solution of HSA (Cys-34 free form, 43.9 μL , 384 μM in Tris·HCl (pH 8, 50mM)). After incubation at 37 $^{\circ}\text{C}$ for 2 h, the solution was purified *via* Zeba Spin desalting column (7k MWCO, ThermoFisher, pre-equilibrated with Tris·HCl (pH 8, 50 mM)) to give **26**.

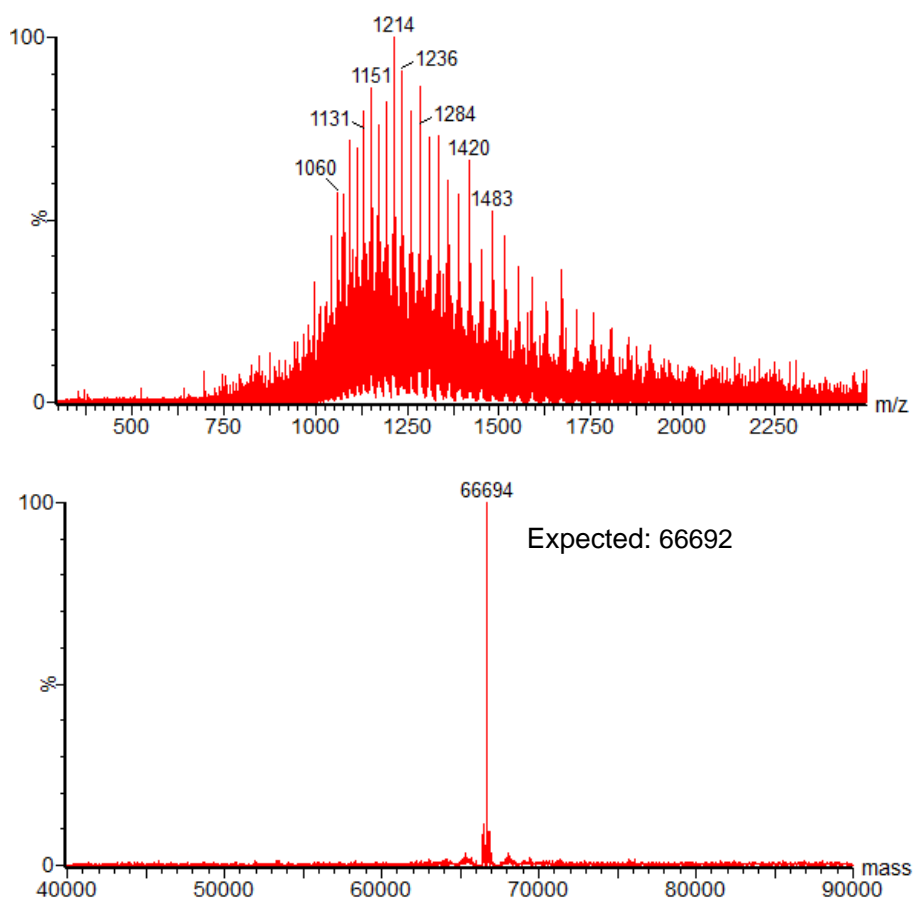
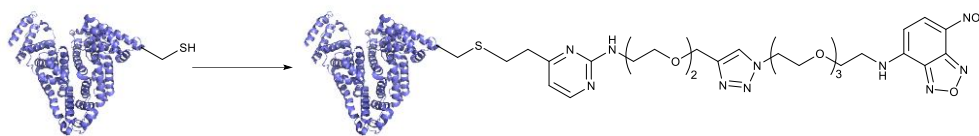


Figure 44. Non-deconvoluted (top) and deconvoluted (bottom) mass spectrum of **26**. Expected 66692 Da; observed 66694 Da.

Synthesis of **27**



Linker **22** (0.58 μL , 20 mM in DMSO), Tris·HCl (14.1 μL , pH 8, 50 mM) and DMSO (0.25 μL) were added to a solution of HSA (Cys-34 free form, 1.5 μL , 384 μM in Tris·HCl (pH 8, 50 mM)). After incubation at 37 °C for 2 h in the dark, the solution was purified *via* Zeba Spin desalting column (7k MWCO, ThermoFisher, pre-equilibrated with Tris·HCl (pH 8, 50 mM)) to give **27**.

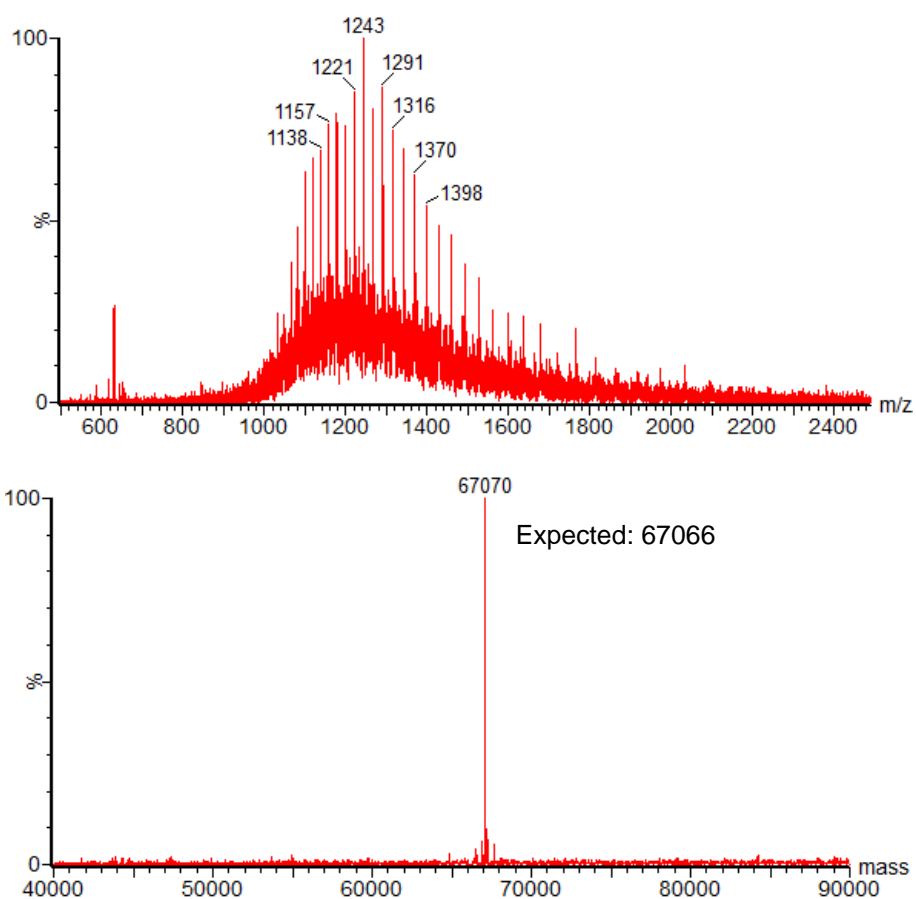
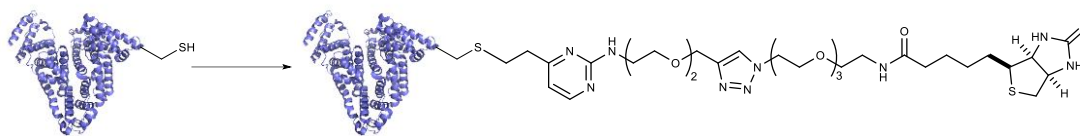


Figure 45. Non-deconvoluted (top) and deconvoluted (bottom) mass spectrum of **27**. Expected 67066 Da; observed 67070 Da.

Synthesis of **28**



Linker **25** (0.58 μL , 20 mM in DMSO), Tris·HCl (14.1 μL , pH 8, 50 mM) and DMSO (0.25 μL) were added to a solution of HSA (Cys-34 free form, 1.5 μL , 384 μM in Tris·HCl (pH 8, 50mM)). After incubation at 37 °C for 2 h, the solution was purified *via* Zeba Spin desalting column (7k MWCO, ThermoFisher, pre-equilibrated with Tris·HCl (pH 8, 50 mM)) to give **28**.

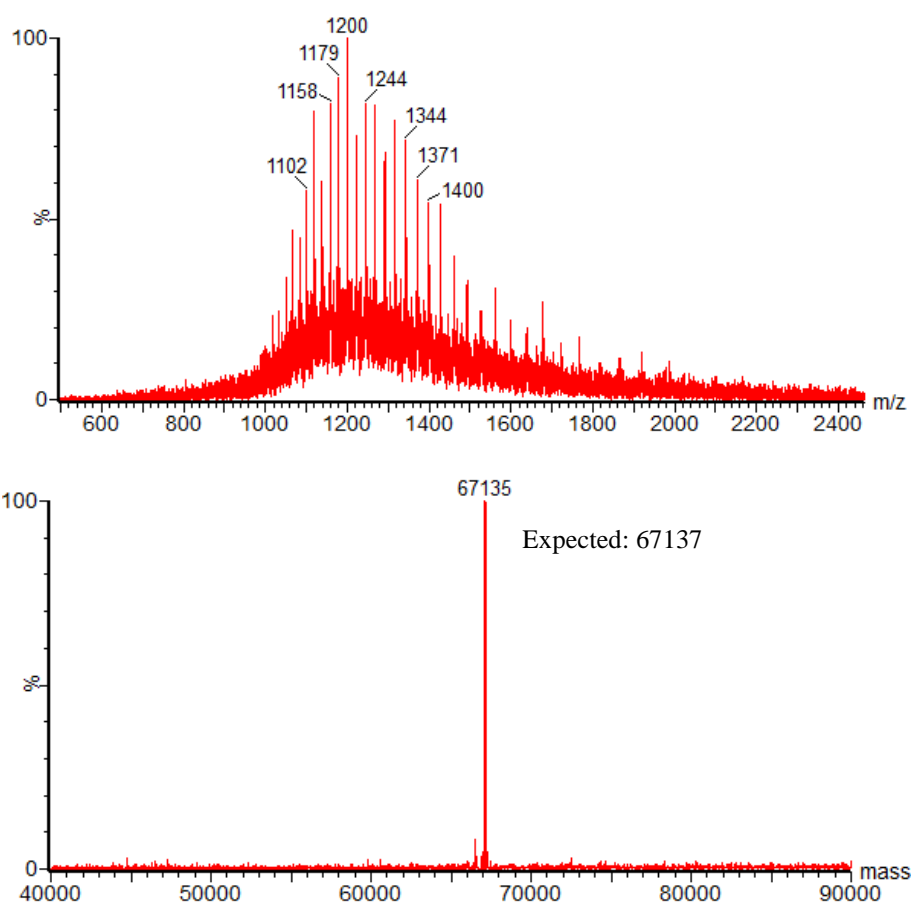
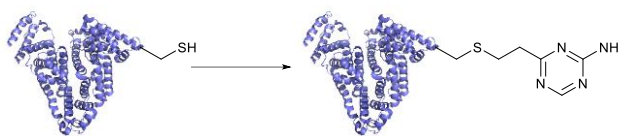


Figure 46. Non-deconvoluted (top) and deconvoluted (bottom) mass spectrum of **28**. Expected 67137 Da; observed 67135 Da.

Synthesis of **29**



Linker **7** (0.35 μL , 20 mM in DMSO), PBS (8.01 μL , $\times 1$) and DMSO (0.15 μL) were added to a solution of HSA (Cys-34 free form, 1.56 μL , 226 μM in PBS ($\times 1$)). After incubation at 37 $^{\circ}\text{C}$ for 1 h, the solution was purified *via* Zeba Spin desalting column (7k MWCO, ThermoFisher, pre-equilibrated with PBS ($\times 1$)) to give **29**.

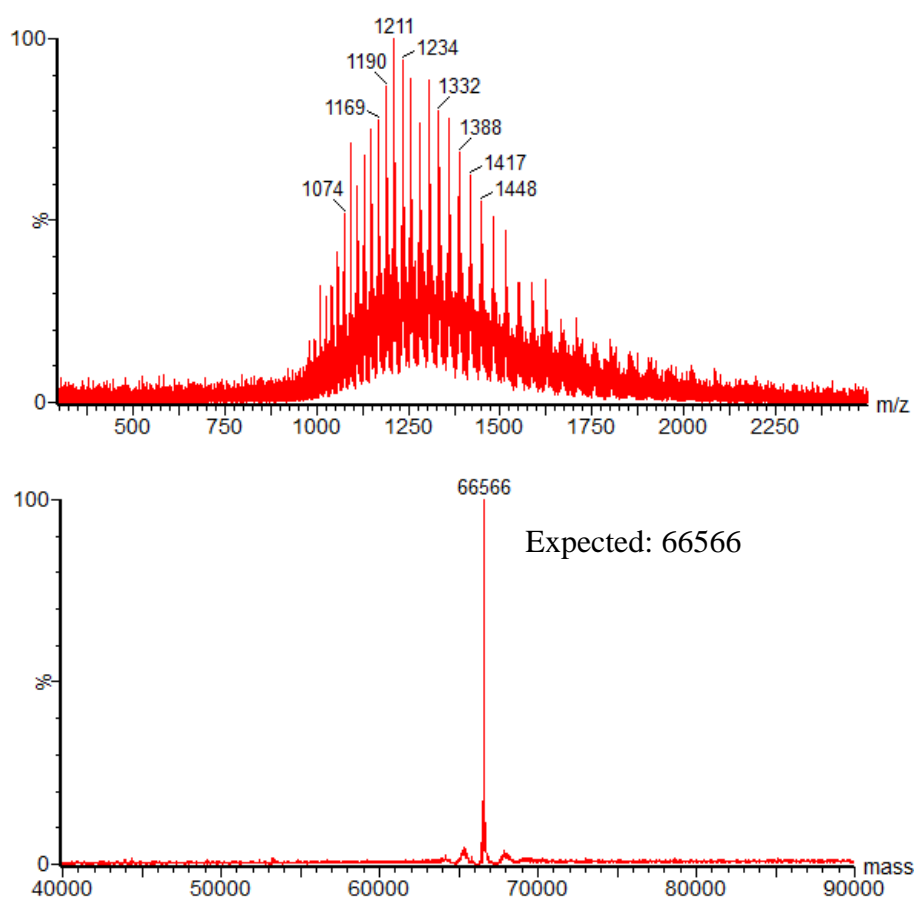


Figure 47. Non-deconvoluted (top) and deconvoluted (bottom) mass spectrum of **29**. Expected 66567 Da; observed 66566 Da.

SDS-PAGE analysis of human serum albumin conjugates

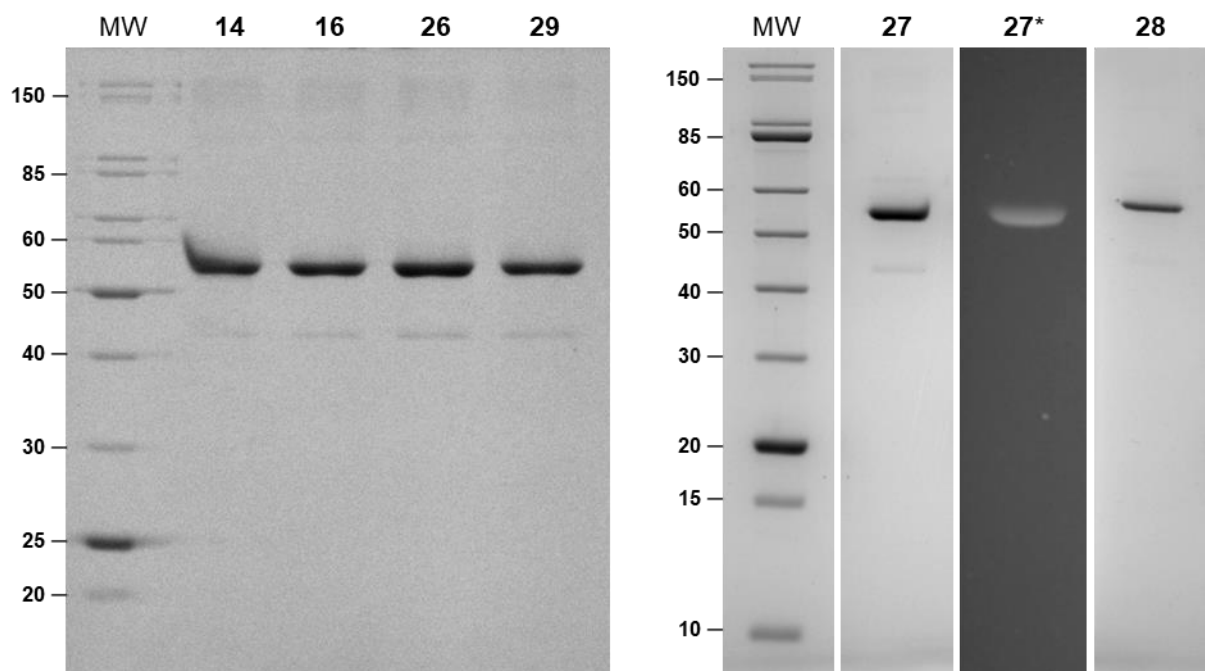
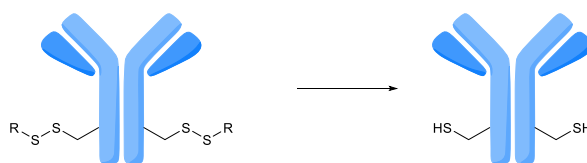


Figure 48. SDS-PAGE analysis with 12% acrylamide gel under non-reducing conditions for HSA **14** and HSA conjugates **16**, **26**, **29**, **27**, and **28**. SDS-PAGE was analysed by coomassie brilliant blue staining (and in-gel fluorescence for the lane labelled **27***). MW=molecular weight marker in kDa.

4.6.2. Modification of cysteine-engineered antibody

Reduction of cysteine-engineered antibody **35**



Based on a literature protocol,¹²⁹ the engineered cysteines of **33** were uncapped.

TCEP·HCl (4.5 μ L, 50 mM in H₂O) and Tris·HCl (40 μ L, pH 8, 50 mM containing 1 mM EDTA) were added to a solution of **33** (40 μ L, 70.7 μ M in PBS (\times 1)), and the resulting solution was incubated at 37 °C for 4 h. Removal of excess reagents and buffer exchange to the required solvent was achieved by repeated ultracentrifugation into Tris·HCl (pH 8, 50 mM containing 1 mM EDTA) using an Amicon-Ultra centrifugal filter (10k MWCO, Merck Millipore). To this solution, dehydroascorbic acid (2.26 μ L, 25 μ M in H₂O) was added, and was left to stand at rt for 2 h, before the solution was purified *via* Zeba Spin desalting column (7k MWCO, ThermoFisher, pre-equilibrated with Tris·HCl (pH 8, 50 mM containing 1 mM EDTA)) to give **35**. Prior to LCMS analysis, samples were deglycosylated and reduced with TCEP·HCl.

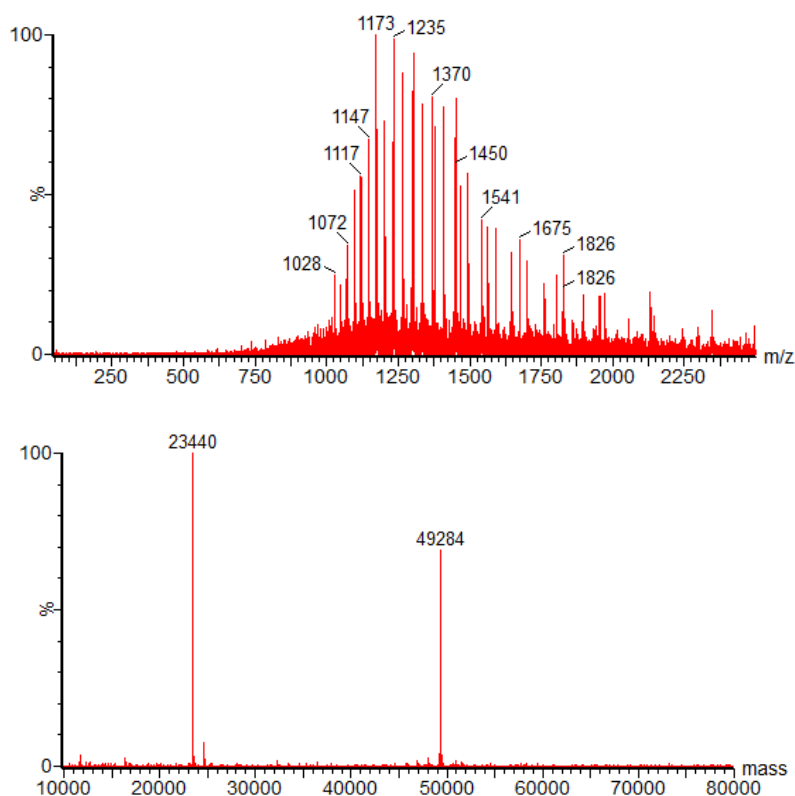
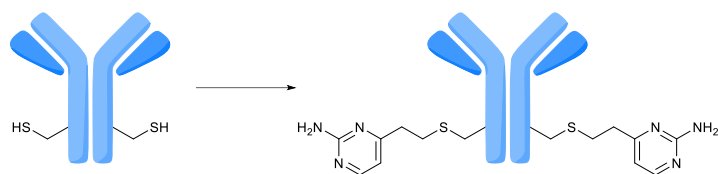


Figure 49. Non-deconvoluted (top) and deconvoluted (bottom) mass spectrum of **35** after deglycosylation with PNGase F and reduction with TCEP·HCl. Observed 23440 Da (LC) and 49284 Da (HC).

Synthesis of **36**



Linker **4** (0.29 μ L, 20 mM in DMSO) and DMSO (0.22 μ L) were added to a solution of **35** (cysteine uncapped form, 9.5 μ L, 31.6 μ M in Tris·HCl (pH 8, 50 mM containing 1 mM EDTA)), and the resulting solution was incubated at 37 $^{\circ}$ C for 4 h. The solution was purified *via* Zeba Spin desalting column (7k MWCO, ThermoFisher, pre-equilibrated with Tris·HCl (pH 8, 50 mM containing 1 mM EDTA)) to give **36**. Prior to LCMS analysis, samples were deglycosylated with PNGase F and reduced with TCEP·HCl.

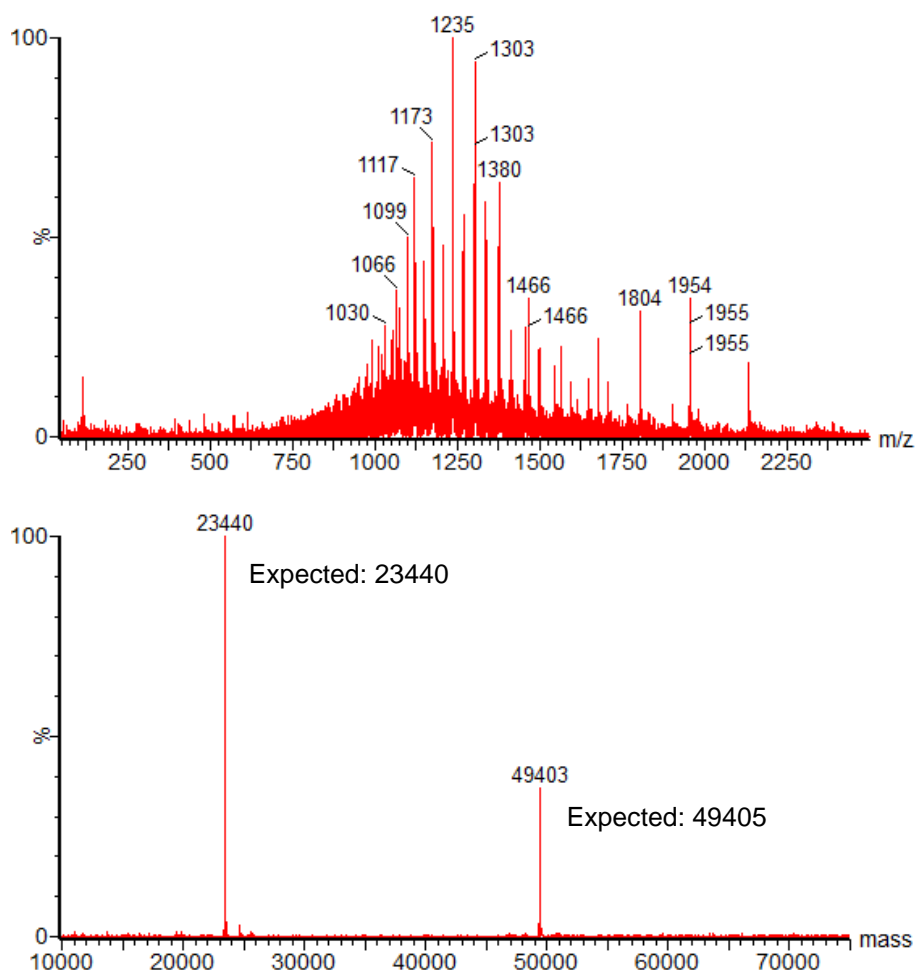
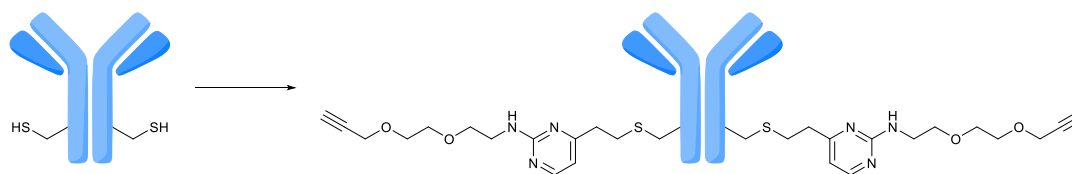


Figure 50. Non-deconvoluted (top) and deconvoluted (bottom) mass spectrum of **36**. Expected 23440 Da (LC) and 49405 Da (HC); observed 23440 Da (LC) and 49403 Da (HC). Prior to LCMS analysis, samples were deglycosylated with PNGase F and reduced with TCEP·HCl.

Synthesis of **37**



Linker **19** (0.50 μ L, 30 mM in DMSO) was added to a solution of **35** (cysteine uncapped form, 9.5 μ L, 31.6 μ M in Tris·HCl (pH 8, 50 mM containing 1 mM EDTA)), and the resulting solution was incubated at 37 $^{\circ}$ C for 4 h. The solution was purified *via* Zeba Spin desalting column (7k MWCO, ThermoFisher, pre-equilibrated with Tris·HCl (pH 8, 50 mM)) to give **37**. Prior to LCMS analysis, samples were deglycosylated with PNGase F and reduced with TCEP·HCl.

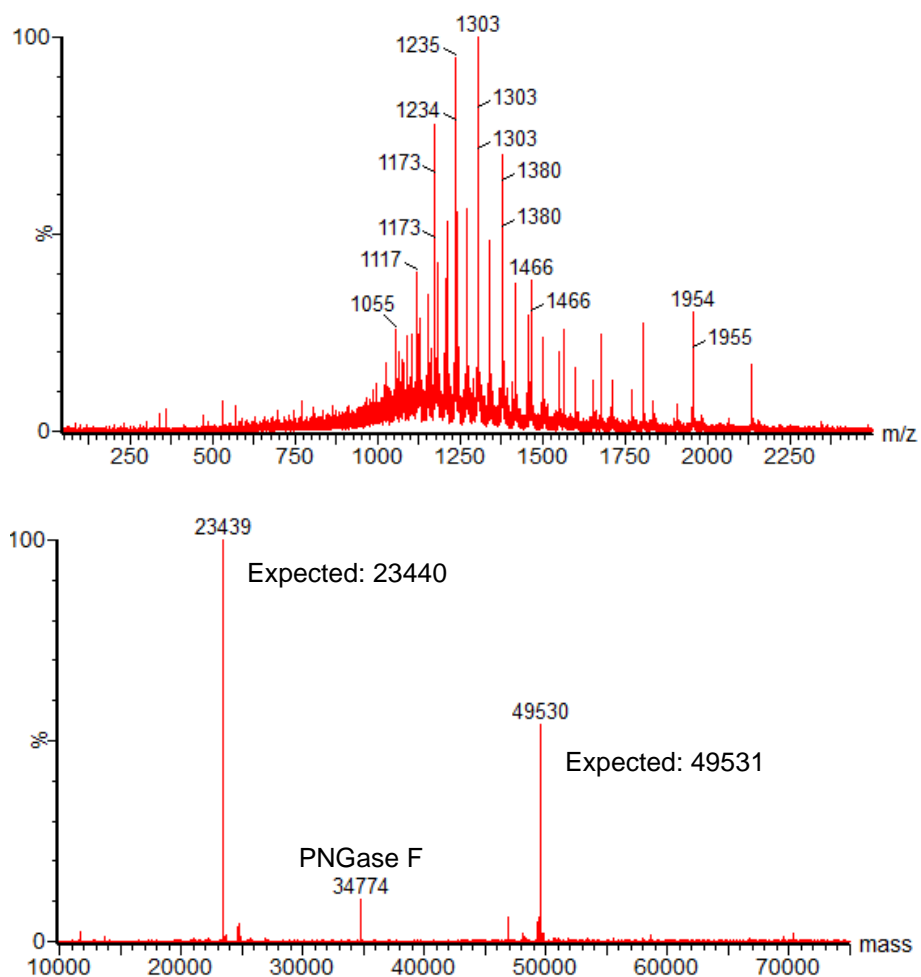
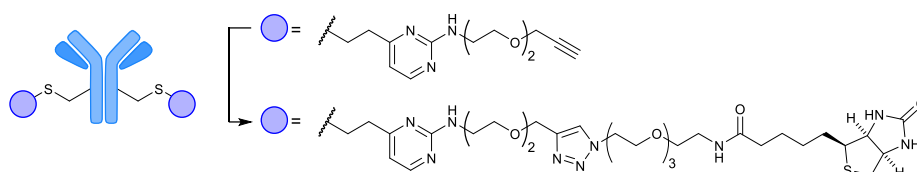


Figure 51. Non-deconvoluted (top) and deconvoluted (bottom) mass spectrum of **37**. Expected 23440 Da (LC) and 49531 Da (HC); observed 23439 Da (LC) and 49530 Da (HC). Prior to LCMS analysis, samples were deglycosylated with PNGase F and reduced with TCEP·HCl. The signal at 34774 Da corresponds to PNGase F.

Synthesis of **38**



THPTA (0.29 μL 20 mM in H_2O), $\text{CuSO}_4 \cdot 5\text{H}_2\text{O}$ (0.23 μL , 5 mM in H_2O), sodium ascorbate (0.34 μL , 50 mM in H_2O), DMSO (1 μL) and azido-biotin **25** (0.57 μL , 20 mM in DMSO) were added sequentially to a solution of **37** (10 μL , 11.4 μM in PBS ($\times 1$)). The resulting solution was incubated at 37 $^\circ\text{C}$ for 15 h before purification *via* Zeba Spin desalting column (7k MWCO, ThermoFisher, pre-equilibrated with PBS ($\times 1$)) to give **38**. Prior to LCMS analysis, samples were deglycosylated with PNGase F and reduced with TCEP-HCl.

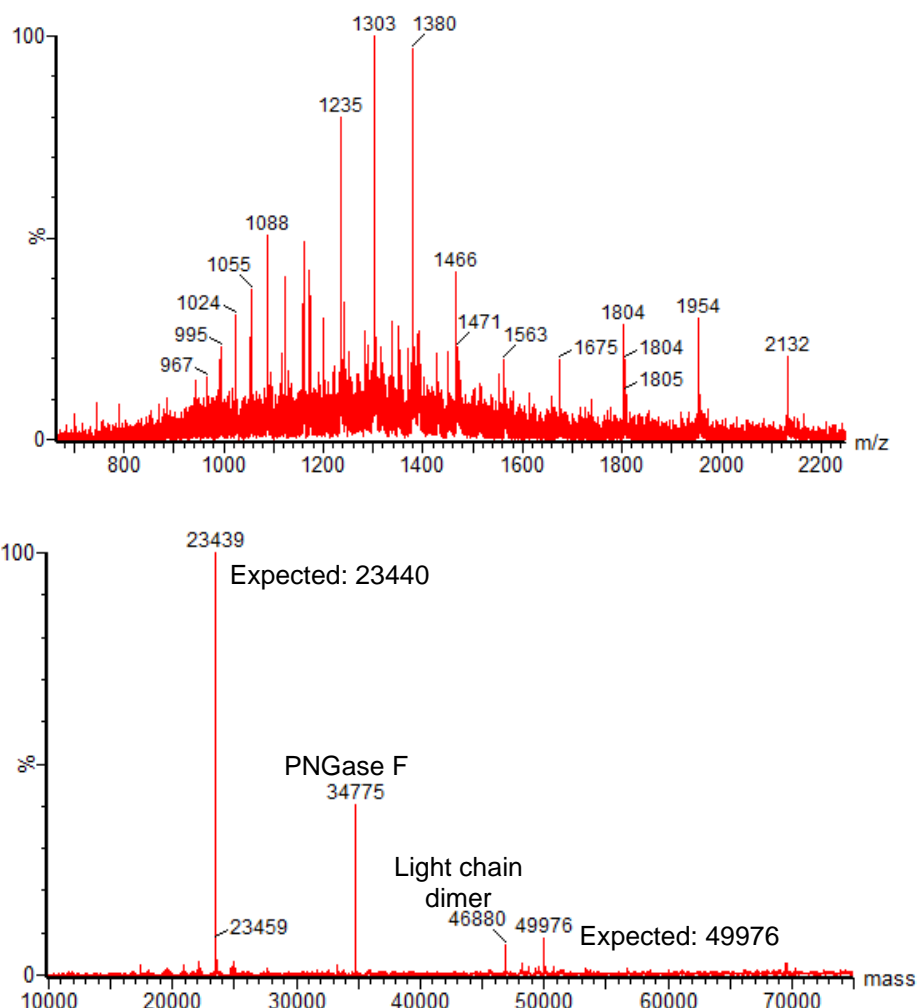
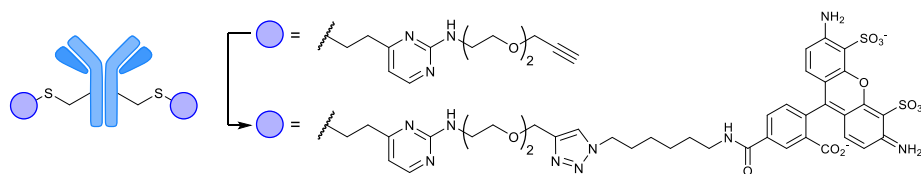


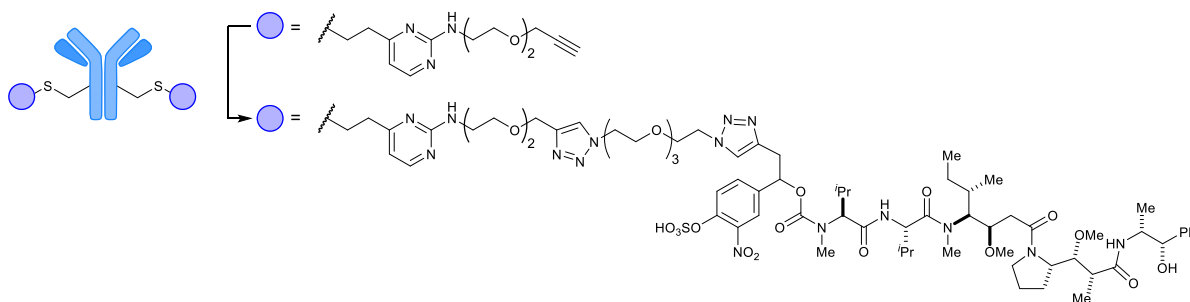
Figure 52. Non-deconvoluted (top) and deconvoluted (bottom) mass spectrum of **38**. Expected 23440 Da (LC) and 49976 Da (HC); observed 23440 Da (LC) and 49976 Da (HC). Prior to LCMS analysis, samples were deglycosylated with PNGase F and reduced with TCEP-HCl. The signals at 34774 Da and 46880 Da corresponds to PNGase F and light chain dimer, respectively.

Synthesis of 39



THPTA (0.29 μL , 80 mM in H_2O), $\text{CuSO}_4 \cdot 5\text{H}_2\text{O}$ (0.23 μL , 20 mM in H_2O), sodium ascorbate (0.34 μL , 200 mM in H_2O), DMSO (1 μL) and Alexa Fluor 488 azide **40** (0.57 μL , 20 mM in DMSO, purchased from Invitrogen) were added sequentially to a solution of **37** (10 μL , 11.4 μM in PBS ($\times 1$)). The resulting solution was incubated at 37 $^\circ\text{C}$ for 6 h before purification *via* Zeba Spin desalting column (7k MWCO, ThermoFisher, pre-equilibrated with PBS ($\times 1$)). The resulting conjugate was analysed by UV-Vis spectroscopy, which revealed conjugate **39** to have a fluorophore-to-antibody ratio of 1.9.

Synthesis of 41



THPTA (2.5 μL , 80 mM in H_2O), $\text{CuSO}_4 \cdot 5\text{H}_2\text{O}$ (3.5 μL , 20 mM in H_2O), sodium ascorbate (1.7 μL , 200 mM in H_2O) and azido-MMAE **42** (1.7 μL , 20 mM in DMSO) were added sequentially to a solution of **37** (25 μL , 27.3 μM in PBS ($\times 1$)). The resulting solution was incubated at 37 $^\circ\text{C}$ for 6 h before purification *via* Zeba Spin desalting column (two rounds of purification, 7k MWCO, ThermoFisher, pre-equilibrated with PBS ($\times 1$)) and further ultracentrifugation to PBS ($\times 1$) using Amicon-Ultra centrifugal filter (10k MWCO, Merck Millipore) to give **41**. Prior to LCMS analysis, samples were deglycosylated with PNGase F and reduced with TCEP $\cdot\text{HCl}$.

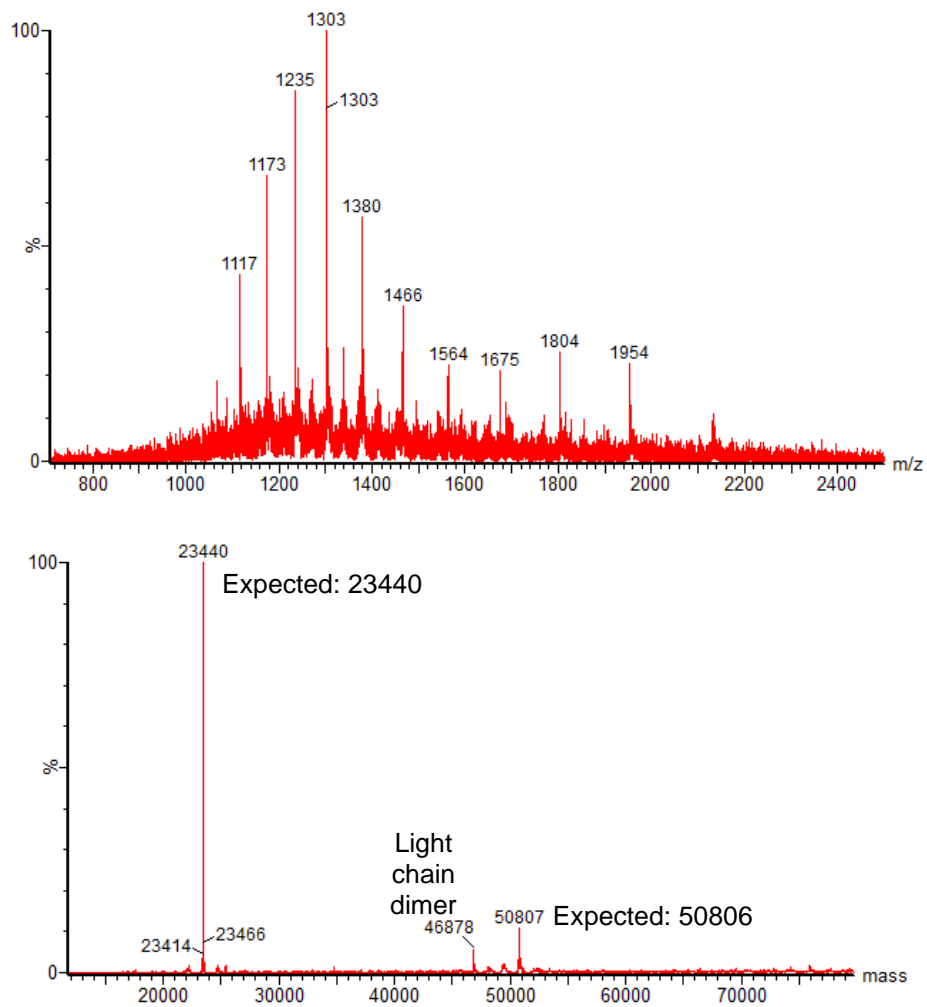


Figure 53. Non-deconvoluted (top) and deconvoluted (bottom) mass spectrum of **41**. Expected 23440 Da (LC; no modification) and 50806 Da (HC); observed 23440 Da (LC) and 50707 Da (HC). Prior to LCMS analysis, samples were deglycosylated with PNGase F and reduced with TCEP-HCl. The signal at 46878 Da corresponds to light chain dimer.

SDS-PAGE analysis of 33 and its conjugates

SDS-PAGE analysis of **33** and its conjugates under non-reducing (NR) and reducing (R) conditions. Analysis of **36**, **37**, **38**, and **39** reveals that conjugates are found predominantly as the “full antibody” forms (~146 kDa), with all native interchain disulfide bonds present. In-gel fluorescence of Alexa Fluor 488 conjugate **39** under reducing conditions revealed the linker modification to be on the heavy chain (~51 kDa), consistent with mass spectrometry analysis; fluorescence was not observed for the light chain (~23 kDa).

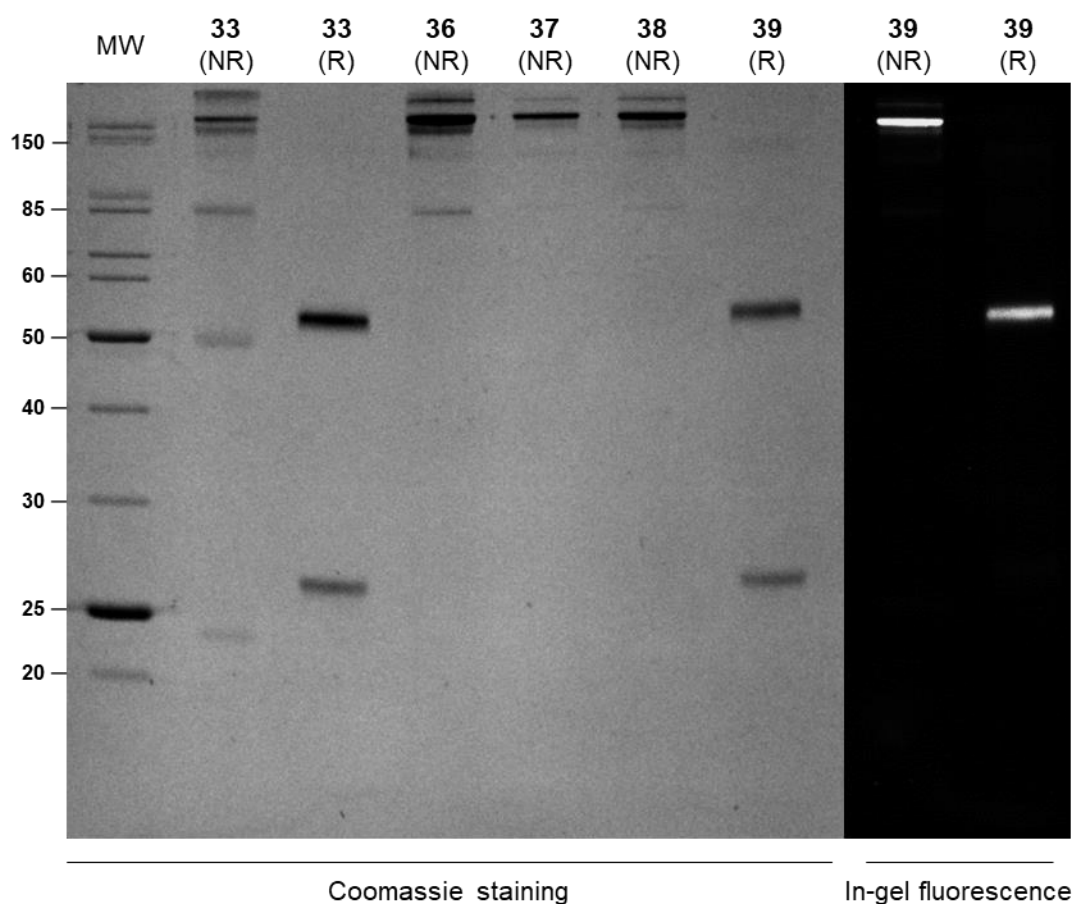


Figure 54. SDS-PAGE analysis with 12% acrylamide gel for antibody species **33**, **36**, **37**, **38**, and **39** under non-reducing (NR) and reducing (R) conditions. SDS-PAGE was analysed by in-gel fluorescence and coomassie brilliant blue staining. MW=molecular weight marker in kDa.

4.6.3. Preparation of fluorophore-modified trastuzumab and plasma stability

Mass spectra of native trastuzumab 45

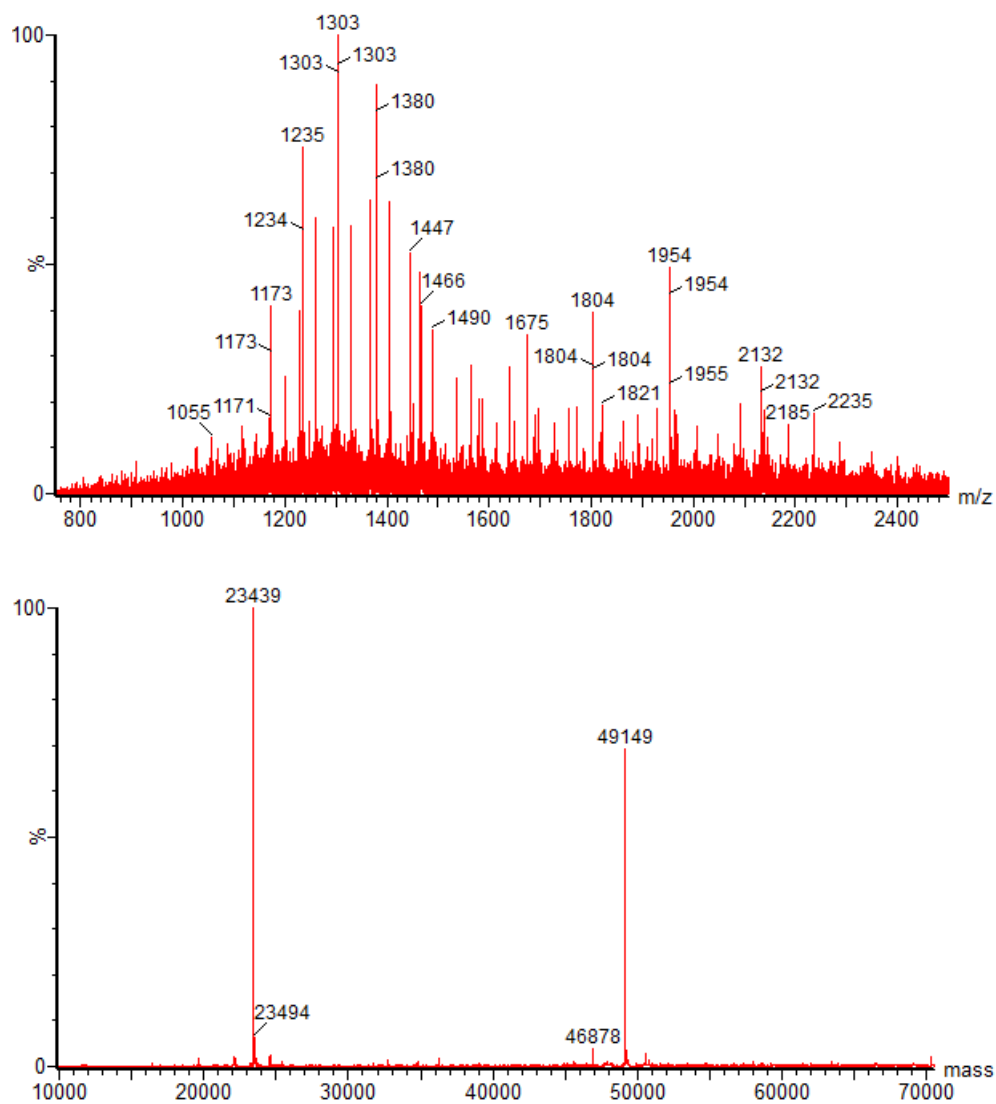
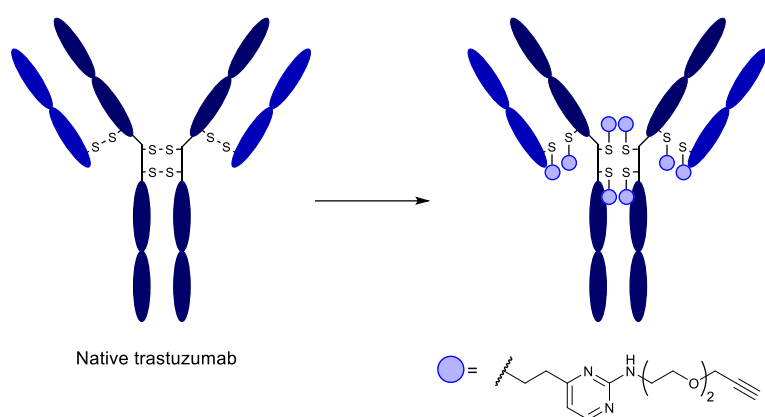


Figure 55. Non-deconvoluted (top) and deconvoluted (bottom) mass spectrum of native trastuzumab 45. Prior to LCMS analysis, samples were deglycosylated with PNGase F and reduced with TCEP-HCl.

Synthesis of **46**



Tris-buffered saline (pH 8, 25 mM in H₂O, 9.0 μL [consists of Tris·HCl, 25 mM NaCl, 0.5 mM EDTA]) and TCEP·HCl (0.4 μL, 5 mM in H₂O) were added to a solution of native trastuzumab **45** (3.0 μL, 45 μM), and the resulting solution was incubated at 37 °C for 1 h. To this solution, DMSO (0.27 μL) and **19** (1.07 μL, 12.5 mM in DMSO) were added, and the resultant solution was incubated at 37 °C for 6 h, before purification *via* Zeba Spin desalting column (7k MWCO, ThermoFisher, pre-equilibrated with PBS (×1)). Finally, buffer exchange to PBS (×1) was achieved by repeated ultracentrifugation using an Amicon-Ultra centrifugal filter (10k MWCO, Merck Millipore) to give **46**. Prior to LCMS analysis, samples were deglycosylated with PNGase F and treated with TCEP·HCl.

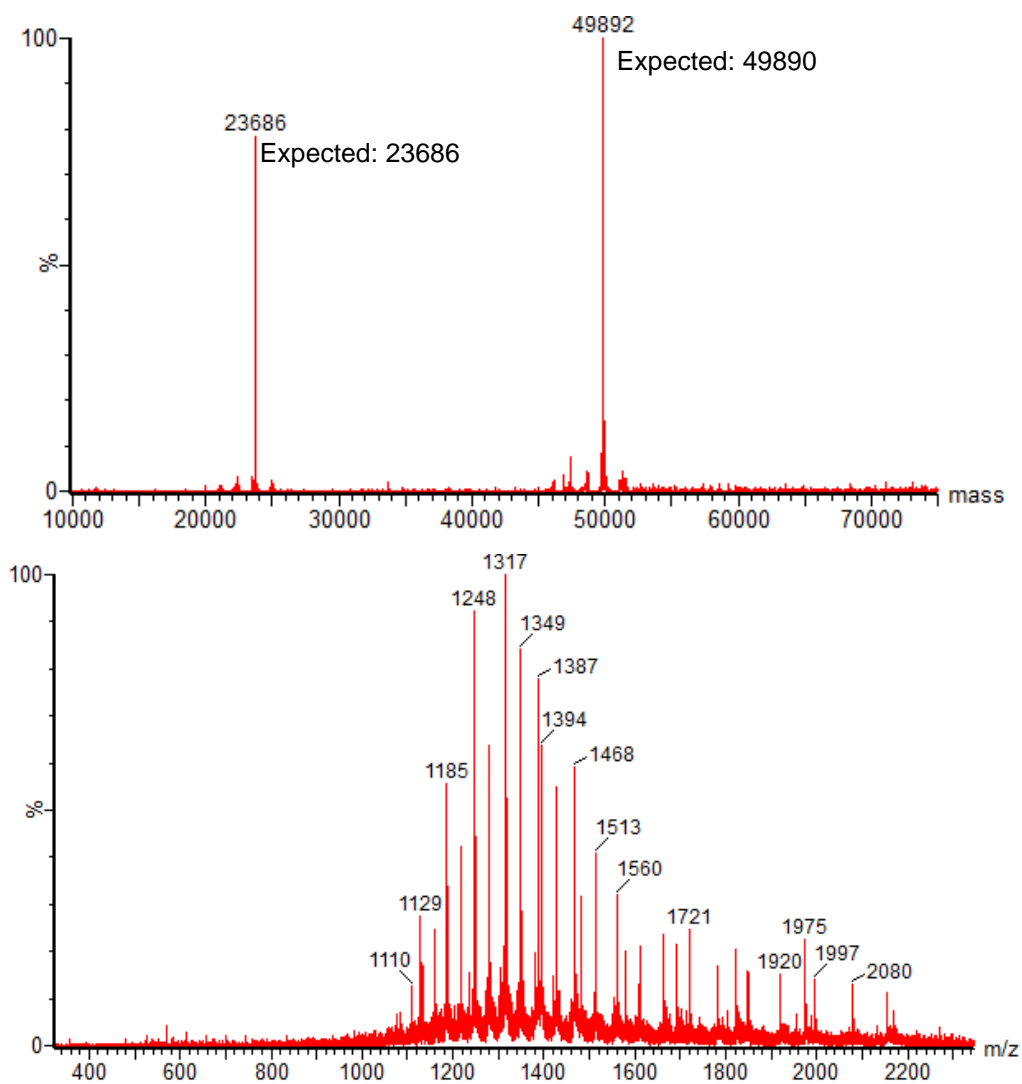
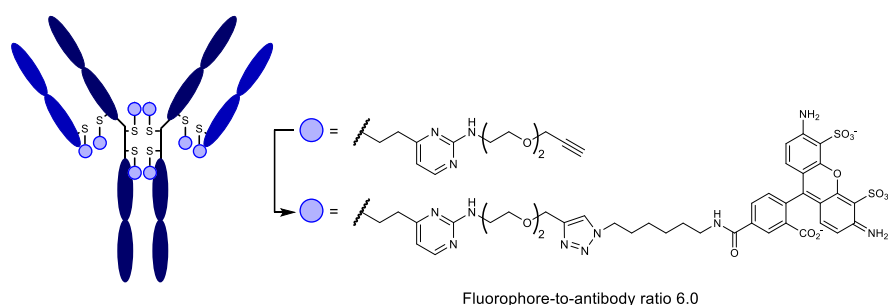


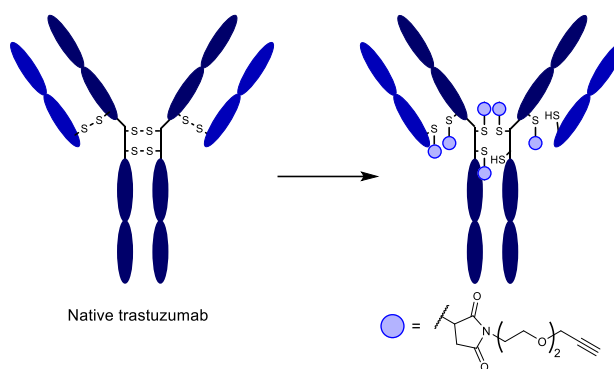
Figure 56. Non-deconvoluted (top) and deconvoluted (bottom) mass spectrum of **46**. The light chain and heavy chain are modified with one and three linkers, respectively, to give a linker-to-antibody ratio of 8. Expected 23686 Da (LC) and 49890 Da (HC). Found 23686 Da (LC) and 49892 Da (HC). Prior to LCMS analysis, samples were deglycosylated with PNGase F and treated with TCEP·HCl.

Synthesis of 47



THPTA (1.62 μL , 80 mM in H_2O), $\text{CuSO}_4 \cdot 5\text{H}_2\text{O}$ (1.08 μL , 20 mM in H_2O), sodium ascorbate (1.08 μL , 200 mM in H_2O), and Alexa Fluor 488 azide **40** (2.16 μL , 20 mM in DMSO, purchased from Invitrogen) were added sequentially to a solution of **46** (30 μL , 12.6 μM in PBS ($\times 1$)). The resulting solution was incubated at 37 $^\circ\text{C}$ for 15 h before purification *via* Zeba Spin desalting column (7k MWCO, ThermoFisher, pre-equilibrated with PBS ($\times 1$)). The resulting conjugate was analysed by UV-Vis spectroscopy, which revealed conjugate **47** to have a fluorophore-to-antibody ratio of 6.0.

Synthesis of 48



This bioconjugate was prepared based on a literature procedure.¹⁵⁶

TCEP·HCl (1.2 μL , 5 mM in H_2O) was added to a solution of native trastuzumab **45** (20 μL , 29.7 μM in PBS ($\times 1$)) and the solution was incubated at 37 $^\circ\text{C}$ for 1 h. To this solution, DMSO (1.7 μL) and maleimide **44** (0.6 μL , 20 mM in DMSO) were added. The resulting solution was left to stand at rt for 1.5 h, before purification *via* Zeba Spin desalting column (7k MWCO, ThermoFisher, pre-equilibrated with PBS ($\times 1$)) to give **48**. Prior to LCMS analysis, samples were deglycosylated with PNGase F and treated with TCEP·HCl.

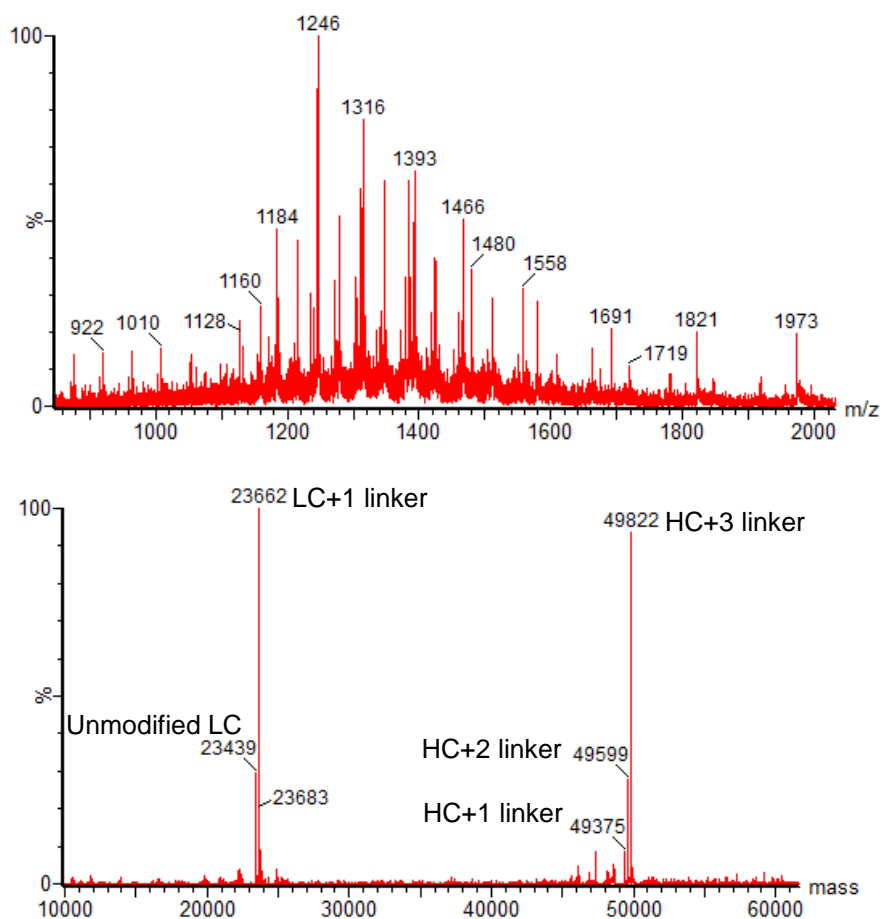
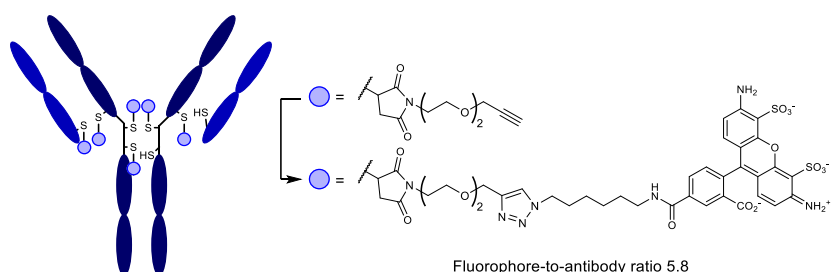


Figure 57. Non-deconvoluted (top) and deconvoluted (bottom) mass spectrum of **48**. The reaction gave a mixture of reacted and unreacted cysteine residues. Light chain and heavy chain are modified with one and three linkers, respectively, to give a linker-to-antibody ratio of 8. The observed masses correspond to the following species: 23439 Da (unmodified LC; expected 23439 Da); 23662 Da (LC modified with one linker; expected 23662 Da); 49375 Da (HC modified with one linker; expected 49372 Da); 49599 Da (HC modified with two linkers; expected 49595 Da); 49822 Da (HC modified with three linkers; expected 49818 Da). Prior to LCMS analysis, samples were deglycosylated with PNGase F and treated with TCEP·HCl.

Synthesis of **49**



THPTA (1.62 μL , 80 mM in H_2O), $\text{CuSO}_4 \cdot 5\text{H}_2\text{O}$ (1.08 μL , 20 mM in H_2O), sodium ascorbate (1.08 μL , 200 mM in H_2O) and Alexa Fluor 488 azide **40** (2.16 μL , 20 mM in DMSO, purchased from Invitrogen) were added sequentially to a solution of **48** (30 μL , 12.6 μM in

PBS ($\times 1$)). The resulting solution was incubated at 37 °C for 15 h before purification *via* Zeba Spin desalting column (7k MWCO, ThermoFisher, pre-equilibrated with PBS ($\times 1$)). The resulting conjugate was analysed by UV-Vis spectroscopy, which revealed conjugate **49** to have a fluorophore-to-antibody ratio of 5.8.

Plasma stability studies

Solutions containing 0.5 μM of bioconjugate **47** (fluorophore-to-antibody ratio = 6.0) or **49** (fluorophore-to-antibody ratio = 5.8) were prepared in PBS ($\times 1$) containing 10% human plasma. These solutions were incubated at 37 °C. On day 0, 2, 4, 6 and 8, aliquots were taken and frozen at -80 °C until analysis. These samples were analysed by sodium dodecyl sulfate-polyacrylamide gel electrophoresis (SDS-PAGE), where 1.25 pmol of antibody was loaded in each lane.

4.6.4. Cell lysate labelling

Preparation of cell lysate

Cell lysates were prepared by Dr. Stephen Walsh.

MCF7 cells ($2 \times$ T175 flasks) were trypsinised and washed with PBS (3×10 mL). Cell pellets were reconstituted in RIPA buffer (Thermo, 89900) supplemented with protease inhibitors (Roche). Cells were then lysed by sonication (Diagenode, 2×30 s cycles) and centrifuged at $21,000 \times g$ at 4 °C for 15 min. The protein-containing supernatant was removed, and protein concentration (~ 5 mg/mL) measured using a Direct Detect Spectrometer (Millipore). Samples were diluted to 1 mg/mL with PBS, aliquoted, flash frozen and stored at -20 °C until use.

Labelling of cell lysate

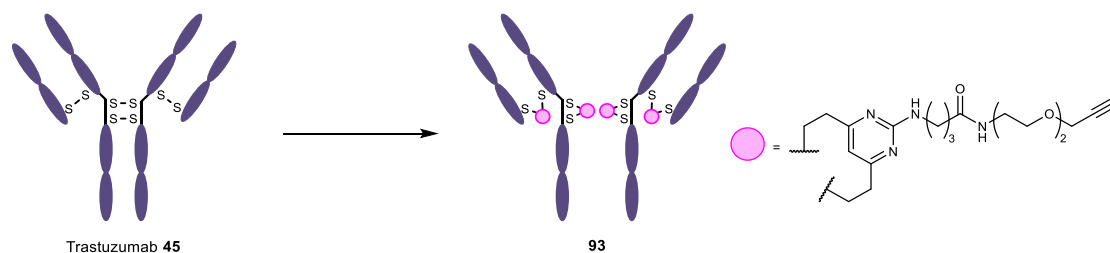
A $\times 20$ stock solution of vinylpyrimidine-alkyne **19** (2.5 μL ; 20 μL , 200 μL , 1 mM, 2 mM, 4 mM, or 8mM in DMSO) or neat DMSO (2.5 μL ; control reaction) was added to MCF7 cell lysate (50 μL , 1 mg/mL), to give final linker concentrations of 1 μM , 10 μM , 50 μM , 100 μM , 200 μM , 400 μM , and 0 μM , respectively. The resulting solutions were left to stand at rt for 2 h, before purification *via* Zeba Spin desalting column (7k MWCO, ThermoFisher, pre-

equilibrated with PBS ($\times 1$)). To each solution, THPTA (500 mM in H₂O, 1 μ L, 500 pmol), CuSO₄·5H₂O (50 mM in H₂O, 1 μ L, 50 pmol), sodium ascorbate (1 M in H₂O, 1 μ L, 1 μ mol) and Alexa Fluor 488 azide **40** (5 mM in DMSO, 2 μ L, 10 pmol) were added sequentially, and the resulting mixture was left to stand at rt for 1.5 h, before purification *via* Zeba Spin desalting column (7k MWCO, ThermoFisher, pre-equilibrated with PBS ($\times 1$)). Material corresponding to a 7.5 μ L aliquot of this resulting solution was used for SDS-PAGE analysis. Samples were prepared under reducing conditions and run using methods described in the general experimental.

For cysteine blockade studies, MCF7 cell lysate (50 μ L, 1 mg/mL) was pre-incubated with iodoacetamide (20 mM) at rt for 1 h, prior to the addition of vinylpyrimidine-alkyne **19**.

4.7. Protein chemistry – Chapter 3

Synthesis of **93**



TCEP·HCl (9.3 μL , 5 mM in H_2O) was added to a solution of native trastuzumab **45** (320 μL , 14.5 μM in PBS ($\times 1$)) and the solution was incubated at 37 $^\circ\text{C}$ for 1 h. To this solution, **92** (6.3 μL , 20 mM in DMSO) was added. The resulting solution incubated at 37 $^\circ\text{C}$ for 2 h, before purification *via* Zeba Spin desalting column (7k MWCO, ThermoFisher, pre-equilibrated with PBS ($\times 1$)) and diafiltration into PBS ($\times 1$) using an Amicon-Ultra centrifugal filter (10k MWCO, Merck Millipore). to give **93**. Prior to LCMS analysis, samples were deglycosylated with PNGase F.

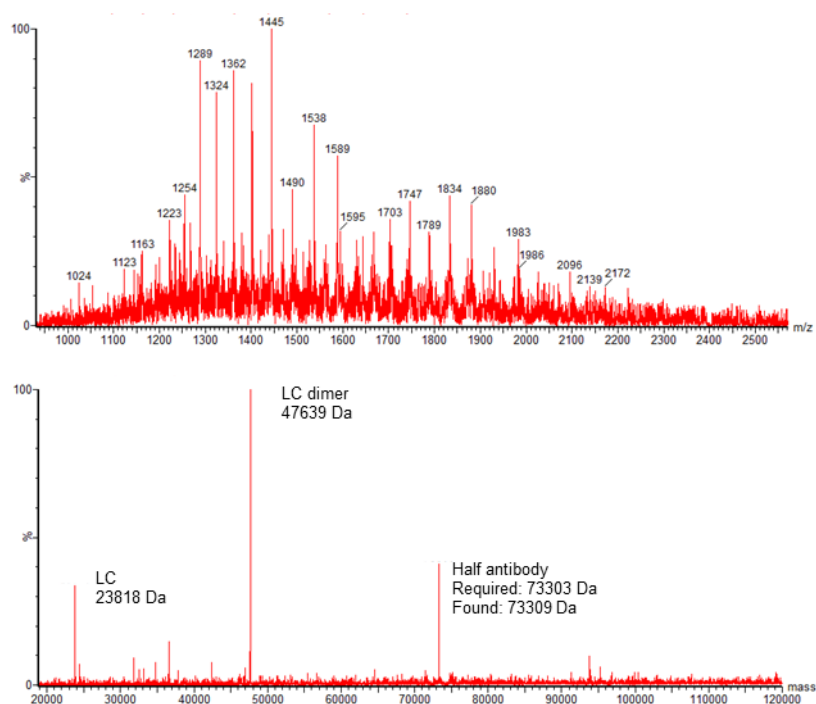
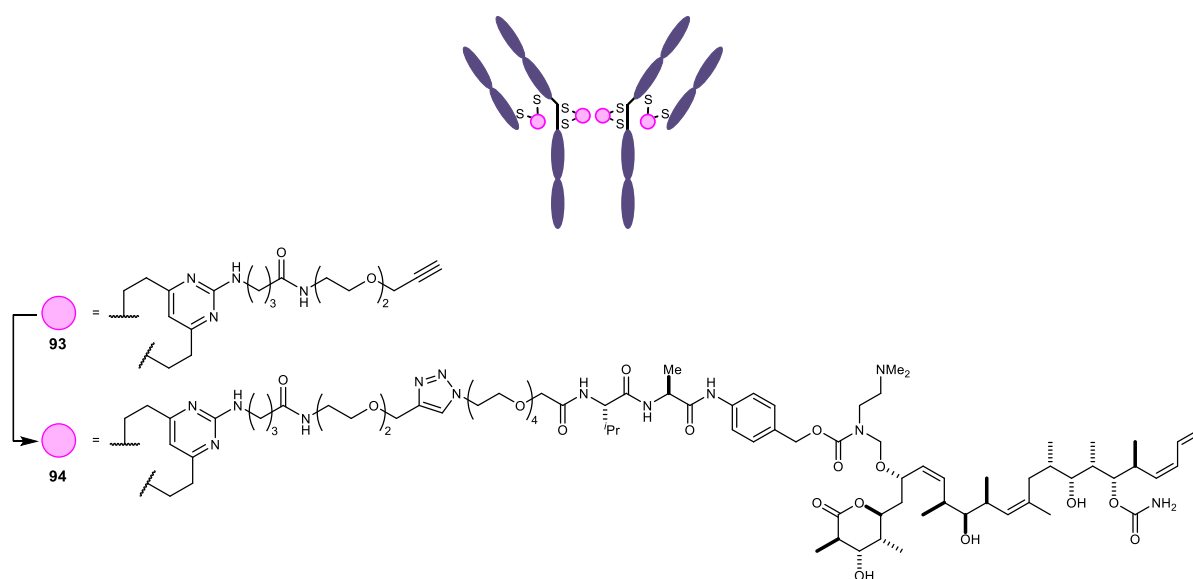


Figure 58. Non-deconvoluted (top) and deconvoluted (bottom) mass spectrum of **93**. The rebridged half antibody species is found together with unreacted light chain (LC) and light chain dimer

Synthesis of **94**



Reaction conducted by Dr. Stephen Walsh.

THPTA (1.2 μL , 20 mM in H_2O), $\text{CuSO}_4 \cdot 5\text{H}_2\text{O}$ (1.6 μL , 5 mM in H_2O), sodium ascorbate (0.9 μL , 20 mM in H_2O), DMSO (1 μL) and azide-discodermolide **76** (4 μL , 20 mM in DMSO) were added sequentially to a solution of **93** (40 μL , 10.3 μM in PBS ($\times 1$)). The resulting solution was incubated at 37 $^\circ\text{C}$ for 6 h before purification *via* Zeba Spin desalting column (7k MWCO, ThermoFisher, pre-equilibrated with PBS ($\times 1$)) to give **94**. Prior to LCMS analysis, samples were deglycosylated with PNGase F.

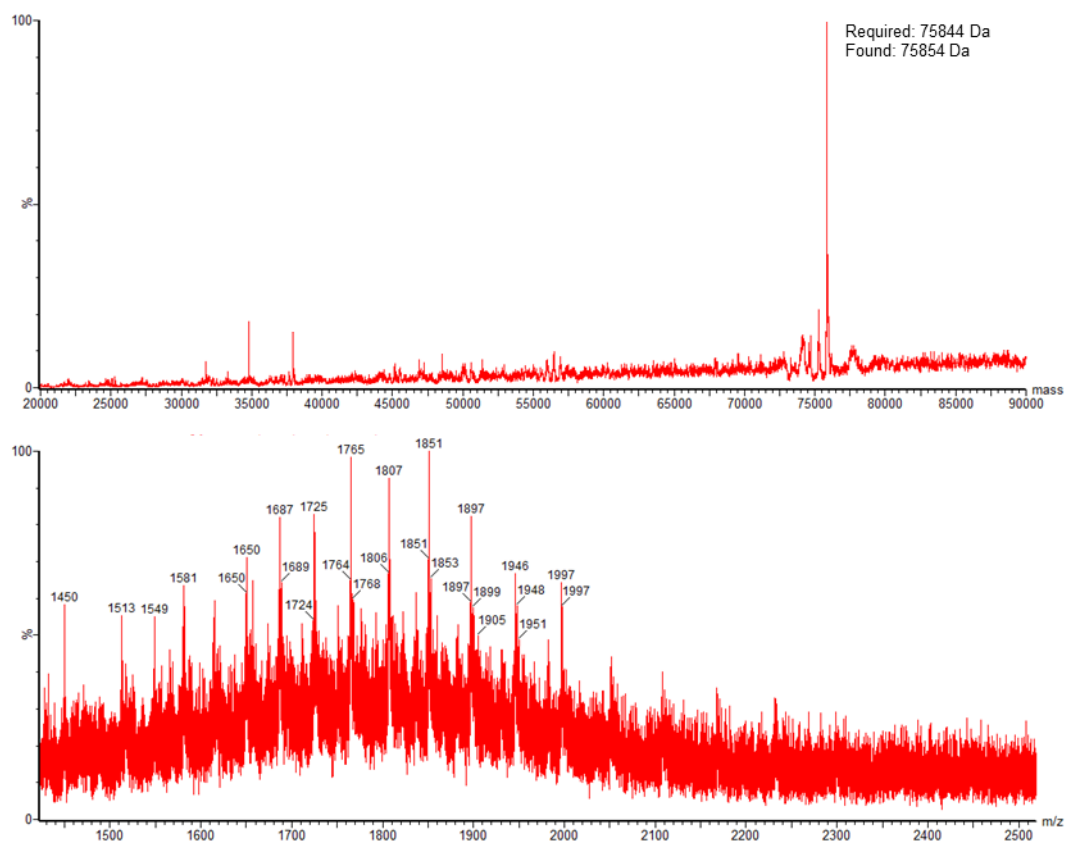


Figure 59. Non-deconvoluted (top) and deconvoluted (bottom) mass spectrum of **94**. The rebridged half antibody species is observed.

Chapter 5. References

- (1) Chabner, B. A.; Roberts, T. G. *Nat. Rev. Cancer* **2005**, *5*, 65.
- (2) World Health Organization. Cancer <https://www.who.int/en/news-room/fact-sheets/detail/cancer> (accessed Nov 13, 2021).
- (3) Danaei, G.; Vander Hoorn, S.; Lopez, A. D.; Murray, C. J. L.; Ezzati, M. *Lancet* **2005**, *366*, 1784.
- (4) Shurin, M. *ImmunoTargets Ther.* **2012**, *36*, 1.
- (5) *Chemical Linkers in Antibody-Drug Conjugates (ADCs)*; van Delft, F., Lambert, J. M., Eds.; Drug Discovery; Royal Society of Chemistry: Cambridge, 2021.
- (6) Schirrmacher, V. *Int. J. Oncol.* **2019**, *54*, 407.
- (7) Debela, D. T.; Muzazu, S. G.; Heraro, K. D.; Ndalama, M. T.; Mesele, B. W.; Haile, D. C.; Kitui, S. K.; Manyazewal, T. *SAGE Open Med.* **2021**, *9*, 1.
- (8) Scott, A. M.; Wolchok, J. D.; Old, L. J. *Nat. Rev. Cancer* **2012**, *12*, 278.
- (9) Izquierdo, M. *Cancer Gene Ther.* **2005**, *12*, 217.
- (10) Dean, N. M.; Frank Bennett, C. *Oncogene* **2003**, *22*, 9087.
- (11) Beck, A.; Goetsch, L.; Dumontet, C.; Corvaia, N. *Nat. Rev. Drug Discov.* **2017**, *16*, 315.
- (12) Lehar, S. M.; Pillow, T.; Xu, M.; Staben, L.; Kajihara, K. K.; Vandlen, R.; DePalatis, L.; Raab, H.; Hazenbos, W. L.; Hiroshi Morisaki, J.; et al. *Nature* **2015**, *527*, 323.
- (13) Peck, M.; Rothenberg, M. E.; Deng, R.; Lewin-Koh, N.; She, G.; Kamath, A. V.; Carrasco-Triguero, M.; Saad, O.; Castro, A.; Teufel, L.; et al. *Antimicrob. Agents Chemother.* **2019**, *63*.
- (14) Chari, R. V. J.; Miller, M. L.; Widdison, W. C. *Angew. Chem. Int. Ed.* **2014**, *53*, 3796.
- (15) Drago, J. Z.; Modi, S.; Chandarlapaty, S. *Nat. Rev. Clin. Oncol.* **2021**, *18*, 327.
- (16) Bross, P. F.; Beitz, J.; Chen, G.; Chen, X. H.; Duffy, E.; Kieffer, L.; Roy, S.; Sridhara, R.; Rahman, A.; Williams, G.; et al. *Clin. Cancer Res.* **2001**, *7*, 1490.
- (17) Goodwin, C. D.; Gale, R. P.; Walter, R. B. *Leukemia* **2017**, *130*, 2373.
- (18) Nicolaou, K. C.; Rigol, S. *Angew. Chem. Int. Ed.* **2019**, *58*, 11206.
- (19) Lamb, Y. N. *Drugs* **2017**, *77*, 1603.
- (20) Ballantyne, A.; Dhillon, S. *Drugs* **2013**, *73*, 755.
- (21) Richardson, N. C.; Kasamon, Y. L.; Chen, H.; de Claro, R. A.; Ye, J.; Blumenthal, G. M.; Farrell, A. T.; Pazdur, R. *Oncologist* **2019**, *24*, e180.
- (22) Deeks, E. D. *Drugs* **2019**, *79*, 1467.
- (23) Hanna, K. S. *Drugs* **2020**, *80*, 1.
- (24) Ebied, A. M.; Patel, K. H.; Cooper-DeHoff, R. M. *Am. J. Med.* **2020**, *133*, 675.
- (25) FDA. FDA grants accelerated approval to tisotumab vedotin-tftv for recurrent or metastatic cervical cancer <https://www.fda.gov/drugs/resources-information-approved-drugs/fda-grants-accelerated-approval-tisotumab-vedotin-tftv-recurrent-or-metastatic-cervical-cancer> (accessed Sep 30, 2021).
- (26) Keam, S. J. *Drugs* **2020**, *80*, 501.
- (27) Syed, Y. Y. *Drugs* **2020**, *80*, 1019.
- (28) Markham, A. *Drugs* **2020**, *80*, 1607.
- (29) Lee, A. *Drugs* **2021**, *81*, 1229.
- (30) Chudasama, V.; Maruani, A.; Caddick, S. *Nat. Chem.* **2016**, *8*, 114.
- (31) Kontermann, R. E. *Curr. Opin. Biotechnol.* **2011**, *22*, 868.
- (32) Panowski, S.; Bhakta, S.; Raab, H.; Polakis, P.; Junutula, J. R. *MAbs* **2014**, *6*, 34.
- (33) Kennedy, P. J.; Oliveira, C.; Granja, P. L.; Sarmiento, B. *Pharmacol. Ther.* **2017**, *177*, 129.
- (34) Trail, P. A.; Willner, D.; Lasch, S. J.; Henderson, A. J.; Hofstead, S.; Casazza, A. M.; Firestone, R. A.; Hellström, I.; Hellström, K. E. *Science* **1993**, *261*, 212.
- (35) Tang, H.; Liu, Y.; Yu, Z.; Sun, M.; Lin, L.; Liu, W.; Han, Q.; Wei, M.; Jin, Y. *Front. Pharmacol.* **2019**, *10*, 373.
- (36) Doronina, S. O.; Toki, B. E.; Torgov, M. Y.; Mendelsohn, B. A.; Cervený, C. G.; Chace, D. F.; DeBlanc, R. L.; Gearing, R. P.; Bovee, T. D.; Siegall, C. B.; et al. *Nat. Biotechnol.* **2003**, *21*, 778.
- (37) Doronina, S. O.; Mendelsohn, B. A.; Bovee, T. D.; Cervený, C. G.; Alley, S. C.; Meyer, D. L.; Oflazoglu, E.; Toki, B. E.; Sanderson, R. J.; Zabinski, R. F.; et al. *Bioconjug. Chem.* **2006**, *17*, 114.
- (38) Kupchan, S. M.; Komoda, Y.; Court, W. A.; Thomas, G. J.; Smith, R. M.; Karim, A.; Gilmore, C. J.; Haitiwanger, R. C.; Bryan, R. F. *J. Am. Chem. Soc.* **1972**, *94*, 1354.
- (39) Remillard, S.; Rebhun, L. I.; Howie, G. A.; Kupchan, S. M. *Science* **1975**, *189*, 1002.
- (40) Chari, R. V. J. *Acc. Chem. Res.* **2008**, *41*, 98.
- (41) Maiese, W. M.; Korshalla, J.; Kuck, N.; Fantini, A.; Wildey, M. J.; Thomas, J.; Greenstein, M.; Lechevalier, M. P.; Lechevalier, H. A. *J. Antibiot.* **1989**, *42*, 558.

- (42) Gredičak, M.; Jerić, I. *Acta Pharm.* **2007**, *57*, 133.
- (43) Tanizawa, A.; Fujimori, A.; Fujimori, Y.; Pommier, Y. *J. Natl. Cancer Inst.* **1994**, *86*, 836.
- (44) Conilh, L.; Fournet, G.; Fourmaux, E.; Murcia, A.; Matera, E. L.; Joseph, B.; Dumontet, C.; Viricel, W. *Pharmaceuticals* **2021**, *14*, 247.
- (45) Hartley, J. A. *Expert Opin. Investig. Drugs* **2011**, *20*, 733.
- (46) Mantaj, J.; Jackson, P. J. M.; Rahman, K. M.; Thurston, D. E. *Angew. Chem. Int. Ed.* **2017**, *56*, 462.
- (47) Pysz, I.; Jackson, P. J. M.; Thurston, D. E. In *Cytotoxic Payloads for Antibody–Drug Conjugates*; 2019; pp 1–30.
- (48) Shen, B. Q.; Xu, K.; Liu, L.; Raab, H.; Bhakta, S.; Kenrick, M.; Parsons-Reponce, K. L.; Tien, J.; Yu, S. F.; Mai, E.; et al. *Nat. Biotechnol.* **2012**, *30*, 184.
- (49) Strop, P.; Liu, S. H.; Dorywalska, M.; Delaria, K.; Dushin, R. G.; Tran, T. T.; Ho, W. H.; Farias, S.; Casas, M. G.; Abdiche, Y.; et al. *Chem. Biol.* **2013**, *20*, 161.
- (50) Hamblett, K. J.; Senter, P. D.; Chace, D. F.; Sun, M. M. C.; Lenox, J.; Cerveny, C. G.; Kissler, K. M.; Bernhardt, S. X.; Kopcha, A. K.; Zabinski, R. F.; et al. *Clin. Cancer Res.* **2004**, *10*, 7063.
- (51) Lyon, R. P.; Bovee, T. D.; Doronina, S. O.; Burke, P. J.; Hunter, J. H.; Neff-Laford, H. D.; Jonas, M.; Anderson, M. E.; Setter, J. R.; Senter, P. D. *Nat. Biotechnol.* **2015**, *33*, 733.
- (52) Sun, X.; Ponte, J. F.; Yoder, N. C.; Laleau, R.; Coccia, J.; Lanieri, L.; Qiu, Q.; Wu, R.; Hong, E.; Bogalhas, M.; et al. *Bioconjug. Chem.* **2017**, *28*, 1371.
- (53) Dorywalska, M.; Strop, P.; Melton-Witt, J. A.; Hasa-Moreno, A.; Farias, S. E.; Galindo Casas, M.; Delaria, K.; Lui, V.; Poulsen, K.; Loo, C.; et al. *Bioconjug. Chem.* **2015**, *26*, 650.
- (54) Walsh, S. J.; Bargh, J. D.; Dannheim, F. M.; Hanby, A. R.; Seki, H.; Counsell, A. J.; Ou, X.; Fowler, E.; Ashman, N.; Takada, Y.; et al. *Chem. Soc. Rev.* **2021**, *50*, 1305.
- (55) Chaubet, G.; Thoreau, F.; Wagner, A. *Drug Discov. Today Technol.* **2018**, *30*, 21.
- (56) Wakankar, A.; Chen, Y.; Gokarn, Y.; Jacobson, F. S. *MAbs* **2011**, *3*, 161.
- (57) Sun, M. M. C.; Beam, K. S.; Cerveny, C. G.; Hamblett, K. J.; Blackmore, R. S.; Torgov, M. Y.; Handley, F. G. M.; Ihle, N. C.; Senter, P. D.; Alley, S. C. *Bioconjug. Chem.* **2005**, *16*, 1282.
- (58) Tumey, L. N.; Charati, M.; He, T.; Sousa, E.; Ma, D.; Han, X.; Clark, T.; Casavant, J.; Loganzo, F.; Barletta, F.; et al. *Bioconjug. Chem.* **2014**, *25*, 1871.
- (59) Szijj, P. A.; Bahou, C.; Chudasama, V. *Drug Discov. Today Technol.* **2018**, *30*, 27.
- (60) Ravasco, J. M. J. M.; Faustino, H.; Trindade, A.; Gois, P. M. P. *Chem. - Eur. J.* **2019**, *25*, 43.
- (61) Lyon, R. P.; Setter, J. R.; Bovee, T. D.; Doronina, S. O.; Hunter, J. H.; Anderson, M. E.; Balasubramanian, C. L.; Duniho, S. M.; Leiske, C. I.; Li, F.; et al. *Nat. Biotechnol.* **2014**, *32*, 1059.
- (62) Christie, R. J.; Fleming, R.; Bezabeh, B.; Woods, R.; Mao, S.; Harper, J.; Joseph, A.; Wang, Q.; Xu, Z. Q.; Wu, H.; et al. *J. Control. Release* **2015**, *220*, 660.
- (63) Forte, N.; Chudasama, V.; Baker, J. R. *Drug Discov. Today Technol.* **2018**, *30*, 11.
- (64) Smith, M. E. B.; Schumacher, F. F.; Ryan, C. P.; Tedaldi, L. M.; Papaioannou, D.; Waksman, G.; Caddick, S.; Baker, J. R. *J. Am. Chem. Soc.* **2010**, *132*, 1960.
- (65) Maruani, A.; Smith, M. E. B.; Miranda, E.; Chester, K. A.; Chudasama, V.; Caddick, S. *Nat. Commun.* **2015**, *6*, 1.
- (66) Badescu, G.; Bryant, P.; Bird, M.; Henseleit, K.; Swierkosz, J.; Parekh, V.; Tommasi, R.; Pawlisz, E.; Jurlewicz, K.; Farys, M.; et al. *Bioconjug. Chem.* **2014**, *25*, 1124.
- (67) Stieger, C. E.; Franz, L.; Körlin, F.; Hackenberger, C. P. R. *Angew. Chem. Int. Ed.* **2021**, *60*, 15359.
- (68) Parker, J. S.; Sore, H. F.; Spring, D. R.; Walsh, S. J. WO 2020/025108, 2020.
- (69) Counsell, A. J.; Walsh, S. J.; Robertson, N. S.; Sore, H. F.; Spring, D. R. *Org. Biomol. Chem.* **2020**, *18*, 4739.
- (70) Kemp, G. C.; Tiberghien, A. C.; Patel, N. V.; D’Hooge, F.; Nilapwar, S. M.; Adams, L. R.; Corbett, S.; Williams, D. G.; Hartley, J. A.; Howard, P. W. *Bioorganic Med. Chem. Lett.* **2017**, *27*, 1154.
- (71) Nunes, J. P. M.; Vassileva, V.; Robinson, E.; Morais, M.; Smith, M. E. B.; Pedley, R. B.; Caddick, S.; Baker, J. R.; Chudasama, V. *RSC Adv.* **2017**, *7*, 24828.
- (72) Bernardim, B.; Cal, P. M. S. D.; Matos, M. J.; Oliveira, B. L.; Martínez-Saéz, N.; Albuquerque, I. S.; Perkins, E.; Corzana, F.; Burtoloso, A. C. B.; Jiménez-Osés, G.; et al. *Nat. Commun.* **2016**, *7*, 13128.
- (73) Oliveira, B. L.; Stenton, B. J.; Unnikrishnan, V. B.; De Almeida, C. R.; Conde, J.; Negrão, M.; Schneider, F. S. S.; Cordeiro, C.; Ferreira, M. G.; Caramori, G. F.; et al. *J. Am. Chem. Soc.* **2020**, *142*, 10869.
- (74) Matos, M. J.; Navo, C. D.; Hakala, T.; Ferhati, X.; Guerreiro, A.; Hartmann, D.; Bernardim, B.; Saar, K. L.; Compañón, I.; Corzana, F.; et al. *Angew. Chem. Int. Ed.* **2019**, *58*, 6640.
- (75) Pillow, T. H.; Sadowsky, J. D.; Zhang, D.; Yu, S.-F.; Del Rosario, G.; Xu, K.; He, J.; Bhakta, S.; Ohri, R.; Kozak, K. R.; et al. *Chem. Sci.* **2017**, *8*, 366.
- (76) Sadowsky, J. D.; Pillow, T. H.; Chen, J.; Fan, F.; He, C.; Wang, Y.; Yan, G.; Yao, H.; Xu, Z.; Martin, S.; et al. *Bioconjug. Chem.* **2017**, *28*, 2086.
- (77) Strop, P. *Bioconjug. Chem.* **2014**, *25*, 855.

- (78) Axup, J. Y.; Bajjuri, K. M.; Ritland, M.; Hutchins, B. M.; Kim, C. H.; Kazane, S. A.; Halder, R.; Forsyth, J. S.; Santidrian, A. F.; Stafin, K.; et al. *Proc. Natl. Acad. Sci. U. S. A.* **2012**, *109*, 16101.
- (79) Oller-Salvia, B.; Kym, G.; Chin, J. W. *Angew. Chem. Int. Ed.* **2018**, *57*, 2831.
- (80) Zimmerman, E. S.; Heibeck, T. H.; Gill, A.; Li, X.; Murray, C. J.; Madlansacay, M. R.; Tran, C.; Uter, N. T.; Yin, G.; Rivers, P. J.; et al. *Bioconjug. Chem.* **2014**, *25*, 351.
- (81) Li, X.; Nelson, C. G.; Nair, R. R.; Hazlehurst, L.; Moroni, T.; Martinez-Acedo, P.; Nanna, A. R.; Hymel, D.; Burke, T. R.; Rader, C. *Cell Chem. Biol.* **2017**, *24*, 433.
- (82) Ochtrop, P.; Hackenberger, C. P. R. *Curr. Opin. Chem. Biol.* **2020**, *58*, 28.
- (83) Smith, N. J.; Rohlfing, K.; Sawicki, L. A.; Kharkar, P. M.; Boyd, S. J.; Kloxin, A. M.; Fox, J. M. *Org. Biomol. Chem.* **2018**, *16*, 2164.
- (84) Kolodych, S.; Koniev, O.; Baatarkhuu, Z.; Bonnefoy, J. Y.; Debaene, F.; Cianféroni, S.; Van Dorsselaer, A.; Wagner, A. *Bioconjug. Chem.* **2015**, *26*, 197.
- (85) Gil de Montes, E.; Jiménez-Moreno, E.; Oliveira, B. L.; Navo, C. D.; Cal, P. M. S. D.; Jiménez-Osés, G.; Robina, I.; Moreno-Vargas, A. J.; Bernardes, G. J. L. *Chem. Sci.* **2019**, *10*, 4515.
- (86) Hansen, B. K.; Loveridge, C. J.; Thyssen, S.; Wørmer, G. J.; Nielsen, A. D.; Palmfeldt, J.; Johannsen, M.; Poulsen, T. B. *Angew. Chem. Int. Ed.* **2019**, *58*, 3533.
- (87) Leriche, G.; Chisholm, L.; Wagner, A. *Bioorganic Med. Chem.* **2012**, *20*, 571.
- (88) Zhang, Y.; Zhou, X.; Xie, Y.; Greenberg, M. M.; Xi, Z.; Zhou, C. *J. Am. Chem. Soc.* **2017**, *139*, 6146.
- (89) Yu, J.; Yang, X.; Sun, Y.; Yin, Z. *Angew. Chem. Int. Ed.* **2018**, *57*, 11598.
- (90) Chalker, J. M.; Gunnoo, S. B.; Boutureira, O.; Gerstberger, S. C.; Fernández-González, M.; Bernardes, G. J. L.; Griffin, L.; Hailu, H.; Schofield, C. J.; Davis, B. G. *Chem. Sci.* **2011**, *2*, 1666.
- (91) Vinogradova, E. V.; Zhang, C.; Spokoynny, A. M.; Pentelute, B. L.; Buchwald, S. L. *Nature* **2015**, *526*, 687.
- (92) Dhanjee, H. H.; Saebi, A.; Buslov, I.; Loftis, A. R.; Buchwald, S. L.; Pentelute, B. L. *J. Am. Chem. Soc.* **2020**, *142*, 9124.
- (93) Bargh, J. D.; Isidro-Llobet, A.; Parker, J. S.; Spring, D. R. *Chem. Soc. Rev.* **2019**, *48*, 4361.
- (94) Devay, R. M.; Delaria, K.; Zhu, G.; Holz, C.; Foletti, D.; Sutton, J.; Bolton, G.; Dushin, R.; Bee, C.; Pons, J.; et al. *Bioconjug. Chem.* **2017**, *28*, 1102.
- (95) Erickson, H. K.; Widdison, W. C.; Mayo, M. F.; Whiteman, K.; Audette, C.; Wilhelm, S. D.; Singh, R. *Bioconjug. Chem.* **2010**, *21*, 84.
- (96) Alley, S. C.; Okeley, N. M.; Senter, P. D. *Curr. Opin. Chem. Biol.* **2010**, *14*, 529.
- (97) Hamann, P. R.; Hinman, L. M.; Hollander, I.; Beyer, C. F.; Lindh, D.; Holcomb, R.; Hallett, W.; Tsou, H. R.; Upešlacis, J.; Shochat, D.; et al. *Bioconjug. Chem.* **2002**, *13*, 47.
- (98) Moon, S. J.; Govindan, S. V.; Cardillo, T. M.; D'Souza, C. A.; Hansen, H. J.; Goldenberg, D. M. *J. Med. Chem.* **2008**, *51*, 6916.
- (99) Govindan, S. V.; Cardillo, T. M.; Sharkey, R. M.; Tat, F.; Gold, D. V.; Goldenberg, D. M. *Mol. Cancer Ther.* **2013**, *12*, 968.
- (100) Lu, J.; Jiang, F.; Lu, A.; Zhang, G. *Int. J. Mol. Sci.* **2016**, *17*, 561.
- (101) Dubowchik, G. M.; Firestone, R. A.; Padilla, L.; Willner, D.; Hofstead, S. J.; Mosure, K.; Knipe, J. O.; Lasch, S. J.; Trail, P. A. *Bioconjug. Chem.* **2002**, *13*, 855.
- (102) Wang, Y.; Fan, S.; Zhong, W.; Zhou, X.; Li, S. *Int. J. Mol. Sci.* **2017**, *18*, 1860.
- (103) Dubowchik, G. M.; Firestone, R. A. *Bioorganic Med. Chem. Lett.* **1998**, *8*, 3341.
- (104) Tiberghien, A. C.; Levy, J. N.; Masterson, L. A.; Patel, N. V.; Adams, L. R.; Corbett, S.; Williams, D. G.; Hartley, J. A.; Howard, P. W. *ACS Med. Chem. Lett.* **2016**, *7*, 983.
- (105) Kolodych, S.; Michel, C.; Delacroix, S.; Koniev, O.; Ehkirch, A.; Eberova, J.; Cianféroni, S.; Renoux, B.; Krezel, W.; Poinot, P.; et al. *Eur. J. Med. Chem.* **2017**, *142*, 376.
- (106) Kolakowski, R. V.; Haelsig, K. T.; Emmerton, K. K.; Leiske, C. I.; Miyamoto, J. B.; Cochran, J. H.; Lyon, R. P.; Senter, P. D.; Jeffrey, S. C. *Angew. Chem. Int. Ed.* **2016**, *55*, 7948.
- (107) Kern, J. C.; Dooney, D.; Zhang, R.; Liang, L.; Brandish, P. E.; Cheng, M.; Feng, G.; Beck, A.; Bresson, D.; Firdos, J.; et al. *Bioconjug. Chem.* **2016**, *27*, 2081.
- (108) Kern, J. C.; Cancilla, M.; Dooney, D.; Kwasnjuk, K.; Zhang, R.; Beaumont, M.; Figueroa, I.; Hsieh, S. C.; Liang, L.; Tomazela, D.; et al. *J. Am. Chem. Soc.* **2016**, *138*, 1430.
- (109) Bargh, J. D.; Walsh, S. J.; Isidro-Llobet, A.; Omarjee, S.; Carroll, J. S.; Spring, D. R. *Chem. Sci.* **2020**, *11*, 2375.
- (110) Bargh, J. D.; Walsh, S. J.; Ashman, N.; Isidro-Llobet, A.; Carroll, J. S.; Spring, D. R. *Chem. Commun.* **2021**, *57*, 3457.
- (111) Hoyt, E. A.; Cal, P. M. S. D.; Oliveira, B. L.; Bernardes, G. J. L. *Nat. Rev. Chem.* **2019**, *3*, 147.
- (112) Tamura, T.; Hamachi, I. *J. Am. Chem. Soc.* **2019**, *141*, 2782.
- (113) Walsh, S. J.; Omarjee, S.; Galloway, W. R. J. D.; Kwan, T. T.-L.; Sore, H. F.; Parker, J. S.; Hyvönen, M.; Carroll, J. S.; Spring, D. R. *Chem. Sci.* **2019**, *10*, 694.

- (114) Robertson, N. S.; Walsh, S. J.; Fowler, E.; Yoshida, M.; Rowe, S.; Wu, Y.; Sore, H.; Parker, J.; Spring, D. R. *Chem. Commun.* **2019**, *55*, 9499.
- (115) Walsh, S. J.; Iegre, J.; Seki, H.; Bargh, J. D.; Sore, H. F.; Parker, J. S.; Carroll, J. S.; Spring, D. R. *Org. Biomol. Chem.* **2020**, *18*, 4224.
- (116) Charoenpattarapreeda, J.; Walsh, S. J.; Carroll, J. S.; Spring, D. R. *Angew. Chem. Int. Ed.* **2020**, *59*, 23045.
- (117) Seki, H.; Walsh, S. J.; Bargh, J. D.; Parker, J. S.; Carroll, J.; Spring, D. R. *Chem. Sci.* **2021**, *12*, 9060.
- (118) Novák, Z.; Bostai, B.; Csékei, M.; Lőrincz, K.; Kotschy, A. *Heterocycles* **2003**, *60*, 2653.
- (119) Bender, A. M.; Chopko, T. C.; Bridges, T. M.; Lindsley, C. W. *Org. Lett.* **2017**, *19*, 5693.
- (120) Lang, K.; Chin, J. W. *ACS Chem. Biol.* **2014**, *9*, 16.
- (121) Kamber, D. N.; Liang, Y.; Blizzard, R. J.; Liu, F.; Mehl, R. A.; Houk, K. N.; Prescher, J. A. *J. Am. Chem. Soc.* **2015**, *137*, 8388.
- (122) Umlauf, B. J.; Mix, K. A.; Grosskopf, V. A.; Raines, R. T.; Shusta, E. V. *Bioconjug. Chem.* **2018**, *29*, 1605.
- (123) Brewer, C. F.; Riehm, J. P. *Anal. Biochem.* **1967**, *18*, 248.
- (124) Kasper, M. A.; Glanz, M.; Stengl, A.; Penkert, M.; Klenk, S.; Sauer, T.; Schumacher, D.; Helma, J.; Krause, E.; Cardoso, M. C.; et al. *Angew. Chem. Int. Ed.* **2019**, *58*, 11625.
- (125) Václavík, J.; Zschoche, R.; Klimánková, I.; Matoušek, V.; Beier, P.; Hilvert, D.; Togni, A. *Chem. - Eur. J.* **2017**, *23*, 6490.
- (126) Wall, A.; Nicholls, K.; Caspersen, M. B.; Skrivergaard, S.; Howard, K. A.; Karu, K.; Chudasama, V.; Baker, J. R. *Org. Biomol. Chem.* **2019**, *17*, 7870.
- (127) Junutula, J. R.; Raab, H.; Clark, S.; Bhakta, S.; Leipold, D. D.; Weir, S.; Chen, Y.; Simpson, M.; Tsai, S. P.; Dennis, M. S.; et al. *Nat. Biotechnol.* **2008**, *26*, 925.
- (128) McKeage, K.; Perry, C. M. *Drugs* **2002**, *62*, 209.
- (129) Dimasi, N.; Fleming, R.; Zhong, H.; Bezabeh, B.; Kinneer, K.; Christie, R. J.; Fazenbaker, C.; Wu, H.; Gao, C. *Mol. Pharm.* **2017**, *14*, 1501.
- (130) Bernardim, B.; Dunsmore, L.; Li, H.; Hocking, B.; Nuñez-Franco, R.; Navo, C. D.; Jiménez-Osés, G.; Burtoloso, A. C. B.; Bernardes, G. J. L.; Bernardes, G. J. L. *Bioconjug. Chem.* **2020**, *31*, 1604.
- (131) Siegl, S. J.; Dzajak, R.; Vázquez, A.; Pohl, R.; Vrabel, M. *Chem. Sci.* **2017**, *8*, 3593.
- (132) Kamber, D. N.; Nguyen, S. S.; Liu, F.; Briggs, J. S.; Shih, H. W.; Row, R. D.; Long, Z. G.; Houk, K. N.; Liang, Y.; Prescher, J. A. *Chem. Sci.* **2019**, *10*, 9109.
- (133) Row, R. D.; Prescher, J. A. *Acc. Chem. Res.* **2018**, *51*, 1073.
- (134) Horner, K. A.; Valette, N. M.; Webb, M. E. *Chem. - Eur. J.* **2015**, *21*, 14376.
- (135) Reisacher, U.; Ploschik, D.; Rönicke, F.; Cserép, G. B.; Kele, P.; Wagenknecht, H.-A. *Chem. Sci.* **2019**, *10*, 4032.
- (136) Reisacher, U.; Groitl, B.; Strasser, R.; Cserép, G. B.; Kele, P.; Wagenknecht, H.-A. *Bioconjug. Chem.* **2019**, *30*, 1773.
- (137) Gunasekera, S. P.; Gunasekera, M.; Longley, R. E.; Schulte, G. K. *J. Org. Chem.* **1990**, *55*, 4912.
- (138) Hung, D. T.; Nerenberg, J. B.; Schreiber, S. L. *Chem. Biol.* **1994**, *1*, 67.
- (139) Kowalski, R. J.; Giannakakou, P.; Gunasekera, S. P.; Longley, R. E.; Day, B. W.; Hamel, E. *Mol. Pharmacol.* **1997**, *52*, 613.
- (140) Kalesse, M. *ChemBioChem* **2000**, *39*, 171.
- (141) Ter Haar, E.; Kowalski, R. J.; Hamel, E.; Lin, C. M.; Longley, R. E.; Gunasekera, S. P.; Rosenkranz, H. S.; Day, B. W. *Biochemistry* **1996**, *35*, 243.
- (142) Paterson, I.; Florence, G. J. In *Topics in Current Chemistry*; 2009; Vol. 286, pp 73–119.
- (143) Nerenberg, J. B.; Hung, D. T.; Somers, P. K.; Schreiber, S. L. *J. Am. Chem. Soc.* **1993**, *115*, 12621.
- (144) Smith, A. B.; Beauchamp, T. J.; Lamarche, M. J.; Kaufman, M. D.; Qiu, Y.; Arimoto, H.; Jones, D. R.; Kobayashi, K. *J. Am. Chem. Soc.* **2000**, *122*, 8654.
- (145) Harried, S. S.; Yang, G.; Strawn, M. A.; Myles, D. C. *J. Org. Chem.* **1997**, *62*, 6098.
- (146) Marshall, J. A.; Johns, B. A. *J. Org. Chem.* **1998**, *63*, 7885.
- (147) Mickel, S. J.; Sedelmeier, G. H.; Niederer, D.; Daeffler, R.; Osmani, A.; Schreiner, K.; Seeger-Weibel, M.; Bérod, B.; Schaer, K.; Gamboni, R.; et al. *Org. Process Res. Dev.* **2004**, *8*, 92.
- (148) Mickel, S. J.; Sedelmeier, G. H.; Niederer, D.; Schuerch, F.; Grimler, D.; Koch, G.; Daeffler, R.; Osmani, A.; Hirni, A.; Schaer, K.; et al. *Org. Process Res. Dev.* **2004**, *8*, 101.
- (149) Mickel, S. J.; Sedelmeier, G. H.; Niederer, D.; Schuerch, F.; Koch, G.; Kuesters, E.; Daeffler, R.; Osmani, A.; Seeger-Weibel, M.; Schmid, E.; et al. *Org. Process Res. Dev.* **2004**, *8*, 107.
- (150) Mickel, S. J.; Sedelmeier, G. H.; Niederer, D.; Schuerch, F.; Seger, M.; Schreiner, K.; Daeffler, R.; Osmani, A.; Bixel, D.; Loiseleur, O.; et al. *Org. Process Res. Dev.* **2004**, *8*, 113.
- (151) Mickel, S. J.; Niederer, D.; Daeffler, R.; Osmani, A.; Kuesters, E.; Schmid, E.; Schaer, K.; Gamboni, R.; Chen, W.; Loeser, E.; et al. *Org. Process Res. Dev.* **2004**, *8*, 122.
- (152) Kern, J. C.; Dooney, D.; Zhang, R.; Liang, L.; Brandish, P. E.; Cheng, M.; Feng, G.; Beck, A.; Bresson,

- D.; Firdos, J.; et al. *Bioconjug. Chem.* **2016**, *27*, 2081.
- (153) Kern, J. C.; Cancilla, M.; Dooney, D.; Kwasnjuk, K.; Zhang, R.; Beaumont, M.; Figueroa, I.; Hsieh, S. C.; Liang, L.; Tomazela, D.; et al. *J. Am. Chem. Soc.* **2016**, *138*, 1430.
- (154) Spencer, C. M.; Faulds, D. *Drugs* **1994**, *48*, 794.
- (155) Wiseman, L. R.; Markham, A. *Drugs* **1996**, *52*, 606.
- (156) Li, W.; Veale, K. H.; Qiu, Q.; Sinkevicius, K. W.; Maloney, E. K.; Costoplus, J. A.; Lau, J.; Evans, H. L.; Setiady, Y.; Ab, O.; et al. *ACS Med. Chem. Lett.* **2019**, *10*, 1386.

Chapter 6. Appendix

6.1. Spectra from kinetic studies

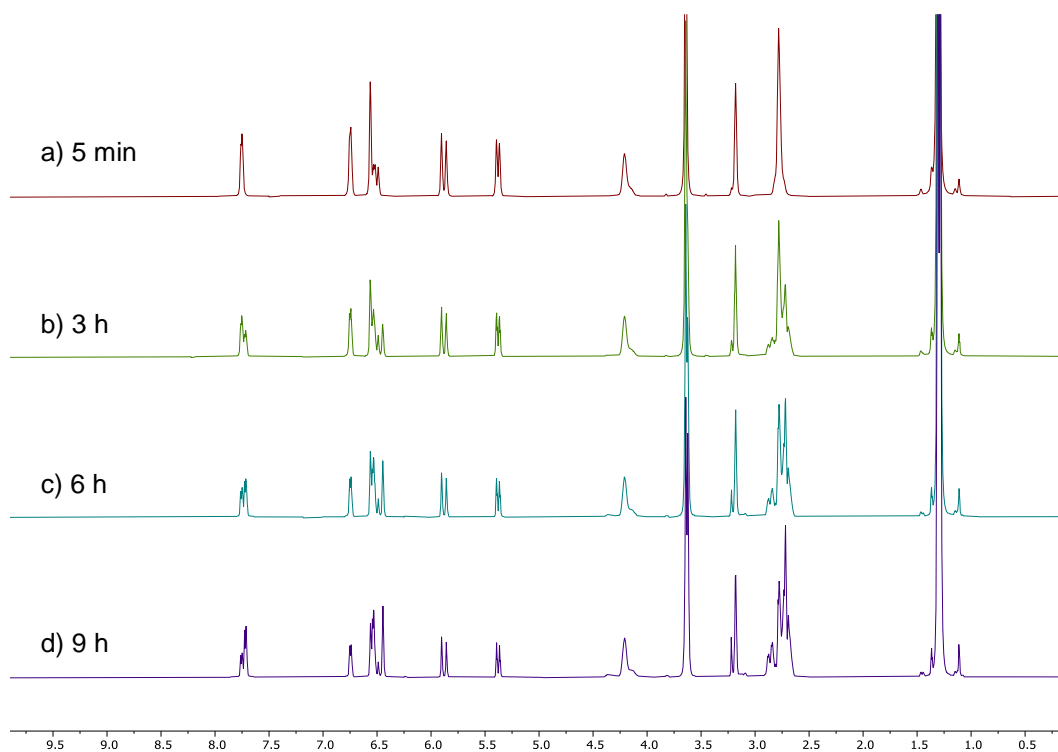


Figure S1. Representative ¹H NMR spectra of the reaction of vinylpyridine **2** with Boc-Cys-OMe in 3:7 CD₃OD/NaPi (pH 8, 50 mM in D₂O).

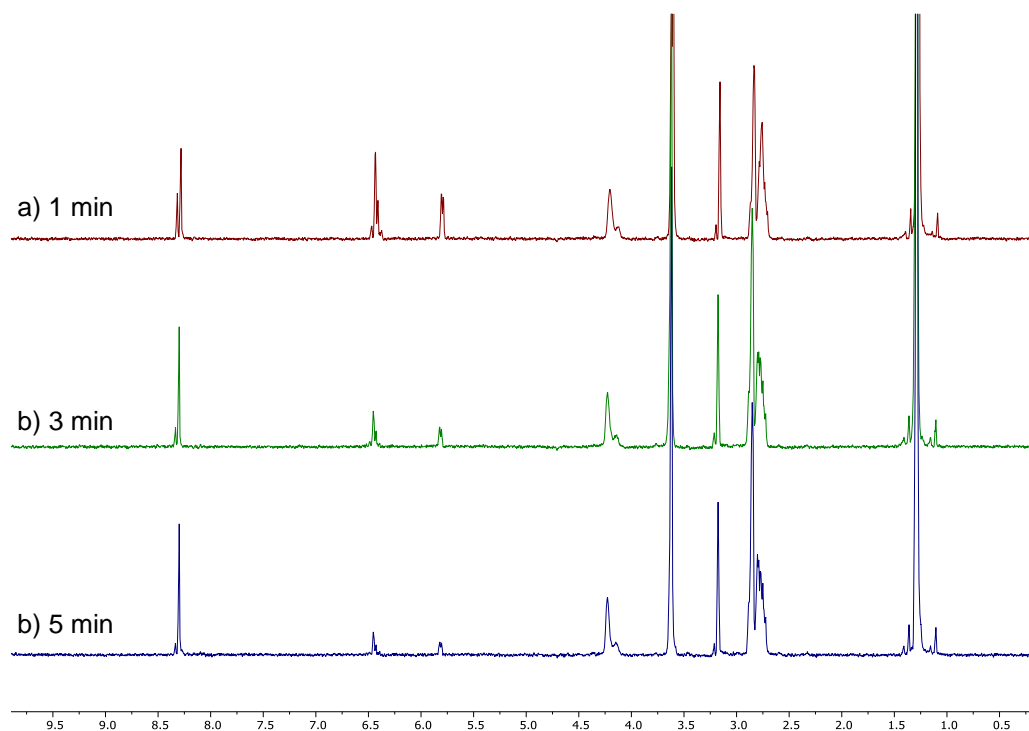


Figure S2. Representative ¹H NMR spectra of the reaction of vinyltriazine **7** with Boc-Cys-OMe in 3:7 CD₃OD/NaPi (pH 8, 50 mM in D₂O).

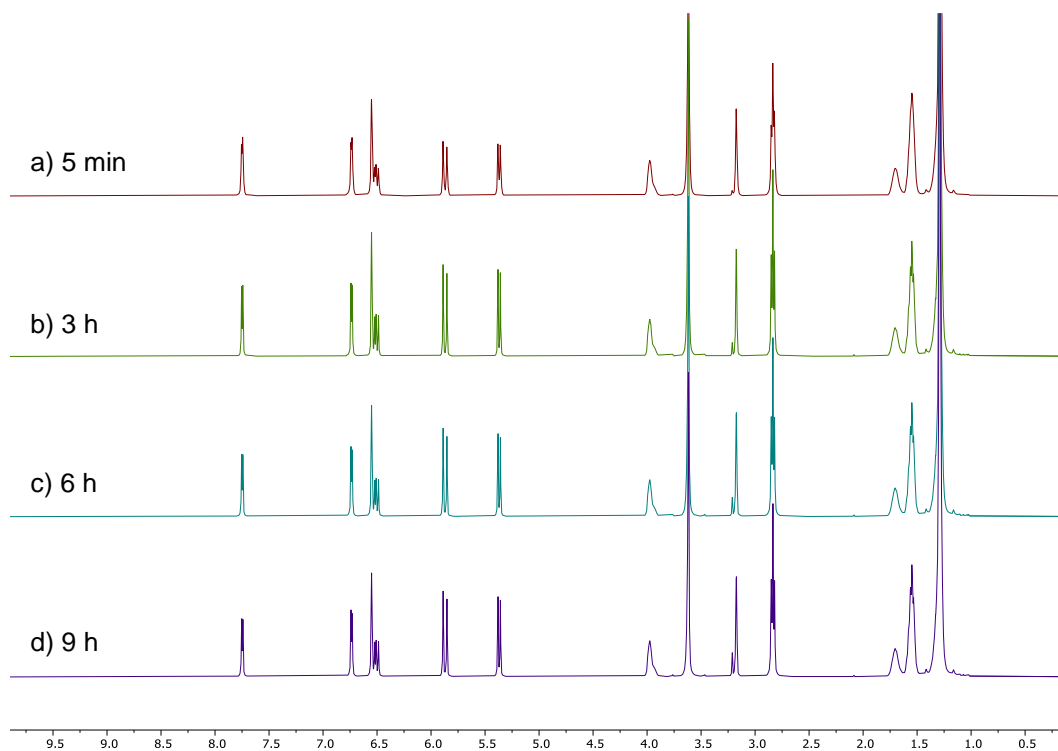


Figure S3. Representative ^1H NMR spectra of the reaction of vinylpyridine **2** with Boc-Lys-OMe·HCl in 3:7 $\text{CD}_3\text{OD}/\text{NaPi}$ (pH 8, 50 mM in D_2O).

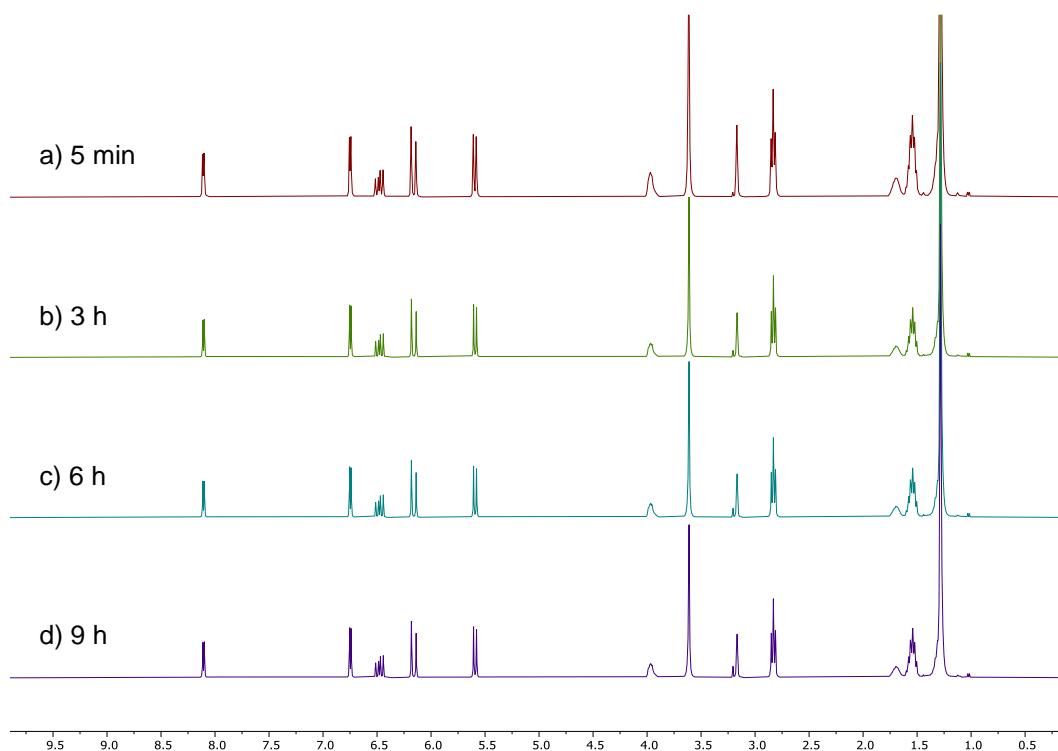


Figure S4. Representative ^1H NMR spectra of the reaction of vinylpyrimidine **4** with Boc-Lys-OMe·HCl in 3:7 $\text{CD}_3\text{OD}/\text{NaPi}$ (pH 8, 50 mM in D_2O).

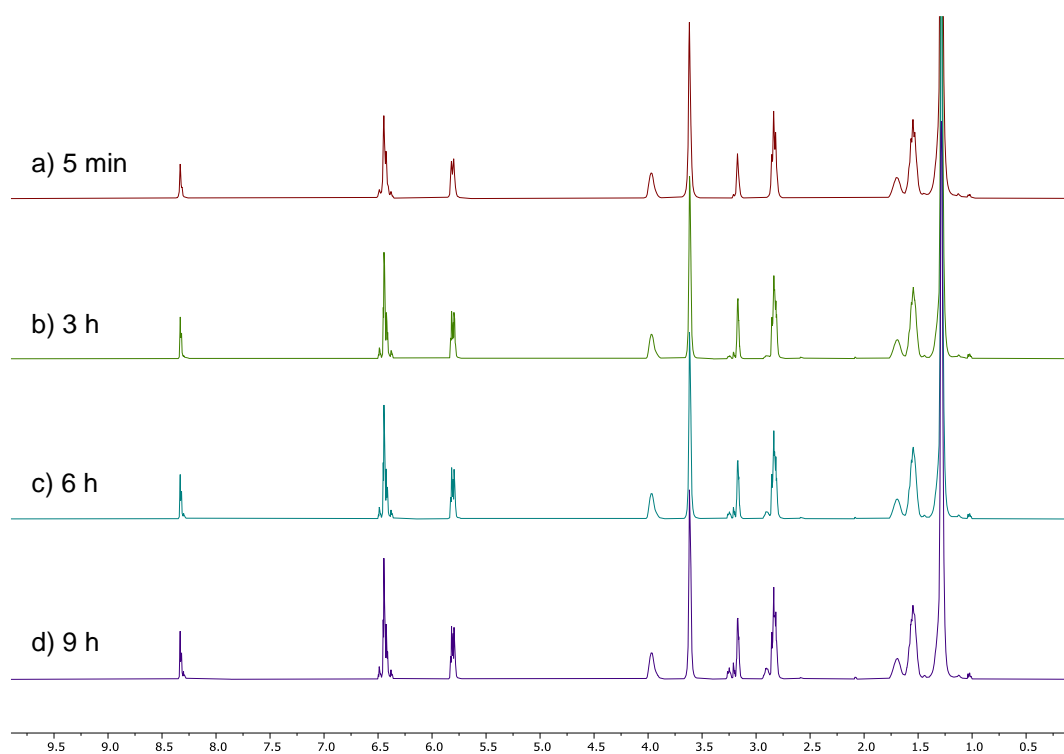


Figure S5. Representative ^1H NMR spectra of the reaction of vinyltriazine **7** with Boc-Lys-OMe·HCl in 3:7 $\text{CD}_3\text{OD}/\text{NaPi}$ (pH 8, 50 mM in D_2O).

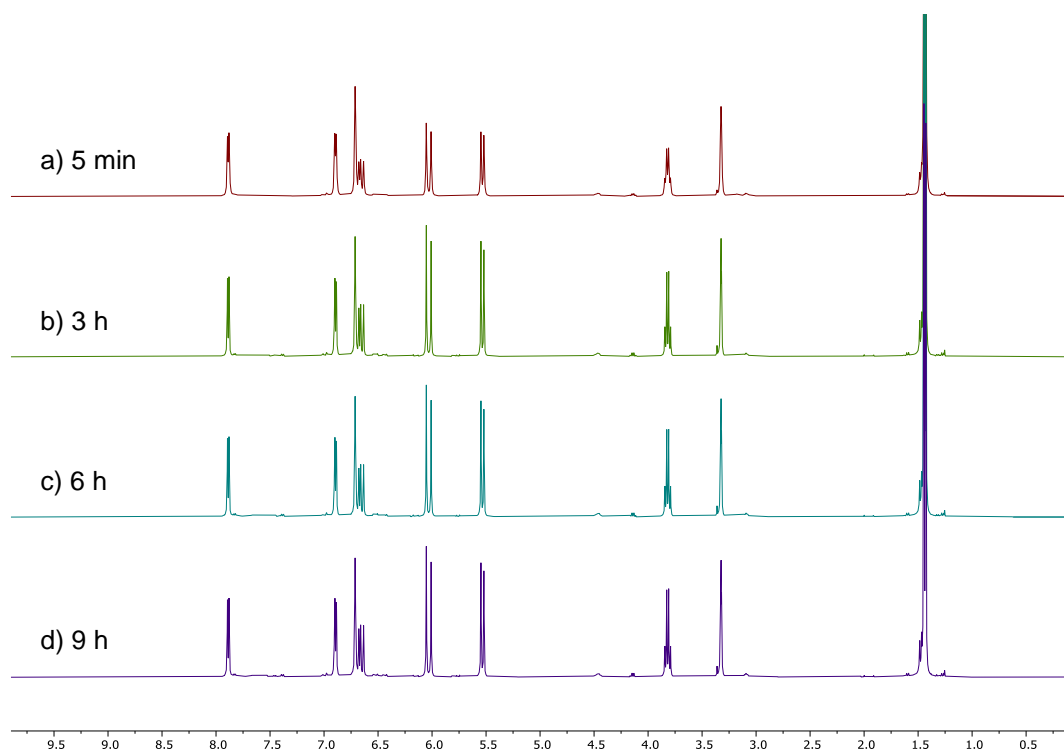


Figure S6. Representative ^1H NMR spectra of the reaction of vinylpyridine **2** with H-Ala- $\text{NH}_2\cdot\text{HCl}$ in 3:7 $\text{CD}_3\text{OD}/\text{NaPi}$ (pH 8, 50 mM in D_2O).

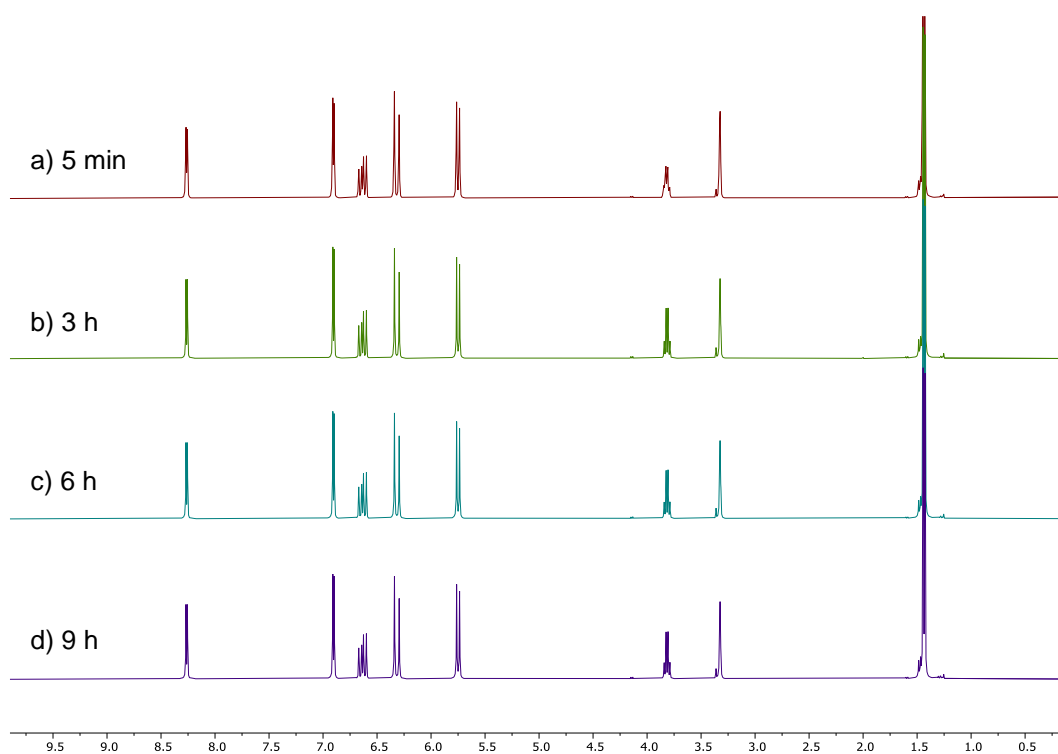


Figure S7. Representative ^1H NMR spectra of the reaction of vinylpyrimidine **4** with H-Ala-NH₂·HCl in 3:7 CD₃OD/NaPi (pH 8, 50 mM in D₂O).

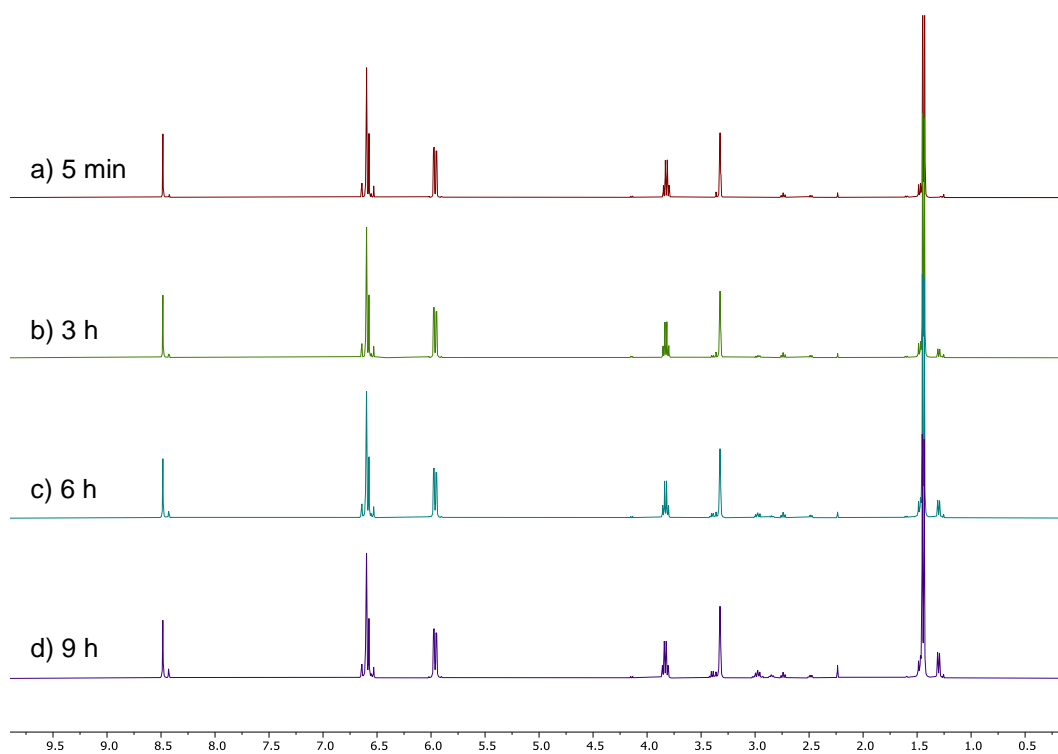


Figure S8. Representative ^1H NMR spectra of the reaction of vinyltriazine **7** with H-Ala-NH₂·HCl in 3:7 CD₃OD/NaPi (pH 8, 50 mM in D₂O).

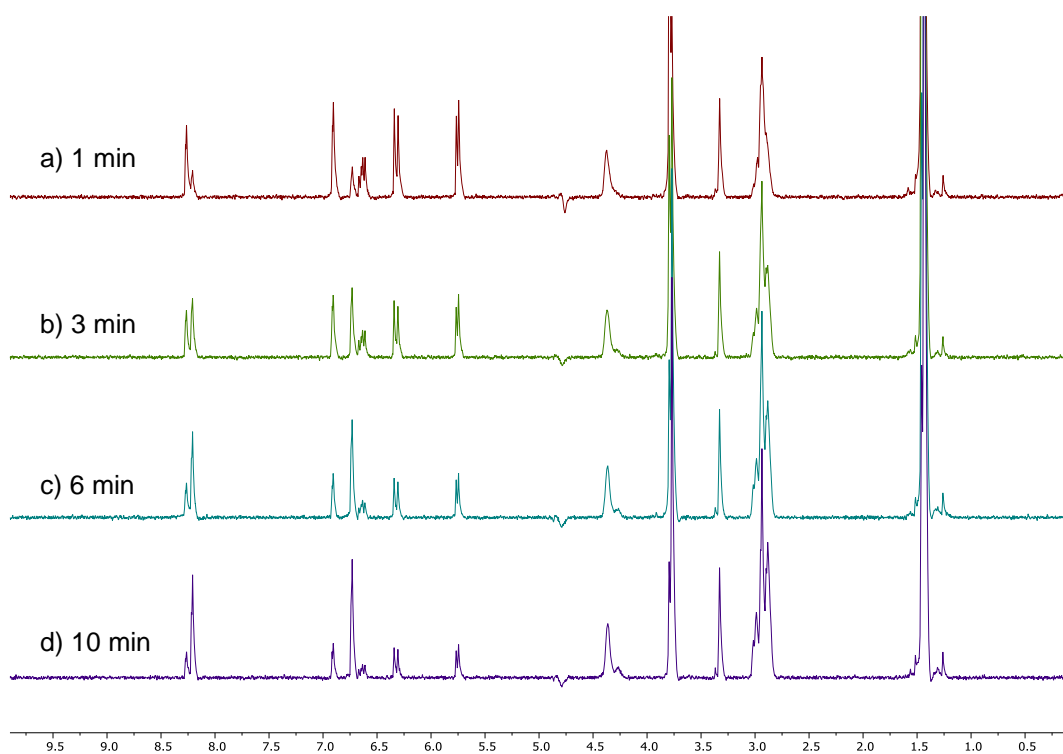


Figure S9. Representative ^1H NMR spectra of the reaction of vinylpyrimidine **4** with Boc-Cys-OMe in 3:7 $\text{CD}_3\text{OD}/\text{NaPi}$ (pH 7, 50 mM in D_2O).

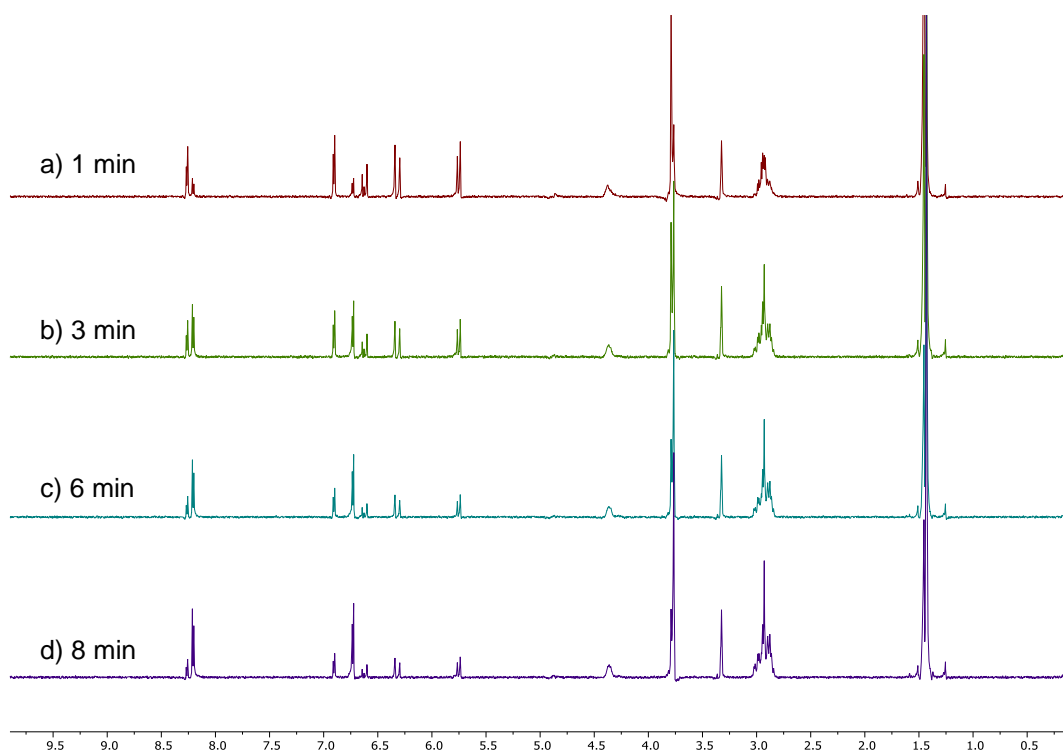


Figure S10. Representative ^1H NMR spectra of the reaction of vinylpyrimidine **4** with Boc-Cys-OMe in 3:7 $\text{CD}_3\text{OD}/\text{NaPi}$ (pH 6, 50 mM in D_2O).

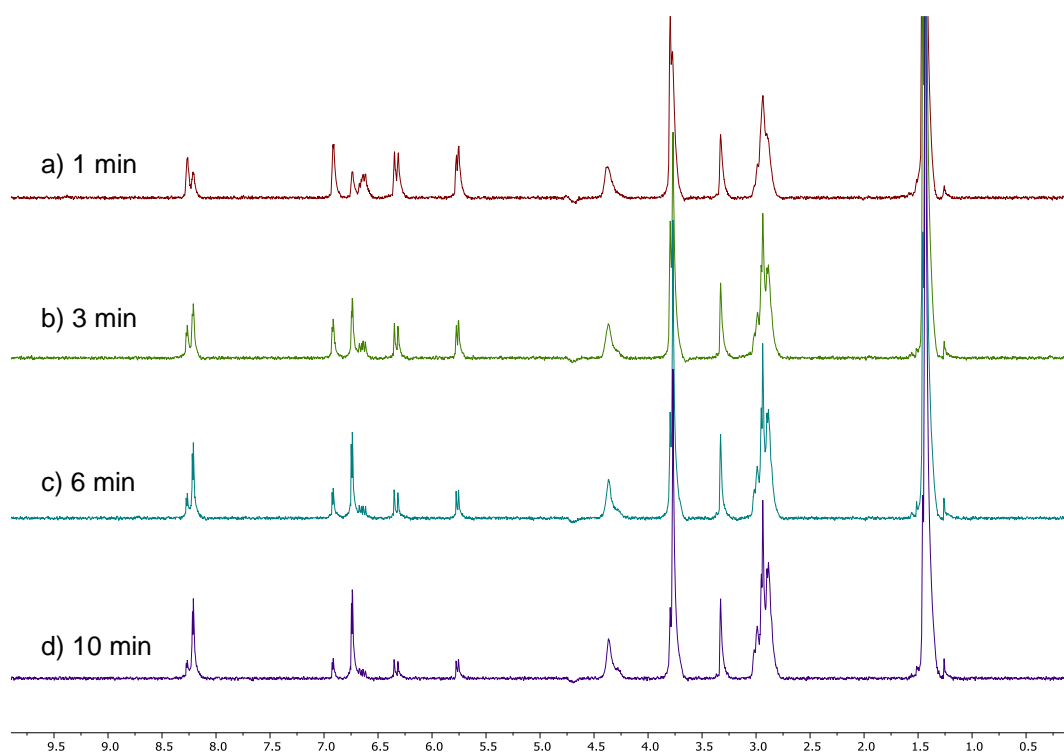


Figure S11. Representative ^1H NMR spectra of the reaction of vinylpyrimidine **4** with Boc-Cys-OMe in 3:7 $\text{CD}_3\text{OD}/\text{CD}_3\text{CO}_2\text{Na}$ (pH 5, 50 mM in D_2O).

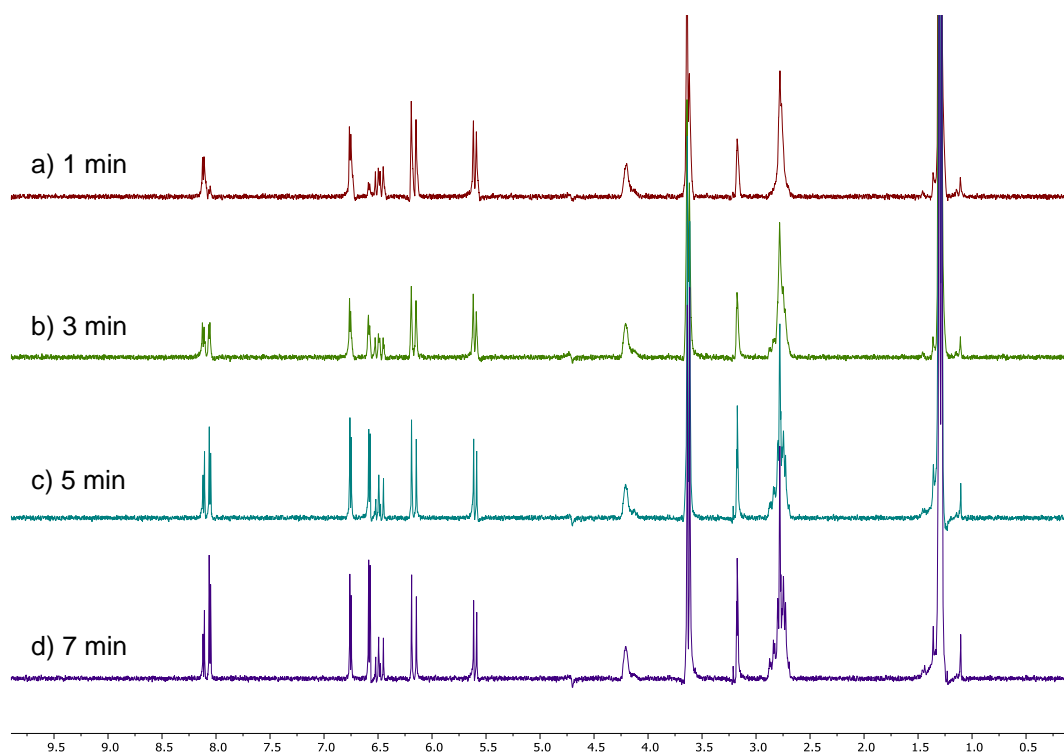


Figure S12. Representative ^1H NMR spectra of the reaction of vinylpyrimidine **4** with Boc-Cys-OMe in 3:7 $\text{CD}_3\text{OD}/\text{NaPi}$ (pH 8, 25 mM in D_2O).

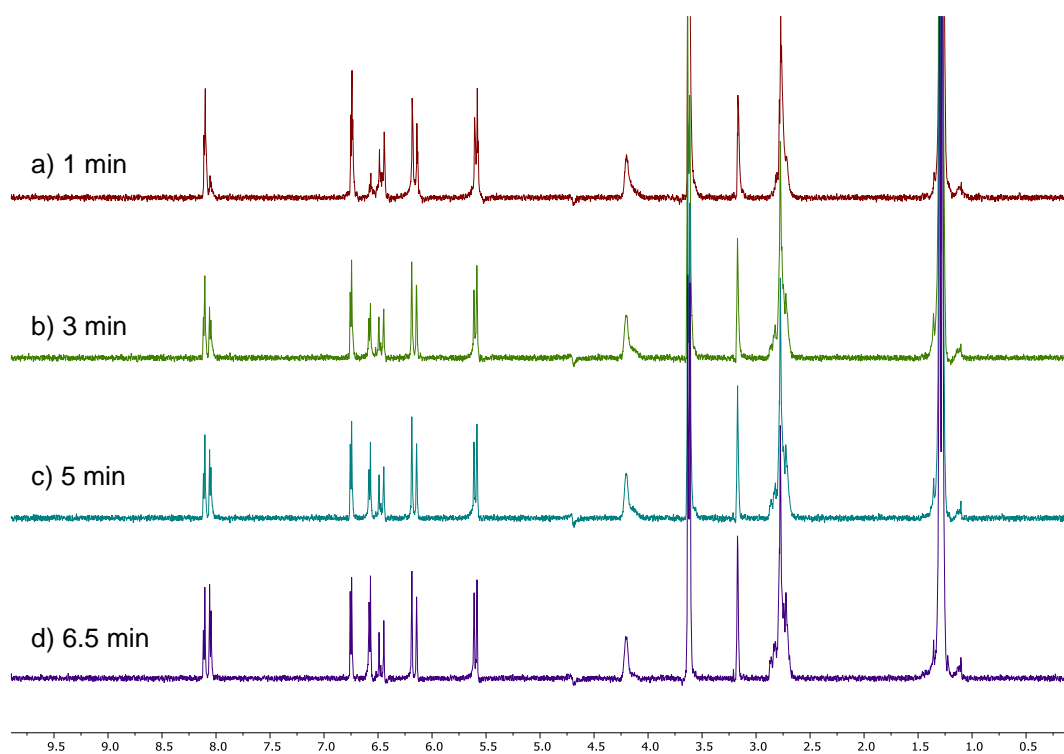


Figure S13. Representative ¹H NMR spectra of the reaction of vinylpyrimidine **4** with Boc-Cys-OMe in 3:7 CD₃OD/NaPi (pH 8, 10 mM in D₂O).

6.2. Spectra from thioether stability studies

Stability data for pyrimidine 10

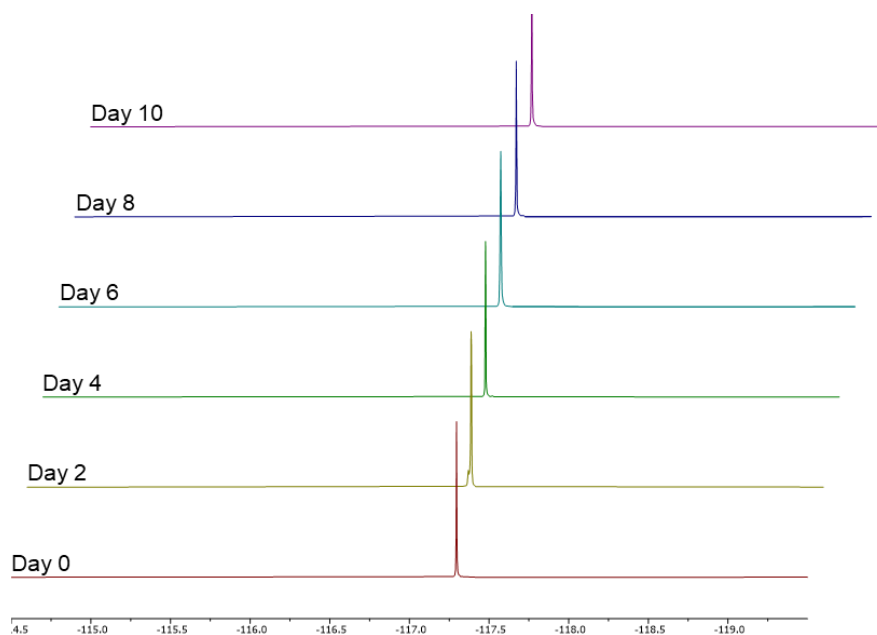


Figure S14. Representative ^{19}F NMR spectra for the stability study of pyrimidine **10** in the presence of 1-thioglycerol, CD_3CN , and NaPi (pH 7.4, 50 mM in H_2O).

Stability data for triazine 11

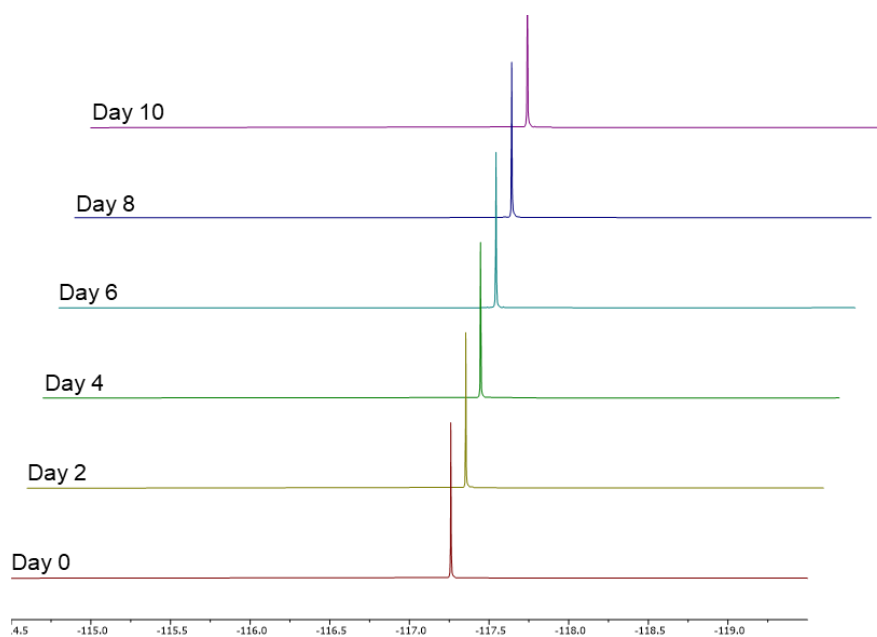


Figure S15. Representative ^{19}F NMR spectra for the stability study of triazine **11** in the presence of 1-thioglycerol, CD_3CN , and NaPi (pH 7.4, 50 mM in H_2O).

Stability data for succinimide **13**

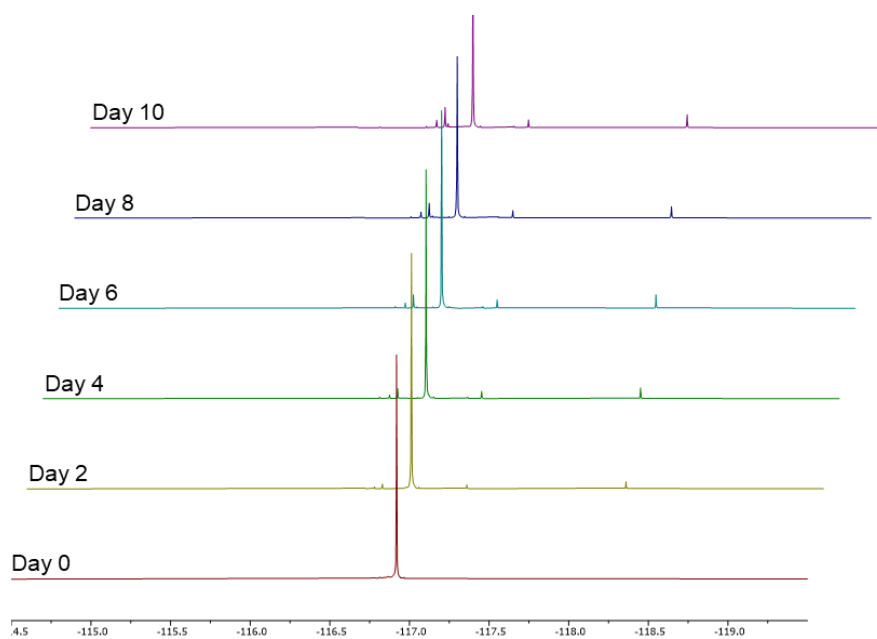
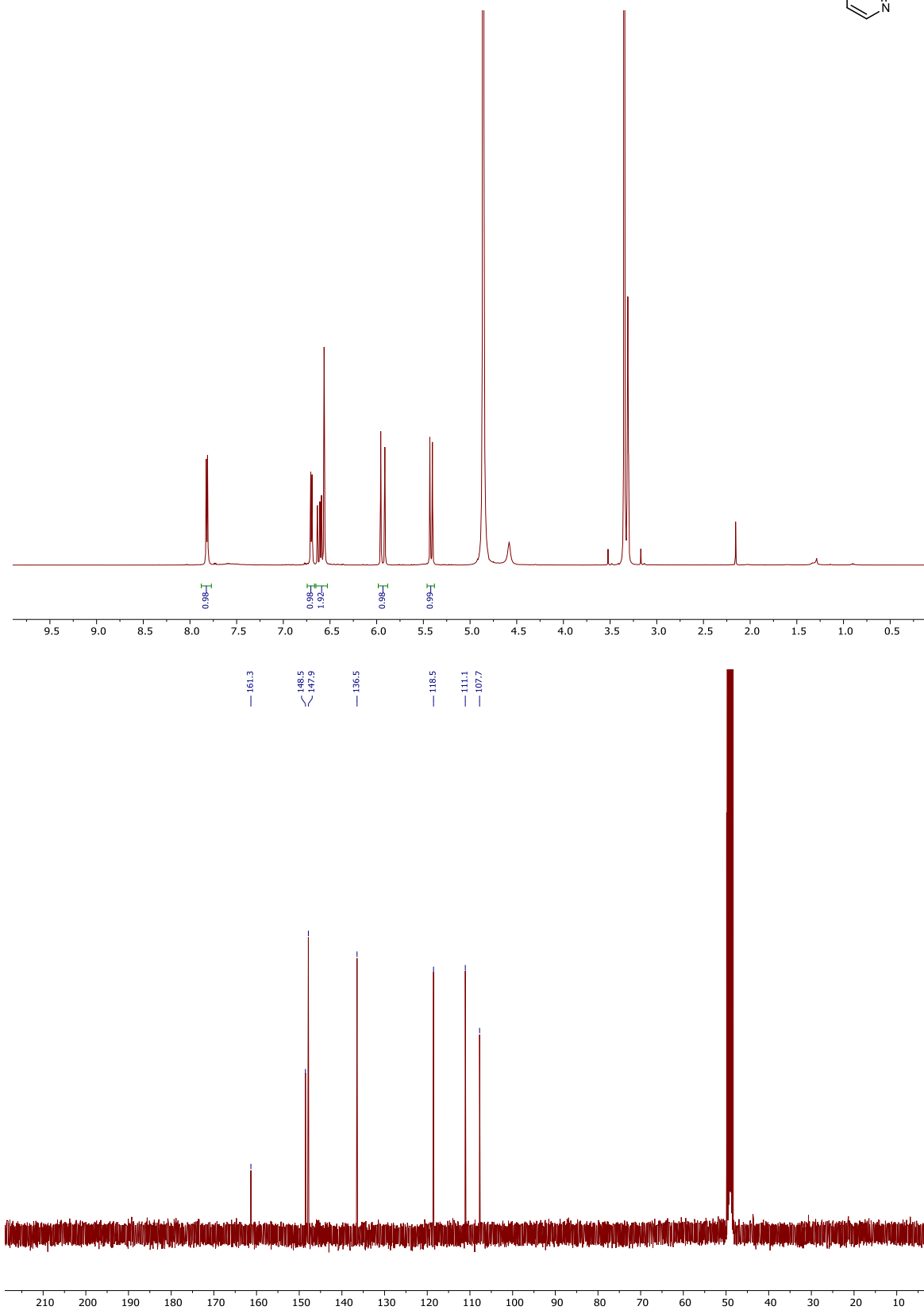
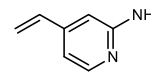


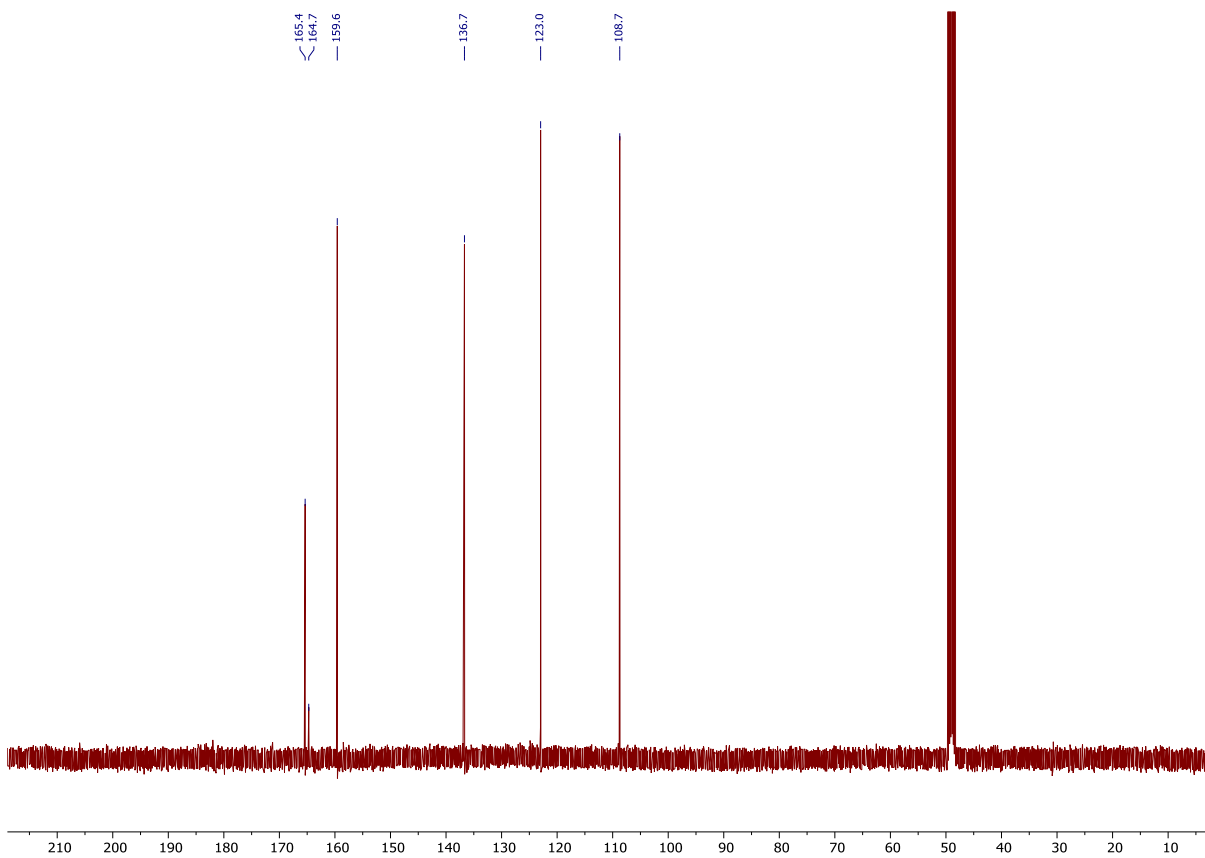
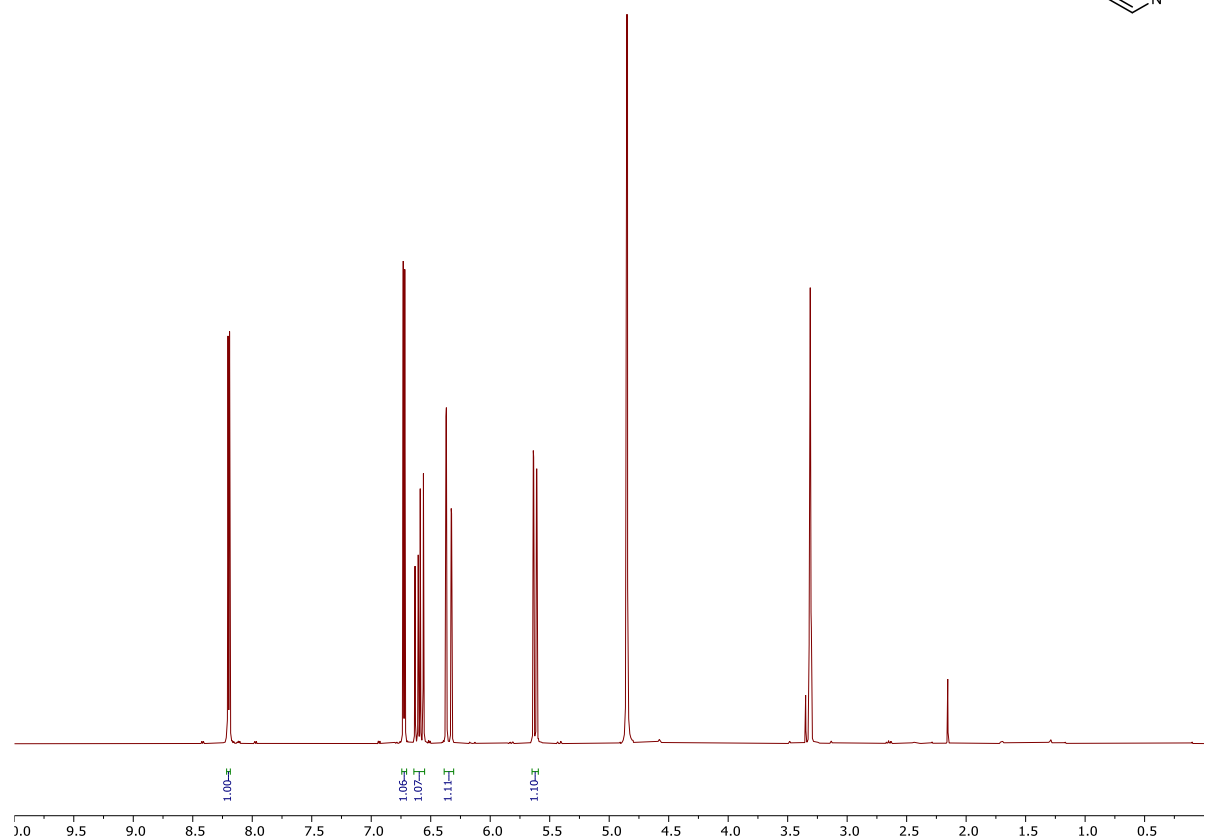
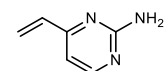
Figure S16. Representative ^{19}F NMR spectra for the stability study of succinimide **13** in the presence of 1-thioglycerol, CD_3CN , and NaPi (pH 7.4, 50 mM in H_2O). A number of new fluorinated peaks emerged over the ten-day incubation period.

6.3. Spectra of small molecules

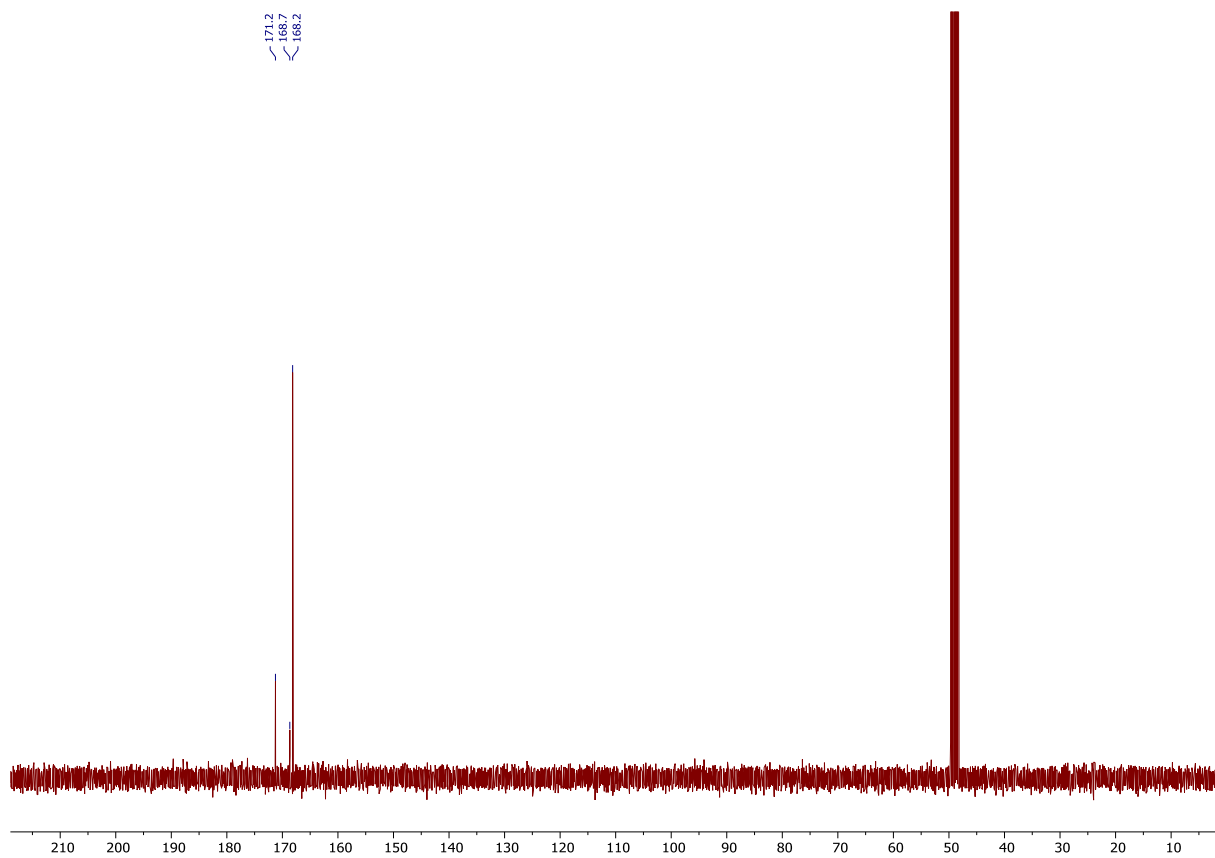
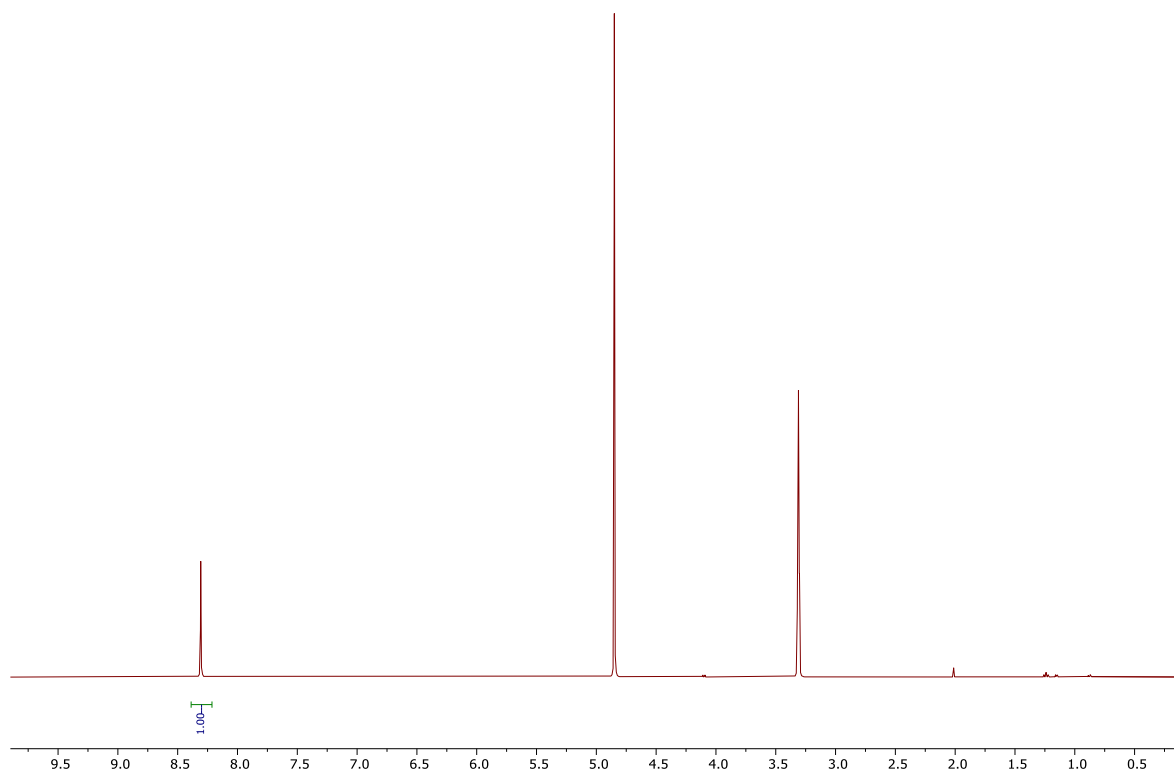
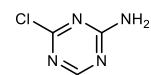
4-Vinylpyridin-2-amine (2)



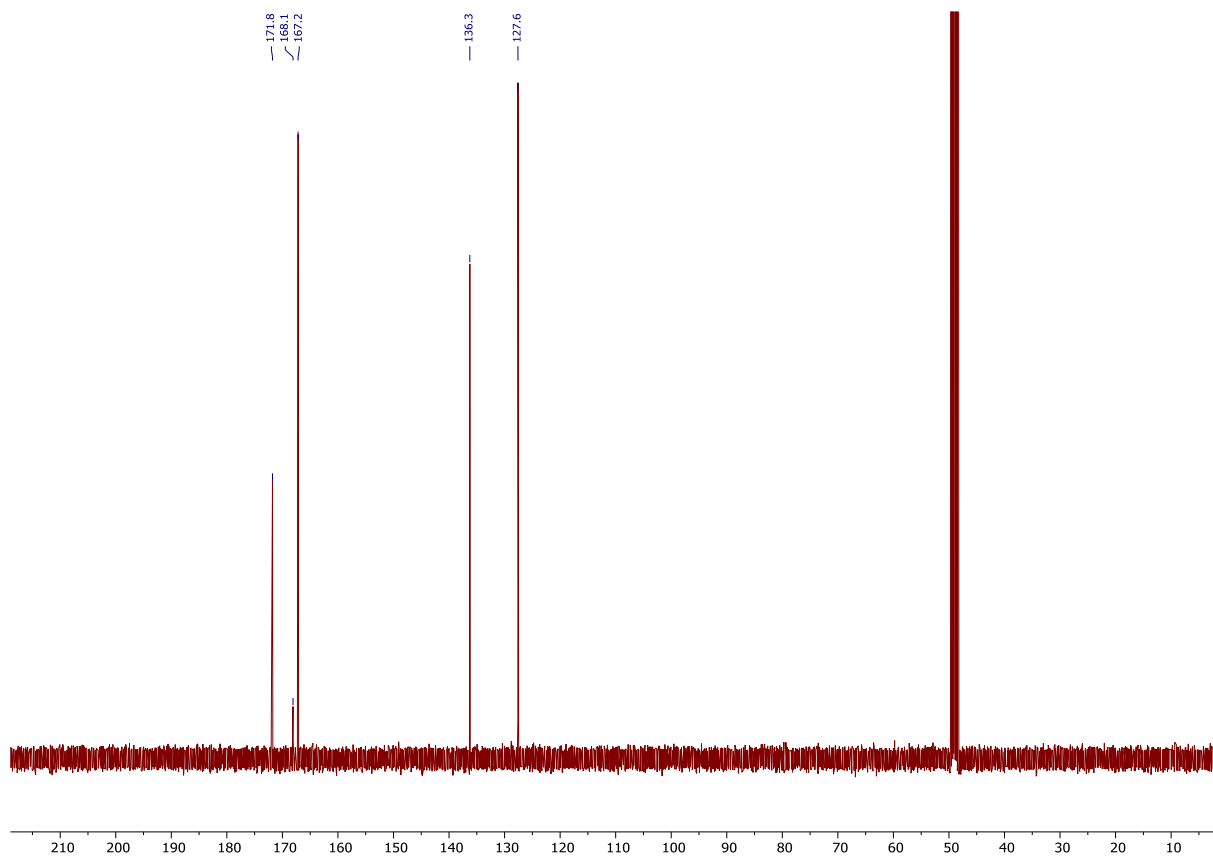
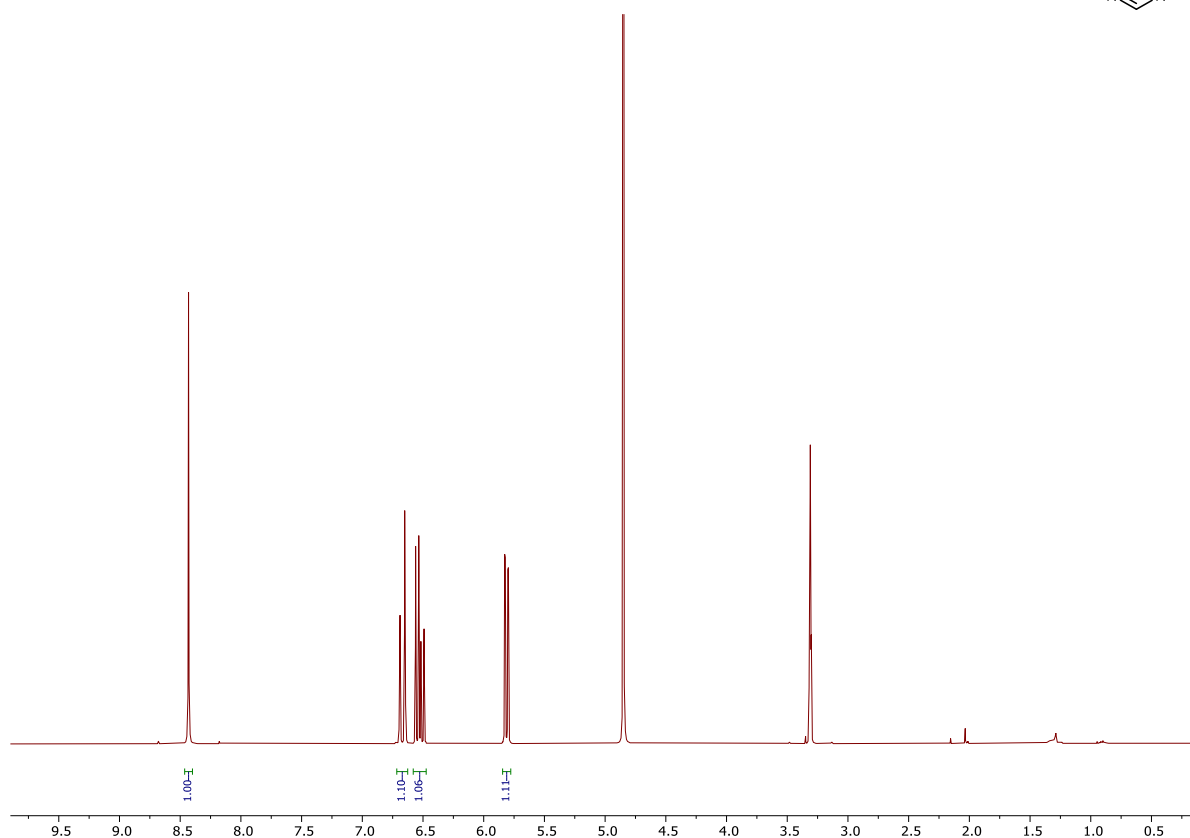
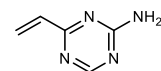
4-Vinylpyrimidin-2-amine (4)



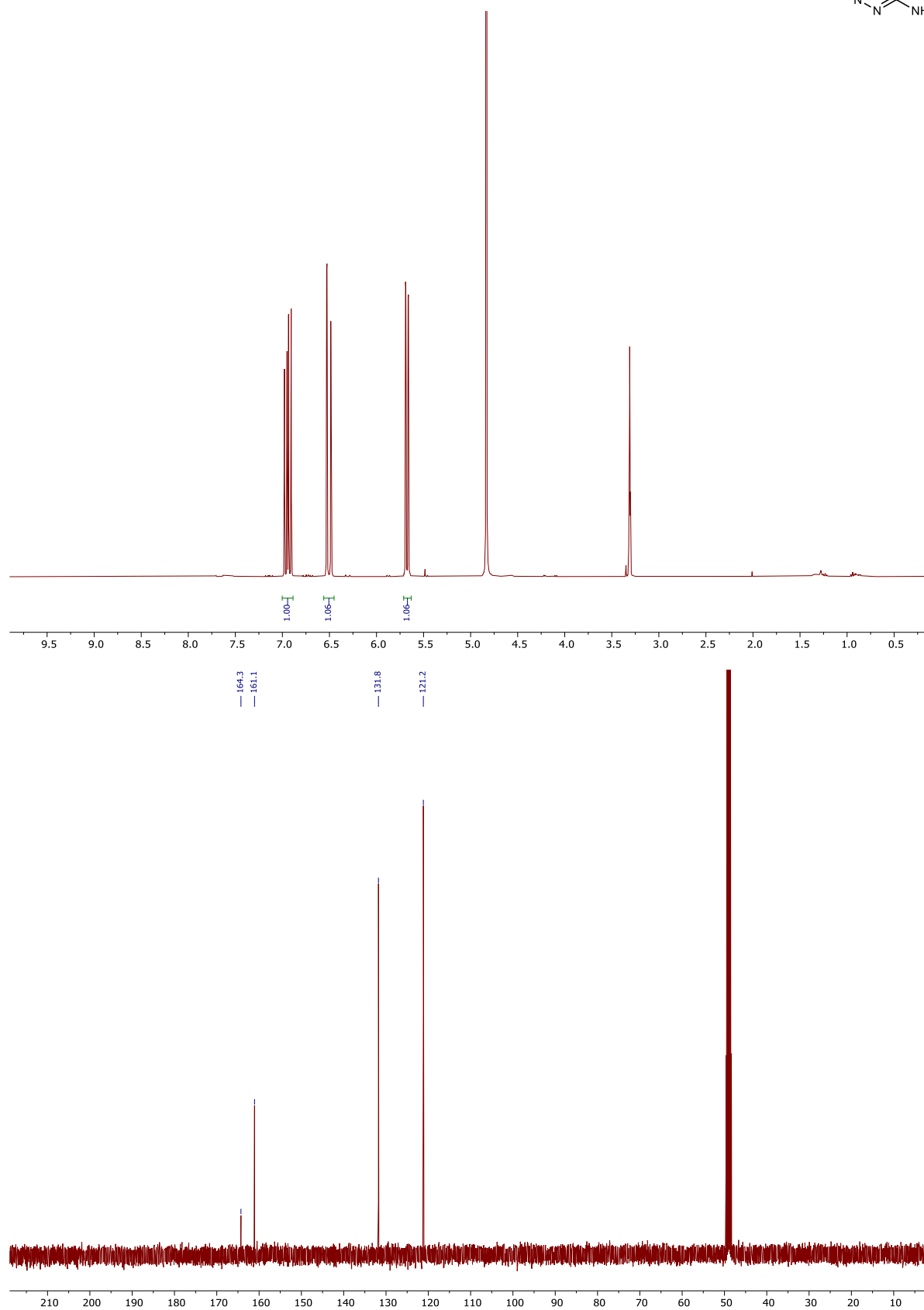
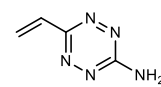
4-Chloro-1,3,5-triazin-2-amine (6)



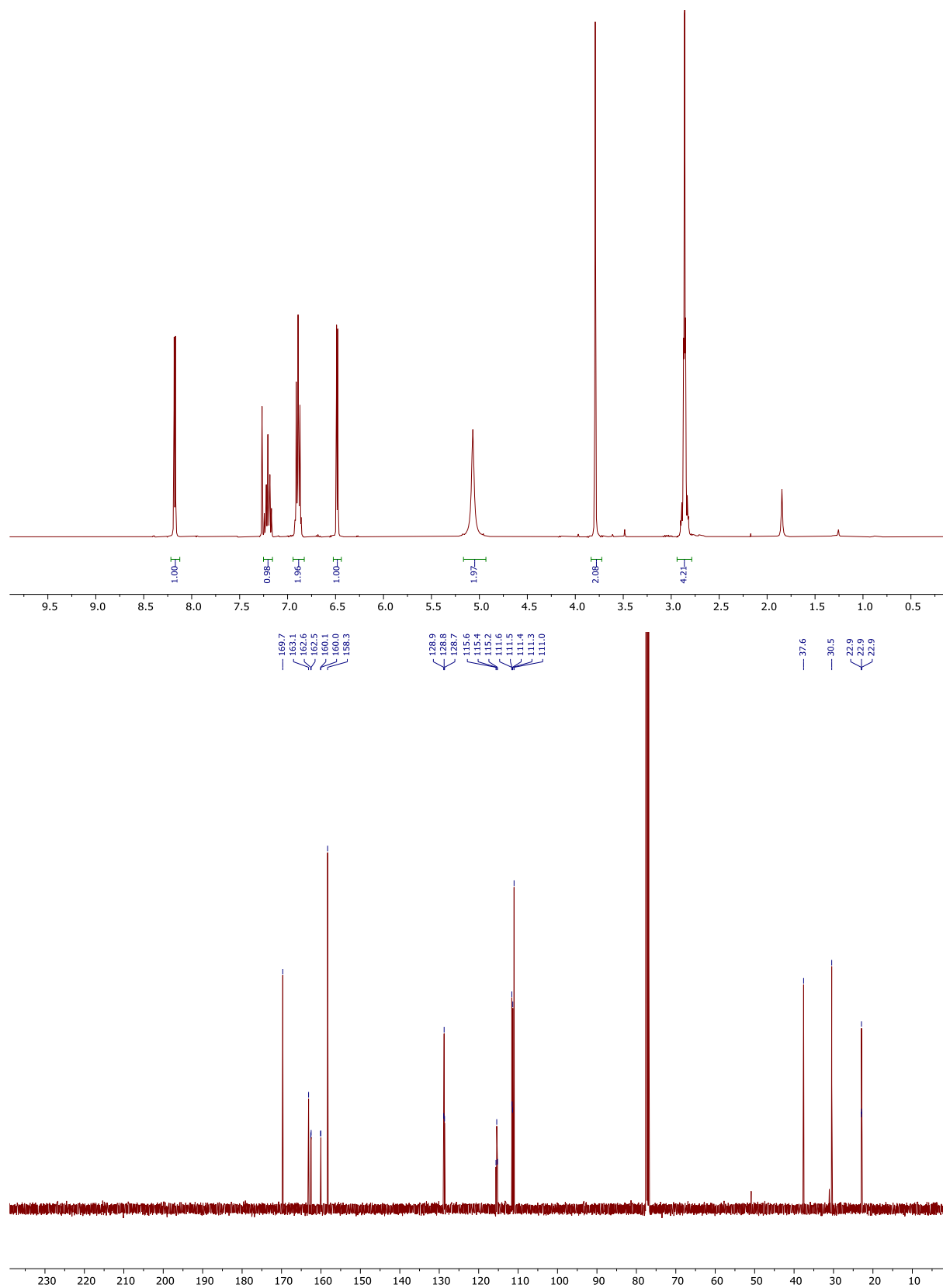
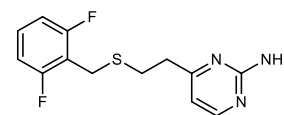
4-Vinyl-1,3,5-triazin-2-amine (7)

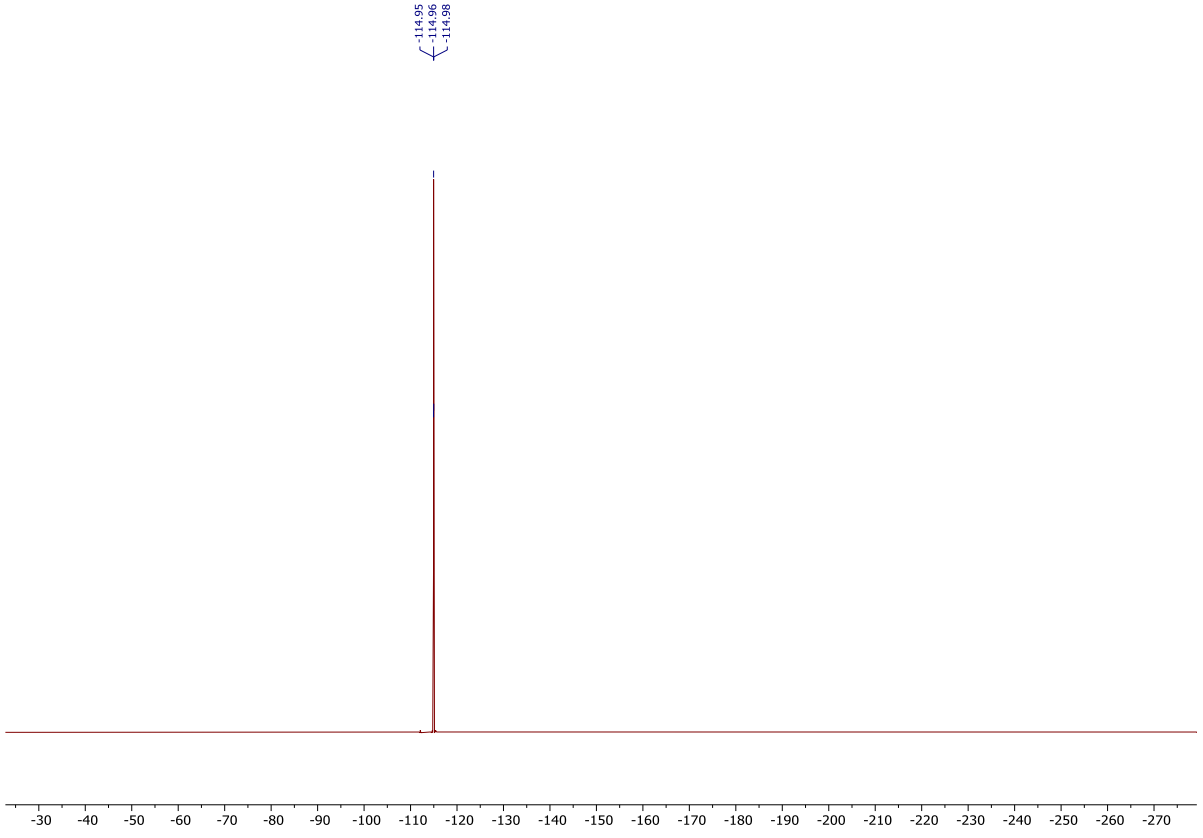


6-Vinyl-1,2,4,5-tetrazin-3-amine (9)

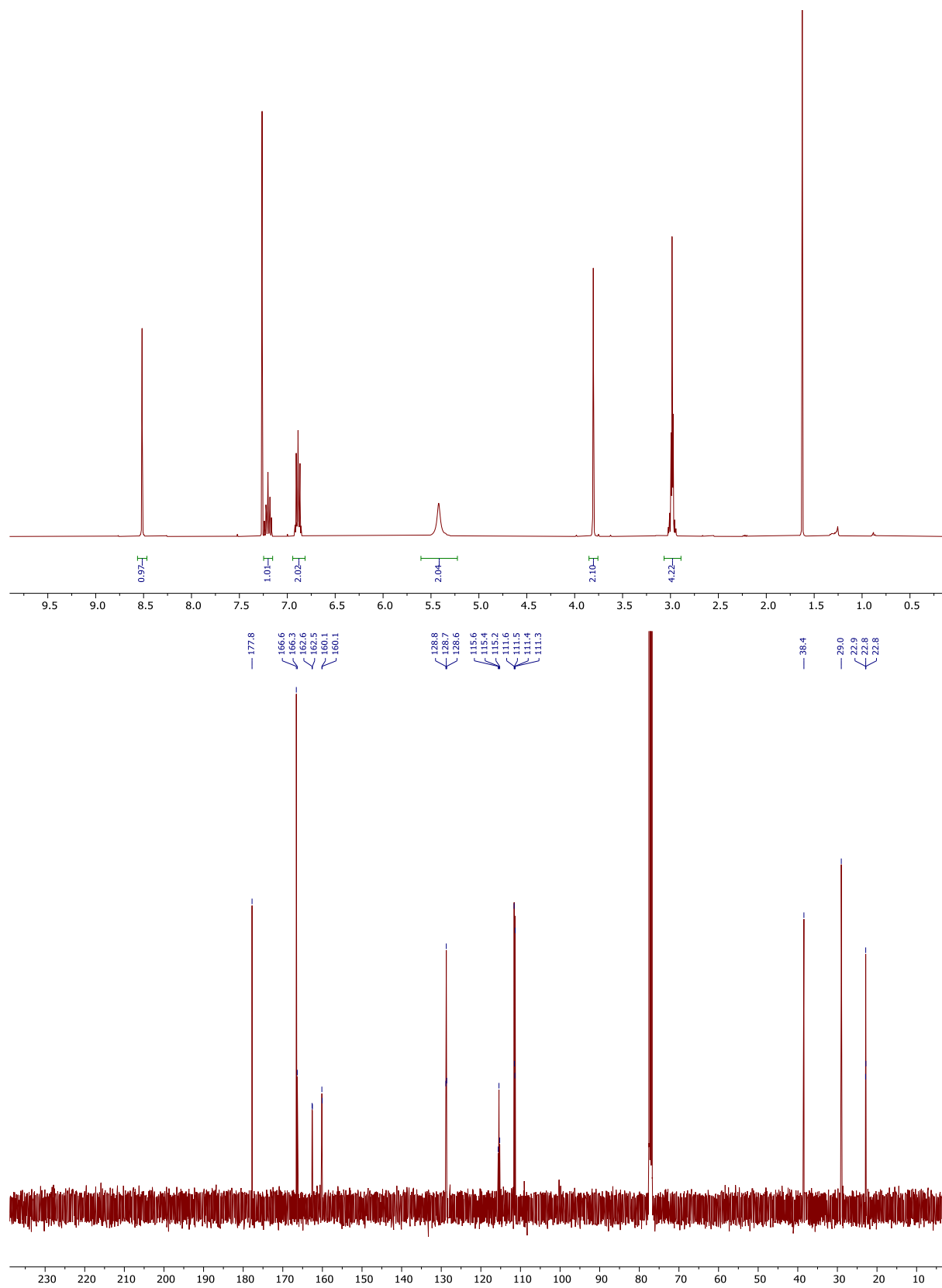
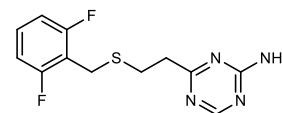


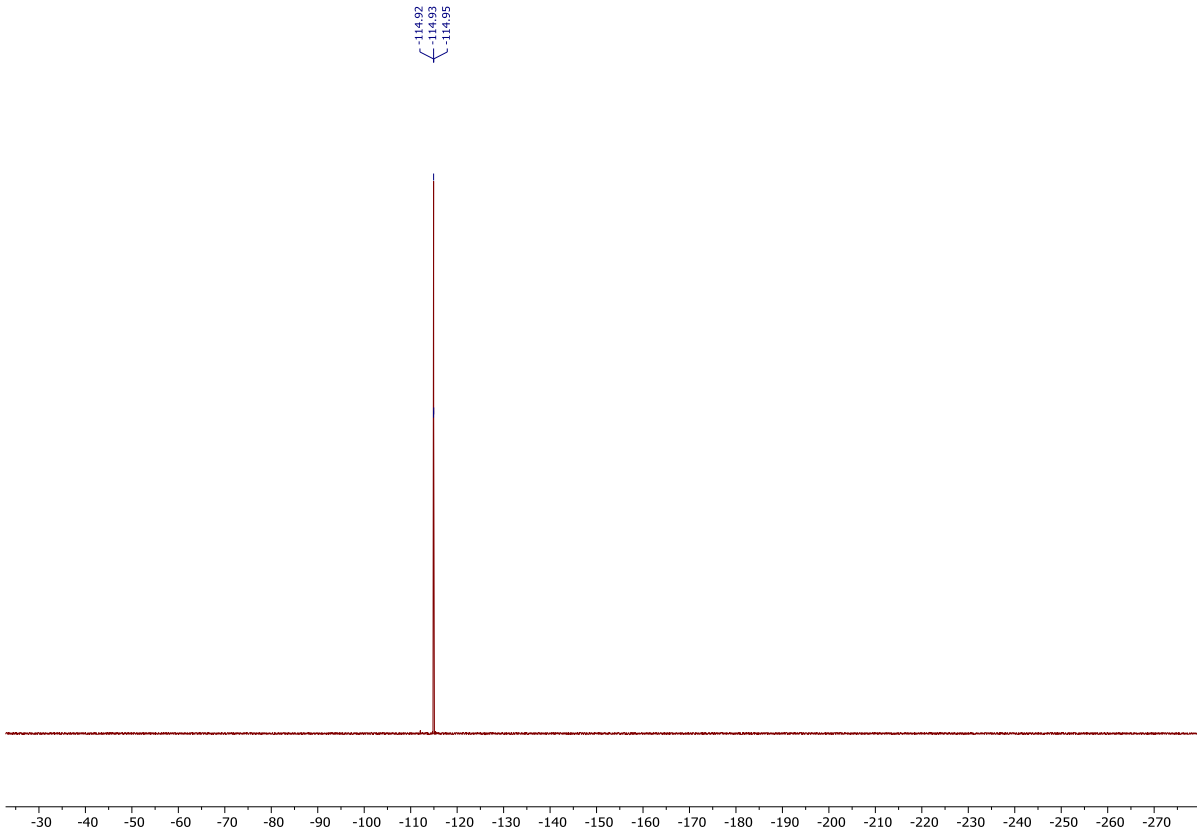
4-(2-((2,6-Difluorobenzyl)thio)ethyl)pyrimidin-2-amine (10)



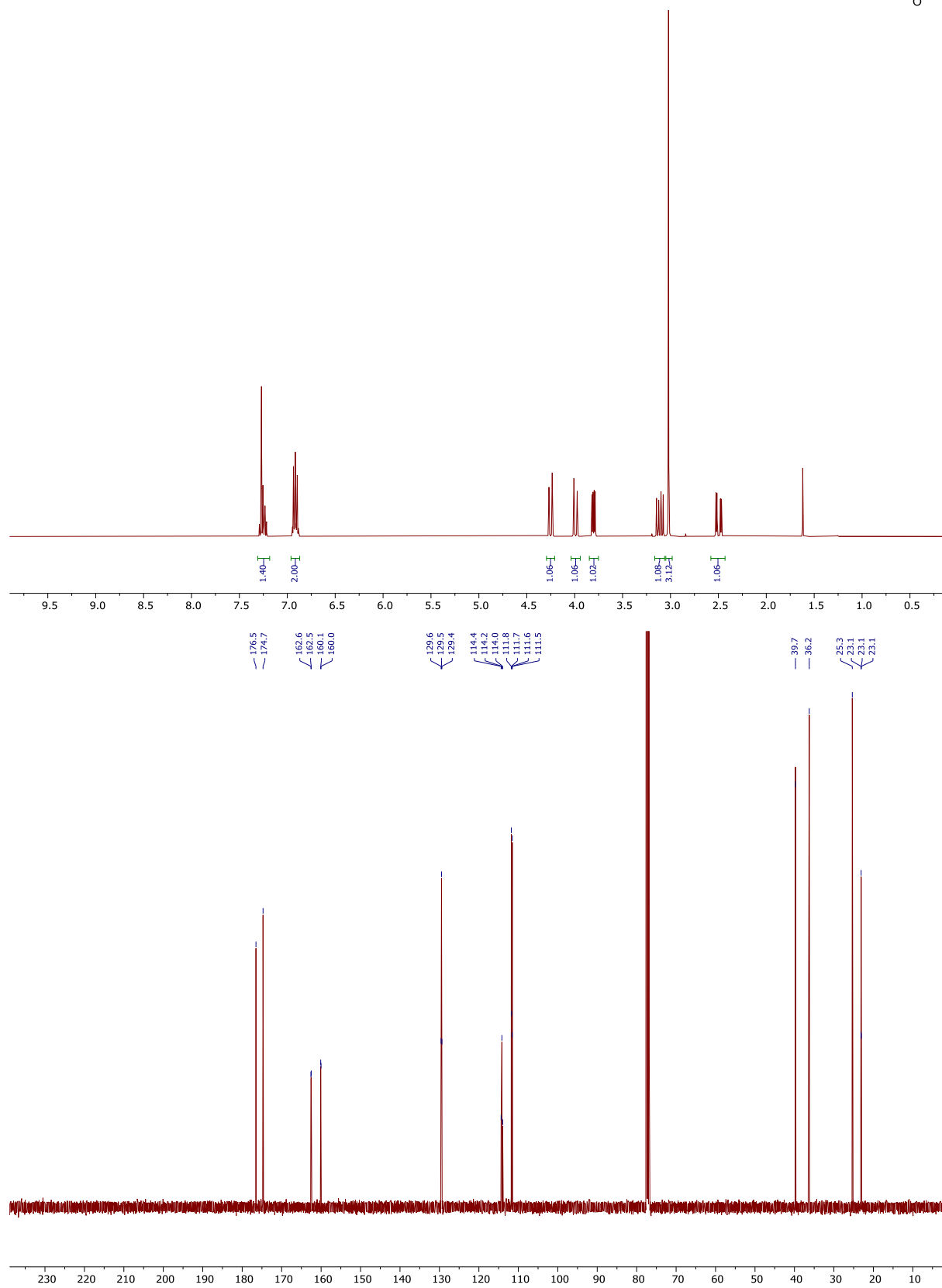
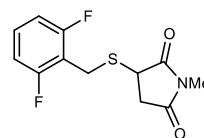


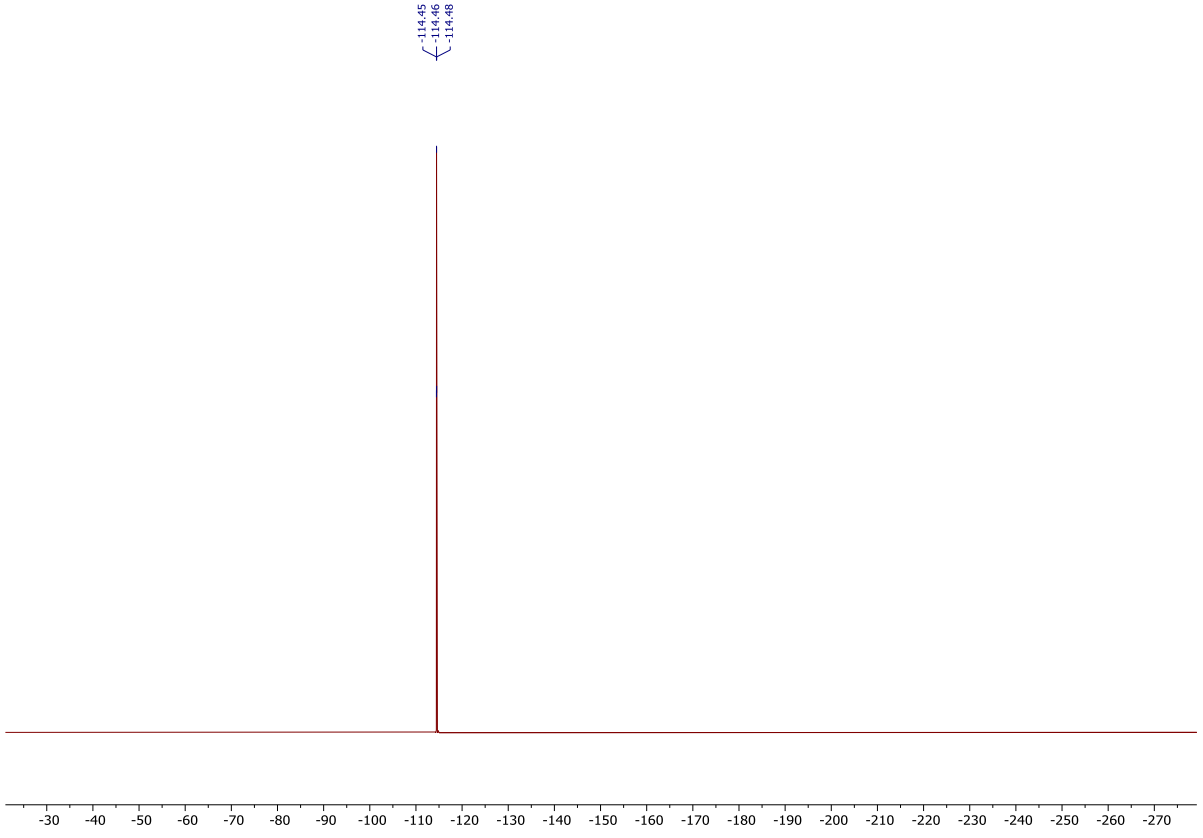
4-(2-((2,6-Difluorobenzyl)thio)ethyl)-1,3,5-triazin-2-amine (11)



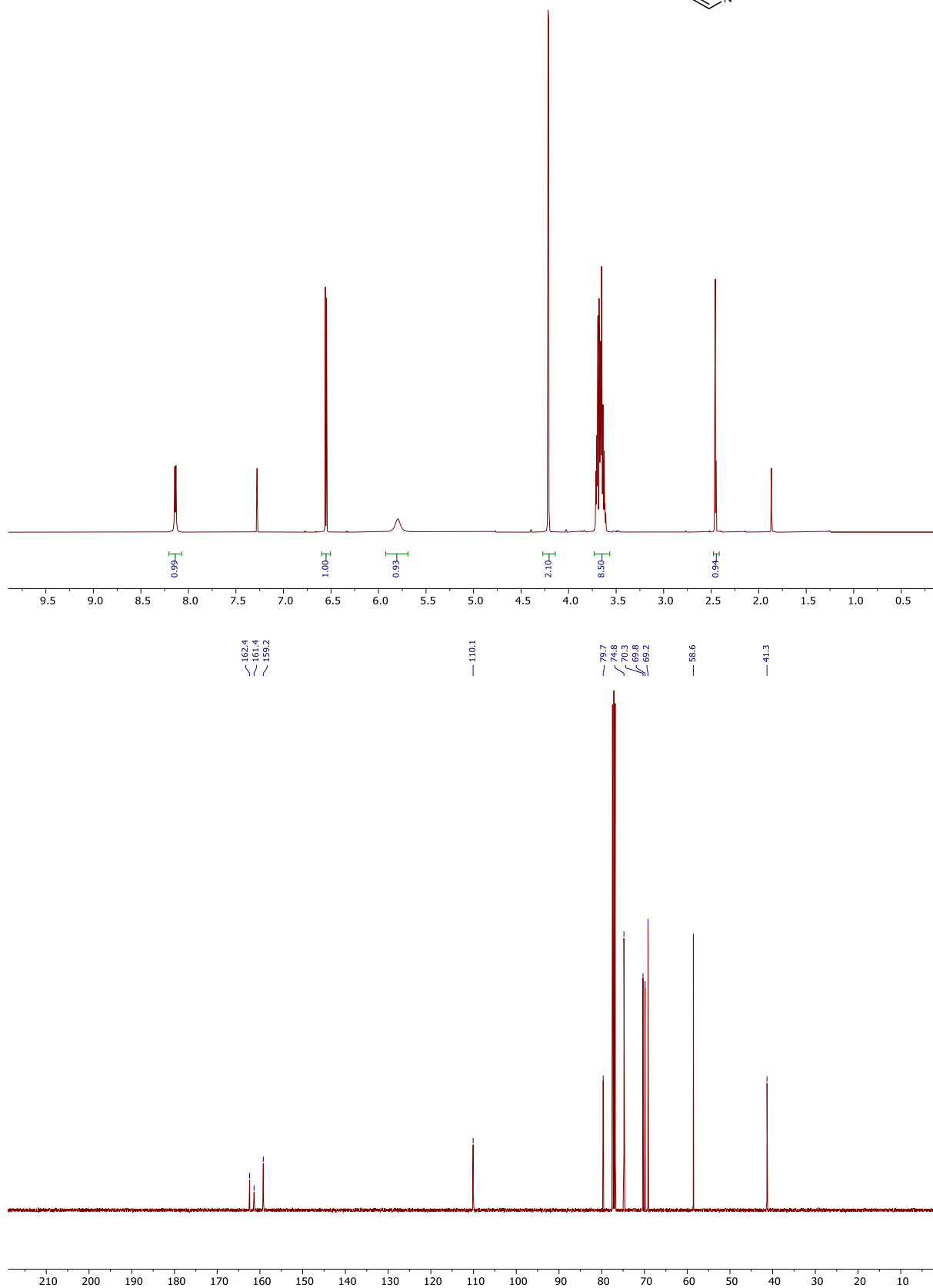
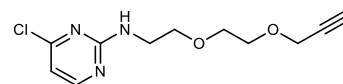


3-((2,6-Difluorobenzyl)thio)-1-methylpyrrolidine-2,5-dione (13)

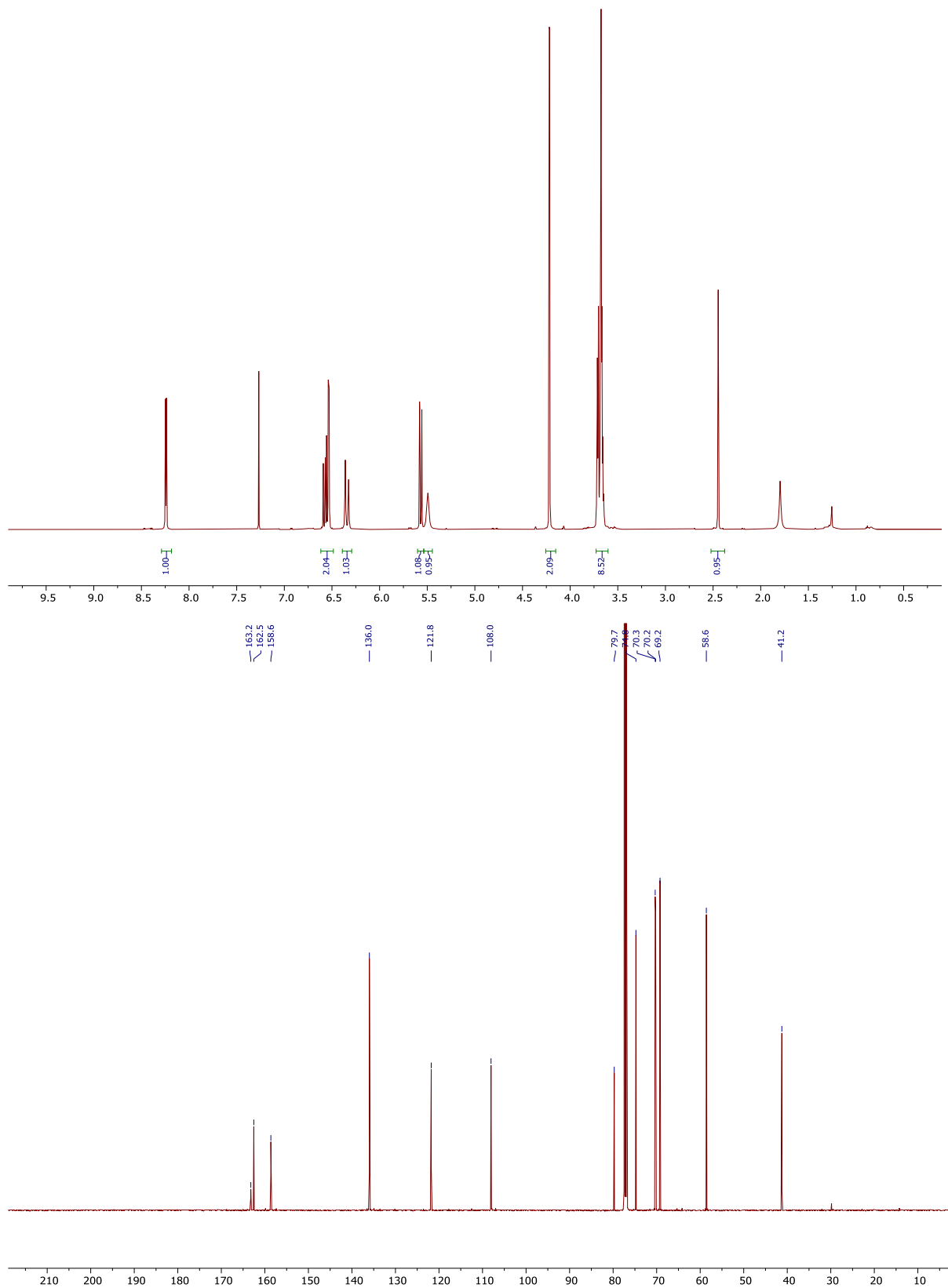
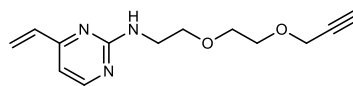




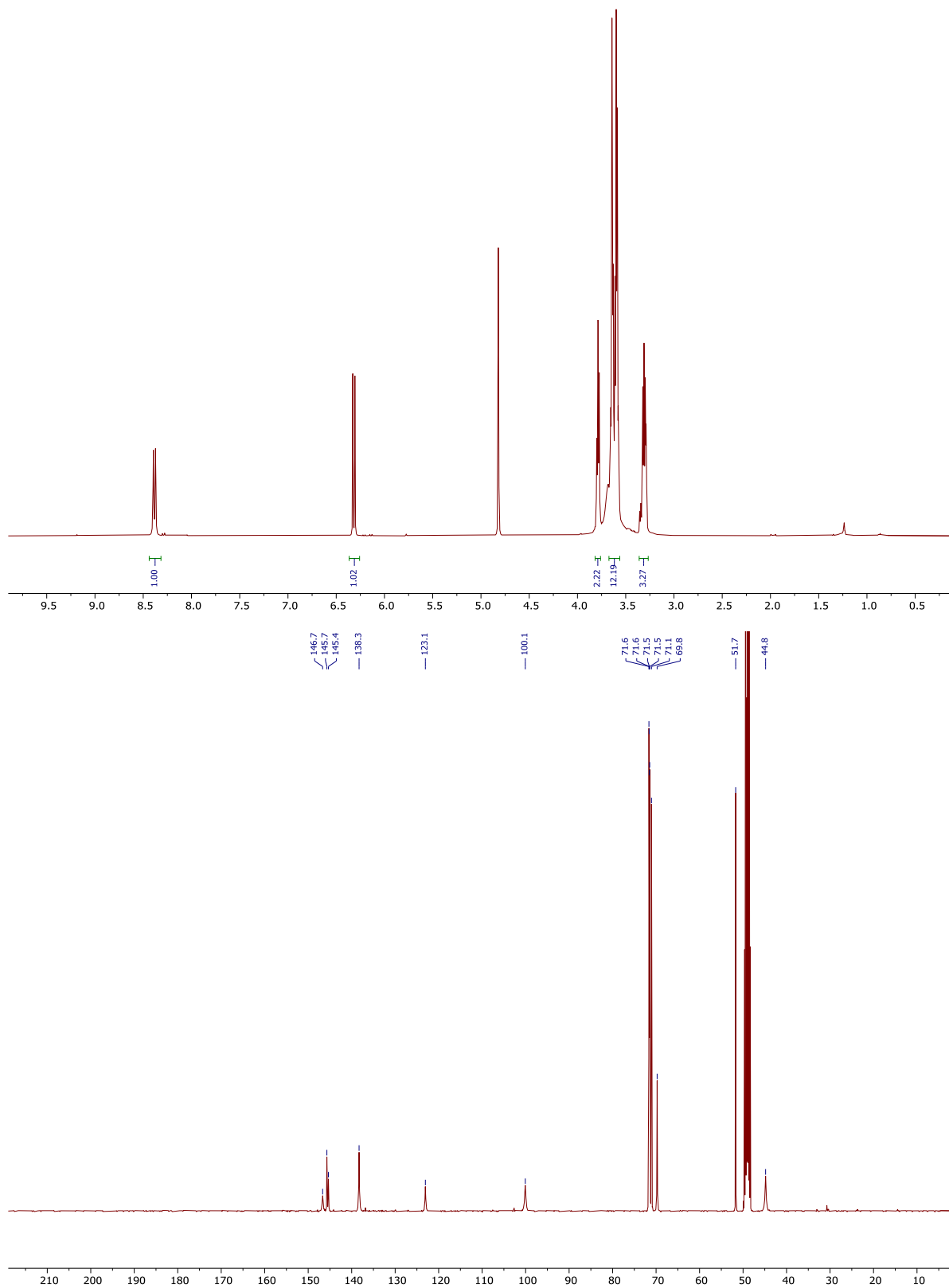
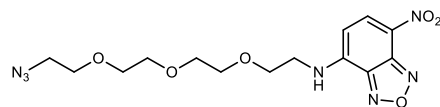
4-Chloro-N-(2-(2-(prop-2-yn-1-yloxy)ethoxy)ethyl)pyrimidin-2-amine (18)



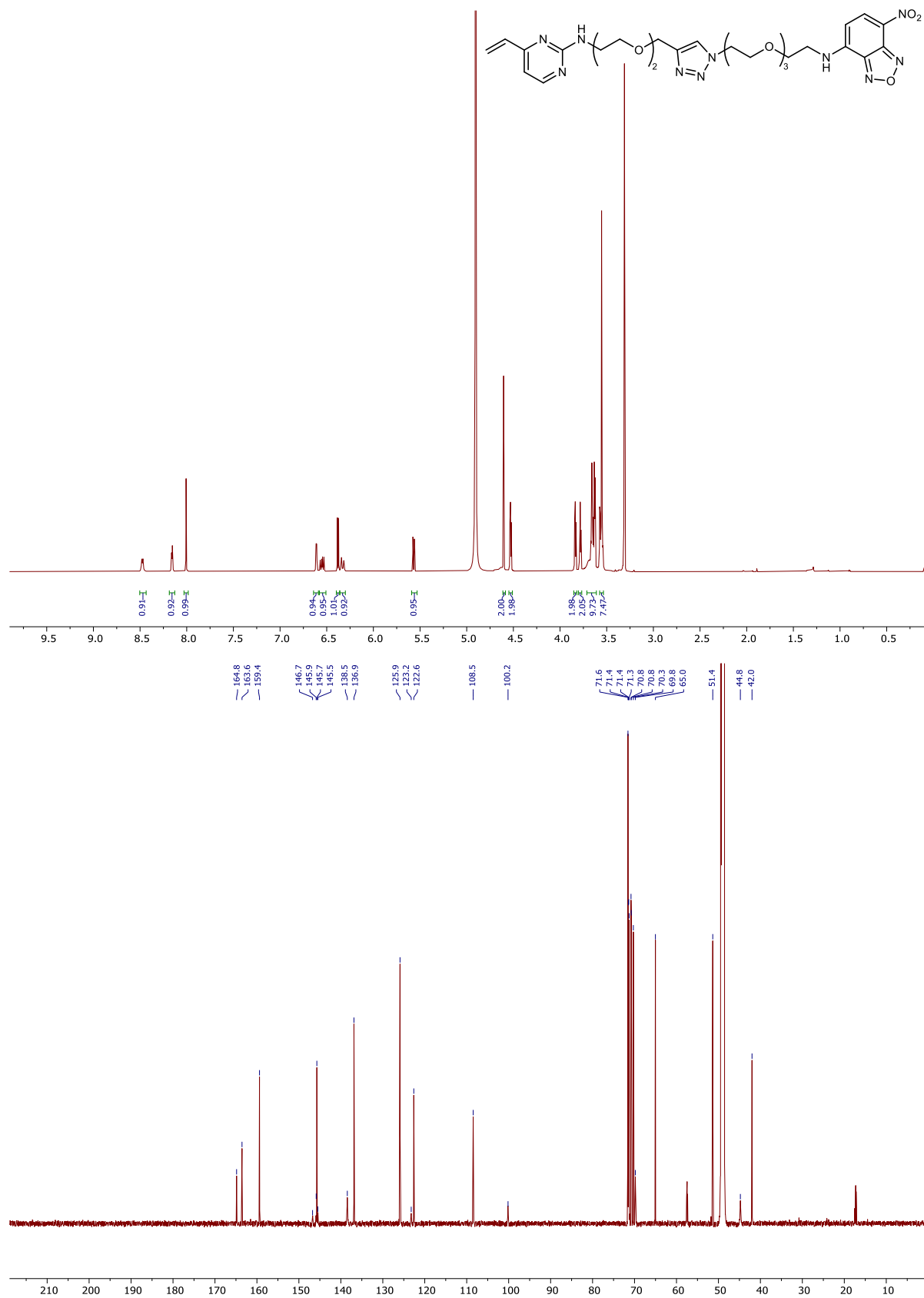
***N*-2-(2-(Prop-2-yn-1-yloxy)ethoxy)ethyl)-4-vinylpyrimidin-2-amine (19)**



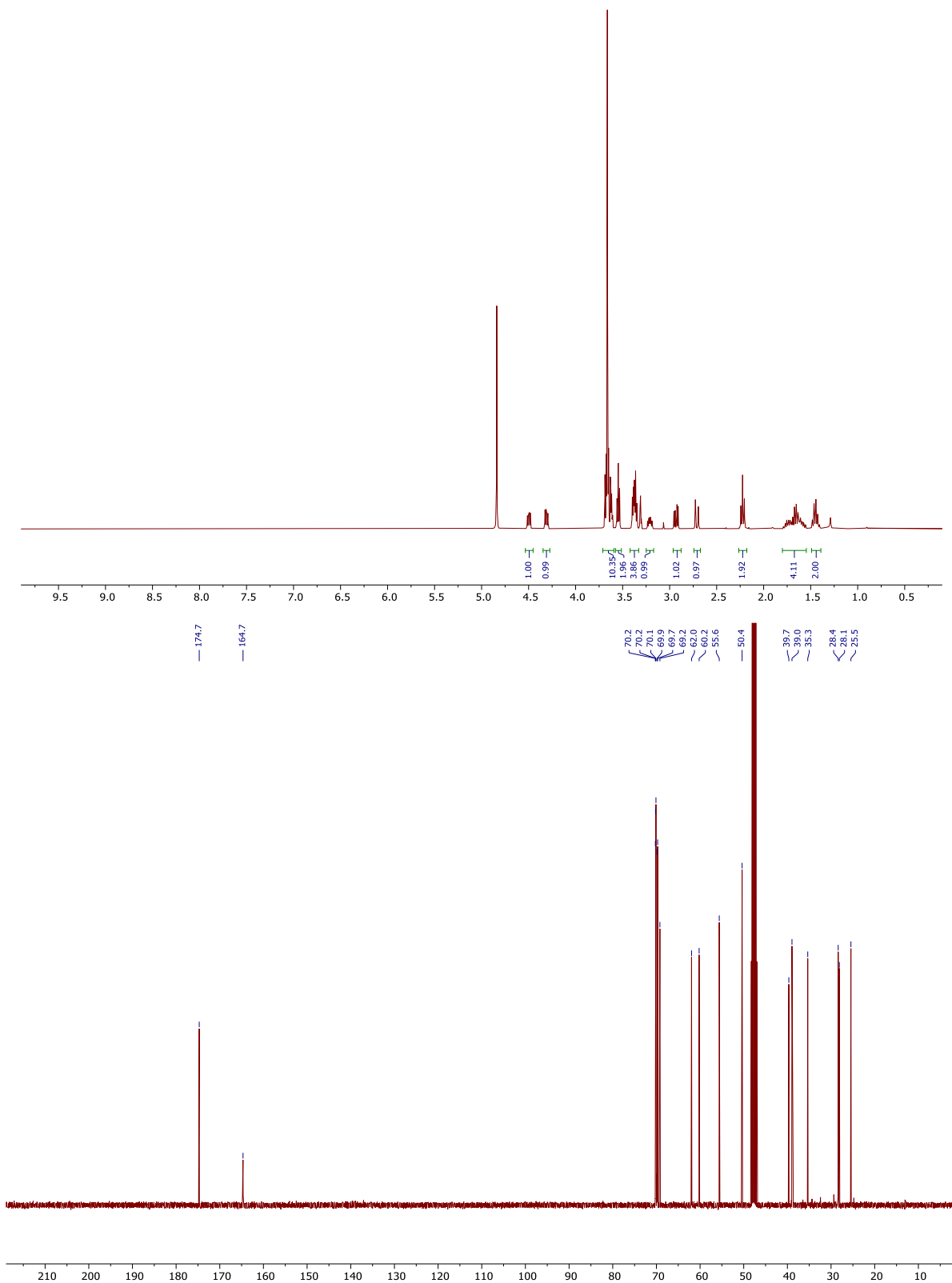
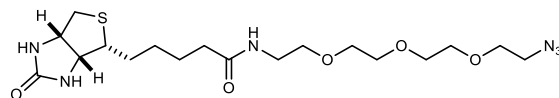
***N*-(2-(2-(2-(2-Azidoethoxy)ethoxy)ethoxy)ethyl)-7-nitrobenzo[*c*][1,2,5]oxadiazol-4-amine**
(21)



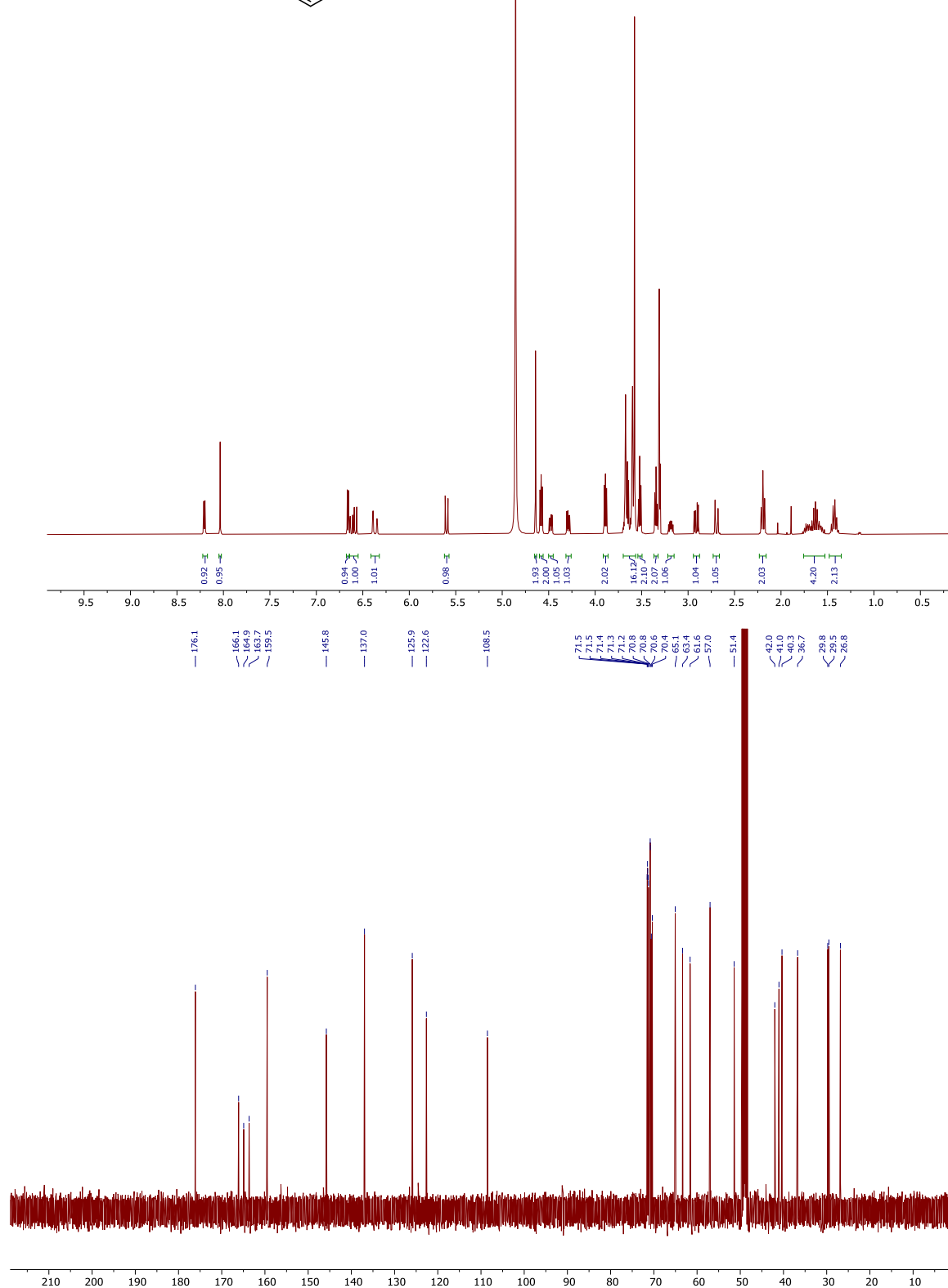
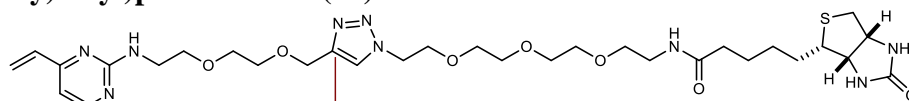
7-Nitro-N-(2-(2-(2-(2-(4-((2-(2-((4-vinylpyrimidin-2-yl)amino)ethoxy)ethoxy)methyl)-1H-1,2,3-triazol-1-yl)ethoxy)ethoxy)ethyl)benzo[c][1,2,5]oxadiazol-4-amine (22)



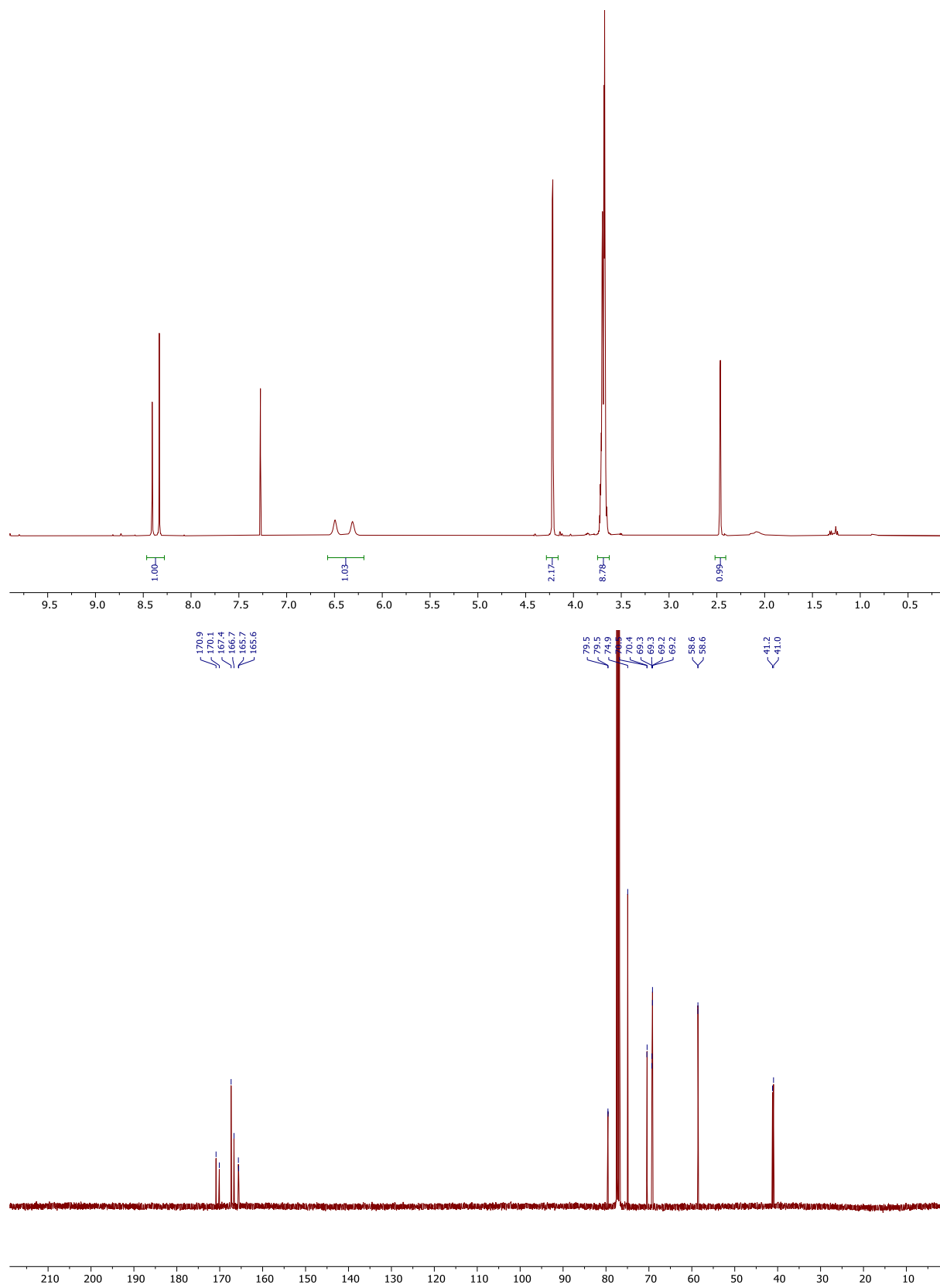
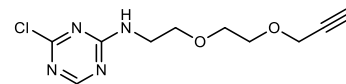
***N*-(2-(2-(2-(2-Azidoethoxy)ethoxy)ethoxy)ethyl)-5-((3*aR*,4*R*,6*aS*)-2-oxohexahydro-1*H*-thieno[3,4-*d*]imidazol-4-yl)pentanamide (24)**



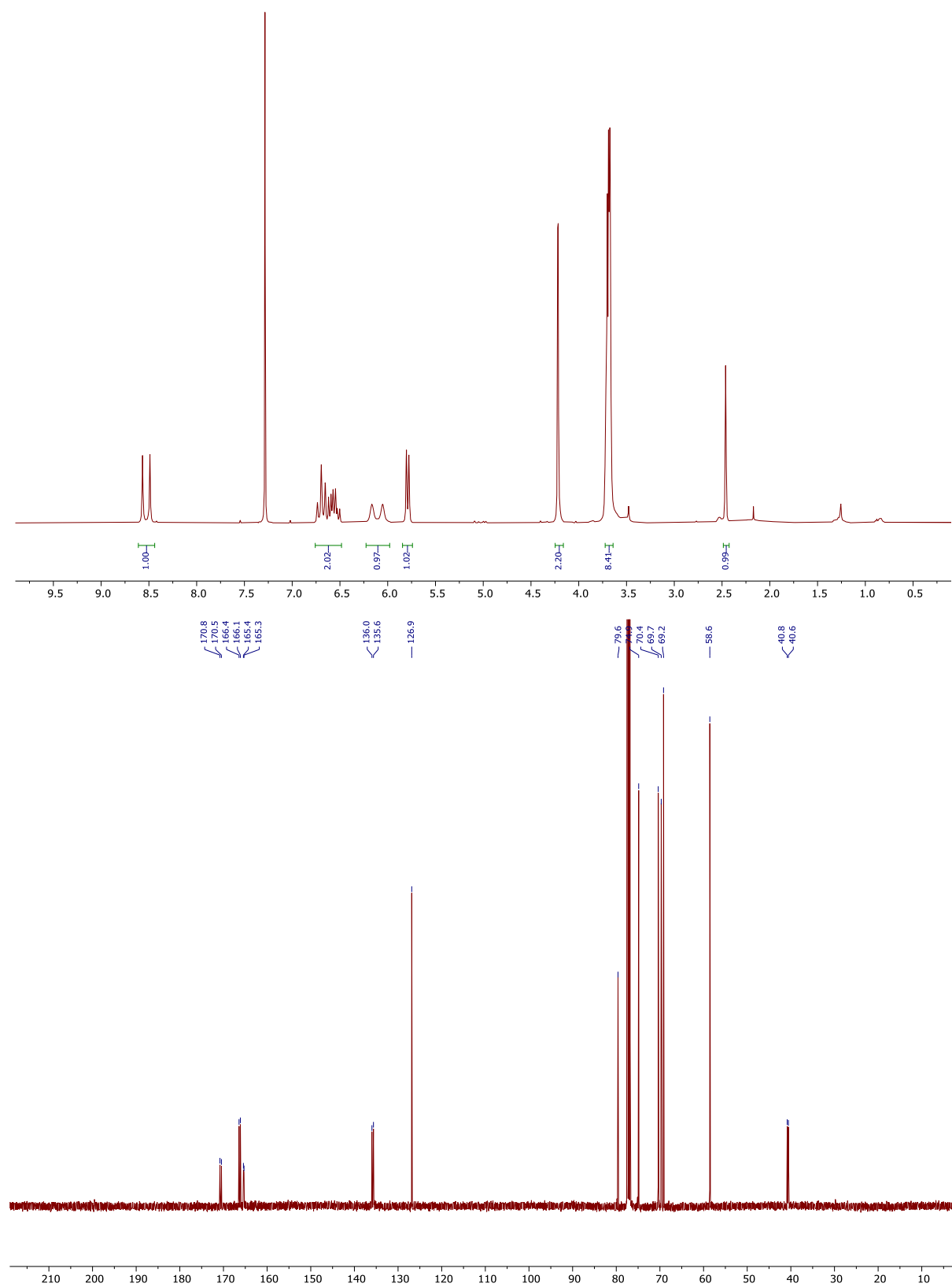
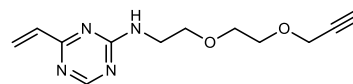
5-((3a*S*,4*S*,6a*R*)-2-Oxohexahydro-1*H*-thieno[3,4-*d*]imidazol-4-yl)-N-(2-(2-(2-(2-(4-((2-(2-((4-vinylpyrimidin-2-yl)amino)ethoxy)ethoxy)methyl)-1*H*-1,2,3-triazol-1-yl)ethoxy)ethoxy)ethoxy)ethyl)pentanamide (25)



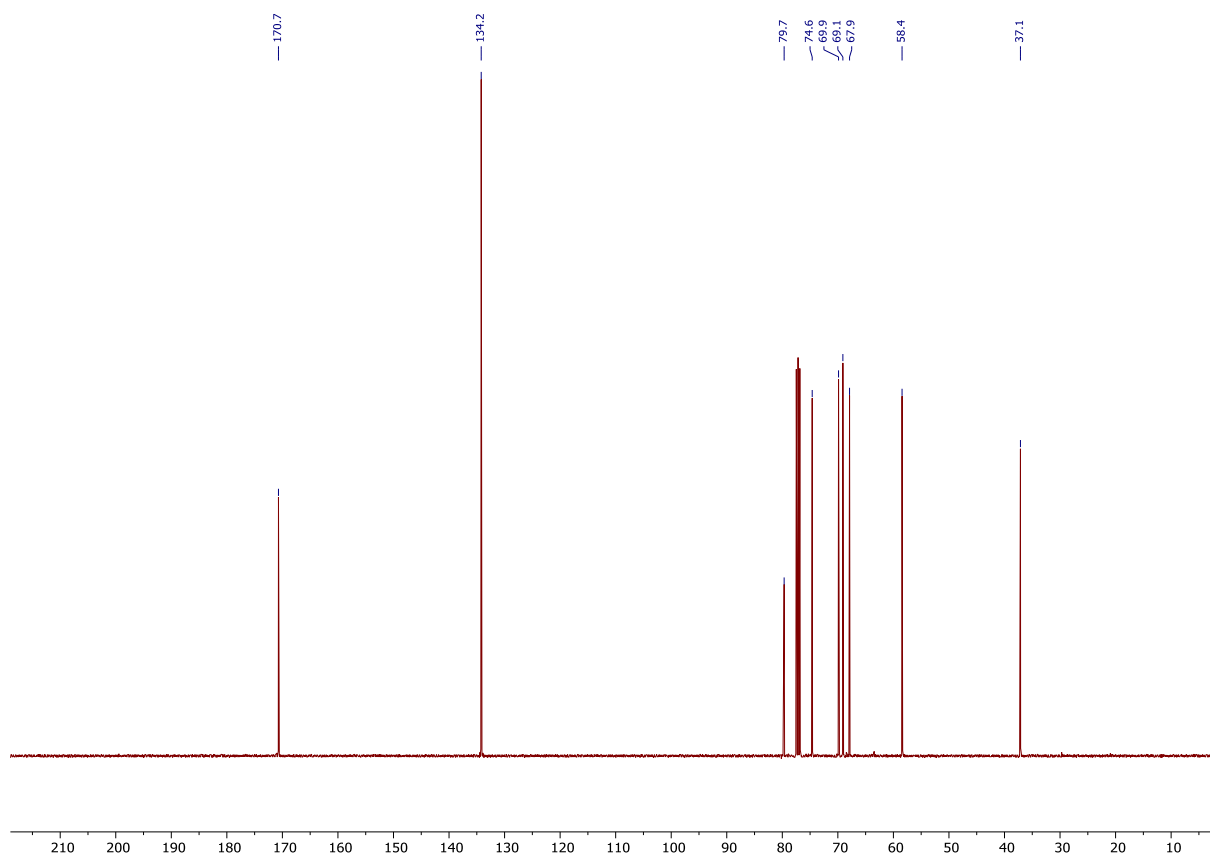
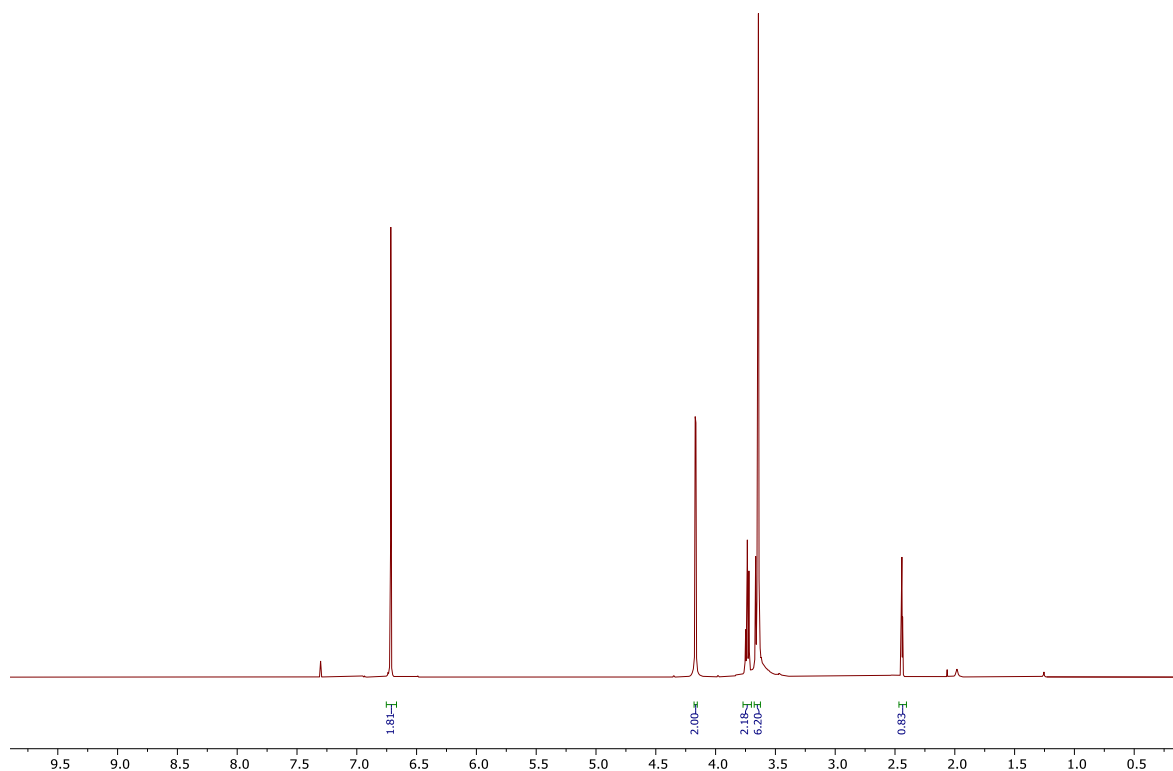
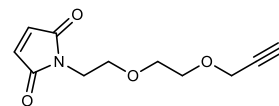
4-Chloro-*N*-(2-(2-(prop-2-yn-1-yloxy)ethoxy)ethyl)-1,3,5-triazin-2-amine (31)



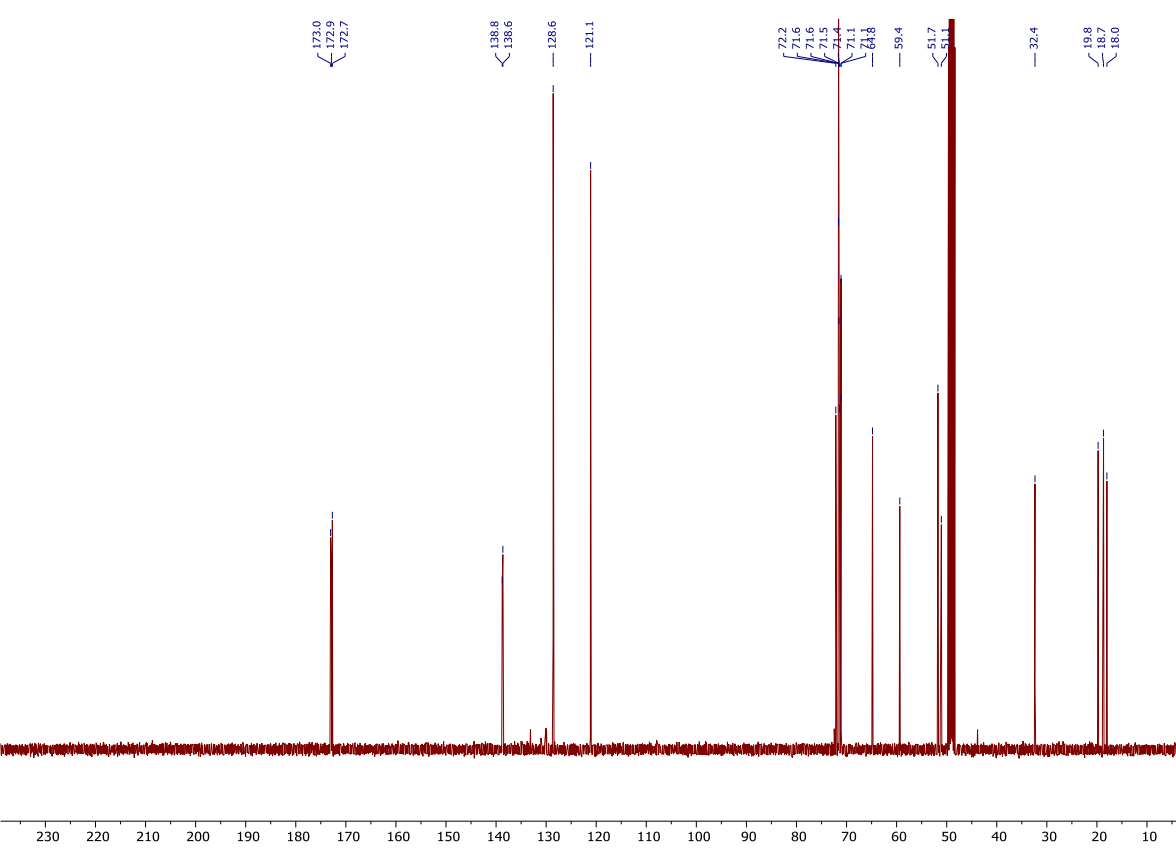
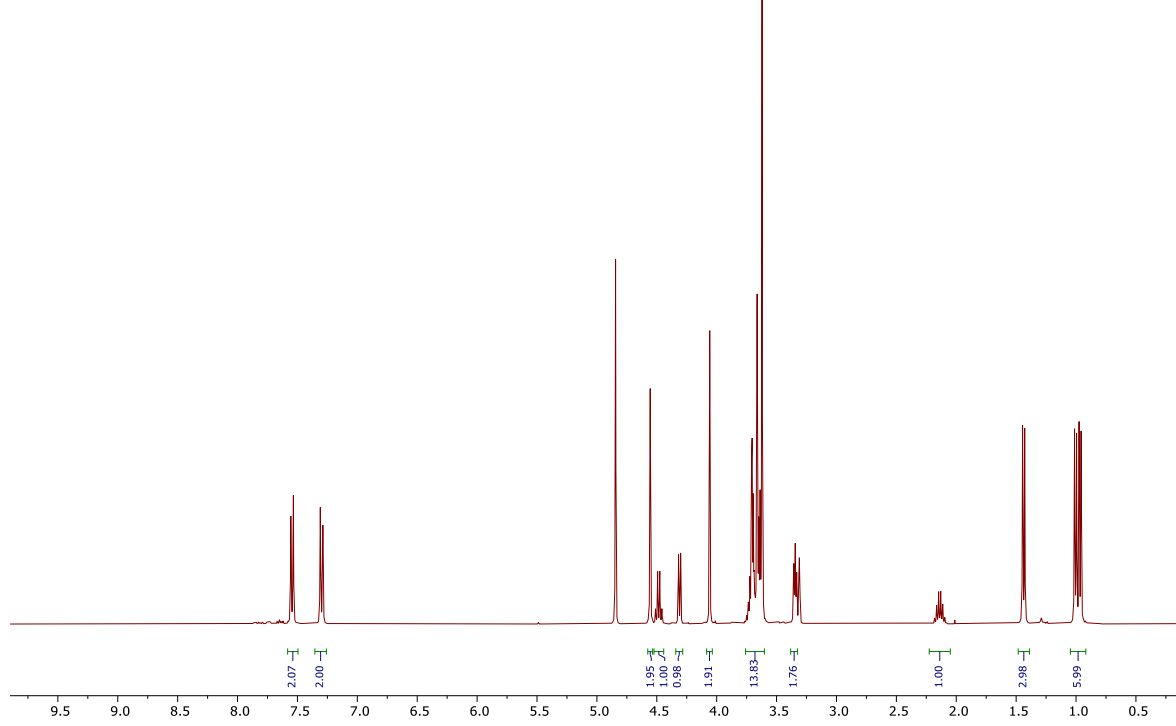
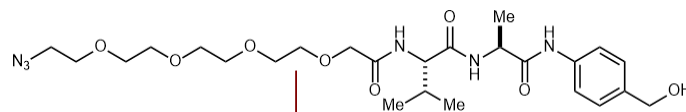
***N*-(2-(2-(Prop-2-yn-1-yloxy)ethoxy)ethyl)-4-vinyl-1,3,5-triazin-2-amine (32)**



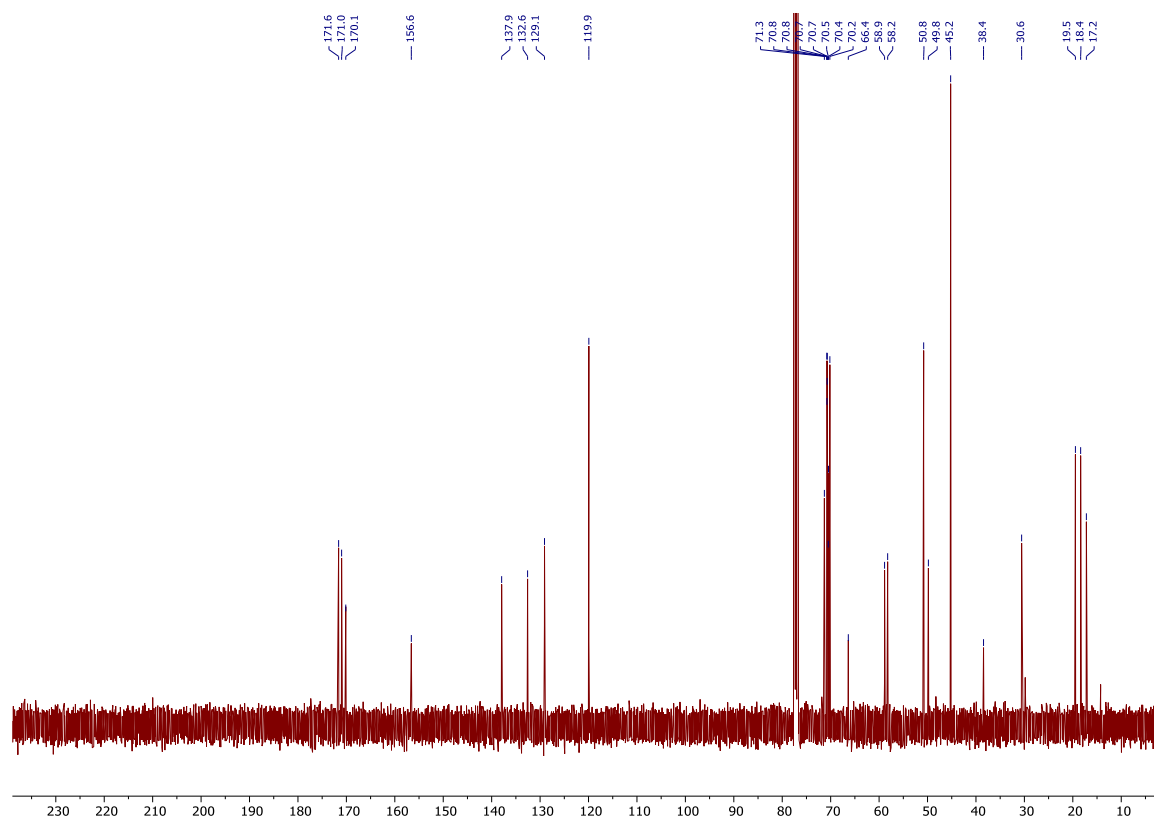
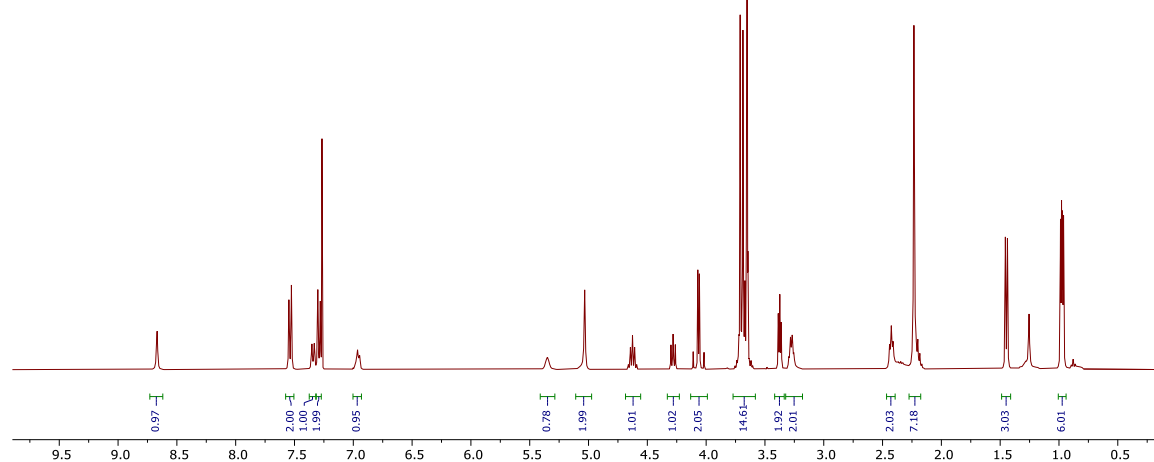
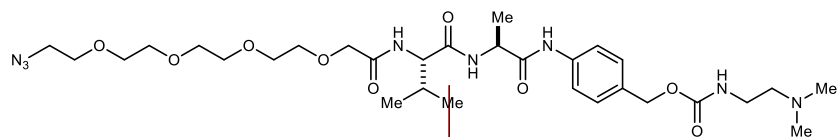
1-(2-(2-(Prop-2-yn-1-yloxy)ethoxy)ethyl)-1H-pyrrole-2,5-dione (44)



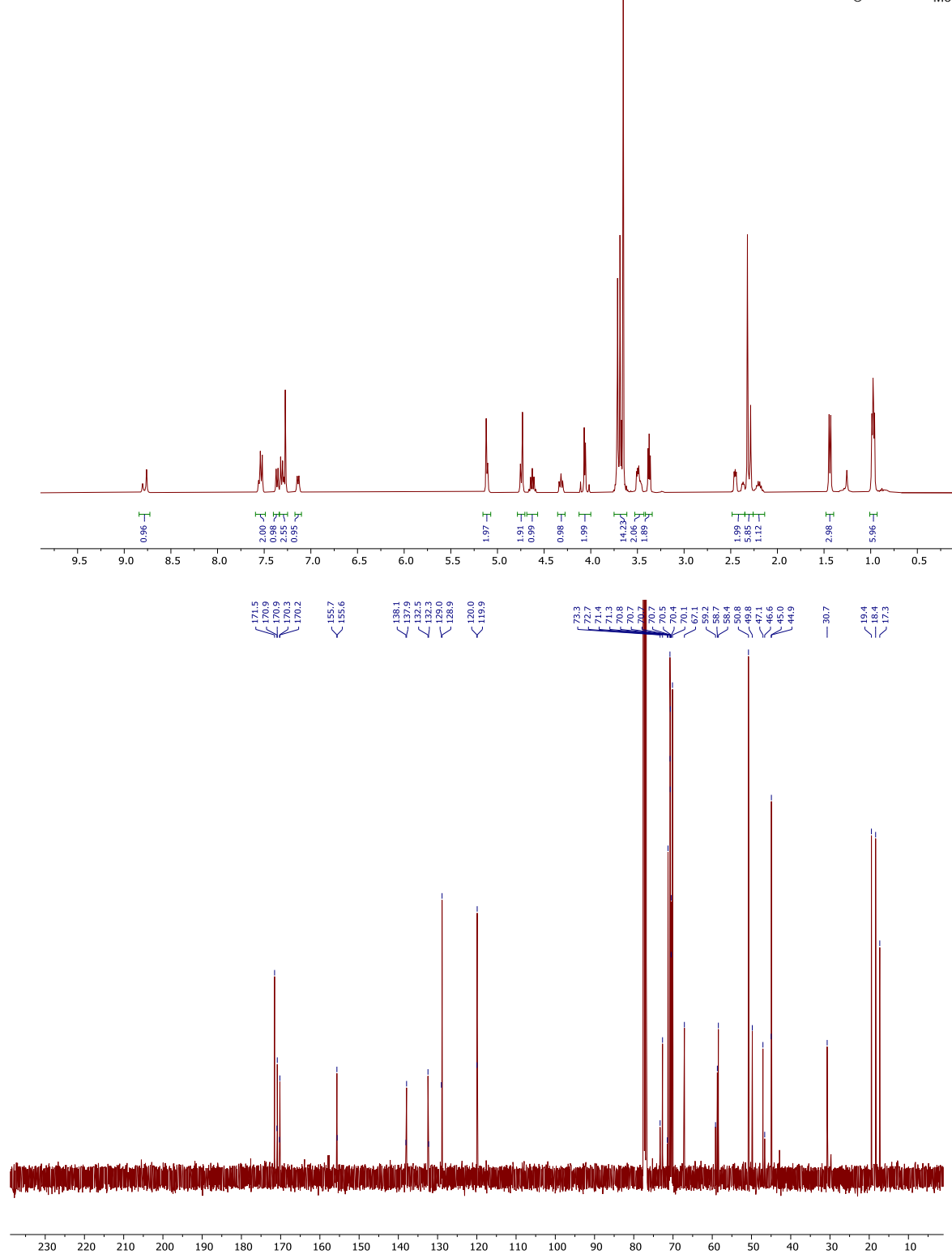
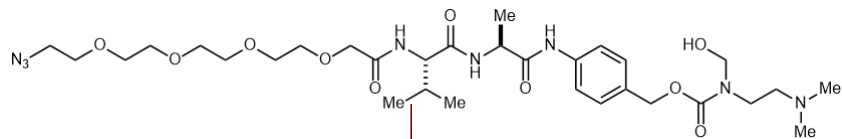
14-Azido-N-((S)-1-(((S)-1-(4-(hydroxymethyl)phenyl)amino)-1-oxopropan-2-yl)amino)-3-methyl-1-oxobutan-2-yl)-3,6,9,12-tetraoxatetradecanamide (80)



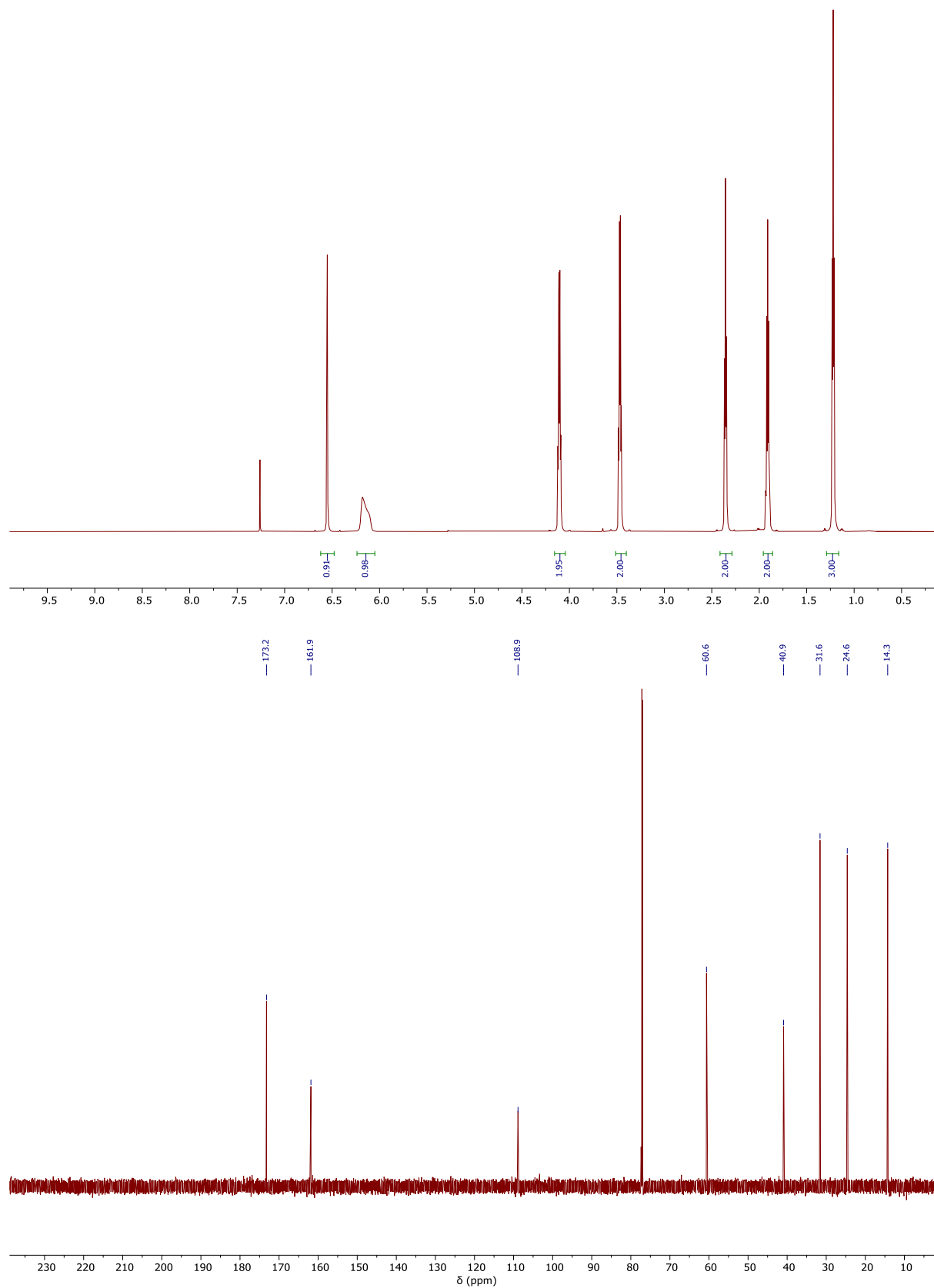
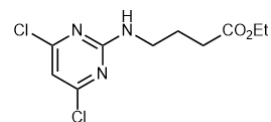
4-((2*S*,5*S*)-20-Azido-5-isopropyl-2-methyl-4,7-dioxo-9,12,15,18-tetraoxa-3,6-diazaicosanamido)benzyl (2-(dimethylamino)ethyl)carbamate (82)



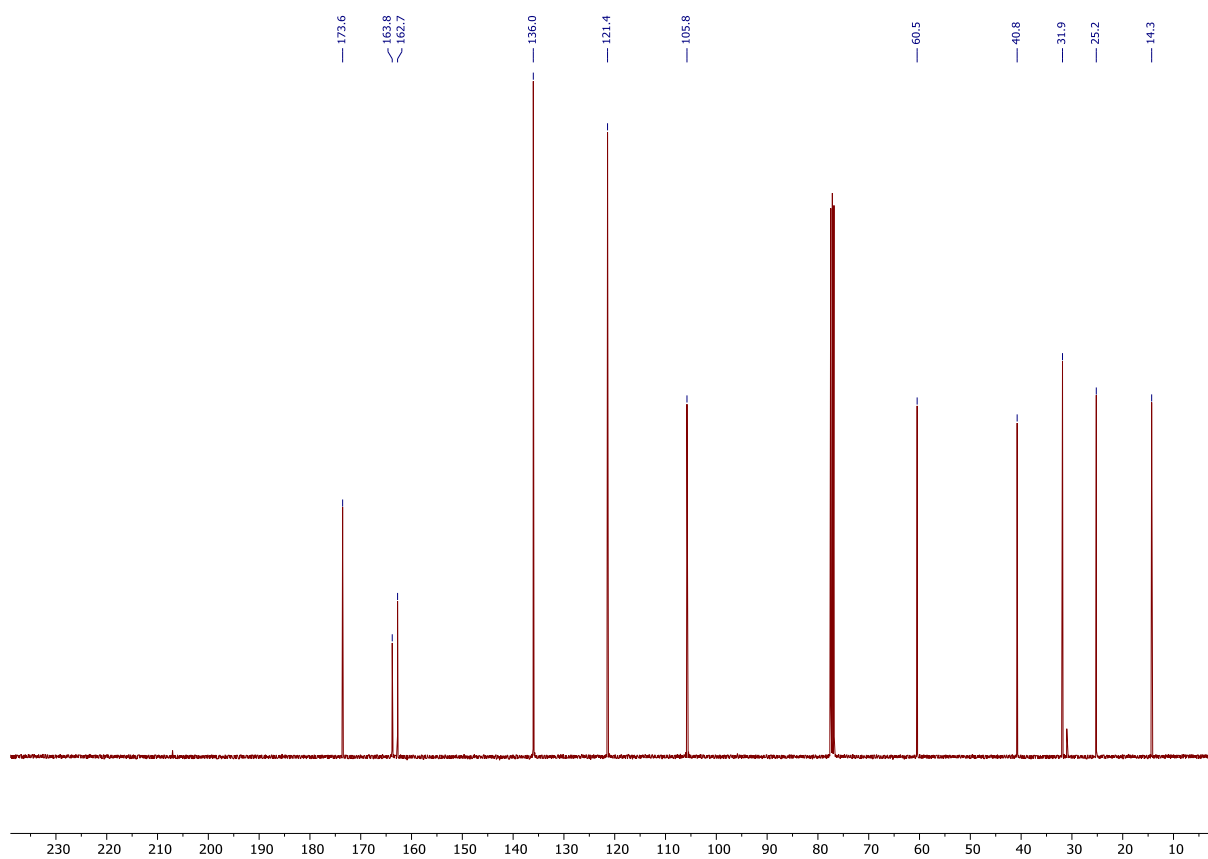
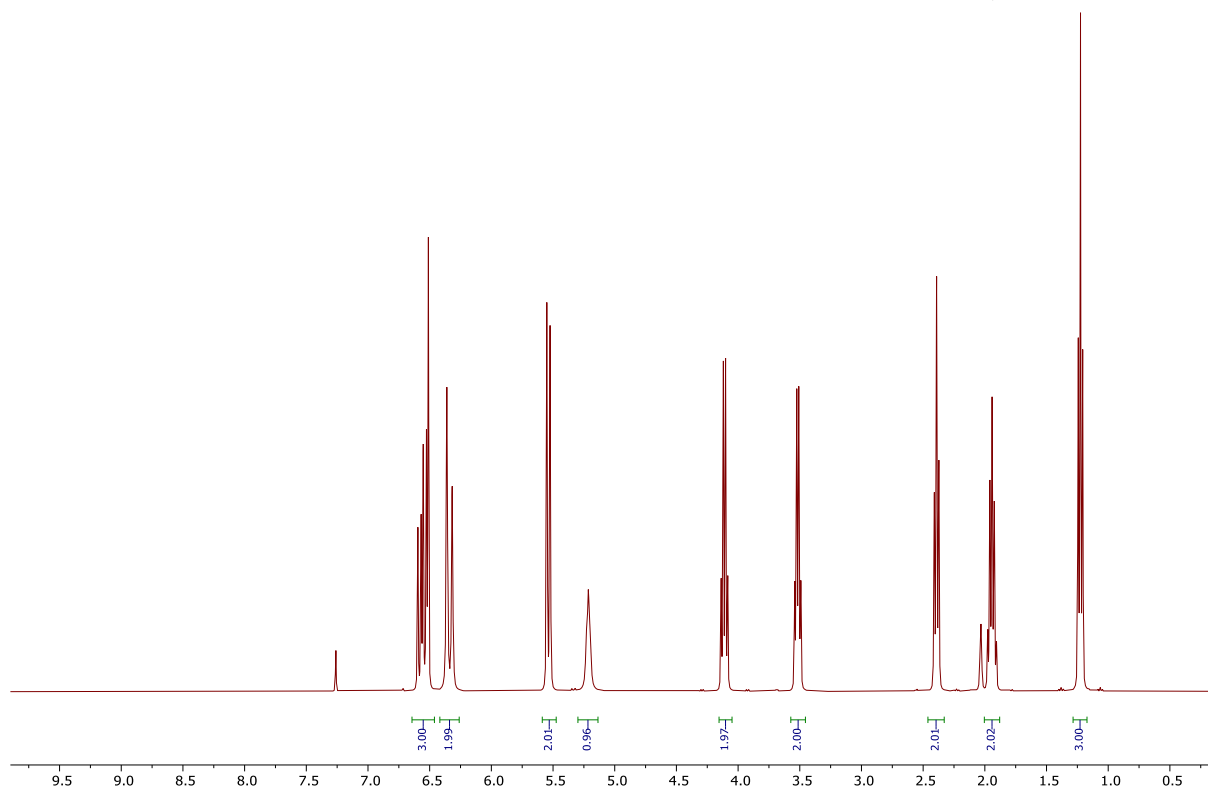
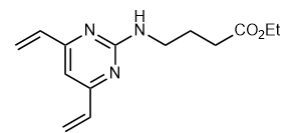
4-((2S,5S)-20-Azido-5-isopropyl-2-methyl-4,7-dioxo-9,12,15,18-tetraoxa-3,6-diazaicosanamido)benzyl (2-(dimethylamino)ethyl)(hydroxymethyl) carbamate (83)



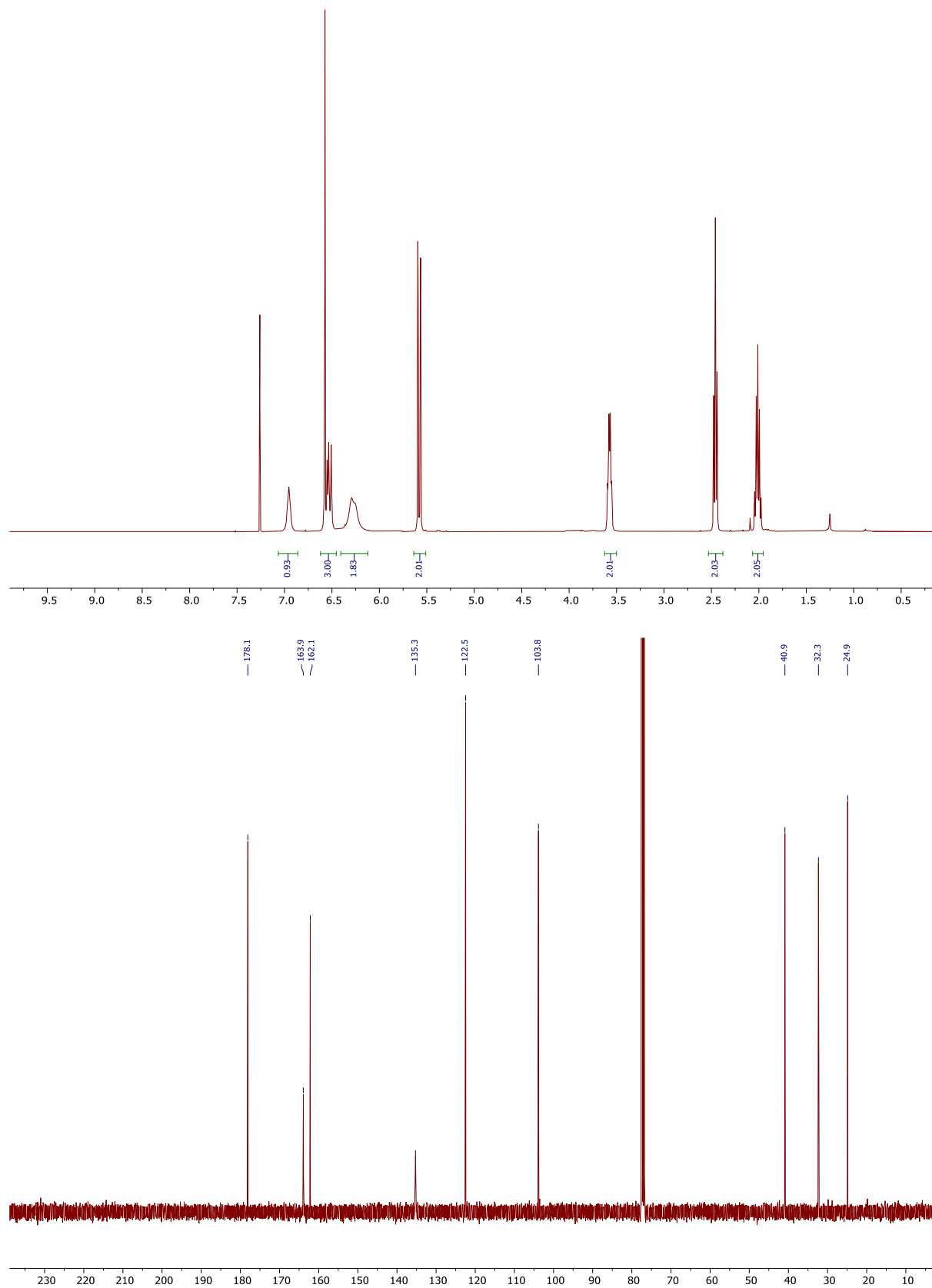
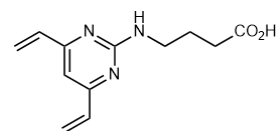
Ethyl 4-((4,6-dichloropyrimidin-2-yl)amino)butanoate (89)



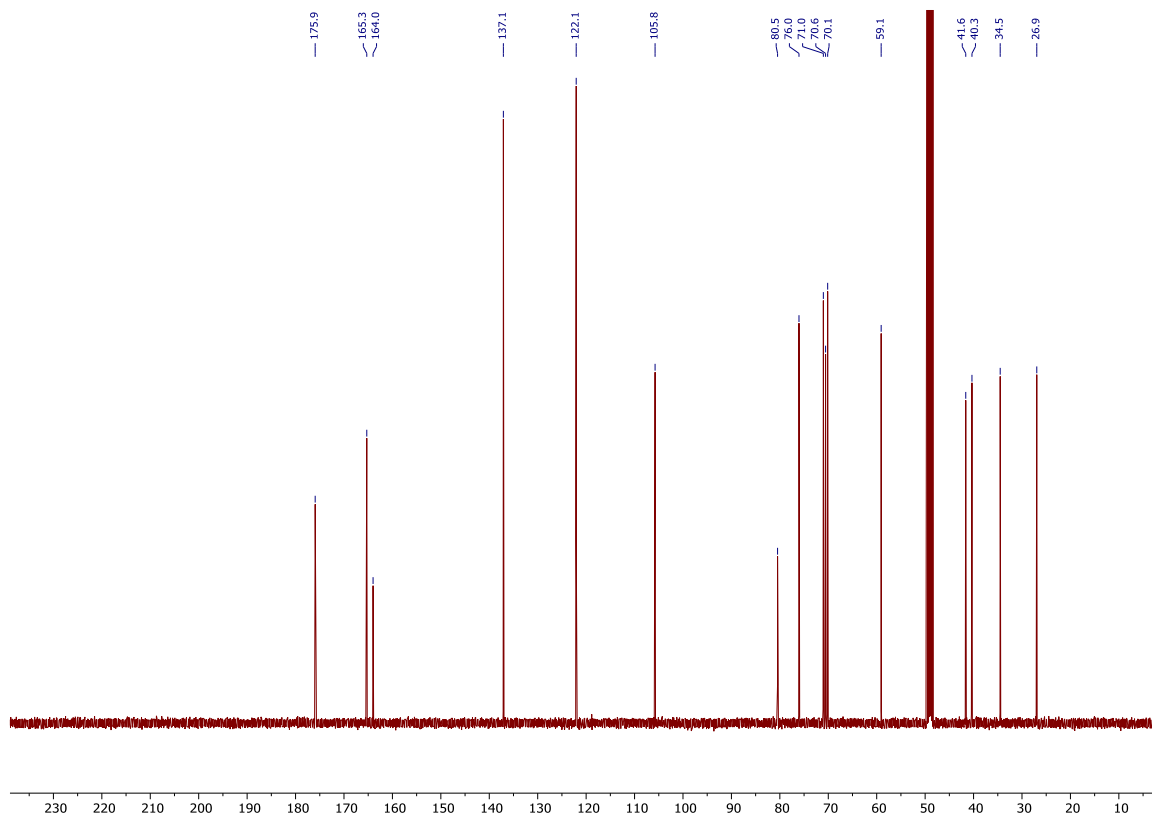
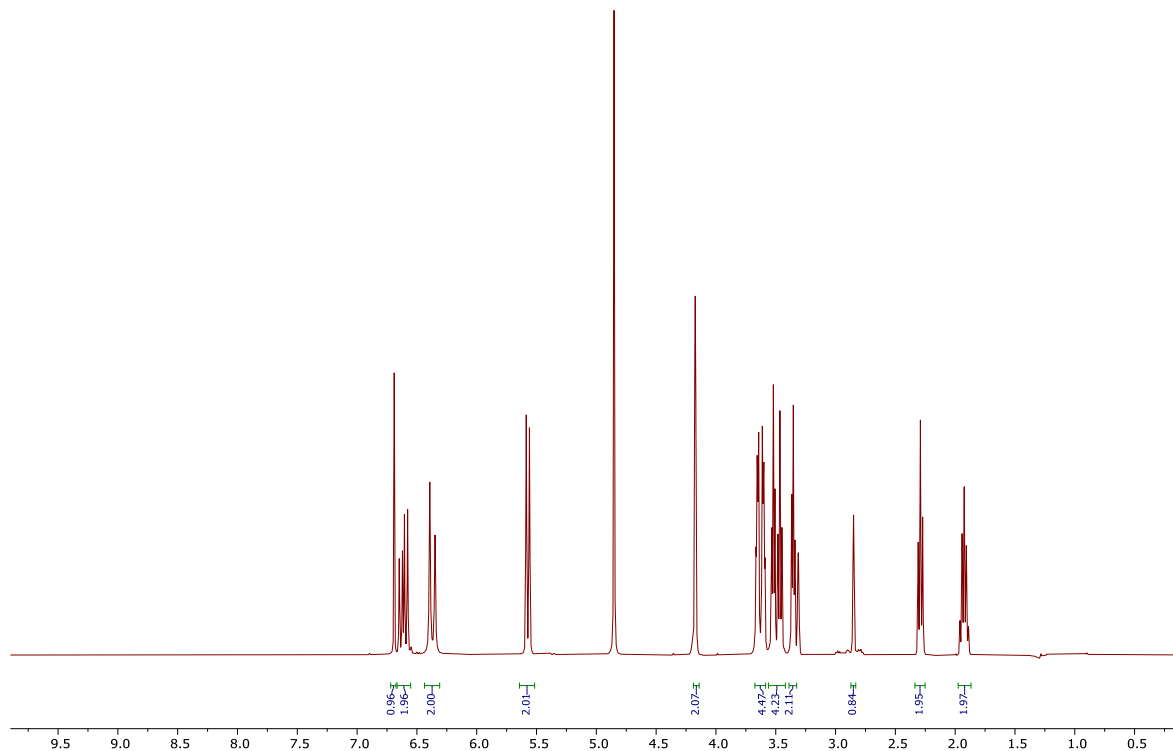
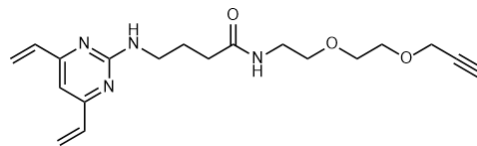
Ethyl 4-((4,6-divinylpyrimidin-2-yl)amino)butanoate (90)



4-((4,6-Divinylpyrimidin-2-yl)amino)butanoic acid (91)



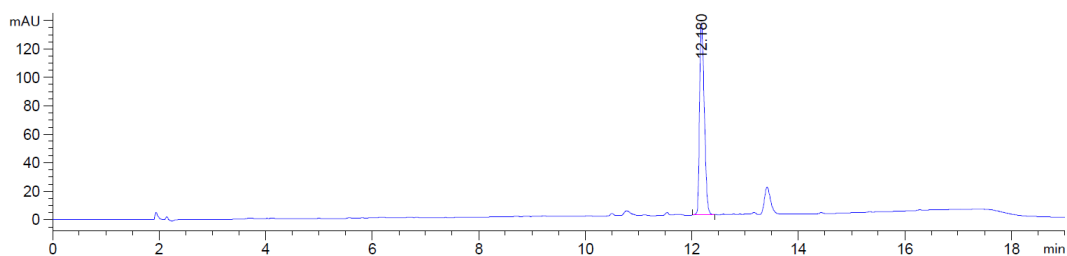
4-((4,6-Divinylpyrimidin-2-yl)amino)-N-(2-(2-(prop-2-yn-1-yloxy)ethoxy)ethyl)butanamide (92)



6.4. Chromatography traces

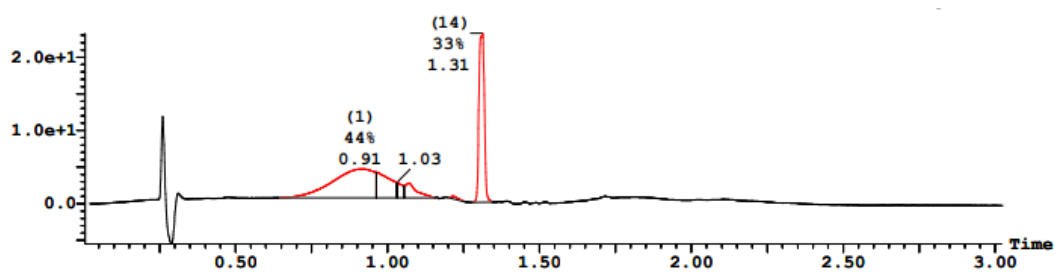
Azide-PEG₃-arylsulfate-MMAE (42)

HPLC: Absorbance at 254 nm.



Azido-discodermolide (76)

Liquid chromatography: Combined absorbance between 220 to 800 nm.



6.5. Publication list

Rapid and robust cysteine bioconjugation with vinylheteroarenes, **Seki, H.**; Walsh, S. J.; Bargh, J. D.; Parker, J. S.; Carroll, J. S.; Spring, D. R. *Chem. Sci.*, **2021**, *12*, 9060.

An automated computational approach to kinetic model discrimination and parameter estimation, Taylor, C. J.; **Seki, H.**; Dannheim, F. M.; Willis, M.; J.; Clemens, G.; Taylor, B. A.; Chamberlain, T. W.; and Bourne, R. A. *React. Chem. Eng.*, **2021**, *6*, 1404.

Site-selective modification strategies in antibody–drug conjugates, Walsh, S. J.[^]; Bargh, J. D.[^]; Dannheim, F. M.[^]; Hanby, A. R.[^]; **Seki, H.**[^]; Counsell, A. J.[^]; Ou, X.[^]; Fowler, E.[^]; Ashman, N.[^]; Takada, Y.[^]; Isidro-Llobet, A.; Parker, J. S.; Carroll, J. S.; and Spring, D. R. *Chem. Soc. Rev.*, **2021**, *50*, 1305. ([^]Equal contribution)

General dual functionalisation of biomacromolecules via a cysteine bridging strategy, Walsh, S. J.[^]; Iegre, J.[^]; **Seki, H.**[^]; Bargh, J. D.; Sore, H. F.; Parker, J. S.; Carroll, J. S.; Spring, D. R. *Org. Biomol. Chem.*, **2020**, *18*, 4224. ([^]Equal contribution)